Aspergillus fumigatus F-box protein Fbx15 functions are dependent on its nuclear localisation signals and are partially conserved between *A. fumigatus* and *A. nidulans*

Dissertation

for the award of the degree

“Doctor rerum naturalium”

Division of Mathematics and Natural Sciences

of the Georg-August-Universität Göttingen

within the doctoral program “Microbiology and Biochemistry” of the

Georg-August University School of Science (GAUSS)

submitted by

Anja Abelmann

from Alfeld (Leine)

Göttingen 2020

Thesis Committee:

Referee: Prof. Dr. Gerhard H. Braus,
Department of Molecular Microbiology and Genetics,
Georg-August University Göttingen

2nd referee: Jun.-Prof. Dr. Kai Heimel,
Department of Molecular Microbiology and Genetics,
Georg-August University Göttingen

3rd referee: Prof. Dr. Ralph Kehlenbach,
Department of Molecular Biology,
Georg-August University Göttingen

Members of the Examination Board:

Prof. Dr. Stefanie Pöggeler,
Department of Genetics of Eukaryotic Microorganisms, Georg-August University Göttingen

Prof. Dr. Rolf Daniel,
Department of Genomic and Applied Microbiology, Georg-August University Göttingen

PD Dr. Michael Hoppert,
Department of General Microbiology, Georg-August University Göttingen.

Date of the oral examination: 16th March 2020

This work was accomplished in the group of Prof. Dr. Gerhard H. Braus, at the Department of Molecular Microbiology and Genetics, Institute of Microbiology and Genetics, Georg-August University Göttingen.

Table of Contents

Summary

Aspergillus fumigatus is a globally distributed opportunistic filamentous fungal pathogen mainly found in compost and represents the main cause of pulmonary aspergillosis in immunocompromised individuals. Fungal development and virulence require a highly controlled balance of regulatory protein biosynthesis, posttranslational modification and degradation for signal transduction and DNA maintenance to colonise various habitats and hosts. F-box proteins are part of the Skp1/A-Cullin -F-Box (SCF) ubiquitin RING ligase complex acting as substrate receptors for target proteins, which become posttranslational ubiquitinated for 26S proteasome mediated degradation. The *Aspergillus*-specific F-Box protein Fbx15 was initially described in *Aspergillus nidulans* as developmentally relevant protein. *A. fumigatus* Fbx15 is needed for the regulation of secondary metabolism such as the control of gliotoxin synthesis, as well as stress response and pathogenicity. *A. fumigatus* Fbx15 is unusual because a function in protein ubiquitination through SCF^{Fbx15} complex was not yet identified, but it is required for the nuclear localisation of the essential co-repressor subunit SsnF. *A. fumigatus* Fbx15 carries two predicted nuclear localisation signals (NLS) within its primary amino acid sequence. This study had three issues: (i) The functions of Fbx15 and putative interaction partners were compared between *A. fumigatus* and *A. nidulan*s. (ii) It was analysed whether Fbx15-mediated stress response and virulence of *A. fumigatus* depends on its control of the synthesis of gliotoxin or other mycotoxins. (iii) The molecular function of the two NLS of *A. fumigatus* Fbx15 and their impact on SsnF localisation was explored.

(i) This study revealed a partial overlap in the functions of the two Aspergillus Fbx15 counterparts. Both heterologous expressed Fbx15 proteins complemented each other's functions in secondary metabolite control and in Fbx15-mediated *A. nidulans* asexual and sexual development regulation. In contrast, *A. nidulans* Fbx15 is only partially required for stress response contrary to the crucial role in stress response of *A. fumigatus* Fbx15. Analysis of the interplay of Fbx15 with the transcription factors OefC and SrbB, the putative transcription factor FiAt, and the putative part of a F-type ATPase, FidA, did not elucidate a clear link to Fbx15 functions in development, stress response and/or pathogenicity.

(ii) *A. fumigatus* Fbx15 is not only required for the regulation gliotoxin, but also for the biosynthesis of the mycotoxin fumagillin at vegetative growth. *A. fumigatus* Fbx15-dependent regulation of gliotoxin biosynthesis is dispensable for Fbx15-mediated stress response at minimal growth and pathogenicity in the *Galleria mellonella* model.

(iii) Either *A. fumigatus* Fbx15 NLS1 or NLS2 are sufficient to support nuclear import of Fbx15 during vegetative growth under non-stress conditions. NLS1 is insensitive against stress when NLS2 is absent. NLS2 is required to exclude Fbx15 from the nuclear matrix to the nuclear periphery during oxidative stress. NLS2 is also sufficient to locate SsnF to the nuclear matrix in the absence of stress, and to the nuclear periphery with stress, whereas the sole presence of NLS1 results in constitutive nuclear SsnF. Therefore, NLS2 is the stress-responding element to control and shift the distribution of Fbx15 and of SsnF from the nuclear matrix to the periphery presumably to release the fungal cell from SsnF dependent gene repression. Fbx15 phosphorylation represents an additional layer of location control, which is not relevant during non-stress conditions. Fbx15 phosphorylation or dephosphorylation do not require intact NLS1- or NLS2 sequences. Fbx15 cellular location during oxidative stress depends on the phosphorylation or dephosphorylation status at residue S468|9. The major finding of this thesis is the identification of *A. fumigatus* NLS2 as control element to exclude Fbx15 and simultaneously the corepressor SsnF from the nuclear matrix during oxidative stress resulting in derepression of genes e.g. for mycotoxin formation.

Zusammenfassung

Aspergillus fumigatus ist ein weltweit verbreiteter, filamentöser Pilz, der hautsächlich auf kompostierbarem Medium vorkommt. Als opportunistischer Krankheitserreger repräsentiert *A. fumigatus* die Hauptursache für atemwegsinvasive Aspergillose in immungeschwächten Individuen. Pilzspezifische Entwicklungsprozesse und Virulenz bedürfen eines kontrollierten Gleichgewichts der Synthese, des Abbaus sowie der posttranslationalen Modifikation regulatorischer Proteine. Solche regulatorischen Proteine werden für Entwicklungsprozesse, Signaltransduktionen und die DNA-Instandhaltung während der Kolonisierung verschiedenster Habitate oder Wirten benötigt. F-box Proteine sind Teil des Skp1/A-F-box-Cullin (SCF) Ubiquitin RING Ligasekomplexes. Sie fungieren als Substratrezeptoren für Proteine, die für ihren Abbau am 26S Proteasom posttranslational ubiquitiniert werden. Das *Aspergillus*-spezifische F-box Protein Fbx15 wurde erstmals in *A. nidulans* als entwicklungsrelevantes Protein beschrieben. *A. fumigatus* Fbx15 ist entscheidend für die Regulation des Sekundärmetabolismus, wobei die Biosynthese des Mykotoxins Gliotoxin reguliert wird. Zudem wird *A. fumigatus* Fbx15 für die Stresstoleranz und Pathogenität des Pilzes benötigt. *A. fumigatus* Fbx15 ist für seinen Proteintyp untypisch, da bis jetzt keine Funktion bezüglich der Proteindegradation mittels Ubiquitinierung durch den SCF^{Fbx15}-Komplex identifiziert wurde. Stattdessen wurde eine Fbx15-abhängige Kernlokalisierung der essentiellen Ko-Repressoruntereinheit SsnF festgestellt. *A. fumigatus* Fbx15 besitzt zwei potentielle nukleare Lokalisierungssignale (NLS) in seiner primären Aminosäuresequenz. Diese Arbeit hatte drei Themen: (i) Die Funktionen von Fbx15 und potentieller Interaktionspartner wurden in *A. nidulans* und *A. fumigatus* miteinander verglichen. (ii) Es wurde untersucht, ob die in Abhängigkeit von *A. fumigatus* Fbx15 entstehende Stressantwort und Virulenz im Zusammenhang mit seiner regulatorischen Wirkung auf die Gliotoxinbiosynthese oder andere Mykotoxine steht. (iii) Die molekulare Funktion der beiden NLSs von *A. fumigatus* Fbx15 wurde untersucht, sowie dessen Einfluss auf die Lokalisierung von SsnF.

(i) Diese Arbeit hat gezeigt, dass es eine partielle Übereinstimmung in den Funktionen der beiden *Aspergillus* Fbx15-Proteine gibt. Beide heterolog exprimierte Fbx15-Proteine komplementieren gegenseitig ihre jeweiligen Funktionen hinsichtlich des Sekundärmetabolismus, sowie der Fbx15-abhängigen asexuellen und sexuellen Entwicklung in *A. nidulans*. Im Gegensatz dazu ist *A. nidulans* Fbx15 nur partiell für Stresstoleranz relevant, wohingegen *A. fumigatus* Fbx15 eine Hauptfunktion in Stresstoleranz vorweist. Die Untersuchung der möglichen Wechselwirkung von Fbx15 mit den Transkriptionsfaktoren OefC und SrbB, des potentiellen Transkriptionsfaktors FiAt, und FidA, der potentielle Teil einer F-ATPase, wies keinen eindeutigen Zusammenhang zu Fbx15 in Entwicklung, Stressantwort und/oder Pathogenität auf.

(ii) *A. fumigatus* Fbx15 ist nicht nur für die Regulierung von Gliotoxin verantwortlich. Es wird ebenfalls für die Regulation der Biosynthese des Mykotoxins Fumagillin während des vegetativen Wachstums benötigt. Darüber hinaus sind die regulatorischen Eigenschaften von *A. fumigatus* Fbx15 in Bezug auf Gliotoxin nicht für die von Fbx15 geleitete Stressantwort während des Minimalwachstums und der Pathogenität im *Galleria mellonella*-Model von Bedeutung.

(iii) Beide NLS-Sequenzen von *A. fumigatus* Fbx15 werden unabhängig voneinander für den Kerntransport von Fbx15 während des vegetativen Wachstums benötigt. Dabei ist NLS1 ist für sich alleine unempfindlich gegenüber Stress. NLS2 wird hingegen für den Transport von Fbx15 von der Kernmatrix zur Kernperipherie bei oxidativem Stress benötigt. Außerdem wird NLS2 für die erfolgreiche Lokalisierung von SsnF in der Kernmatrix in Abwesenheit von Stress benötigt, sowie den Transport von SsnF zur Kernperipherie bei Stress. In diesem Prozess führt Präsenz von NLS1 ohne NLS2 zu einer kontinuierlichen Kernlokalisierung von SsnF. NLS2 ist hierbei ein Element für die Stressantwort, das für den Shift von Fbx15 und SsnF von der Kernmatrix zur Kernperipherie verantwortlich ist, um vermutlich die von SsnF verursachte Repression der Genregulation in der Zelle zu unterbinden. Die Phosphorylierung von Fbx15 repräsentiert

dabei eine zusätzliche Lokalisierungskontrolle, die jedoch nicht bei vegetativen Wachstum entscheidend ist. Dephosphorylierung oder Phosphorylierung von Fbx15 benötigt keine intakte NLS1- oder NLS2-Sequenz. Dennoch ist die zelluläre Lokalisierung von Fbx15 bei oxidativem Stress abhängig von der Phosphorylierung oder Dephosphorylierung an den Aminosäuren S468|9. Das Hauptergebnis dieser Dissertation besteht in der Identifizierung von *A. fumigatus* Fbx15 NLS2 als Kontrollelement, um Fbx15 und SsnF simultan aus der Kernmatrix während oxidativen Stresses zu transportieren, was zu einer Derepression von Genen führt, die z.B. für die Produktion von Mykotoxinen zuständig sind.

I Introduction

1 *Aspergillus fumigatus* - an opportunistic human pathogen

1.1 Nutrient versatility of *A. fumigatus* and its global distribution

The ubiquitous airborne saprotrophic fungus *Aspergillus fumigatus* has its natural niche in the soil on decaying organic matter where the fungus makes an important contribution to the recycling of carbon and nitrogen (Latgé, 1999). The fungus is able to degrade almost all components of organic waste such as cellulose, fatty acids, pectin, proteins, sugars and xylane (Adav *et al.*, 2015; Fogarty, 1994; Wang *et al.*, 2012). This ability is due to its high metabolic versatility, e.g. demonstrated by the capability to utilise diverse carbon sources like D-galactose, L-arabinose and D-xylose or alcohols instead of its favoured carbon source glucose (Flipphi *et al.*, 2009; Zhang *et al.*, 2018). Despite of this, *A. fumigatus* is able to recycle nitrogen out of amino acids (aa), nitrate and purines if the favoured ammonium, glutamate or glutamine is not available (Krappmann and Braus, 2005; Lee *et al.*, 2013). The ability to utilise different compounds for carbon and nitrogen recycling contribute to *A. fumigatus* successful competition with other mesophilic, thermotolerant and thermophilic aerobic microorganisms, e.g. different bacteria like actinomycetes and fungi such as molds (Bhatti *et al.*, 2017; Fang and Latgé, 2018; Singh and Satyanarayana, 2019). Whereas most other fungi are mesophilic and grow at temperatures between 25-35°C, *A. fumigatus* is highly thermotolerant with a growth ability between 30 to 52°C what depicts the ideal proliferation conditions in young composts (Beffa *et al*., 1998; St-Germain and Summerbell, 2003; Cooney and Emerson, 1964). The ability to adapt to a wide range of environmental conditions makes *A. fumigatus* one of the most ubiquitous distributed fungi in the world with a very high genetic diversity (Debeaupuis *et al.*, 1997; Rocchi *et al.*, 2015). Analysis of over 2,000 *A. fumigatus* isolates from 13 countries in four continents revealed eight genetic clusters of which seven showing a broad geographic distribution. These global populations of *A. fumigatus* are structured by contemporary gene flow, historical differentiation, sexual reproduction and local distributed antifungal drug resistance (Ashu *et al.*, 2017).

1.2 Developmental stages of *A. fumigatus*

A. fumigatus reproduces itself either asexually or sexually. The sexual life cycle is induced under specific conditions including heat and a duration of six month resulting in fruiting bodies, so called cleistothecia (Dyer and O'Gorman, 2012; Ene and Bennett, 2014; Mullins *et al.*, 1976; O'Gorman *et al.*, 2009). *Neosartorya* as a new Latin genus name was given to the telomorphic (sexual) state next to the already existing anamorphic (asexual) state

Aspergillus (O'Gorman *et al.*, 2009). During the asexual life cycle airborne haploid spores are produced, named conidiospores or conidia (Mullins *et al*., 1976). Conidia are released into the environment from multicellular conidiophores that are produced by vegetative hyphae developing specialised foot-cells. Those foot-cells terminate in a stalk with a clavate vesicle, which is covered with a layer of green phialides, which act as spore forming cells in a budding-like process. From the polar phialides green-pigmented conidia are produced by mitotic division and subsequent constriction (Figure 1) (Bayram *et al.*, 2008; Brakhage and Langfelder, 2002; Tao and Yu, 2011).

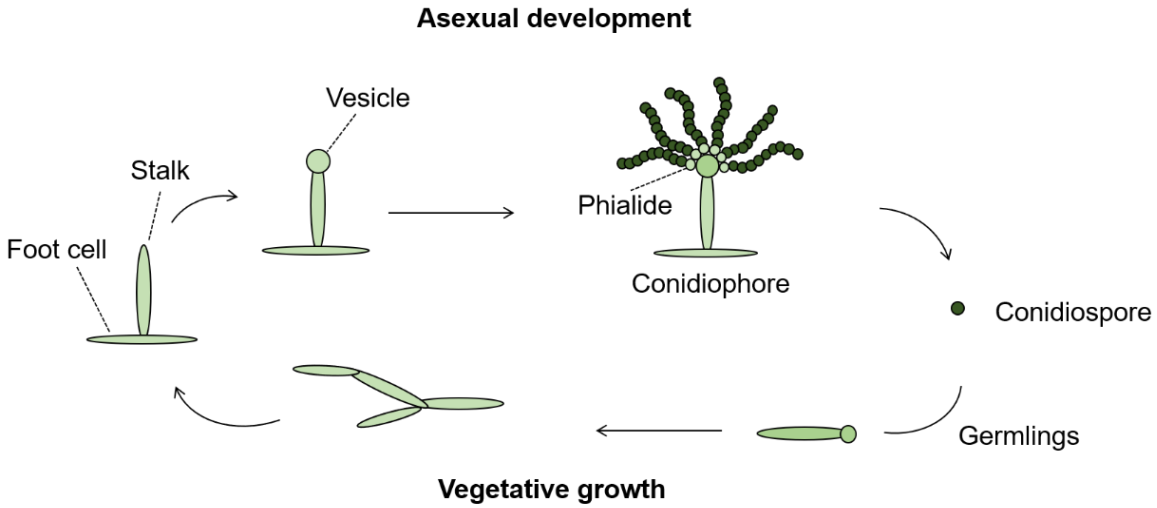

Figure 1: *A. fumigatus* asexual life cycle. *A. fumigatus* airborne conidiospores germinate on a medium containing suitable nutrient – and energy sources. The fungus grows vegetatively out of airborne conidia till a new conidiophore is produced, whose first developmental stage is the formation of a foot cell. From the foot cell a stalk and a vesicle arise. The full-developed conidiophore contains phialides at the vesicle site with chains of conidiospores. Modified from Bayram *et al.*, 2008.

The conidia of *A. fumigatus* are long-term resting structures that are resistant against a wide range of environmental stress inducers such as oxidative stress, ultraviolet radiation and heat (Corrochano, 2007; Hagiwara *et al.*, 2014; Kozakiewicz and Smith, 1994). Several layers are covering *A. fumigatus* conidia and protect them from stressors. The outer layer is the rodlet layer that consists of amyloid fibres that are composed of the hydrophobin family member protein RodA. So far seven different hydrophobins are identified (RodA-RodG) whereby RodA is solely important for the formation of the rodlet layer, conidial hydrophobicity, sporulation and resistance to physical injury and immunological inertia (Paris, Debeaupuis, *et al.*, 2003; Valsecchi *et al.*, 2018; Wyatt *et al.*, 2013). The cell wall of *A. fumigatus* conidia consist of different polysaccharides, α-(1,3)-glucan, chitin, galactomannan, ß-(1,3)-glucan and mycelial-specific

galactosamino-galactan (Alkhayyat *et al.*, 2015; Hohl and Feldmesser, 2007; Samar *et al.*, 2015; Valiante *et al.*, 2015). The reorganization of the conidial cell wall during germination is mediated by the glycosyl hydrolase GH55 members (Millet *et al.*, 2019). Two types of melanin are parts of the conidia cell wall: Pyomelanin and 1,8-dihydroxynaphthalene (DHN)-melanin. Pyomelanin is a brown, water-soluble compound protecting the conidia against cell wall stress and reactive oxygen species (ROS) whereas DHN-melanin is a blue-green pigment accumulated in the conidia and has an additional protective function against ROS (Heinekamp *et al.*, 2012; Rambach *et al.*, 2015; Schmaler-Ripcke *et al.*, 2009; Sugareva *et al.*, 2006).

1.3 *A. fumigatus* as opportunistic human pathogen

A. fumigatus represents the most common and opportunistic aerial fungal pathogen as it causes 90% of all cases of invasive aspergillosis in immunosuppressed individuals next to other pathogenic fungi such as *A. niger*, *A. flavus* or *A. terreus* (Fang and Latgé, 2018; Perfect *et al.*, 2001). The airborne conidia of *A. fumigatus* with a size of 2 to 3 µm are small enough to reach the lung alveoli (Christensen *et al.*, 1989; Yaguchi, 2011). In fact, mammals inhale daily several hundreds of *A. fumigatus* conidia (Chazalet *et al.*, 1998; Goodley *et al.*, 1994; Hospenthal *et al.*, 1998). These conidia are normally eliminated in immunocompetent individuals, e.g. by engulfing or inactivation through recruited neutrophils and Ly6Chi inflammatory monocytes of the innate immune system (Bonnett *et al.*, 2006; Espinosa *et al.*, 2014; Jhingran *et al.*, 2012; Mircescu *et al.*, 2009; Shlezinger *et al.*, 2017). Immunosuppression is a cause of chemotherapies, diseases like tuberculosis, AIDS, neutropenic diseases or as a result of organ transplantations. In these individuals inhaled conidia are able to enter the lung where they start to germinate (Figure 2) (Tekaia and Latgé, 2005). Invasive aspergillosis can lead to death and is characterized by angioinvasion with sinopulmonary involvement while disseminating to the central nervous system (Fayed, 2018; Pauw *et al.*, 2008). Invasion to the gastrointestinal tract, skin or contiguously belongs to the characteristics of invasive aspergillosis (Pauw *et al.*, 2008). Depending on the degree of immune suppression *A. fumigatus* causes allergic, saprophytic, partially invasive or acute invasive aspergillosis clinical syndromes. Allergic reactions result in extrinsic asthma including allergic fungal sinusitis, severe asthma with fungal sensitization and allergic bronchopulmonary aspergillosis (Chaudhary and Marr, 2011; Ghosh *et al.*, 2015; Knutsen *et al.*, 2012). Saprophytic syndromes are categorised in chronic cavitary or fibrosing aspergillosis and Aspergilloma (Denning *et al.*, 2016; Steinbach, 2018). Recent global estimations accomplished in 2017 projected over 3,000,000 cases of chronic pulmonary aspergillosis and around 250,000 cases of invasive

aspergillosis annually (Bongomin *et al.*, 2017). The mortality rate of patients suffering from chronic pulmonary aspergillosis ranges from 14% to 53% after one to ten years post infection (Lowes *et al.*, 2017).

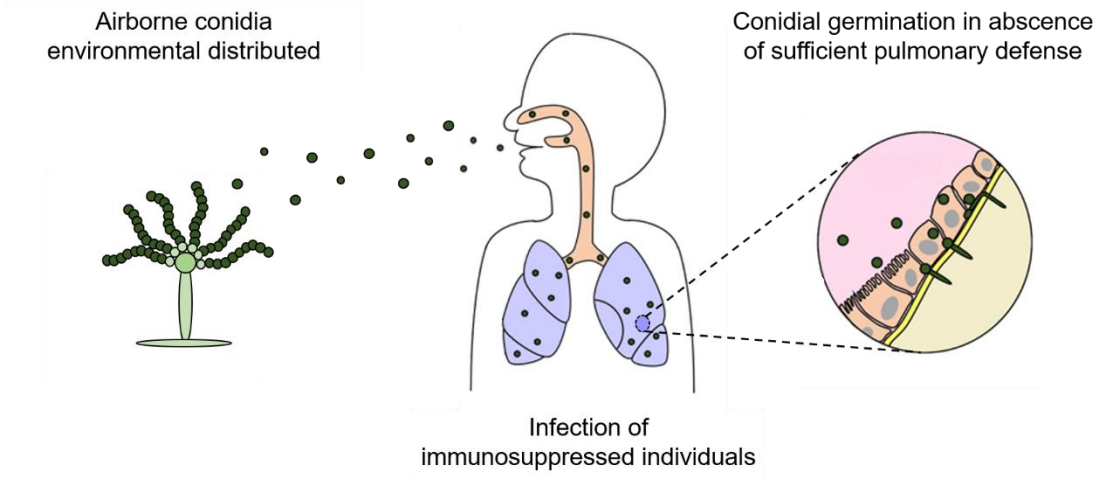

Figure 2: Infection life cycle of *A. fumigatus*. Inhalation of environmental distributed airborne *A. fumigatus* conidia can distribute through the lung alveoli in immunosuppressed individuals. Pulmonary aspergillosis can break out in the absence of a sufficient pulmonary defence leading to the germination of conidia through the lung tissue. Modified from Tekaia and Latgé, 2005.

2 *Aspergillus nidulans* - a genetic model organism for filamentous fungi

Aspergillus nidulans represents a model organism for the genome research, cell development and gene regulation of filamentous fungi (Martinelli, 1994; Osmani and Mirabito, 2004). In contrast to the heterothallic *A. fumigatus*, *A. nidulans* is homothallic and undergoes an asexual and sexual life cycle under moderate growth conditions (Bayram *et al.*, 2010a; O'Gorman *et al.*, 2009; Ruger-Herreros *et al.*, 2011).

The asexual life cycle of *A. nidulans* is favoured by a combination of factors including light and characterized by the production of conidia that origin from conidiophores (Adams *et al.*, 1998; Bayram *et al.*, 2010; Mooney and Yager, 1990). The conidiophores of *A. nidulans* contain an additional cell type, called metula, in contrast to *A. fumigatus* conidiophores (Adams *et al.*, 1998; Mims *et al.*, 1988). The metula origins from the conidiophore stalk, called conidiophore vesicle, and comprises a single nucleus (Mims *et al.*, 1988). From the metula the spore forming phialides arise whose asymmetric budding-like division results in the formation of conidia chains (Adams *et al.*, 1998). The sexual life cycle is favoured in darkness with limited oxygen levels (Park *et al.*, 2019). After cultivation *A. nidulans* needs

20h at 37°C to initiate sexual development (Seo *et al.*, 2004). In *A. nidulans* dikaryon formation occurs either homothallic (self-fertilized) or heterothallic (two compatible partners) (Galagan *et al.*, 2005; Paoletti *et al.*, 2007; Scazzocchio, 2006). Hülle cells cluster around the dikaryotic hyphae appearing in a "nest" and differentiate to thick-walled globose cells (Pöggeler *et al.*, 2018). They are assumed to function as nurse cells for cleistothecia and are not directly connected to sexuality (Braus *et al.*, 2002; Hermann *et al.*, 1983; Scherer and Fischer, 1998). Inside the dikaryotic cells, which form a network of ascogenous hyphae, nuclear fusion takes place (Pöggeler *et al.*, 2018). Young ascis are formed containing eight nuclei synthesized by meiotic division and a post-meiotic mitosis. These young ascis are comprised in a pre-mature cleistothecium, the primordium (Sohn and Yoon, 2002). In numbers over 10.000 asci are comprised in one cleistothecium. The formation of a mature cleistothecium with a size of 125-200 µm in diameter takes 96h (Seo *et al.*, 2004). Asexual conidia and sexual ascospores can germinate and undergo either the asexual or sexual life cycle depending on the environmental conditions after vegetative growth (Figure 3).

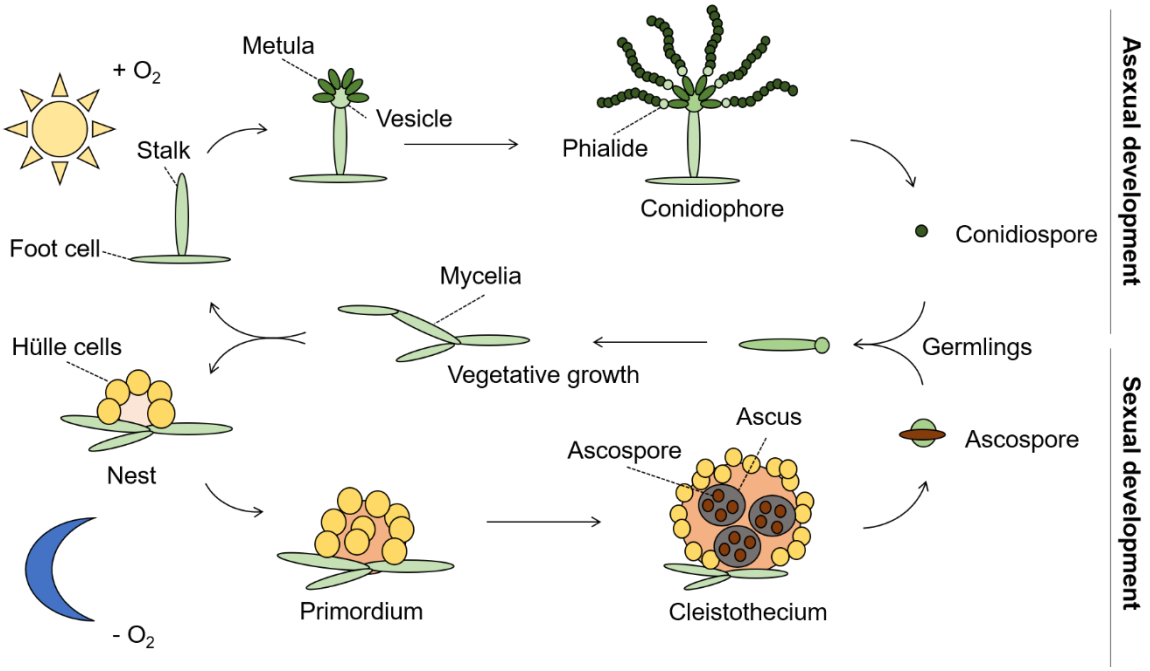

Figure 3: Developmental stages of *A. nidulans*. In light with sufficient oxygen supply the fungus favours the asexual development producing conidiophores. Conidiophores contain a foot cell, a stalk and a vesicle with metulae, on which spore-forming phialides produce large numbers of conidiospores. In darkness with reduced oxygen supply the sexual development is favoured resulting in the production of the fruiting bodies, cleistothecia. Cleistothecia arise from Hülle cells surrounding nest structures, of which a primordium is developed. Mature cleistothecia contain ascospores with inside of each four ascis are present. A released ascospore can germinate like a conidiospore producing a mycelium network at vegetative growth. Modified from Bayram *et al.*, 2008.

Reorganisation of the morphogenesis due to environmental changes or by passing developmental stages like from filamentous growth to other reproductive stages needs the synthesis and degradation of certain proteins as most recently described in *Candida albicans* by an increased ubiquitin polypeptide-dependent protein degradation during hyphal growth (Yang *et al.*, 2020). The autophagy as well as degradation of corresponding proteins through the ubiquitin-dependent 26S proteasome represent important tasks during these processes (Glickman and Ciechanover, 2002; Pollack *et al.*, 2009). Proteins degraded by the 26S proteasome need to be marked with K48-polyubiquitin (Petroski and Deshaies, 2005b). This labelling is required for development, which process itself reversable (Meister *et al.*, 2019; Tyers and Jorgensen, 2000; von Zeska Kress *et al.*, 2012).

3 The fungal F-Box protein Fbx15

3.1 F-Box proteins as part of the SCF E3 ubiquitin RING ligases

3.1.1 SCF E3 ubiquitin RING ligases mediate ubiquitination followed by proteasomal degradation

The tetrameric Skp1-cullin-F-box protein (SCF) E3 ubiquitin ligases are one of the best-understood families of the cullin-based 'really interesting new gene' (RING) ligases and were first characterized in *Saccharomyces cerevisiae* (Bai *et al.*, 1996). They are of high importance in biological processes such as cell cycle progression, development, DNA replication, gene transcription and signal transduction (Nakayama and Nakayama, 2006; Petroski and Deshaies, 2005a; Ren *et al.*, 2008). Most recently, a specific mammalian SCF^{FBXO3} E3 ligase was identified to modulate inflammation in atherosclerosis (Chandra *et al.*, 2019). The fungal SCF E3 ubiquitin RING ligase consists of a scaffold protein, cullin (5 family members), an F-box protein as substrate receptor (approx. 70 family members), an adapter protein Skp1/SkpA and a catalytic RING component (2 members: RBX1 and RBX2) (Deshaies and Joazeiro, 2009; Sarikas *et al.*, 2011; Willems *et al.*, 2004). Dysfunctions in the regulation of cellular processes by the SCF E3 ubiquitin RING ligases can cause severe diseases such as human cancer and have a direct influence on the embryonic development (Nakayama and Nakayama, 2006; Wei and Sun, 2010).

The SCF E3 ubiquitin RING ligases are required to control the life span of regulatory proteins involved in coordinating development, signal transduction and DNA maintenance in the ubiquitin 26S proteasome system (UPS). Hence, around 90% of protein breakdowns in mammalian cells are mediated by proteasome degradation (Lee and Goldberg, 1998). Well studied substrates are short-lived proteins such as transcription factors, cyclins, cyclin-dependent kinases and their inhibitors (Glotzer *et al.*, 1991; Ko and Cho, 2018;

McNeilly *et al.*, 2018; Pagano *et al.*, 1995). The degradation of substrates by the proteasome occurs either in the nucleus or in the cytoplasm (Berner *et al.*, 2018; Serrano-Bueno *et al.*, 2019). Target proteins are recruited to the proteasome if labelled with a specific ubiquitin chain in a sequential action of E1, E2 and E3 enzymes, of which E3 ubiquitin RING ligases are responsible for the substrate specificity through their F-box proteins (Clague *et al.*, 2015; Skaar *et al.*, 2013). The 76 aa long comprising ubiquitin is highly conserved in eukaryotic organisms. First, monomeric ubiquitin is bound to the E1 ubiquitin-activating enzyme and transferred to cysteine residues of E2 ubiquitin-conjugating enzyme, both in an adenosine triphosphate (ATP)-dependent manner. The ubiquitin-bound E2 enzyme binds to the E3 ubiquitin ligase. After the substrate is bound to E3 through its F-box protein, the ubiquitin of the E2 enzyme is transferred to a lysine residue of the substrate (Glickman and Ciechanover, 2002; Lennarz and Lane, 2013).

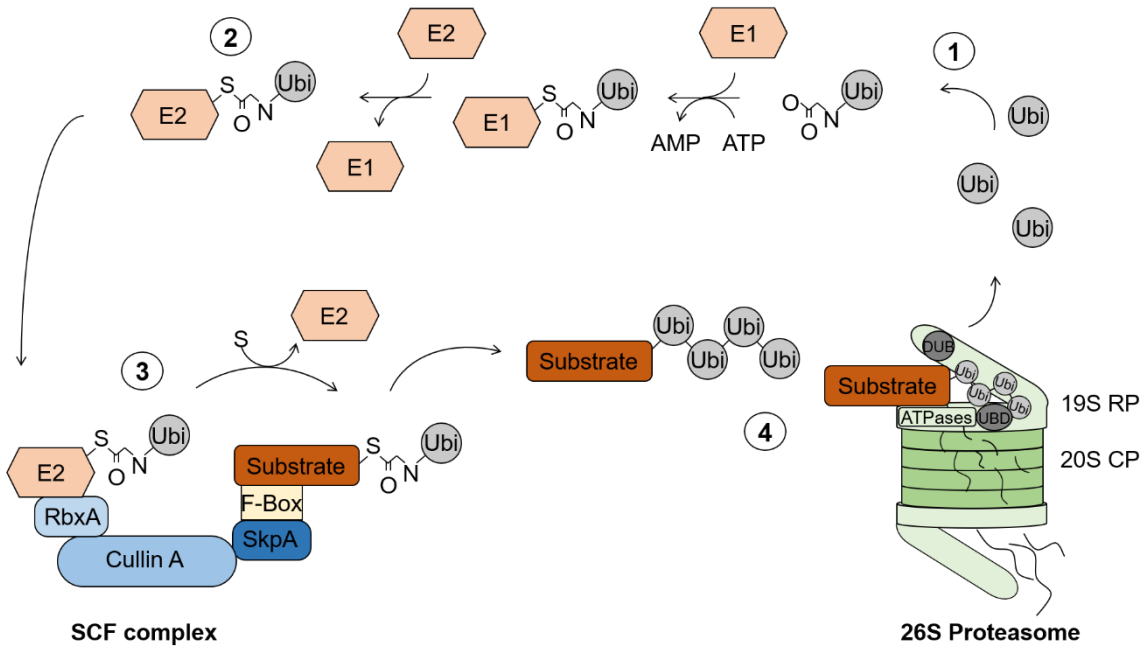

Figure 4: Substrate degradation by the ubiquitin 26S proteasome system (UPS). (**1**) Linking substrates to ubiquitin for degradation by the 26S proteasome starts with activating and binding of free monomeric ubiquitin (Ubi) to the E1 ubiquitin-activating enzyme in an energy-consuming step. (**2**) Ubiquitin is transferred to the ubiquitin-conjugating enzyme E2 binding on an internal cysteine residue. (**3**) The E2-Ubiquitin bundle binds to the RbxA adapter of the E3 ubiquitin ligase (here: Skp1-cullin/Rbx-F-box protein (SCF) complex), where the transfer of active ubiquitin to a lysine residue of the substrate, bound to the F-box protein, is catalysed. (**4**) A final polyubiquitin chain is built by attachment of single ubiquitin to a previous attached ubiquitin through its internal Lys48 residue and recognized by the ubiquitin binding domains (UBD) in the 19S proteasomal regulatory particle (RP). The substrate enters the proteolytic chamber of the 20S core particle (CP) after a ring of six ATPases unfolded it. Hereby, the ubiquitin-tag was removed from the substrate by a deubiquitinating enzyme (DUB) and releases inactive monoubiquitin. Modified from Jöhnk, 2016.

In case of proteasomal degradation of the substrate a polyubiquitin chain is formed by the covalent attachment of monomeric ubiquitins achieved by an isopeptide bound of the C-terminal glycine residue at aa 76 of the new ubiquitin to Lys48 (one of seven lysine residues) of the already attached substrate-bound ubiquitin (Komander and Rape, 2012). Polyubiquitinated substrates at Lys48 are recognized by two ubiquitin receptors with ubiquitin binding domains (UBD) of the 19S proteasomal regulatory particle (RP) and get unfolded by six ATPases in the RP. During this process the ubiquitin chain gets cleaved and recycled from the target protein by deubiquitinating enzymes (DUBs) (Bhattacharyya *et al.*, 2014; Gu and Enenkel, 2014). The unfolded protein exits the proteolytic core of the proteasome, the 20S core particle (CP), though its two entrance pores with specific sizes allowing only unfolded proteins to pass through (Figure 4) (Bhattacharyya *et al.*, 2014). Most recently it has been identified that SCF E3 ligases can regulate the modelling of other SCF E3 ligases by coupled monoubiquitylation (Kelsall *et al.*, 2019).

3.1.2 Regulation of the SCF E3 ubiquitin RING ligase

A specific lysine at the C-terminus of the cullin of the SCF E3 ubiquitin RING ligases gets modified in its binding affinity to the other SCF subunits by the neural-precursor-cell-expressed developmentally down-regulated 8 (NEDD8) cascade (Huang *et al.*, 2009; Osaka *et al.*, 1998; Pan *et al.*, 2004). Neddylation promotes the activity of SCF E3 ligases by a NEDD8 cascade (Gong and Yeh, 1999). Thereby, the catalytic efficiency is increased, which results in promoting RBX-cullin dimerization by a conformational change in the cullin scaffold. Moreover, NEDD8 supports the assembly of polyubiquitin chains by allowing the E2 enzyme to move in closer proximity to the acceptor lysine residue of the substrate protein (Duda *et al.*, 2008; Merlet *et al.*, 2009). The COP9 (constitutive photomorphogenesis 9) signalosome (CSN) recognizes cullin ring ligases such as SCF E3 ubiquitin RING ligases, which are not bound to substrates. The binding leads to a deactivation resulting in the deneddylation of the cullin by the recruitment of the cullin-associated neddylation-dissemination 1 (CAND1), which leads to a disassembly of the SCF E3 ubiquitin RING ligase components (Goldenberg *et al.*, 2004; Köhler *et al.*, 2019; J. Zheng *et al.*, 2002). Most recently it was shown that six subunits of the CSN interact with a novel ubiquitin-specific protease UspA in *A. nidulans* (Meister *et al.*, 2019). UspA is one of 22 DUBs in *A. nidulans*, which can reverse the ubiquitination processes (Abdul Rehman *et al.*, 2016; Meister *et al.*, 2019). UspA negatively regulates the amount of ubiquitinated proteins during developmental processes and is itself repressed by a functional CSN as well as reduces the protein level of the secondary metabolism-regulating NF-κB-like velvet domain protein VeA (Kato *et al.*, 2003; Meister *et al.*, 2019).

3.2 F-Box proteins in fungi

F-box proteins contain a F-box domain and function as protein receptors for substrates of SCF E3 ubiquitin RING ligases for ubiquitination through the adaptor Skp1/A to Cul1/A scaffold (Schmidt *et al.*, 2009). The amount of F-box proteins differ among species. For instance, humans, *A. fumigatus* and *A. nidulans* comprise approx. 70 F-box associated genes whereas 897 F-box-coding genes were found in *Arabidopsis thaliana* (Galagan *et al.*, 2005; Hua and Vierstra, 2011; Orejas *et al.*, 2001; Skaar *et al.*, 2009). Based on further protein interaction domains, F-box proteins can be subdivided into three classes: FBXW, FBXL, FBXO (Shen and Spruck, 2017). The class of the FBXW interaction domains contains one or more WD40 domains and ß-propeller structures that are required to recognize the specific consensus sequence DSGXXX(X)S, which must be phosphorylated on its serine (Ser) residues. FBXL proteins contain a C-terminal leucine-rich repeat (LRR) domain as well as an α-β-repeat structure. The last class with FBXO interaction domains contains different, partially uncharacterized motifs. Identified motifs of FBXO proteins are include carbo-hydrate-binding proteins and sugar hydrolases (CASH), Kelch-repeats (double glycine repeats forming ß-propellers), zinc finger and proline rich domains (Cardozo and Pagano, 2004; Jöhnk, 2016; Shen and Spruck, 2017; Skaar *et al.*, 2013).

F-box proteins are involved in different molecular pathways in ascomycetes. For example, the F-box protein GrrA is required for the development of matured ascospores during meiosis in *A. nidulans* (Krappmann *et al.*, 2006). In contrast, *A. nidulans* SconB is a negative regulator of the sulphur metabolism by repressing the MetR transcription factor, which represents an activator of sulphur metabolism (Natorff *et al.*, 2003; Sieńko *et al.*, 2014). Fbx23 and Fbx47 of *A. nidulans* regulate the CreA-mediated catabolite repression. Thereby, Fbx23 as part of the SCF^{Fbx23} E3 ubiquitin RING ligase complex is bridged to the CreA-SsnF-RcoA repressor complex through the GskA protein kinase, which leads to the degradation of the multi-repressor complex during xylan-induced derepressing conditions (de Assis *et al.*, 2018). Most recently, Fbx19 and Fbx22 were fund to be required in carbon catabolite repression responses in *Neurospora crassa* as Fbx19 is required to promote growth on medium containing arabinan and pectin whereas Fbx22 is needed to negatively control growth on D-glucose and glucomannan (Horta *et al.*, 2019).

The fungal specific Fbx15 is conserved among *Aspergillus* spp. and was primarily characterized in *A. nidulans*, where it has critical functions for asexual and sexual development as well as secondary metabolite homeostasis (Jöhnk *et al.*, 2016; von Zeska Kress *et al.*, 2012). The *A. fumigatus* Fbx15 protein sequence comprises several domains. The N-terminal F-box domain at aa position 6 to 53 is followed by the genus-specific interaction motif 1 at aa position 223 to 272 and the non-genus-specific second motif 2 at aa 313 to 362. Motif 2 is found in different other members of the genus such as

Penicillium chrysogenum. Both motifs do not contain FBXW belonging WD40 repeats or FBXL belonging LRR, which categorises Fbx15 to the FBXO class of interaction domains in F-box proteins (Jöhnk *et al.*, 2016; Skaar *et al.*, 2013). At the C-terminus two predicted monopartite nuclear localisation signals (mp NLS) at aa position 407 to 418 (NLS1: YERPRKRLRRYY) and 485 to 494 (NLS2: VSRKRKSPID) were identified. Two serine (Ser) residues were identified as putative phosphorylation sites by LCMS-analysis at aa 468 and 469 in between of the NLS sequences. S469 is most likely the critical putative phosphorylated residue with a probability of 98% compared to 2% for S468 (Figure 5) (Jöhnk *et al.*, 2016).

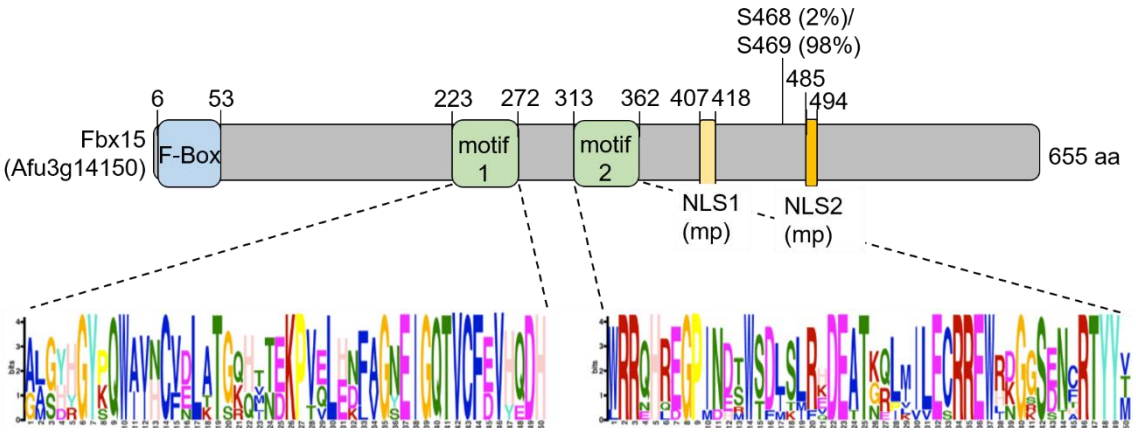

Figure 5: Domain architecture of the *A. fumigatus* F-box protein Fbx15. The F-box protein Fbx15 is 655 amino acids (aa) long. The characteristic F-box domain acting as interface to the SCF complex is located at the N-terminus at aa position 6 to 53. Two additional interaction motifs that contain no WD40 repeats or leucin-rich repeats (LRR) are positioned in the middle of the protein sequence: genus-specific motif 1 at aa position 223 to 272 and non-genus specific motif 2 at aa position 313 to 372. Two predicted monopartite nuclear localisation signals (mp NLS) are present at the C-terminus: NLS1 at aa position 407 at 418, NLS2 at aa position 485 and 494. Two serine (S) residues are probable phosphorylated: S468 (2%) and S469 (98%) are positioned between NLS1 and NLS2. Modified from Jöhnk *et al*., 2016.

Whereas F-box proteins are often rather instable, Fbx15 is a stable protein compared to the F-box protein SconB in *A. fumigatus,* whose homolog Met30 in *S. cerevisiae* is known to be short lived (Jöhnk *et al.*, 2016; Pashkova *et al.*, 2010). An active SCF^{Fbx15} complex formation occurs in the cytoplasm when Fbx15 is phosphorylated. However, binding to SkpA also occurs in the nucleus when Fbx15 is mimicked to be dephosphorylated at S468 and S469 by exchanging the Ser residues to alanine (Ala) residues. Increased dephosphorylation of Fbx15 protein is triggered by oxidative stress induced by hydrogen peroxide (H_2O_2), which is probably driven by the GlcA/BimG phosphatase. Nonetheless, the overall ubiquitin pattern in *A. fumigatus* is not significantly altered in absence of *fbx15*,

indicating the SCF^{Fbx15} E3 ubiquitin RING ligases bind a rare number of substrates for proteasomal degradation (Jöhnk *et al.*, 2016).

3.2.1 Oxidative stress response is supported by fungal F-box proteins

Aspergillus spp. must cope with diverse stressors during colonization of various habitats or invasion of potential host organism including oxidative stress induced by ROS (Fountain *et al.*, 2016; Jia *et al.*, 2018). The most critical host immune defence mechanism is the NADPH-oxidase-mediated production of ROS by alveolar macrophages and neutrophils (Grimm *et al.*, 2013). ROS are divided into three major ROS molecules: superoxide anion (O_2^-), hydroxyl radical ($HO^•$) and H_2O_2. O_2^- is produced by the reduction of molecular oxygen (O^2). H_2O_2 is produced by the conversion of O_2^- through superoxide dismutases (SODs). A full reduction is performed by catalases or glutathione peroxidases to water. $HO^•$ results in a partially reduction of O_2^- through Fenton reaction catalysed by ferrous ions. Targets of O_2^- are proteins with prosthetic Fe-S groups, whereas the extremely oxidizing $HO^•$ can damage all major groups of biomolecules. The relatively stable, non-charged H_2O_2 can diffuse through biological membranes causing damages to Fe-S proteins (Breitenbach *et al.*, 2015; Daly, 2009; Sato *et al.*, 2009). Thioredoxin functions as oxidoreductase, which acts as electron donor for the thioredoxin peroxidase, comparable to glutathione (Sato *et al.*, 2009; Thön *et al.*, 2007). The glutathione system is the major cellular oxidative stress defence system (Bakti *et al.*, 2017; Breitenbach *et al.*, 2015). The glutathione peroxidase is an electron donor while reducing H_2O_2 to H_2O (Breitenbach *et al.*, 2015; Meister and Anderson, 1983; Sato *et al.*, 2009). Menadione generates O_2^- and is suggested to affect the reduced glutathione (GSH) pool by a detoxification reaction catalysed by glutathione *S*-transferase (Pócsi *et al.*, 2004). Ascomycetes can actively regulate the elimination of ROS by e.g. catalases that act as ROS scavengers (Green and Johnson, 2004; Paris, Wysong, *et al.*, 2003; Pöggeler *et al.*, 2018). During host invasion *A. fumigatus* has to scope with host-specific ROS of the innate immune system. In this context it was examined that the protein AfBIR1 acts as inhibitor of the fungal caspase activity, which is controlled by conidial susceptibility to NADPH oxidase-dependent killing (Shlezinger *et al.*, 2017).

Besides, it has been shown that *A. fumigatus* Fbx15 is required for the fungal tolerance against oxidative stress resulting in a diminished growth ability in absence of *fbx15*. On molecular level Fbx15 is required for the downregulation of the catalase associated gene *cat1*. Moreover, *fbx15* gene expression and Fbx15 protein amounts are increased in presence of H_2O_2 (Jöhnk *et al.*, 2016). In *S. cerevisiae* the intrinsically instable F-box protein Pof14 is required for oxidative stress response induced by H_2O_2 in a SCF^{Pof14}-

independent manner (Tafforeau *et al.*, 2006). Most recently, it was investigated that the *Magnaporthe oryzae* F-box protein gene MoFWD1 is required for oxidative stress release during conidial germination (Shi *et al.*, 2019).

3.2.2 F-box proteins are involved in secondary metabolite homeostasis in Aspergilli

Fungi produce a wide range of natural products such as the spore- and fruiting body-containing pigment melanin (Kimura and Tsuge, 1993; Rambach *et al.*, 2015; Schmaler-Ripcke *et al.*, 2009). These natural products can be subdivided in essential (primary metabolites) and non-essential (secondary metabolites) natural products. Secondary metabolite genes occur in clusters contrary to the primary metabolite genes that are scattered in the whole genome (Keller *et al.*, 2005; Malik, 1980). A wide range of structurally heterogenous secondary metabolites with high interest to research, medicine and biotechnology are produced by *Aspergillus* spp. (Singh *et al.*, 2016; Yoon *et al.*, 2013). Synthesis of the secondary metabolites is performed in two steps: the core backbone is processed either by a polyketide synthase (PKS) which can be divided into non-reducing PKS and highly-reducing PKS, a non-ribosomal peptide synthetase (NRPS), a PKS–NRPS hybrid, a dimethylallyl tryptophan synthase (DMATS) or a terpene cyclase (TC) . The carbon skeleton is diversified by enzymes, which genes are usually clustered with the secondary metabolites core backbone gene (Fischbach and Walsh, 2006). Under standard laboratory growth secondary metabolites are usually repressed in filamentous fungi because secondary metabolite production is likely triggered under specific circumstances, e.g. to adapt to changed environmental conditions (Bode *et al.*, 2002; Gerke and Braus, 2014). Some pathogenic Aspergilli produce useful secondary metabolites for biotechnology industry like citric acid, enzymes and therapeutically relevant secondary metabolites as antimicrobial aurasperone A of *A. niger* (Schuster *et al.*, 2002; Shaaban *et al.*, 2012). So far, for the *Aspergillus* spp. members *A. nidulans*, *A. fumigatus*, *A. niger* and *A. terreus* several secondary metabolite-linked enzymes were identified. Of 66 core synthase genes for secondary metabolite production 29 were verified to secondary metabolite production in *A. nidulans*. In comparison, 19 out of 44 identified genes were linked to secondary metabolite production in *A. fumigatus*. In *A. niger* only 14 out of 99 total identified genes were linked to secondary metabolite production and in *A. terreus* 20 out of 74 genes (Table 1) (Romsdahl and Wang, 2019).

Table 1: Status of linked *Aspergillus* secondary metabolite core synthase genes to downstream products. PKS = Polyketide synthase, NRPS = Non-ribosomal peptide synthetase, Hybrid = Mixture of PKS and NRPS, DMATS = Dimethylallyl tryptophan synthase, TC = Terpene cyclase, SM = Secondary metabolite (Romsdahl and Wang, 2019).

	A. nidulans		***A. fumigatus***		***A. niger***		***A. terreus***	
	Linked	**Total**	**Linked**	**Total**	**Linked**	**Total**	**Linked**	**Total**
PKS	16	33	6	16	8	46	9	29
NRPS	11	25	9	18	4	35	9	36
Hybrid	1	1	1	2	2	9	1	1
DMATS	0	5	2	3	0	2	0	5
TC	1	2	1	1	0	7	1	3
SM	29	66	19	40	14	99	20	74

Fbx15 of *A. fumigatus* and *A. nidulans* control the secondary metabolite homeostasis as the absence of *fbx15* results in an orange (*A. fumigatus*) or dark reddish (*A. nidulans*) pigmented colony during asexual development, which is presumably due to the regulation of so far unidentified or uncharacterised secondary metabolites (Jöhnk *et al.*, 2016; von Zeska Kress *et al.*, 2012).

Previous studies have confirmed that secondary metabolism is directly linked to asexual and sexual development (Bayram *et al.*, 2008; Elramli *et al.*, 2019; Zhou *et al.*, 2019). For instance, the global regulator, regulation of secondary metabolism and development (RsdA), regulates secondary metabolism accompanied by the repression of asexual development (Zhou *et al.*, 2019). Also, the assembly of a heptameric striatin-interacting phosphatase and kinase (STRIPAK) complex is required for the coordination of light-dependent fungal development with secondary metabolism in *A. nidulans* (Elramli *et al.*, 2019). Thereby, the STRIPAK complex is involved in the proper expression of the VeA-VelB-LaeA complex, which is required to coordinate secondary metabolism such as the production of the mycotoxin sterigmatocystein and fungal development (Bayram and Braus, 2012; Elramli *et al.*, 2019).

Some secondary metabolites produced by fungi have toxic features. The secondary metabolite gliotoxin is an intensively studied mycotoxin in *A. fumigatus*. The *gli*-cluster consists of 13 genes (Figure 7) (Gardiner and Howlett, 2005; Schrettl *et al.*, 2010). Gliotoxin has antioxidant properties by promoting the degradation and recycling of GSH and is considered to be directly linked to virulence (Gallagher *et al.*, 2012; Kwon-Chung and Sugui, 2009; Owens *et al.*, 2014; Scharf *et al.*, 2012). However, various studies on gliotoxin in context to virulence revealed contradictory findings. Gliotoxin was described as virulence factor in a non-neutropenic mouse model as tested with the *gliP* mutant (Sugui *et al.*, 2007). Thereby, it was discovered that gliotoxin impairs the function of neutrophils

by inhibiting the formation of neutrophil-recruiting leukotriene A_4 hydrolase (König *et al.*, 2019). However, in neutropenic mice no altered pathogenicity in *A. fumigatus* lacking gliotoxin synthesis by *gliP* deletion was observable (Spikes *et al.*, 2008; Kupfahl *et al.*, 2006).

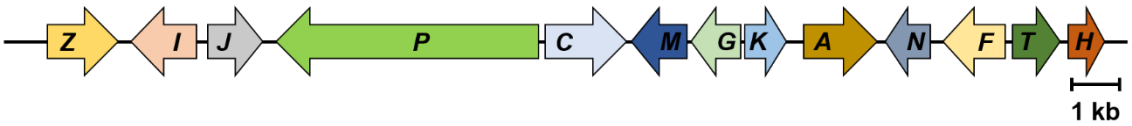

Figure 6: Structure of the *gli*-cluster genes in *A. fumigatus*. Gliotoxin biosynthesis is encoded by the 13 *gli*-cluster genes (in colour and labelled with their last letter), that are located at chromosome 6. Modified from Dolan *et al.*, 2015.

The gene product of *gliZ* is a Zn_2Cys_6 finger binuclear transcription factor, which is required for the induction of gliotoxin production and its regulation (Bok *et al.*, 2006; Kwon-Chung and Sugui, 2009; Scharf *et al.*, 2012). Lacking *gliZ* gene expression results in a block of all other gliotoxin cluster genes except *gliT*. The bioactivity of gliotoxin is controlled by the multimodular NRPS GliP (Balibar and Walsh, 2006). Upstream regulation of the gliotoxin gene cluster is performed by transcription factors like VeA or MtfA and the methyltransferase LaeA, known as global secondary metabolite regulators (Dhingra *et al.*, 2012; Perrin *et al.*, 2007; Schoberle *et al.*, 2014; Smith and Calvo, 2014).
Fbx15 is required for the downregulation of *gli*-cluster genes such as *gliP* and *gliZ*, which encoding products are essential for the biosynthesis of the mycotoxin gliotoxin (Gardiner and Howlett, 2005; Jöhnk *et al.*, 2016). Moreover, mimicking dephosphorylation of Fbx15 at S468 and S469 by exchanging Ser to Ala also promotes the induction of *gli*-gene expression but does not influence the gliotoxin biosynthesis (Jöhnk *et al.*, 2016).

3.3 Transcriptional regulators as (potential) interaction partners of *A. fumigatus* Fbx15

Putative interacting proteins for *A. fumigatus* Fbx15 were identified by Tandem-Affinity Chromatography Purification (TAP). Next to the subunits of the SCF^{Fbx15} complex, nuclear proteins, proteins with functions in transcriptional regulation, RNA processing, signal transduction, metabolism, fungal morphology, as well as three proteins of unknown function were identified, in total 38 proteins (Table 2) (Jöhnk *et al.*, 2016).

Table 2: Fbx15 putative interacting proteins - co-purified proteins with Fbx15 identified by TAP analysis in *A. fumigatus*. *S. cerevisiae* homologous proteins with a known function are given in brackets. Co-purified with Fbx15: Putative interacting proteins with Fbx15 had to appear at least twice in two independent Fbx15-purifications. Already used proteins for analysing the interaction with Fbx15 are shaded in grey. Putative Fbx15-interacting transcription factors are shaded in blue. Modified from Jöhnk *et al*., 2016.

***A. fumigatus* Fbx15 co-purified proteins**	**Protein description**
SCF-subunits & related proteins	
AFUA_1G12960 (CulA)	SCF ubiquitin ligase subunit
AFUA_5G06060 (SkpA)	SCF ubiquitin ligase subunit
AFUA_4G10350 (UbiD)	Polyubiquitin
AFUA_4G10780 (Tom1)	ubiquitin-protein ligase
AFUA_8G05500 (CsnD)	COP9 signalosome subunit
AFUA_5G07260 (CsnF)	COP9 signalosome subunit
AFUA_4G12630 (CsnG)	COP9 signalosome subunit
Transcription factors & nuclear proteins	
AFUA_3G09670 (OefC)	C6 transcription factor
AFUA_4G03460 (SrbB)	bHLH transcription factor, involved in hypoxia and virulence
AFUA_4G08930	Putative nucleolar GTPase (Nog2p)
AFUA_2G11840 (SsnF)	Transcriptional corepressor (Ssn6p)
AFUA_6G05150 (RcoA)	Transcriptional corepressor (Tup1p)
AFUA_5G11390	APSES transcription factor, putative
AFUA_2G06140	uracil DNA N-glycosylase activity, DNA repair
AFUA_5G07890	single-stranded DNA binding protein (Rim1p)
RNA processing	
AFUA_3G06440	Splicing factor with U2 snRNP localisation (Prp21p)
AFUA_5G04420	Splicing factor with U2 snRNP localisation (Cus1p)
AFUA_6G08610	RNA trimethyl guanosine synthase, role in 7-methylguanosine cap hypermethylation (Tgs1p)
AFUA_5G09670	RNase III domain protein
AFUA_7G05810	Putative ribonucleoprotein, nucleic acid binding (Mrd1p)
Ribosomal proteins	
AFUA_1G05990	60S ribosomal protein (Rpl16Ap)
AFUA_2G04130	40S ribosomal protein (Rps11A)
AFUA_2G01830	Protein with putative ribosomal activity
Signal-transduction	
AFUA_1G11730 (ArfA)	GTPase activity, role in ER/Golgi transport
AFUA_2G07600	GTP binding, signal recognition activity
AFUA_6G07980 (NimX)	Cyclin-dependent serine/threonine kinase
AFUA_6G06750	14-3-3 family protein; predicted gene pair with ArtA
Metabolic enzymes	
AFUA_1G12800	Putative NADPH isocitrate dehydrogenase (Idh2p)
AFUA_2G04520	Protein with metal ion binding domains, oxidoreductase activity (Adh4p)
AFUA_2G10920 (EchA)	Putative enoyl-CoA hydratase/isomerase family protein, role in beta oxidation of fatty acids
AFUA_3G08660 (IdpA)	Putative isocitrate dehydrogenase
AFUA_6G10660 (AclA)	Putative ATP citrate lyase subunit
AFUA_3G11070 (PdaC)	Putative pyruvate decarboxylase
Fungal morphology	
AFUA_4G08770	Protein with putative microtubule binding activity
AFUA_5G03080 (AspC)	Septin, role in cell polarity and hyphal growth
Unknown function	
AFUA_1G09610	Conserved hypothetical protein
AFUA_3G13930	Conserved hypothetical protein

Interactions with *A. fumigatus* Fbx15 were analysed with the Ser/threonine (Thr) kinase NimX and the transcriptional co-repressor subunit SsnF (Table 2, grey). A cytoplasmic interaction of *A. fumigatus* Fbx15 with NimX was investigated considering to trigger Fbx15 phosphorylation (Jöhnk *et al.*, 2016).

Three transcription factors were found to be potential interaction partners of *A. fumigatus* Fbx15: OefC (overexpressed fluffy C), SrbB and the putative APSES transcriptional regulator AFUA_5G11390 (later called FiAt (Fbx15-interacting putative APSES transcription factor)) (Table 2, blue shaded). The regulation of the cellular localisation by transcriptional regulators is essential to cope with environmental changes or internal constitutions. In general, transcription factors regulate gene transcription through binding to DNA motifs or other transcriptional regulators as monomers or in a complex to control gene expression, either positively or negatively (Goodbourn and R., 1990; Horikoshi *et al.*, 1988; Levine and Manley, 1989; Ptashne, 1988; Sigler, 1988; Xiong *et al.*, 2019). In *A. fumigatus* transcriptional regulation is mandatory during adaptation to environmental changes and in virulence mechanisms (Bahn, 2015). 6.19% (618/9.981) from annotated genes in *A. fumigatus* genome are specific for DNA binding. Similar proportions are predicted in other fungi like *A. nidulans* FGSC A4 with 5.95% (651/10.931), *A. oryzae* RIB40 with 4.10% (499/12.164) or *S. cerevisiae* with 4.06% (281/6.918) (Bultman *et al.*, 2017).

3.3.1 Nuclear localisation of the co-repressor subunit SsnF is mediated by Fbx15 in *A. fumigatus*

The interaction of *A. fumigatus* Fbx15 with SsnF was analysed in more detail (Jöhnk *et al.*, 2016). SsnF or Ssn6 in *Saccharomyces cerevisiae* represents a co-repressor subunit forming a complex with homo-tetramers of Tup1 (Gounalaki *et al.*, 2000; Palaiomylitou *et al.*, 2008). During transcriptional repression SsnF/Ssn6 functions as an adaptor between the specific DNA-binding proteins and the Tup1 tetramer, whereas Tup1 comprises the repressive function of the co-repressor complex (García-Sánchez *et al.*, 2005; Liu and Karmarkar, 2008; Tzamarias and Struhl, 1994). Remarkable, the Tup1-Ssn6 complex belongs to the conserved orthologous protein groups OG5_128428 and OG5_131310 in fungi and represses approx. 3 to 5% of the whole yeast genome (http://orthomcl.org) (DeRisi *et al.*, 1997; Li *et al.*, 2003; Parnell and Stillman, 2011).

The wide range of gene regulation is due to its property not to bind directly to DNA but to other DNA-binding proteins, demonstrating its flexibility in respect to target a variety of proteins (Hanlon *et al.*, 2011; Roy *et al.*, 2013). For instance, the *S. cerevisiae* TupA-Ssn6 co-repressor complex is needed to position nucleosomes across the entire coding

sequence of the DNA damage-inducible gene *RNR3* together with Imitation SWItch (ISWI) chromatin remodelling factors (Zhang and Reese, 2004). Moreover, the *FLO1* gene, whose gene product is responsible for cell-cell adhesion during *S. cerevisiae* flocculation in terms of survival under adverse conditions, is repressed by the TupA-SsnF complex during nutrient rich conditions (Church *et al.*, 2017; Teunissen *et al.*, 1995; Verstrepen and Fink, 2009). Most recently, a TupA-independent network of *S. cerevisiae* SsnF with other transcriptional regulators was elucidated in copper homeostasis by the regulating the *CTR1* gene, which encodes the Ctr1 copper transporter (Dancis *et al.*, 1994; Voutsina *et al.*, 2019). SsnF represses *CTR1* gene expression in dependency of the transcriptional activator Mac1 (Jungmann *et al.*, 1993; Voutsina *et al.*, 2019). Moreover, SsnF interacts physically and genetically with the transcriptional repressor Hir1, a histone chaperon, resulting in an inactivation of Hir1 transcription if *CTR1* gene expression is repressed (Amin *et al.*, 2013; Voutsina *et al.*, 2019). Comparable co-repressor systems are existing in mammals. For instance, a well-studied physiological relevant co-regulator complex is the NR-co-repressor complex, which includes 6 subunits. The complex is required to coordinate the metabolism in hepatocytes (Liang *et al.*, 2019).

The Fbx15-interacting protein SsnF has essential functions in *A. fumigatus* and is transported through the nuclear core membrane in dependency of Fbx15 and its phosphorylation status at S469 and S468. The phosphorylation status is presumably controlled by the essential NimX kinase and GlcA phosphatase. It is assumed that On the one hand, mimicking dephosphorylation of Fbx15 at S468 and S469 results in a nuclear clearance of SsnF during vegetative growth. The physical interaction of Fbx15 and SsnF is thereby shifted to the nucleus. On the other hand, mimicking phosphorylation at the most likely phosphorylated S469 through replacing the Ser residue with asparagine residue results in an accumulation of SsnF in the nucleus during oxidative stress conditions (Figure 7) (Jöhnk *et al.*, 2016).

SsnF is located in the nucleus and suggested to be transported to the nuclear envelop in a Fbx15-dependent manner during oxidative stress in *A. fumigatus* (Jöhnk *et al.*, 2016). The molecular traffic through the nuclear core is essential for many cellular processes in all multicellular organisms and is mediated either passive through diffusion or active transport coupled with energy consumption (Görlich and Kutay, 2002; Mattaj and Englmeier, 1998; Nakielny and Dreyfuss, 1999). NLS-containing proteins like *A. fumigatus* Fbx15 are associated with an active nuclear transport mechanism through the nuclear pore complex (NPC) contrary to passive diffusion, which is achieved for molecules with a size up to 110 kilodalton (kDa) (Jöhnk *et al.*, 2016; Lange *et al.*, 2007; Wang and Brattain, 2007). Classical NLS sequences are categorised into two subgroups: monopartite (mp) NLS consist of single stretches of basic aa and bipartite (bip) NLSs consisting of two

stretches of basic aa separated by a linker region (Dingwall and Laskey, 1991; Kalderon *et al.*, 1984; Robbins *et al.*, 1991).

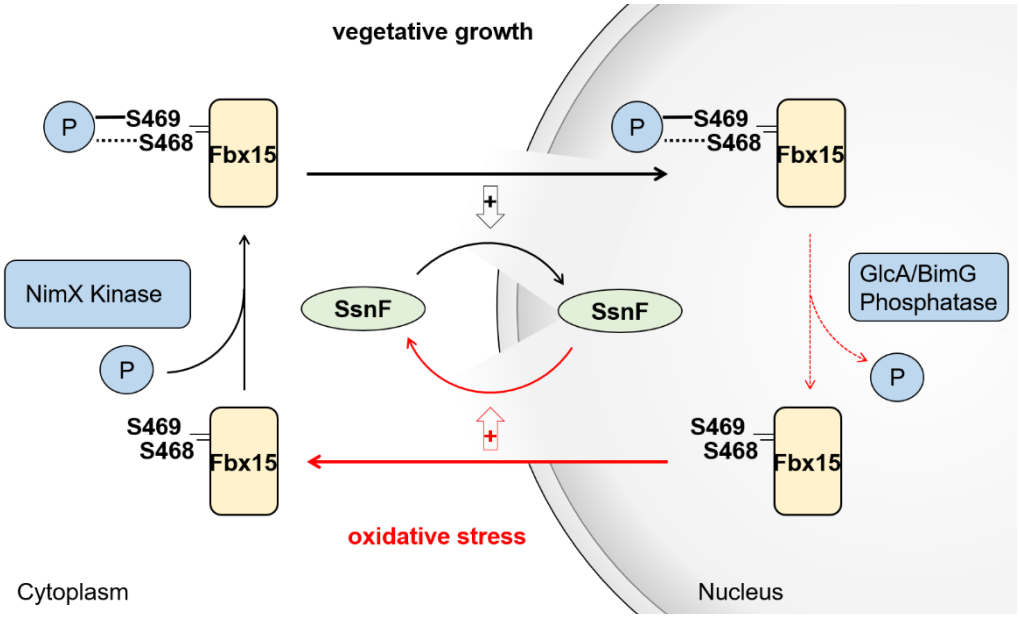

Figure 7: **Simplified model of SsnF shuttle mechanism through the nuclear membrane depending of *A. fumigatus* Fbx15.** SsnF gets transferred into the nucleus during vegetative growth when Fbx15 is phosphorylated most likely at S469 prior to S468, which is presumably driven by the NimX kinase in the cytoplasm. Upon oxidative stress conditions SsnF and Fbx15 RE shuttled outside the nucleus whereby SsnF is transported to the nuclear envelop depending on dephosphorylated Fbx15 at S468|9. Dephosphorylation of Fbx15 is presumably triggered by the GlcA/BimG phosphatase. Modified from Jöhnk *et al.*, 2016.

Most of the active nuclear import is driven by importin ß-related transport receptors which are constantly circulating between the nucleus and cytoplasm. Recognized cargo molecules are guided through NPCs whereby a physical interaction between the receptors and the NPCs is formed. This nuclear trafficking mechanism is regulated by a RanGTP gradient, in which low concentrations are present in the cytoplasm and high concentrations in the nucleus (Görlich *et al.*, 1996; Mattaj and Englmeier, 1998). Release of cargo molecules in the nucleus is triggered by RanGTP binding (Chi *et al.*, 1996; Rexach and Blobel, 1995). In contrast to nuclear import where importins are involved, the nuclear export is mediated by exportins that bind cargo molecules at high RanGTP concentrations in the nucleus (Fornerod *et al.*, 1997; Kutay *et al.*, 1997). Cargo proteins consisting of nuclear export signals (NESs) are bound to an exportin and guided through the NPC outside the nucleus (Fridell *et al.*, 2002; Murphy and Wente, 1996; Nakielny and Dreyfuss, 1999; Wen *et al.*, 1995). Exported cargos are released from the cargo-exportin-RanGTP complex by GTP hydrolysis, whereby Ran is removed from exportin (Bischoff and Görlich, 1997; Görlich *et al.*, 1997; Kutay *et al.*, 1997). A higher concentration of RanGTP in the

nucleus is ensured by RanGDP nuclear import by nuclear transport factor 2 (NTF2) and followed by a RanGEF-mediated re-charging of Ran with GTP (Figure 8) (Bauer *et al.*, 2015; Bischoff and Ponstingl, 1991; Ribbeck *et al.*, 1998; Smith *et al.*, 2004). Noteworthy, in the *A. fumigatus* Fbx15 protein sequence no NES sequences were identified (Jöhnk *et al.*, 2016).

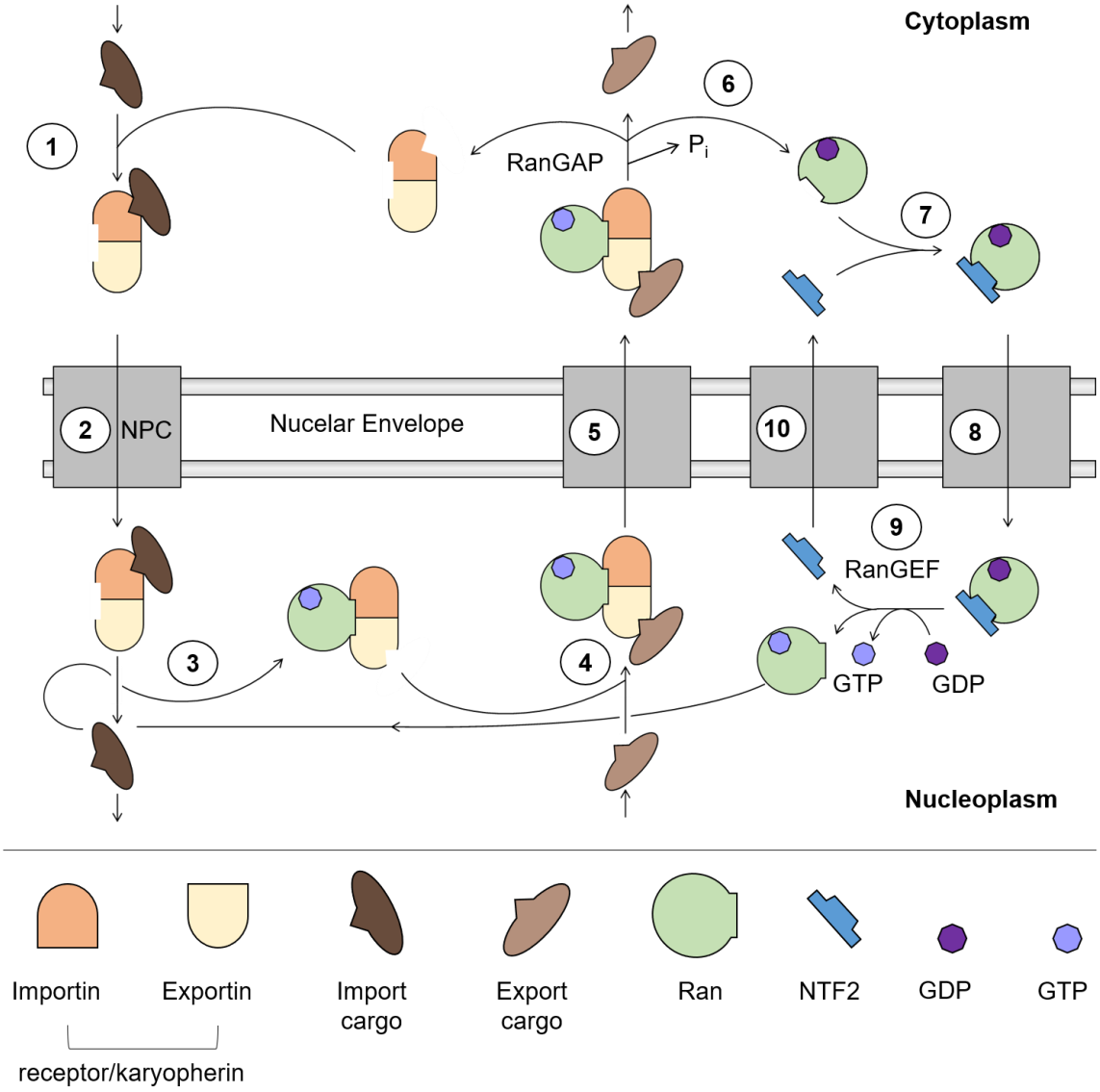

Figure 8: Model of the nuclear transport cycle. (**1**) Import cargo binds to transport receptor/karyopherin in the cytoplasm and (**2**) moves through the nuclear pore complex (NPC) into the nucleus. There, (**3**) Ran-GTP binds to the karyopherin resulting in the release of the imported cargo. (**4**) Export cargo binds to karyopherin-Ran-GTP complex, which (**5**) transits through the NPC into the cytoplasm. (**6**) RanGAP triggers the conversion of Ran-GTP to Ran-GDP resulting in the dissociation of the karyopherin from Ran and export cargo. Recovering nuclear pools of Ran-GTP is mediated by (**7**) Ran-GDP, which binds to the non-karyopherin transport receptor NTF2, and (**8**) moves into the nucleus, where (**9**) RanGEF triggers the conversion of Ran-GDP to Ran-GTP. NTF2 is released and (**10**) moves back into the cytoplasm. Modified from Bauer *et al.*, 2015.

Nuclear traffic can be regulated by e.g. masking or posttranslational modifications of NLS sequences (Poon and Jans, 2005). NLS sequences can be masked and unmasked intra – or intermolecular in order to control nuclear import as shown for the intramolecular masking of the p105 NLS, which gets unmasked upon the immune response through specific phosphorylation and degradation of the proteins C-terminus (Henkel *et al.*, 1992; Poon and Jans, 2005; Rivière *et al.*, 1991). Intermolecular masking is caused by the binding to an additional protein which shields the NLS of the corresponding protein and thereby controls its nuclear import as shown for the inhibitor of κB. The inhibitor masks the NLS of the transcriptional regulator NF-κB and shields the protein from nuclear import when NF-κB has to be inactivated (Beg *et al.*, 1992; Ganchi *et al.*, 1992; McLane and Corbett, 2009; Zabel *et al.*, 1993). Another regulation of the nuclear import is obtained by a covalent modification through phosphorylation as known for *S. cerevisiae* Gln3p. *S. cerevisiae* Gln3p is a transcription factor, whose activity is dependent on the quality of nitrogen and carbon sources. Cytoplasmic abundance of phosphorylated Gln3p is given in case of nitrogen sources such as glutamine. Whereas Gln3p is transferred into the nucleus via karyopherin α/Srp1p in a dephosphorylated version during nitrogen starvation or nonpreferred nitrogen sources. The phosphorylation status of Gln3p is hereby controlled by TOR1 and TOR2 (Beck and Hall, 1999; Bertram *et al.*, 2000; Carvalho and Zheng, 2003).

3.3.2 Several (putative) transcription factors are potential interaction partners of *A. fumigatus* Fbx15

The overexpressed fluffy C (OefC) zinc binuclear transcription factor, SrbB as transcription factor of the sterol regulatory element binding protein family (SREBP) and the putative APSES transcription factor FiAt are potential interaction partner of *A. fumigatus* Fbx15 (Figure 9) (Jöhnk *et al.*, 2016).

OefC was primarily described in *A. nidulans* due to a screening of growth- or development-related genes. Multiple copies of OefC under the *niiA*-promoter result in “fluffy” hyphae formation with aerial hyphae production independent of the promoter induction (Lee *et al.*, 2005). *A. fumigatus* OefC is 669 aa long and contains a well-conserved $Zn(II)_2Cys_6$ binuclear cluster domain (Figure 9A). The $Zn(II)_2Cys_6$ binuclear cluster domain comprises a zinc finger motif as part of a DNA-binding domain (DBD), in which six cysteine residues are bound to two zinc atoms uniquely in this type of transcription factors (Lohr *et al.*, 1995; Todd and Andrianopoulos, 1997). OefC contains a middle homologous region (MHR) at its C-terminus (Figure 9A). MHRs are thought to act as regulators of the protein activity (MacPherson *et al.*, 2006; Schjerling and Holmberg, 1996). The functions of zinc cluster

transcription factors vary from transcriptional regulation to other physiological roles, including mediating chromatin remodelling, lipid binding, protein chaperoning, protein-protein interactions, and zinc sensing (Laity *et al.*, 2001). In pathogenic fungi such as *A. fumigatus* and *Candida albicans* zinc cluster transcription factors are known to be involved in virulence and pathogenicity (Issi *et al.*, 2017; Rybak *et al.*, 2017; Vandeputte *et al.*, 2011).

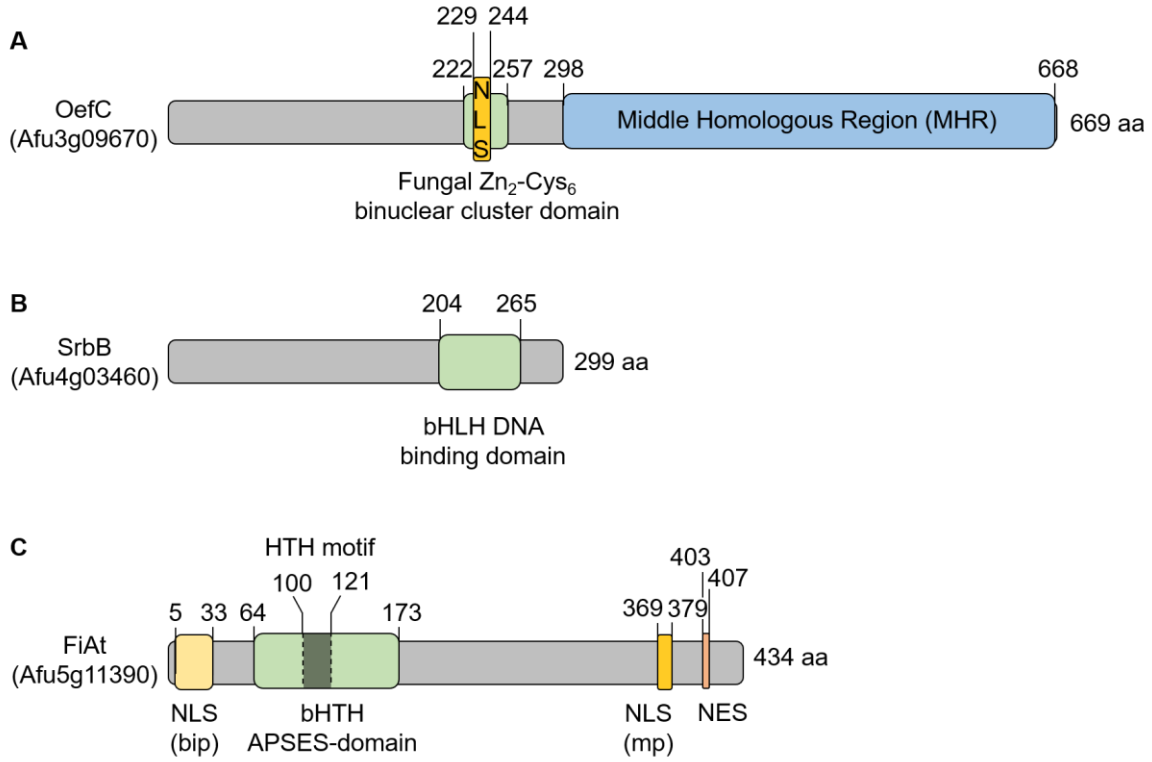

Figure 9: Domain architecture of the transcriptional regulator OefC and SrbB, and the putative transcription factor FiAt in *A. fumigatus*. (**A**) The zinc cluster transcription factor OefC (overexpressed fluffy C) with a protein length of 669 amino acid (aa) contains a fungus-specific zinc binuclear cluster domain (green), which consists of two zinc and two cysteine molecules (Zn_2Cyc_6) at aa position 222 to 257. A monopartite nuclear localisation signal (mp NLS, dark yellow) is present at aa 229 to 244. A middle homologous region (MHR, blue) is present at aa 298 to 668. Modified from Lee *et al.*, 2005. (**B**) The SREBP transcription factor SrbB with a protein length of 299 aa contains a basic helix-loop-helix (bHLH, green) DNA binding domain at aa 204 to 265. Modified from Chung *et al.*, 2014. (**C**) The uncharacterized putative transcription factor FiAt (Fbx15 interacting APSES transcription factor) consists of an ASPES-typical included helix-turn-helix (HTH, green) domain at aa position 64 to 173 with inside a HTH DNA-binding motif at aa 100 to 121 (dark green) (Jöhnk *et al.*, 2016) (https://prosite.expasy.org/scanprosite/). At the N-terminus a putative bipartite (bip) NLS at aa position 5 to 33 (light yellow) was identified. At the C-terminus a mp NLS at aa position 369 to 379 (dark yellow), as well as a nuclear export signal (NES, orange) at aa position 403 to 407 were identified with the cNLS Mapper program (http://nls-mapper.iab.keio.ac.jp/cgi-bin/NLS_Mapper_form.cgi) and the NetNES 1.1 Server program (http://www.cbs.dtu.dk/services/NetNES/).

The 299 aa long transcription factor SrbB has a characteristic basic helix-loop-helix (bHLH) domain with a canonical tyrosine residue at its C-terminus and is conserved among the

Aspergillus family (Figure 9B) (Bien and Espenshade, 2010; Hua *et al.*, 1993; Yokoyama *et al.*, 1993). *A. fumigatus* SrbB was initially identified in CHIP-seq analysis of SrbA, another member of the SREBP family. SrbB is not membrane bound and needs regulated intramembrane proteolysis for activation contrary to SrbA (Chung *et al.*, 2014). It has been shown that the abundance of the *srbB* transcript is regulated by SrbA and *vice versa*. SrbB regulates together with SrbA genes involved in heme biosynthesis and demethylation of C4-sterols upon hypoxia. Independent of SrbA, SrbB is involved in regulating of the carbohydrate metabolism, hypoxia adaptation and virulence (Chung *et al.*, 2014). In several pathogenic fungi SrbB was reported to have an impact on the fungal fitness in response to hypoxia such as *A. fumigatus*, *Cryptococcus neoformans* and *Paracoccidioides brasiliensis* (Willger *et al.*, 2008).

The putative APSES (Asm1p, Phd1p, Sok2p, Efg1p and StuAp) transcription factor FiAt is 434 aa long and contains a basic helix-turn-helix (bHTH) APSES domain with inside a HTH motif, a bip NLS, a mp NLS and a NES (Figure 9C). In general APSES domain-containing proteins represent transcriptional regulators solely present in fungi that share a highly conserved bHLH DNA-binding motif (Aramayo *et al.*, 1996). APSES transcription factors are involved in fungal development such as sporulation, secondary metabolism and pathogenicity (LeeJ. Y. *et al.*, 2013; Yao *et al.*, 2017; Zhao *et al.*, 2014). An already functional analysed APSES transcription factor in *A. fumigatus* is StuA. *A. fumigatus* StuA positively regulates conidiophore development, ergot alkaloid production and is involved in virulence by regulating gene *uge3* encoding for the uridine diphosphate-glucose-epimerase, which is crucial for adherence by mediating the galactosaminogalactan biosynthesis (Gravelat *et al.*, 2013; Sheppard *et al.*, 2005). StuA itself is transcriptional regulated by the SREBP transcription factor SrbA (Willger *et al.*, 2008). Most fungi contain five ASPES proteins. Nonetheless, *Cyrptococcus neoformans* possess only two APSES proteins and *Saccharomyces cerevisiae* six APSES proteins (Zhao *et al.*, 2014). Maturation of ascospores and conidiophores is mediated by Asm1 in *Neurospora crassa* and by StuA in *A. nidulans* (Aramayo *et al.*, 1996; Dutton *et al.*, 1997). The impact on virulence for APSES transcription factors has been shown in *Candida albicans* and *A. flavus*. *Candida albicans* Efg1p is needed for host cell invasion and virulence of disseminated in mice and oral candidiasis next to its function in mating and yeast-to-hypha transition and normal adherence (Doedt *et al.*, 2004; Lo *et al.*, 1997; Park *et al.*, 2005; Sonneborn *et al.*, 1999; Sonneborn *et al.*, 1999; Stoldt *et al.*, 1997). *A. flavus* AfRafA and AfStuA play a central role in fungal development, mycotoxin synthesis including aflatoxin and cyclopiazonic acid and pathogenicity (Yao *et al.*, 2017).

3.3.3 The putative C-terminal part of a F-type ATPase F-subunit FidA as potential interaction partner of Fbx15 in *A. fumigatus*

The protein Afu2G05520 was identified as putative interaction partner of *A. fumigatus* Fbx15 out of 66 total candidates (Table S1). This protein is the putative C-terminal part of an F-type ATPase, later on called FidA (Fbx15-interacting developmental protein A), was identified as the C-terminal part of a F-type ATPase F-subunit in *Penicillium expansum* (gene XP_016595530.1) (Figure 10) (Ballester *et al.*, 2015). This C-terminal part is separated from the N-terminal part in *A. fumigatus* (F-domain: Afu2G05510, FidA: Afu2g05520) (Figure 10).

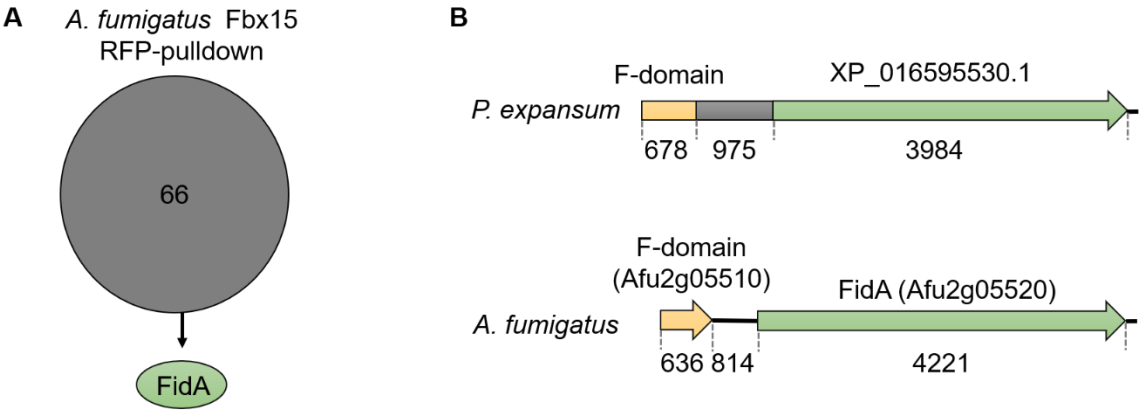

Figure 10: FidA as putative C-terminal part of a F-type ATPase F-subunit is a putative interacting protein of the *A. fumigatus* Fbx15 protein. (**A**) The Fbx15-interacting developmental protein A (FidA) was identified as an uncharacterized, putative interacting protein of Fbx15 out of 66 candidates in *A. fumigatus* from RFP-pulldowns. Data were obtained from LCMS-analysis (see for details Table S1). (**B**) Analysis of sequential composition of FidA. Sizes are indicated in bp. FidA is a potential F-domain-consisting ATPase. The F-domain (yellow) is separated from FidA (green) in *A. fumigatus* (Afu2g05520). In *Penicillium expansum* the orthologue XP_01659553 is composite of FidA together with the corresponding F-domain. Alignments were performed with NCBI-BLAST (https://blast.ncbi.nlm.nih.gov/Blast.cgi?PAGE=Proteins).

Many cellular processes like the UPS or active nuclear traffic consume energy (Bos *et al.*, 2007; Glickman and Ciechanover, 2002). The most common form of intracellular energy carriers is ATP, which is also referred as 'molecular unit of currency' (Knowles, 2003). Depending on the need in metabolic processes ATP can be interconverted into adenosine diphosphate (ADP) or adenosine monophosphate (AMP) in terms of energy consumption (Alberts *et al.*, 2014). ATP synthases (ATPases) hydrolyses ATP to ADP and a free phosphate ion or syntheses ATP out of ADP and free phosphate in a condensate reaction (von Ballmoos *et al.*, 2009; Igamberdiev and Kleczkowski, 2015; Junge and Nelson, 2015; Walker, 2013). ATPases can be subdivided in five classes: F-, V-, A-, P-, N- and E-ATPases. All ATPases are found in eukaryotes except N-type and A-ATPase. N-type ATPases act as F-type ATPases in bacteria whereas A-type ATPases are solely present

in Archaea, also acting like F-type ATPases (Dibrova *et al.*, 2010; Müller *et al.*, 2006; Steinert *et al.*, 1997). In eukaryotic cells most cellular processes are driven by the hydrolysis of ATP in mitochondria by F-type ATPases (von Ballmoos *et al.*, 2009; Junge and Nelson, 2015; Walker, 2013). F-type proton-translocating ATPases are transmembrane-bound protein channels required to synthesize ATP by oxidative phosphorylation. This mechanism is coupled with an electrochemical proton gradient, which is established by an electron transfer chain (Futai *et al.*, 1989, 2000, 2005; Pedersen and Carafoli, 1987).

4 Aim of this study

F-box proteins are substrate adaptors of SCF E3 ubiquitin RING ligases, which target proteins that should be ubiquitinated (Schmidt *et al.*, 2009). F-box proteins were shown to have an influence on multicellular developmental processes and secondary metabolism in *A. nidulans,* among them Fbx15 that is conserved in *A. fumigatus* (Jöhnk *et al.*, 2016; von Zeska Kress *et al.*, 2012). The F-box protein Fbx15 was first identified in *A. nidulans* with a crucial role in asexual and sexual development as well as secondary metabolite homeostasis (von Zeska Kress *et al.*, 2012). *A. nidulans* Fbx15 is to 60% identical to its homolog in *A. fumigatus* (Jöhnk *et al.*, 2016). *A. fumigatus* Fbx15 is essential for the regulation of secondary metabolism, stress response, virulence and was identified as putative shuttle protein for the nuclear localisation of the co-repressor subunit SsnF. Cellular localisation of the co-repressor subunit SsnF is ensured by the presence of *A. fumigatus* Fbx15 depending on the phosphorylation status at the putative phosphorylation residues S468 and S469. The absence of *A. fumigatus* Fbx15 activity results in a complete loss of virulence in mice as well as the regulation of the pathogenicity-associated mycotoxin gliotoxin is mediated by *A. fumigatus* Fbx15 (Jöhnk *et al.*, 2016).
In the first part of this study the stress response-mediating *A. fumigatus* Fbx15 and the development-mediating *A. nidulans* Fbx15 were analysed if they functionally replace each other due to secondary metabolism, stress adaptation and asexual and sexual development as they show structural similarities. Therefore, *A. fumigatus* Fbx15 was integrated in *A. nidulans* and *vice versa* and analysed due to their phenotypes without and with stress detergents. Furthermore, putative interaction partners of Fbx15 were analysed according their local physical interaction via bimolecular fluorescence complementation (BiFC) and the putative interplay in regulatory processes in *A. fumigatus* and/or *A. nidulans* by phenotypical assays without and/or with stress detergents, virulence tests in the *Galleria mellonella* larvae infection assay, localisation determination in dependency of the presence of Fbx15 and/or by aligning their secondary metabolite profiles.

In the second part it was analysed whether *A. fumigatus* Fbx15-dependent regulation in gliotoxin biosynthesis was examined in context to *A. fumigatus* Fbx15-mediated stress response and virulence by deleting *gliP* or *gliZ* genes, whose encoding gene products represent essential components for gliotoxin biosynthesis (Balibar and Walsh, 2006; Bok *et al.*, 2006). Additionally, it was examined if *A. fumigatus* Fbx15 is required for the regulation of other *A. fumigatus*-specific toxic secondary metabolites despite of gliotoxin through HPLC-MS analysis, whose regulation may be required *A. fumigatus* adaptation and/or virulence.

In the third part of this study *A. fumigatus* Fbx15 functionality was further elucidated in dependency of its two NLS sequences. It was examined whether both NLS sequences are required for the same or different functions and/or at different circumstances. Therefore, *A. fumigatus* Fbx15 NLS single and double deficient mutants were generated and analysed in growth tests concerning stress tolerance and localisation without and with oxidative stress. Furthermore, the localisation of the co-repressor subunit SsnF was examined in dependency of *A. fumigatus* Fbx15 NLS1 and NLS2. Respecting *A. fumigatus* Fbx15 cellular localisation dependent on its structural architecture, the impact of S468 and S469 was additionally analysed during non-stress- and oxidative stress conditions.

II Materials and Methods

1 Chemicals and materials

Buffers, media and solutions were prepared with chemicals of the companies AppliChem GmbH (Darmstadt, Germany), BD Biosciences (Heidelberg, Germany), Biozym Scientific GmbH (Hessisch Oldendorf, Germany), Carl Roth GmbH&Co.KG (Karlsruhe, Germany), Fluka (Neu-Ulm, Germany), Invitrogen (Karlsruhe, Germany), Merck KGaA (Darmstadt, Germany), Oxoid Deutschland GmbH (Wesel, Germany), Roche Diagnostics GmbH (Mannheim, Germany), Sigma-Aldrich Chemie GmbH (Munich, Germany), Serva Electrophoresis GmbH (Heidelberg, Germany) and VWR International GmbH (Darmstadt, Germany). The pH was determined with a WTW bench pH/mV Routine meter pH 526 (Sigma-Aldrich Chemie GmbH) was used. For small-scale sterile filtration of solutions Filtropur filters with a pore size of 0.2 and 0.45 µm from Sarstedt AG&Co.KG (Nümbrecht, Germany) were used. All plastic consumables like inoculation loops, petri dishes, pipet tips, and consumables needed for cryo – preservation/-conservation etc. were obtained from Sarstedt AG&Co.KG, Starlab GmbH (Hamburg, Germany) and Nerbe plus GmbH (Winsen/Luhe, Germany).

For selection of microorganisms ampicillin (Carl Roth GmbH&Co.KG), hygromycin B (InvivoGen, San Diego, CA, USA), phleomycin (InvivoGen) and pyrithiamine hydrobromide (Sigma-Aldrich Chemie GmbH) were used. Primers were obtained from Eurofins Genomics GmbH (Ebersberg, Germany) and Sigma-Aldrich Chemie GmbH (Munich, Germany). DNA fragment amplifications were accomplished with the Phusion® High-Fidelity DNA polymerase, appropriated polymerase buffers, synthetic oligonucleotides and restriction enzymes with corresponding buffers from Thermo Fisher Scientific (Schwerte, Germany). The GeneRuler™ 1 kb DNA Ladder (Thermo Fisher Scientific) was utilised for DNA on-gel band size determination in DNA gel electrophoresis. PCR-reactions were performed with the PCR-cyclers Primus96 Thermal Cyclers from MWG-Biotech (Ebersberg, Germany), T Professional Standard 96, T Professional Trio 48, T Professional Standard 96 Gradient thermocycler from Biometra GmbH (Göttingen, Germany) or Mastercycler® gradient from Eppendorf AG (Hamburg, Germany).

Gel electrophoresis was performed in the Sub-Cell® GT Cell gel chamber powered by the Power Pac 300 from Bio-Rad Laboratories GmbH (Munich, Germany). A NanoDrop™ ND-1000 spectrophotometer from PeqLab Biotechnology GmbH

(Erlangen, Germany) was used to measure DNA and RNA concentrations. RNase A was provided by AppliChem GmbH. The DNA polymerases Phusion® High-Fidelity DNA polymerase and *Taq* DNA polymerase with corresponding polymerase buffers and deoxynucleotides were obtained from Thermo Fisher Scientific. Harvesting of *Aspergillus* mycelium was performed with Calbiochem® Miracloth from Merck KGaA. Amersham™ Hybond-N™ nylon membrane was used to bind nucleic acid that was detected by Amersham™ Hyperfilm™-ECL for chemiluminescent signals and the Optimax® X-ray Film Processor from Protec GmbH&Co.KG (Oberstenfeld, Germany). For western hybridisation proteins were measured with an Infinite M200 microplate reader operated with Magellan software (both: Tecan Trading AG, Männedorf, Switzerland). The Mini-Protean® Tetra Cell, Mini Trans-Blot® Electrophoretic Cell and with the PowerPac™ 3000 power supply (Bio-Rad Laboratories GmbH) was utilised to perform SDS polyacrylamide gel electrophoresis. For protein on-gel band size determination the PageRuler™ Prestained Protein Ladder 10-180 kDa (Thermo Fisher Scientific) was used. Proteins were blotted on Amersham™ Protran™ 0.45 µm NC nitrocellulose membrane (GE Healthcare life science) and detected with the Fusion SL7 chemiluminescence detector (PeqLab Biotechnology GmbH) or Amersham™ Hyperfilm™-ECL (GE Healthcare life science). Signal quantification was performed with image processing Fiji software (Schindelin *et al.*, 2009). Protein purification of GFP-/RFP-tagged proteins was performed with GFP-Trap or RFP-Trap agarose beads from Chromotek (Planegg-Martinsried, Germany). The primary antibodies α-HA antibody [clone HA-7] from (Sigma-Aldrich Chemie GmbH), Anti-Phospho - (Ser/Thr) Phe antibody (ab17464) from Abcam (Cambridge, United Kingdom), Anti-Ubiquitin clone P4D1-A11 mouse antibody (Merck KGaA), α-GFP mouse antibody and α-RFP mouse antibody (both: Chromotek) and the secondary antibodies horseradish peroxidase-coupled rabbit G21234 (Invitrogen) and mouse antibody 115-035-003 from Jackson ImmunoResearch (Newmarket, United Kingdom) were used.

The RealMasterMix SYBR ROX 2.5x from 5 PRIME GmbH (Hilden, Germany) and the Light Cycler 2.0 System from Roche Diagnostics GmbH were used for Real-Time PCR. Quantitative analysis was performed with CFX Connect™ Real-Time System (Bio-Rad). For 1.5 ml and 2 ml reaction tube centrifugation Heraeus™ Biofuge Fresco (cooled) and Heraeus™ Pico™ Microcentrifuges from Heraeus Instruments GmbH (Hanau, Germany), Sorvall RC-3B Plus Refrigerated Centrifuge (Thermo Fisher Scientific) and Sorvall RC-5B Plus Refrigerated Centrifuge (Thermo Fisher Scientific) were used. For 10 ml, 15 ml and 50 ml centrifugation tubes Rotixa/RP from Andreas Hettich GmbH & Co. KG (Tuttlingen, Germany), 5804R from Eppendorf AG and

4K15C from Sigma Laborzentrifugen GmbH (Osterode am Harz, Germany) were used.

Fluorescence imaging was performed using an Axiovert Observer Z1 confocal microscope from Carl Zeiss Microscopy GmbH (Jena, Germany) equipped with a CoolSNAP ES2 CCD Camera from Photometrics (Tucson, Arizona, USA) or the Confocal Scanner Unit CSU-X1 from Yokogawa Electric Corporation (Tokyo, Japan) with a QuantEM:512SC EMCCD Camera from Photometrics. Image analysis was performed using the SlideBook 6.0 digital microscopy software (Intelligent Imaging Innovations, Göttingen, Germany). Hoechst 33258 pentahydrate (Invitrogen) or DAPI (Carl Roth GmbH&Co.KG) were used to visualise nuclei. For virulence assays *Galleria mellonella* moth larvae were purchased from Fauna Topics GmbH (Marbach/N. Rielingshausen, Germany).

Materials, instruments and suppliers not mentioned here are indicated in the following chapters.

2 Strains

2.1 *Escherichia coli*

Escherichia coli strain DH5α [F-, Δ (*arg*F-lac)169, φ80d*lac*ZΔM15, Δ*pho*A8, *gln*X44(AS), λ-, *deo*R481, *rfb*C1, *gyr*A96(NalR), *rec*A1, *end*A1, *thi*E1, *sd*R17] (Hanahan, 1985) was utilised.

2.2 *Aspergillus fumigatus* and *Aspergillus nidulans*

In this study generated and used *A. fumigatus* and *A. nidulans* strains are listed in Table 3. Construction details are given below with corresponding plasmids and oligonucleotides listed in Table 4 and Table 5.

Table 3: Generated and used *A. fumigatus* and *A. nidulans* strains in this study. ^{P} = promoter, ^{T} = terminator, ^{NRM} = non-recyclable marker, hph = hygromycin resistance, phleo = phleomycine.

***A. fumigatus* strains generated and used in this study**		
Strain name	**Genotype**	**Reference**
D141	Clinical isolate	Reichard *et al.*, 1990
Af293.1 (FGSC# 1137)	*pyrG1*	Fungal Genetics Stock Center, Kansas City,

		Missouri, USA (McCluskey *et al.*, 2010)
AfS35 (FGSC#1159)	*nkuA*::*loxP*	Krappmann, Sasse and Braus, 2006
AfGB189	Δ*pyroA*; *loxP*	C. Sasse
AfGB118	Δ*pyroA*::*pyroA:tetOn:rfp*	Helmschrott *et al.*, 2013
AfGB128	Δ*nkuA*; *fbx15*::*six*	Jöhnk *et al.*, 2016
AfGB417	Δ*nkuA*; Δ*fbx15*::*fbx15*:*six*	This study
AfGB418	Δ*nkuA*; Δ*fbx15*::^{P}*gpdA*:*fbx15*:*six*	This study
AfGB419	Δ*nkuA*; Δ*fbx15*::^{P}*gpdA*:*fbx15*:*sgfp*:*six*	This study
AfGB420	Δ*nkuA*; Δ*fbx15*::*fbx15*$^{\Delta\|NLS2}$:*six*	This study
AfGB421	Δ*nkuA*; Δ*fbx15*::*fbx15*$^{NLS1\|\Delta}$:*six*	This study
AfGB422	Δ*nkuA*; Δ*fbx15*::*fbx15*$^{\Delta\|\Delta}$:*six*	This study
AfGB423	Δ*nkuA*; Δ*fbx15*::^{P}*gpdA*:*fbx15*$^{\Delta\|NLS2}$:*rfp*:*six*	This study
AfGB424	Δ*nkuA*; Δ*fbx15*::^{P}*gpdA*:*fbx15*$^{NLS1\|\Delta}$:*rfp*:*six*	This study
AfGB425	Δ*nkuA*; Δ*fbx15*::^{P}*gpdA*:*fbx15*$^{\Delta\|\Delta}$:*rfp*:*six*	This study
AfGB426	Δ*nkuA*; Δ*fbx15*::^{P}*gpdA*:*fbx15*$^{S468\|9A}$:*rfp*:*six*	This study
AfGB427	Δ*nkuA*; Δ*fbx15*::^{P}*gpdA*:*fbx15*$^{S468\|9D}$:*rfp*:*six*	This study
AfGB428	Δ*nkuA*; *gliP*::*six*	This study
AfGB429	Δ*nkuA*; *gliZ*::*six*	This study
AfGB430	Δ*nkuA*; Δ*gliP*; *fbx15*::Δ*fbx15*:*six*	This study
AfGB431	Δ*nkuA*; Δ*gliZ*; *fbx15*::Δ*fbx15*:*six*	This study
AfGB432	*pyrG1*::*pyrG,* ^{P}*niiA*:*cyfp*:*fbx15*:^{T}*niiA,* ^{P}*niaA*:*nyfp*:*srbB*:^{T}*niaA*	This study
AfGB433	*pyrG1*::*pyrG,* ^{P}*niiA*:*cyfp*:*fbx15*:^{T}*niiA,* ^{P}*niaA*:*nyfp*:*fiAt*:^{T}*niaA*	This study
AfGB434	*pyrG1*::*pyrG*, ^{P}*niiA*:*fbx15*:*cyfp*:^{T}*niiA,* ^{P}*niaD*:*nyfp*:*fidA*:^{T}*niaD*	This study
AfGB435	*pyrG1*::*pyrG*, ^{P}*niiA*:*cyfp*:*fbx15*:^{T}*niiA*, ^{P}*niaA*:*nyfp*:^{T}*niaA*	This study
AfGB436	*pyrG1*::*pyrG,* ^{P}*niiA*:*cyfp*:^{T}*niiA,* ^{P}*niaA*:*nyfp*:*fiAt*:^{T}*niaA*	This study
AfGB437	*pyrG1*::*pyrG*, ^{P}*niiA*:*cyfp*:^{T}*niiA,* ^{P}*niaD*:*nyfp*:*fidA*:^{T}*niaD*	This study
AfGB438	Δ*nkuA*; *oefC*::*six*	This study
AfGB439	Δ*nkuA*; Δ*oefC*::*sgfp*:*oefC*:*six*	This study
AfGB440	Δ*nkuA*; Δ*oefC*::^{P}*gpdA*:*sgfp*:*oefC*:*six*	This study
AfGB441	Δ*nkuA*; Δ*oefC*; *fbx15*::Δ*fbx15*:*six*	This study
AfGB442	Δ*nkuA*; Δ*fbx15*; *sgfp*:*oefC*:*six*	This study
AfGB443	Δ*nkuA*; Δ*fbx15*; Δ*oefC*::^{P}*gpdA*:*sgfp*:*oefC*:*six*	This study
AfGB444	Δ*nkuA*, *srbB*::*six*	C. Sasse
AfGB445	Δ*nkuA*; Δ*srbB*::*srbB*:*rfp*:*six*	This study
AfGB446	Δ*nkuA*; Δ*fbx15*; *srbB*::Δ*srbB*:*six*	This study
AfGB447	Δ*nkuA;* Δ*srbB*::^{P}*gpdA*:*srbB*:*six*	This study
AfGB448	Δ*nkuA*; Δ*fbx15*; ^{P}*gpdA*:*srbB*:*six*	This study
AfGB449	Δ*nkuA*; *fiAt*::*six*	This study
AfGB450	Δ*nkuA*, Δ*pyroA*::*pyroA:tetOn*:*fiAt*	This study
AfGB451	Δ*nkuA*, Δ*pyroA*::*pyroA:tetOn*:*fiAt*:*sgfp*	This study
AfGB452	Δ*nkuA*, Δ*pyroA*::*pyroA:tetOn*:*fiAt*:*sgfp*; *fbx15*::*six*	This study
AfGB453	Δ*nkuA*; Δ*fbx15*; *fiAt*::*six*	This study
AfGB454	Δ*nkuA*; *fidA*::*six*	This study
AfGB455	Δ*nkuA*; Δ*fidA*::*fidA*:*sgfp*:*six*	This study
AfGB456	Δ*nkuA*; *fidA*::^{P}*gpdA*:*fidA*:*sgfp*:*six*	This study
AfGB457	Δ*nkuA*; *fidA*::*sgfp*:*fidA*:*six*	This study
AfGB458	Δ*nkuA*; *fidA*:: ^{P}*gpdA*:*sgfp*:*fidA*:*six*	This study
AfGB459	Δ*nkuA*; *fidA*::*ha*:*fidA*:*six*	This study
AfGB464	Δ*nkuA*; Δ*fbx15*::^{P}*gpdA*:*fbx15*$^{\Delta\|NLS2}$:*rfp*:*six*; *ssnF*::*ssnF*:*sgfp*:hph^{NRM}	This study
AfGB465	Δ*nkuA*; Δ*fbx15*::^{P}*gpdA*:*fbx15*$^{NLS1\|\Delta}$:*rfp*:*six*; *ssnF*::*ssnF*:*sgfp*:hph^{NRM}	This study

AfGB466	Δ*nkuA*; Δ*fbx15*::^{P}*gpdA*:*fbx15*$^{\Delta\|\Delta}$:*rfp*:*six*; *ssnF*::*ssnF*:*sgfp:*hph^{NRM}	This study
AfGB467	*pyrG1*::*pyrG,* ^{P}*niiA*:*cyfp*:*fbx15*:^{T}*niiA,* ^{P}*niaA*:*nyfp*:*oefC*:^{T}*niaA*	This study
***A. nidulans* strains generated and used in this study**		
ANCS07	*nkuA*::*loxP*	C. Sasse
AGB1265	Δ*nkuA*; *fbx15*::*six*	This study
AGB1266	Δ*nkuA*; Δ*fbx15*::*fbx15*:*strep*:*six*	This study
AGB1267	Δ*nkuA*; Δ*fbx15*::^{P}*gpdA*:*fbx15*:*rfp*:*six*	This study
AGB1268	Δ*nkuA*; ^{P}*niiA*:*cyfp*:*fbx15*:^{T}*niiA,* ^{P}*niaA*:*nyfp*:*oefC*:^{T}*niaA*:phleo^{NRM}	This study
AGB1269	Δ*nkuA*; ^{P}*niiA*:*cyfp*:*fbx15*:^{T}*niiA,* ^{P}*niaA*:*nyfp*:*fidA*:^{T}*niaA*:phleo^{NRM}	This study
AGB1270	Δ*nkuA*; ^{P}*niiA*:*cyfp*:*fbx15*:^{T}*niiA,* ^{P}*niaA*:*nyfp*:^{T}*niaA*:phleo^{NRM}	This study
AGB1271	Δ*nkuA*; ^{P}*niiA*:*cyfp*:^{T}*niiA,* ^{P}*niaA*:*nyfp*:*oefC*:^{T}*niaA*:phleo^{NRM}	This study
AGB1272	Δ*nkuA*; ^{P}*niiA*:*cyfp*:^{T}*niiA,* ^{P}*niaA*:*nyfp*:*fidA*:^{T}*niaA*:phleo^{NRM}	This study
AGB1273	Δ*nkuA*; *oefC*::*six*	This study
AGB1274	Δ*nkuA*; Δ*oefC*::*oefC*:*six*	This study
AGB1275	Δ*nkuA*; Δ*oefC*::*sgfp*:*oefC*:*six*	This study
AGB1276	Δ*nkuA*; Δ*oefC*::^{P}*gpdA*:*sgfp*:*oefC*:*six*	This study
AGB1277	Δ*nkuA*; Δ*fbx15*; *sgfp*:*oefC*:*six*	This study
AGB1278	Δ*nkuA*; *fidA*::*six*	This study
AGB1279	Δ*nkuA*; Δ*fidA*::*fidA*:*sgfp*:*six*	This study
AGB1280	Δ*nkuA*; Δ*fidA*::^{P}*gpdA*:*fidA*:*sgfp*:*six*	This study
AGB1281	Δ*nkuA*; Δ*fidA*::*sgfp*:*fidA*:*six*	This study
AGB1282	Δ*nkuA*; Δ*fidA*::^{P}*gpdA*:*sgfp*:*fidA*:*six*	This study
AGB1283	Δ*nkuA*; Δ*fidA*::*ha*:*fidA*:*six*	This study
***A. fumigatus* and *A. nidulans* crossover complementations**		
AfGB460	Δ*nkuA*; Δ*fbx15*^{AF}::*fbx15*^{AN}:*six*	This study
AfGB461	Δ*nkuA*; Δ*oefC*^{AF}::*oefC*^{AN}:*six*	This study
AGB1284	Δ*nkuA*; Δ*fbx15*^{AN}::*fbx15*^{AF}:*six*	This study
AGB1285	Δ*nkuA*; Δ*oefC*^{AN}::*oefC*^{AF}:*six*	This study

3 Media and growth conditions

Used media and supplemental substances were made in deionized water (dH_2O) and sterilized by autoclaving at 2 bar and 121°C for 20 min or sterile filtrated through a 0.2 µM - or 0.45 µM pore size filter membrane.

3.1 *Escherichia coli* cultivation

E.coli strains were cultivated in liquid lysogeny broth (LB) medium (Bertani, 1951) [1% (w/v) bacto-tryptone, 1% (w/v) NaCl, 2% (w/v) agar for solid medium, 0.5% (w/v) yeast extract, pH 7.5] by shaking on a rotary shaker at 37°C. For transformation of calcium competent *E. coli* cells liquid super optimal broth with catabolite repression (SOC) medium [2% bacto tryptone, 2.5 mM KCl, 10 mM $MgCl_2$, 10 mM $MgSO_4$, 10 mM NaCl, 0.5% yeast extract, supplemented with 20 mM glucose after autoclaving] was used. Solid LB medium plates supplemented with 100 µg/ml ampicillin was used for the selection of transformants. Plasmids conservation was

performed with equal volumes of bacterial overnight (o/n) cultures and 50% glycerol and stored at -80°C.

3.2 *Aspergillus* cultivation

A. fumigatus and *A. nidulans* strains were cultivated in *Aspergillus* minimal medium (AMM) [1% D-glucose, 1 x AspA (7 mM KCl, 11.2 mM KH_2PO_4, 70 mM $NaNO_3$, pH 5.5), 2 mM $MgSO_4$, 1 x trace elements (7.1 µM $CoCl_2$, 6.4 µM $CuSO_4$, 174 µM EDTA, 18 µM $FeSO_4$, 178 µM H_3BO_3, 25 µM $MnCl_2$, 6.2 µM Na_2MoO_4, 76 µM $ZnSO_4$] (Pontecorvo *et al*., 1953) at 37 °C either shaking in liquid cultures to obtain vegetative mycelium, or on solid plates, containing 2% agar for conidiation. *A. fumigatus* strains generated with the TetOn-System (Helmschrott *et al.*, 2013) were grown on solid London medium (LM) [1% (w/v) glucose, 7 mM KCl, 11.2 mM KH_2PO_4, 2 mM $MgSO_4$, 5 mM $(NH_4)_2C_4H_4O_6$, 0.1% (v/v) trace element solution, pH 5.5] (Käfer, 1977) supplemented with 30 µg/ml doxycycline (dox) to induce overexpression.

4 Phenotypical assays

4.1 Fungal stress tests

Phenotypical stress tests were performed by spotting $2*10^3$ or $5*10^3$ conidia on 30 ml AMM or, for overexpression generated with the TetOn-System (Helmschrott *et al.*, 2013), 30 ml LM containing 30 µg/ml dox. Used stressors were H_2O_2 for oxidative stress response, NaCl for osmotic stress response, lactose for carbon source changes, methylmethanesulfonate (MMS), camptothecin (CPT), CongoRed for cell wall stress response, 3-aminotriazole (3-AT) for histidine stress response and amphotericin B (Amp B) as antifungal drug. Also, the heavy metal stressor cadmium sulphate ($CdSO_4$) was tested. Strains were grown for three up to five days at 37°C in light (*A. nidulans*) or darkness (*A. fumigatus*). Results were documented with an Epson Perfection V600 Photo Scanner from Epson (Suwa, Japan).

4.2 Spore and cleistothecia quantification

For spore and cleistothecia quantification 2000 spores of Aspergilli were point inoculated and grown on solid AMM plates for seven days in light or dark with limited oxygen supply at 37°C to induce asexual and sexual development. Quantification of spores was performed by harvesting all spores from one plate in 5 ml NaCl-Tween solution. Spore numbers were determined by using Thoma cell counting chambers

(hemocytometer) from PaulMarienfeld GmbH& Co.KG (Lauda-Königshofen, Germany).

Cleistothecia quantification was performed by cutting out 5 mm^2 agar plugs with the larger opening of a 200 µl pipette tip. Matured cleistothecia were counted by their individualization on a new agar plate with a SZX12-ILLB2-200 binocular microscope (Olympus Deutschland GmbH, Hamburg, Germany). Significances were determined with one-way Anova and Student's t-test by Simple Interactive Statistical Analysis (SISA) (Uitenbroek, 1997).

5 Nucleic acid isolation

5.1 Isolation and purification of plasmid DNA and linearized DNA fragments

The NucleoSpin® Plasmid Kit (Macherey-Nagel) or the QIAprep® Spin Miniprep Kit (Qiagen) were utilised according to manufacturer's specifications to purify plasmid DNA from *E. coli* cultures. Plasmid DNA was eluted from spin columns with 65°C hot ddH_2O and stored at -20°C. Linearized DNA fragments obtained from PCR amplification or digestions with enzymes for plasmid linearization and construct excision were separated by agarose gel electrophoresis using the 10 x DNA loading dye [0.2% (w/v) bromophenol blue, 200 mM EDTA pH 8.0, 10% (v/v) Ficoll 400, 0.2% (w/v) xylene cyanol FF]. Purification of respective collected DNA bands from agarose gels was obtained by utilising the NucleoSpin® Gel and PCR Clean-up Kit (Macherey-Nagel) or the QIAquick® Gel Extraction Kit (Qiagen).

5.2 Extraction and purification of genomic DNA from *Aspergillus*

Overnight cultivated vegetative mycelium of *A. fumigatus* and *A. nidulans* was frozen in liquid nitrogen and pulverized with a MM400 table mill from Retsch Technology GmbH (Haan, Germany). The pulverized mycelium was mixed with 600 µl gDNA lysis buffer (Lee and Taylor, 1990) (50 mM EDTA, 3% (w/v) SDS, 50 mM Tris-HCl pH 7.2, 1% (v/v) β-mercaptoethanol) to a homogenous solution. After 1h incubation at 65°C 200 µl 8 M potassium acetate was added to the mycelium solution, mixed by inversion and centrifuged for 15 min at 13000 rpm at room temperature (RT). The supernatant was subsequently transferred to a clean reaction tube, mixed with 400 µl isopropanol supplemented 20 µl of 1 M NaOAc and centrifuged for two min at 13000 rpm at RT. Obtained DNA was washed with 70% (v/v) ethanol, centrifuged for two min at 13000 rpm at RT and dried at 65°C. DNA was resolved in 20 µg/ml RNAse A-containing

100 µl ddH_2O at 65°C and concentrations were measured with a Nanodrop ND-1000 (Peqlab Biotechnology GmbH).

6 Bioinformatical analysis

Multiple protein sequence alignment was performed using the blastp-algorithm of NCBI-BLAST (https://blast.ncbi.nlm.nih.gov/Blast.cgi?PAGE=Proteins). The ScanProsite tool (https://prosite.expasy.org/scanprosite/) (de Castro *et al.*, 2006) was utilised to determine domains using the aa sequences. NES were identified using the NetNES 1.1 Server program (http://www.cbs.dtu.dk/services/NetNES/) (La Cour *et al.*, 2004) and classical NLS were identified using the cNLS Mapper program (http://nls-mapper.iab.keio.ac.jp/cgi-bin/NLS_Mapper_form.cgi) (Kosugi *et al.*, 2008; Kosugi *et al*., 2009; S. Kosugi, Hasebe, Tomita, & Yanagawa, 2009). Putative phosphosites were identified with the NetPhos 3.1 Server (http://www.cbs.dtu.dk/services/NetPhos/). Disordered region predictions with protein-binding activity were identified with the DISOPRED3 program (http://bioinf.cs.ucl.ac.uk/disopred) (KosugiShunichi *et al.*, 2009).

7 Molecular techniques

7.1 Polymerase chain reaction (PCR)

DNA fragments used for plasmid generation, Southern probes, control of plasmid insertion after *E. coli* transformation through seamless cloning or ligation (colony PCR) were obtained by polymerase chain reaction (PCR) (Saiki *et al.*, 1988, Bergkessel and Guthrie, 2013; Hofmann and Brian, 1991) using the Phusion® High-Fidelity DNA Polymerase (Thermo Fisher Scientific). PCR programs were set according to the manufacturer's instructions. Appropriate annealing and salt adjusted temperatures of primers were determined by utilising the OligoCalc program Oligo Calculator version 3.27 (Kibbe, 2017).

7.2 Agarose gel electrophoresis

For purification or determination of DNA fragments sizes (Lee *et al.*, 2012) and to control RNA quality agarose gel electrophoresis was used. DNA samples were mixed in 10 x loading dye and load on a 1% (v/w) agarose gel in 1 x TAE buffer [2 mM EDTA, 20 mM sodium acetate, 40 mM Tris-acetate, pH 8.3] supplemented with 0.001 mg/ml ethidium bromide. RNA samples were mixed in 0.5 x *Taq* (Thermo Fisher

Scientific) loading dye diluted in RNAse free water. As size standard the GeneRuler™ 1 kb DNA Ladder (Thermo Fisher Scientific) was used. An electric field of 90 V was utilised for separation. In-gel DNA and RNA samples were visualised and documented with UV light (λ = 254 nm) by utilising a TFX-20 MX Vilber Lourmat Super Bright transilluminator (Sigma-Aldrich Chemie GmbH) or the Gel iX20 Imager Windows Version with the Intas GDS gel documentation software from Intas Science Imaging Instruments GmbH (Göttingen, Germany).

8 Construction of plasmids for genetic manipulations of fungi

For plasmid construction DNA fragments were obtained by PCR from gDNA of *A. nidulans* Δ*nkuA* (ACS07) and *A. fumigatus* AfS35 as templates. Fusion of DNA fragments was performed by fusion-PCR (Szewczyk *et al.*, 2006). Obtained DNA fragments and marker cassettes were fused by using the GeneArt®Seamless Cloning and Assembly Kit (Invitrogen) and the GeneArt®Seamless Cloning and Assembly Enzyme Mix (Invitrogen) according the FastCloning protocol (Li *et al.*, 2011) or the T4 DNA ligase (Thermo Fisher Scientific) according to manufactural protocol. The DNA-marker cassette constructs were cloned into the *EcoR*V multiple cloning site of the backbone plasmid pBluescript SK+. Details to plasmid design are described in the following chapter. As selective markers phleomycin (phleo) and pyrithiamine recycle marker cassettes were used. For on-locus integration in fungi all DNA-marker cassettes were excised by splicing to receive a linear construct. Therefore, outermost primers were constructed with either *Mss*I or *Swa*I restriction sites.

8.1 Recyclable marker cassettes as selection markers

Plasmids constructed and used in this study harbour recyclable marker cassettes if not indicated otherwise. The recyclable marker cassettes employ a prokaryotic small ß-Ser recombinase and its *six*-recognition sequences and is based on the bacterial recombination system (Canosa *et al.*, 1996; Hartmann *et al.*, 2010; Rojo *et al.*, 1993; Rojo and Alonso, 1994). By this system excision of the respective marker cassette off the fungal genome after transformation is possible and allows marker-free mutations, only leaving a *six*-recognition sequence of approx. 100 nucleotide base pairs (bp) (Figure 11).

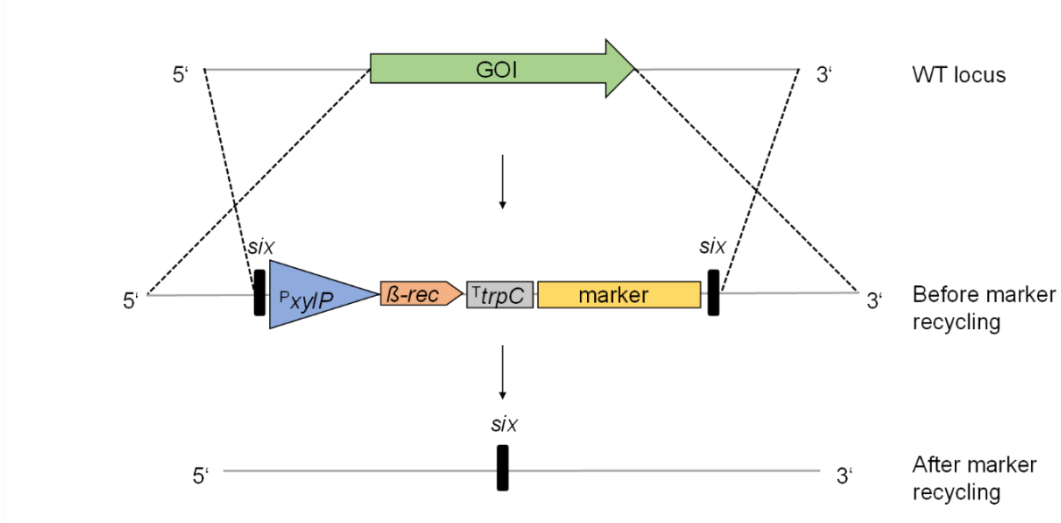

Figure 11: Scheme of the integration and recycling of a recyclable marker cassette. As example a deletion of the gene of interest (GOI) is given. Through homologous recombination the ORF (green) of GOI is replaced by a recyclable marker cassette, containing the β-*serine recombinase* gene (β-*rec*), driven by the xylose-inducible promoter (^{P}*xylP*) and employing the *trpC* terminator (^{T}*trpC*). Supplementation of xylose in the media allows to the induction of ^{P}*xylP:*β-*rec* expression., which triggers the excision of the cassette from the fungal genome, only leaving a small *six*-site as scar. This promotes on-locus integration of the respective construct. Modified from Thieme, 2017.

The selection marker can be reused after successful recycling for further integrations in the same host strain. In that way interference of large resistance cassettes with genetic equipment of the host can be successfully prevent. In this study two different marker cassettes were used. The *A. oryzae* pyrithiamine resistance gene (*ptrA*) included in pSK485 leads to resistance against pyrithiamine and is denoted as ptrA^{RM} (ptrA recyclable marker) in the following subchapters (Kubodera *et al.*, 2000). The plasmid pChS315 (Table 4) harbours the *ble* gene of *Streptoalloteichus hindustanus* that confers to phleomycin resistance (Drocourt *et al.*, 1990). The recyclable phleomycin marker cassette is named phleo^{RM} in the following.

Table 4: Plasmids used in this study. *A. fumigatus* genes are labelled with ^{AF} at the end, *A. nidulans* genes are denoted with ^{AN}. The pBlue Skript II (SK+) was used as backbone plasmid, if not indicated otherwise. ^{P} = promoter, ^{t} = terminator, ^{R} = resistance, phleo^{RM} = phleomycin recyclable resistance marker cassette from pME4305, ptrA^{RM} = pyrithiamine resistance recyclable marker cassette from pSK485, ptrA^{NRM} = pyrithiamine resistance non-recyclable marker cassette, hph^{NRM} = hygromycin resistance non-recyclable marker cassette, phleo^{NRM} = phleomycin resistance non-recyclable marker cassette, prs. com. = personal communication.

Name	Description	Reference/Source
pBlue Skript II (SK+)	Cloning vector, *amp*^{R}	Fermentas GmbH (St. Leon-Rot, Germany)
pSK485	*six*-^{P}*xylP*:ß-*rec*:*trpC*^{t}-ptrA^{R}-*six*	Hartmann *et al.*, 2010
pBJ97	^{P}*niiA*:*cyfp*:*fbx15*^{AF} (gDNA) in *Pme*I restriction site of pME3160	B. Jöhnk
pChS3	*5`pyroA*:*cds*:$^{t}$*trpC*:*tetOn*:*3`pyroA*	C.Sasse
pChS291	Δ*srbB*^{AF}:ptrA^{RM}	C. Sasse
pChS302	^{P}*srbB*:*srbB*^{AF}:*rfp*:ptrA^{RM}	C. Sasse
pChS314	*six*-^{p}*xylP*:ß-*rec*:^{t}*trpC*-ptrA^{RM}-*six*	C. Sasse
pChS315	*six*-^{p}*xylP*:ß-*rec*:^{t}*trpC*-phleo^{RM}-*six*	C. Sasse
pChS379	BiFC vector; ^{t}*niiA*-*Pme*I-^{P}*niiA* / ^{P}*niaD*-*Swa*I-^{t}*niaD*, phleo^{RM}	C. Sasse
pME3160	BiFC vector; ^{t}*niiA*-*Pme*I-^{P}*niiA* / ^{P}*niaD*-*Swa*I-^{t}*niaD*, *pyrG*	Bayram *et al*., 2008
pME4044	^{P}*gpdA*:*fbx15* ^{AF}:s*gfp* in pJET1.2	Jöhnk *et al*., 2016
pME4286	*ssnF*^{AF}:s*gfp*:^{T}*trpC*:^{P}*gpdA*:hph	Jöhnk *et al*., 2016
pME4292	Plasmid contains *sgfp*	B. Jöhnk prs. com.
pME4301	^{P}*niiA*:*cyfp*:*fbx15*^{AF} (cDNA) in *Pme*I restriction site of pME3160	Jöhnk *et al.*, 2016
pME4302	^{P}*niiA*:*cyfp*:*fbx15*^{AF} (cDNA) in *Pme*I restriction site, ^{P}*niaD*:*nyfp*:*ssnF*^{AF} in *Swa*I restriction site of pME3160	Jöhnk *et al.*, 2016
pME4342	^{P}*fbx15*::*fbx15*^{AF}:*rfp*:ptrA^{RM}	Jöhnk *et al*., 2016
pME4345	^{P}*fbx15*::*fbx15*[S468|9A]^{AF}:*rfp*:ptrA^{RM}	Jöhnk *et al*., 2016
pME4350	^{P}*fbx15*::*fbx15*[S468|S469D]^{AF}:*rfp*:ptrA^{RM}	Jöhnk *et al.*, 2016
pME4538	Δ*fbx15*^{AF}:ptrA^{RM}	Jöhnk *et al*., 2016
pME4915	^{P}*fbx15*:*fbx15*^{AF}:ptrA^{RM}	This study
pME4916	^{P}*gpdA*:*fbx15*^{AF}:ptrA^{RM}	This study
pME4917	^{P}*gpdA*:*fbx15*^{AF}:*sgfp*:ptrA^{RM}	This study
pME4918	^{P}*fbx15*:*fbx15*[Δ|NLS2]^{AF}:ptrA^{RM}	This study
pME4919	^{P}*fbx15*:*fbx15*[NLS1|Δ]^{AF}:ptrA^{RM}	This study
pME4920	^{P}*fbx15*:*fbx15*[Δ|Δ]^{AF}:ptrA^{RM}	This study
pME4921	^{P}*gpdA*:*fbx15*[Δ|NLS2]^{AF}:*rfp*:ptrA^{RM}	This study
pME4922	^{P}*gpdA*:*fbx15*[NLS1|Δ]^{AF}:*rfp*:ptrA^{RM}	This study
pME4923	^{P}*gpdA*:*fbx15*[Δ|Δ]^{AF}:*rfp*:ptrA^{RM}	This study
pME4924	^{P}*gpdA*:*fbx15*[S468|9A]^{AF}:*rfp*:ptrA^{RM}	This study
pME4925	^{P}*gpdA*:*fbx15*[S468|9D]^{AF}:*rfp*:ptrA^{RM}	This study
pME4926	Δ*gliP*^{AF}:ptrA^{RM}	This study
pME4927	Δ*gliZ*^{AF}:ptrA^{RM}	This study
pME4928	^{P}*niiA*:*cyfp*:*fbx15*^{AF} (gDNA) in *Pme*I restriction site, ^{P}*niaD*:*nyfp*:*oefC*^{AF} (gDNA) in *Swa*I restriction site of pME3160	This study
pME4929	^{P}*niiA*:*cyfp*:*fbx15*^{AF} (gDNA) in *Pme*I restriction site, ^{P}*niaD*:*nyfp*:*srbB*^{AF} (gDNA) in *Swa*I restriction site of pME3160	This study
pME4930	^{P}*niiA*:*cyfp*:*fbx15*^{AF} (gDNA) in *Pme*I restriction site, ^{P}*niaD*:*nyfp*:*fiAt*^{AF} (gDNA) in *Swa*I restriction site of pME3160	This study
pME4931	^{P}*niiA*:*cyfp*:*fbx15*^{AF} (gDNA) in *Pme*I restriction site, ^{P}*niaD*:*nyfp*:*fidA*^{AF} (gDNA) in *Swa*I restriction site of pME3160	This study
pME4932	^{P}*niiA*:*cyfp*:*fbx15*^{AF} (cDNA) in *Pme*I restriction site, ^{P}*niaD*:*nyfp* in *Swa*I restriction site of pME3160	This study

pME4934	^{P}*niiA*:*cyfp* in *Pme*I restriction site, ^{P}*niaD*:*nyfp*:*fiAt*^{AF}in *Swa*I restriction site of pME3160	This study
pME4935	^{P}*niiA*:*cyfp* in *Pme*I restriction site, ^{P}*niaD*:*nyfp*:*fidA*^{AF} (gDNA) in *Swa*I restriction site of pME3160	This study
pME4936	Δ*oefC*^{AF}:ptrA^{RM}	This study
pME4937	^{P}*oefC*:*sgfp*:*oefC*^{AF}:ptrA^{RM}	This study
pME4938	^{P}*gpdA*:*sgfp*:*oefC*^{AF}:ptrA^{RM}	This study
pME4939	^{P}*oefC*^{AF}:*oefC*^{AN}:ptrA^{RM}	This study
pME4940	^{P}*gpdA*:*srbB*^{AF}:*ptrA*^{RM}	This study
pME4941	Δ*fiAt*^{AF}:ptrA^{RM}	This study
pME4942	*5'pyroA*:*cds*:*trpC*^{t}:^{P}*gpdA*:*tetON*:*fiAt*:*3'pyroA*	This study
pME4943	*5'pyroA*:*cds*:*trpC*^{t}:^{P}*gpdA*:*tetON*:*fiAt*:*sgfp*:*3'pyroA*	This study
pME4944	Δ*fidA*^{AF}:ptrA^{RM}	This study
pME4945	^{P}*fidA*:*fidA*^{AF}:*sgfp*:ptrA^{RM}	This study
pME4946	^{P}*gpdA*:*fidA*^{AF}:*sgfp*:ptrA^{RM}	This study
pME4947	^{P}*fidA*:*sgfp*:*fidA*^{AF}:ptrA^{RM}	This study
pME4948	^{P}*gpdA*:*sgfp*:*fidA*^{AF}:ptrA^{RM}	This study
pME4949	^{P}*fidA*:*ha*:*fidA*^{AF}:ptrA^{RM}	This study
pME4950	^{P}*fbx15*^{AF}:*fbx15*^{AN}:ptrA^{RM}	This study
pME4951	Δ*fbx15*^{AN}:phleo^{RM}	This study
pME4952	^{P}*fbx15*:*fbx15*^{AN}:*strep*:phleo^{RM}	This study
pME4953	^{P}*gpdA*:*fbx15*^{AN}:*rfp*:phleo^{RM}	This study
pME4954	^{P}*fbx15*^{AN}:*fbx15*^{AF}:phleo^{RM}	This study
pME4955	^{P}*niiA*:*cyfp*:*fbx15*^{AN} (gDNA) in *Pme*I restriction site, ^{P}*niaD*:*nyfp*:*oefC*^{AN} (gDNA) in *Swa*I restriction site of pChS379 with phleo^{NRM}	This study
pME4956	^{P}*niiA*:*cyfp*:*fbx15*^{AN} (gDNA) in *Pme*I restriction site, ^{P}*niaD*:*nyfp*:*fidA*^{AN} (gDNA) in *Swa*I restriction site of pChS379 with phleo^{NRM}	This study
pME4957	^{P}*niiA*:*cyfp*:*fbx15*^{AN} (gDNA) in *Pme*I restriction site, ^{P}*niaD*:*nyfp* in *Swa*I restriction site of pChS379 with phleo^{NRM}	This study
pME4958	^{P}*niiA*:*cyfp* in *Pme*I restriction site, ^{P}*niaD*:*nyfp*:*oefC*^{AN} (gDNA) in *Swa*I restriction site of pChS379 with phleo^{NRM}	This study
pME4959	^{P}*niiA*:*cyfp* in *Pme*I restriction site, ^{P}*niaD*:*nyfp*:*fidA*^{AN} (gDNA) in *Swa*I restriction site of pChS379 with phleo^{NRM}	This study
pME4960	Δ*oefC*^{AN}:phleo^{RM}	This study
pME4961	^{P}*oefC*:*oefC*^{AN}:phleo^{RM}	This study
pME4962	^{P}*oefC*:*sgfp*:*oefC*^{AN}:phleo^{RM}	This study
pME4963	^{P}*gpdA*:*sgfp*:*oefC*^{AN}:phleo^{RM}	This study
pME4964	^{P}*oefC*^{AN}:*oefC*^{AF}:phleo^{RM}	This study
pME4965	Δ*fidA*^{AN}:phleo^{RM}	This study
pME4966	^{P}*fidA*:*fidA*^{AN}:*sgfp*:phleo^{RM}	This study
pME4967	^{P}*gpdA*:*fidA*^{AN}:*sgfp*:phleo^{RM}	This study
pME4968	^{P}*fidA*:*sgfp*:*fidA*^{AN}:phleo^{RM}	This study
pME4969	^{P}*gpdA*:*sgfp*:*fidA*^{AN}:phleo^{RM}	This study
pME4970	^{P}*fidA*:*ha*:*fidA*^{AN}:phleo^{RM}	This study

8.2 Primer and Plasmid design

Constructed plasmids used in this study are listed in Table 4. Corresponding primers needed for plasmid design are listed in Table 5. Genetic information was obtained from AspGD (Arnaud *et al.*, 2012) and fungiDB (https://fungidb.org/fungidb/). For

plasmid design the Lasergene software package from DNA STAR Inc. (Madison, WI, USA) was utilised. For seamless cloning reactions primers were constructed with an overhang of 15 bp to the backbone plasmid to create a 15 bp long homologous region. Primers were designed in a way to generate *Mss*I (GTTT/AAAC motive) restriction sites for splicing the DNA-marker cassettes out of the constructed plasmid for further integration into fungi, if not indicated otherwise. Therefore, naturally present ACCC and GTTT were used as part of the restriction sites to limit the integration of synthetic included bps.

Table 5: Oligonucleotides for plasmid construction or fragment amplification used in this study.

Name	5' – sequence – 3'	Size
BJ3	GAT CTT TGC CCG GTG TAT GAA ACC	24-mer
BJ4	GGT GAT GTC TGC TCA AGC GGG	21-mer
BJ43	TGA CGC CCA GGA CCG AG	17-mer
BJ63	ATG ACC GAC ATG AGC AAG AAC C	22-mer
BJ64	GTC ACC GAA GCC AAT ATC CAT G	22-mer
BJ319	GGT GGT AGC GGT GGT GTC	18-mer
BJ320	TCA CTT GTA CAG CTC GTC CAT	21-mer
kt182	CAT CAG TGC CAG CTG TCT TCG	21-mer
kt184	GGC TTT ACA CTT TAT GCT TCC G	22-mer
OZG73	ATG GTG AGC AAG GGC GAG GAG	21-mer
OZG75	ATG GCC GAC AAG CAG AAG AAC	21-mer
OZG78	GTA TAA TCA TAG ATT GTT TAA CAC TAG	27-mer
OZG79	CTC GTT GTG CCA CAC TAT GGA TTC	24-mer
OZG 207	GGT GGT AGC GGT GGT ATG GTG AGC	24-mer
OZG387	CGT GGC GAT GGA GCG CAT GAT ATA G	25-mer
OZG388	GTG GTT CAT GAC CTT CTG TTT CAG GTC	27-mer
srbB-1	CTG CAG GAA TTC GAT GTT TAA ACA AGG CAT TGG ACG GGA	39-mer
AA1	CTG CAG GAA TTC GAT GTT TAA ACA ACG GAG AAT TGA GGC TC	41-mer
AA2	CTA TAG GCC TGA GTG ATT TAA ATG TCC AAA CTG AGA GGA AGA GAT	45-mer
AA3	ATA ATA TGG CCA TCT CGA TCC GTC CTC TCT AGT TG	35-mer
AA4	ATC GAT AAG CTT GAT GTT TAA ACG GCT TGT GCT ATT TGC AG	41-mer
AA5	TCA GTT TGG ACA TTT GAT CTT TGC CCG GTG TAT GAA	36-mer
AA6	CAC TCG GAA TAT CCA CTG GA	20-mer
AA7	TGG ATA TTC CGA GTG GAT TGC CTT ATT CGA CGA ATC TA	38-mer
AA8	AGG CCT GAG TGA TTT TCA CTT GTA CAG CTC GTC CAT	36-mer
AA9	GAG GCA AGC AAC ACC CTC	18-mer
AA10	GGT GTT GCT TGC CTC TGT CCG AAG GCG GAG GC	32-mer
AA24	CGC CCG CCA TCG TTT ATG GCC GAC AAG CAG AAG AA	35-mer
AA25	CAT ACT CTC ACA TTT ATG GTG AGC AAG GGC GAG	33-mer
AA27	GAC CTT GAT CTG GCA TAT CTA C	22-mer
AA28	CAC GGC CGT GTA CAT ATC AT	20-mer
AA33	CGC TCC ATC GCC ACG ATG GCA TAC AAC AAC AGA CCT G	37-mer
AA34	TGC GAA CCC GTA TTT CTA GGT GCG AAA CTT GTC GTT	36-mer
AA44	CCT ATG CGAACCCGTATTTCGTGGCGATGGAGCG	34-mer
AA61	TAG GCC TGA GTA TTT TCA CCG AAG CCA ATA TCC ATG A	37-mer
AA63	ATA ATA TGG CCA TCT GAT CTT TGC CCG GTG TAT GAA A	37-mer
AA64	CTA TAG GCC TGA GTG GGC AGG TGA TGG GAG TTC	33-mer
AA65	CAG ACA TCA CCA TTT ATG GCA TAC AAC AAC AGA CCT G	37-mer

AA66	ATA AGC TTG ATA TTT GTT TAA ACT GCG CGT CCT GCA TG	38-mer
AA75	TCA CCG AAG CCA ATA TCC ATG ATT AAT	27-mer
AA76	CCG CTT GAG CAG ACA TCA CCA TGA CCG ACA TGA GCA AGA AC	41-mer
AA78	GTT TAA ACT ATA TCA CCG ATG ACA CTC	27-mer
AA79	AAA TGA TGT ATG GCT AAT ATG AGT CTA G	28-mer
AA80	GAA ATC TAG TCC CGG CTC TT	20-mer
AA81	GTT TAA ACG TTG TAT TAG CCA TTG CAG	27-mer
AA83	CTA GAA GAA GTA GGG AAT GGA A	22-mer
AA84	TCA TGC GCT CCA TCG CCA CGG TGC GAT CTC TGC CAA AGA	39-mer
AA179	GCC CTT GCT CAC CAT GAA GAA GTA GGG AAT GGA AGC	36-mer
AA186	ATA GGC CTG AGA TTT CTA CTT GTA CAG TTC GTC CAT G	37-mer
AA198	ATA TGG CCA TCT CAC TTC TTC CAC ACG GTA TAC ATT GTA	39-mer
AA199	GAT AAG CTT GAT CAC GTT TAA ACC TGC ACC TGC TGC AT	38-mer
AA200	AGG AAT TCG ATA TTT GTT TAA ACT CAC ATT TCA GGG CAC CA	41-mer
AA201	ATA GGC CTG AGA TTT AAA TGA TGC AGA GCG TAG GGT TGA	39-mer
AA202	ATA TGG CCA TCT CAC GCT GTT CTC ACC TCT TTT TTT TTT TT	41-mer
AA203	GAT AAG CTT GAT CAC GTT TAA ACG ATC GAT TCG AGG CG	38-mer
AA204	AGG AAT TCG ATA TTT GTT TAA ACG ACT CGG GCT TTC CC	38-mer
AA205	ATA GGC CTG AGA TTT AAA TCG CTG ACG AGT AGT TTG CTC	39-mer
AA208	TAG TAG TGC AAG TTT GAA GAA GTA GGG AAT GGA AGC CCT	39-mer
AA209	CAG ACA TCA CCG TTT ATG GTG CGA TCT CTG CCA AA	35-mer
AA265	ATA TGG CCA TCT CAC GCT GGT CTA GCT TAT TCA TGT A	37-mer
AA266	GAT AAG CTT GAT CAC GTT TAA ACC TCC CGT GTT CAC CG	38-mer
AA267	AGG AAT TCG ATA TTT GTT TAA ACA CCG ACT CTC CTT ATC GT	41-mer
AA268	ATA GGC CTG AGA TTT AAA TCT GTT AGA CAC TGG TCT TGT AA	41-mer
AA269	ACC ACC GCT ACC ACC GTG AGA TGC GCT ACT TGT GC	35-mer
AA270	ATA TGG CCA TCT CAC ACA GAT CGA ACA GGC CGCT	34-mer
AA271	GAT AAG CTT GAT CAC GTT TAA ACA TTG GTG ACA TTC AAA ATG CT	44-mer
AA272	AGG AAT TCG ATA TTT GTT TAA ACT TCT ACG CTA AGC TCC C	40-mer
AA273	ATA GGC CTG AGA TTT AAA TAA CAA TTC TCG AGT CTG TGG G	40-mer
AA285	TAG TAG TGC AAG TTT CTA CTT GTA CAG TTC GTC CAT G	37-mer
AA286	ATA TGG CCA TCT CAC CCT TTG TTT CCC CTT CCG TC	35-mer
AA287	GAT AAG CTT GAT CAC ATT TAA ATA TCG AAA TCA TGC CTT ACC A	43-mer
AA288	AGG AAT TCG ATA TTT AAA TGA CTA ACA ATG GTC ACA GC	38-mer
AA289	ATA GGC CTG AGA TTT GTT TAA ACT GAA AGA ATG TGG GCC GCA TA	44-mer
AA310	AGG AAT TCG ATA TTT GTT TAA ACC TTC TCT AGG GTC ATG C	40-mer
AA312	ATA TGG CCA TCT CAC ACT ACC AGG CCT GCA CTT	33-mer
AA313	AGC TTG ATC ACG TTT AAA CGG GAC AGT GTA CGA G	34-mer
AA319	ATA GGC CTG AGA TTT AAA TTT TCT CTG ACC AAA AAA GCG	39-mer
AA325	TGC GAA CCC GTA TTT TTA GTG AGA TGC GCT ACT TGT G	37-mer
AA327	GCC TGA GAT TTG TTT CTA GGT GAT GAG GAA GTC CAT	36-mer
AA328	ACA TTC TTT CAG TTT ATG GTG AGC AAG GGC GAG G	34-mer
AA329	ACC ACC GCT ACC ACC CTT GTA CAG TTC GTC CAT GCC	36-mer
AA330	ACA AGG GTG GTA GCG GTG GTT TGT CCA TGC AAA AGA CGC CC	41-mer
AA332	CGA GAA TTG TTA TTT GAT CTT TGC CCG GTG TAT GAA A	37-mer
AA333	CCG CTT GAG CAG ACA TCA CCG CAG AGC AGA ACG GCC AC	38-mer
AA336	ATA GGC CTG AGA TTT TTA CTT CTC GAA CTG GGG GTG GCT CCA AGC GCT ACG GAG CCA GAA ACC ACG G	67-mer
AA337	AGG AAT TCG ATA TTT AAA TTC AAG GTT CGC TGG TGT C	37-mer
AA338	ATA GGC CTG AGA TTT GTT TAA ACT CCA TTC AGC AAC GAC CCG	42-mer
AA339	ATA TGG CCA TCT CAC TTT TGC TCG GGT CGA GTT CTT	36-mer
AA340	GAT AAG CTT GAT CAC ATT TAA ATC TTT TCT GAC AAA AGG GAG TAA	45-mer
AA342	ACC ACC GCT ACC ACC CTT	18-mer
AA343	GGT GGT AGC GGT GGT TTG TCC ATG CAA AAA TCC CCC	36-mer

AA344	GCC TGA GAT TTG TTT TCA AGT AAT CAG GAA ATC CAT ATT CAT	42-mer
AA346	ATA GGC CTG AGA TTT TCA AGT AAT CAG GAA ATC CAT ATT CA	41-mer
AA347	TGC TGA ATG GAG TTT GAT CTT TGC CCG GTG TAT GAA	36-mer
AA350	CCG CTT GAG CAG ACA TCA CCA TGG TGA GCA AGG GCG AGG	39-mer
AA351	ACA TTC TTT CAG TTT GAT CTT TGC CCG GTG TAT GAA	36-mer
AA354	ATA GGC CTG AGA TTT TTA TTG AGC TGA ACG CAG CTG	36-mer
AA357	ACA TTC TTT CAG TTT ATG TTG TCC ATG CAA AAA TCC CC	38-mer
AA358	TGC TGA ATG GAG TTT ATG TTG TCC ATG CAA AAG ACG C	37-mer
AA359	GTG TCT AAC AGA TTT GAT CTT TGC CCG GTG TAT GAA	36-mer
AA360	TGA GCA GAC ATC ACC TCG CAA CCT GCG GAT CTC A	34-mer
AA361	ATA GGC CTG AGA TTT TTA GTG AGA TGC GCT ACT TGT G	37-mer
AA362	ACA AGG GTG GTA GCG GTG GTT CGC AAC CTG CGG ATC TCA	39-mer
AA364	GTG TCT AAC AGA TTT ATG TAC CCC TAC GAC GTC CCC GAC TAC GCC TCG CAA CCT GCG GAT CTC A	64-mer
AA366	ACA AGG GTG GTA GCG GTG GTG CAG AGC AGA ACG GCC AC	38-mer
AA367	CGA GAA TTG TTA TTT ATG GTG AGC AAG GGC GAG G	34-mer
AA368	CGA GAA TTG TTA TTT ATG TAC CCC TAC GAC GTC CCC GAC TAC GCC GCA GAG CAG AAC GGC CAC	63-mer
AA370	CGC TCC ATC GCC ACG TTG TCC ATG CAA AAA TCC CCC T	37-mer
AA371	TGC GAA CCC GTA TTT TCA AGT AAT CAG GAA ATC CAT ATT CAT	42-mer
AA372	AAG GTC ATG AAC CAC ACC AGG AAC CTG GAC TCC A	34-mer
AA373	TAT CCT CGT CAG TTT CTA ACG GAG CCA GAA ACC AC	35-mer
AA374	CGC TCC ATC GCC ACG GCA GAG CAG AAC GGC CAC	33-mer
AA375	TGC GAA CCC GTA TTT TTA TTG AGC TGA ACG CAG CTG T	37-mer
AA383	ATA GGC CTG AGA TTT TCA CCG AAG CCA ATA TCC ATG A	37-mer
AA384	TCA GTT TGG ACA TTT ATG ACC AGG AAC CTG GAC TC	35-mer
AA385	CTA TAG GCC TGA GTG ATT TCT AAC GGA GCC AGA AAC CAC	39-mer
AA386	GGT CAG AGA AAA TTT GAT CTT TGC CCG GTG TAT GAA A	37-mer
AA387	GGT GAT GTC TGC TCA AGC G	19-mer
AA388	CCG CTT GAG CAG ACA TCA CCA TGA CCA GGA ACC TGG ACT C	40-mer
AA389	ACC ACC GCT ACC ACC ACG GAG CCA GAA ACC ACG G	34-mer
AA390	ATA GGC CTG AGA TTT TCA CTT GTA CAG CTC GTC CAT	36-mer

8.3 Sequencing of plasmids

In this study constructed plasmids were checked for correct integration without mutations by sequencing performed by Seqlab Sequence Laboratories GmbH (Göttingen, Germany). The Lasergene software package (DNA Star Inc.) was used to analyse obtained sequences. The primers kt182 and kt184 were used to sequence plasmids cloned in the pBluescript SK+. Both primers are binding near the *EcoR*V cloning restriction site of the pBluescript SK+ cloning vector. Other sequencing primers are denoted in the following chapter.

8.4 Plasmid construction and strain generation in Aspergilli

A. fumigatus D141 gDNA was used as templates for plasmid construction. For *A. nidulans* based plasmid construction the ANCS07 (WT, Δ*nkuA*) was used as template. Sizes of DNA fragments are rounded in the upcoming sections.

8.5 *A. fumigatus* plasmid and strain construction

Construction of plasmids and strains for Δ*fbx15* and complementation with recyclable marker cassette

The Δ*fbx15* strain was constructed by amplifying 1.2 kb of *fbx15* 5' flanking region of *fbx15* (Afu3g14150) with the primer pair AA1/AA2 including a 15 bp overhang to introduce homolog overhangs to pBluescript SK+ and the ß-*six*-site of the ptrA recyclable marker cassette. 1.2 kb of *fbx15* 3' flanking region was amplified with the primer pair AA3/AA4, introducing a 15 bp overhang homologous to pBluescript SK+ and the *six*-site of the ptrA resistance recyclable marker cassette ($ptrA^{RM}$) including a *Swa*I restriction site for further integrations between *fbx15* 5' flanking region and *six*-site. The *fbx15* 5'- and 3' flanking regions were cloned together with the $ptrA^{RM}$ into the *EcoR*V multiple cloning site of pBluescript SK+ in a seamless cloning reaction, resulting in pME4538 (Jöhnk *et al.*, 2016).

The *fbx15* complementation construct pME4915 was obtained by amplifying the *fbx15* gene with the primer pair BJ63/64. The *fbx15* gene fragment was integrated into the *Swa*I restriction site of pME4538. The constructed deletion as well as the complementation cassette of *fbx15* were excised with *Mss*I. pME4538 was integrated into AfS35, resulting in AfGB128 (Jöhnk *et al.*, 2016), pME4915 was integrated into AfGB128, resulting in AfGB417. Correct replacement of the original gene was verified with Southern hybridisation before and after marker recycling.

Construction of plasmids and strains for overexpressed *fbx15* with recyclable marker cassette without and with GFP-tag

Overexpression of *fbx15* gene was achieved by using the *gpdA*-promoter. pME4916 was constructed by the amplification of ^{P}*gpdA-fbx15* from pME4044 with primer pair AA5/AA61 introducing a stop codon and 15 bp overhangs to *fbx15* 5' flanking region and the *six*-site of the $ptrA^{RM}$. For the construct of pME4917 ^{P}*gpdA*:*fbx15*:*sgfp* was amplified from pME4044 with the primer pair AA3/AA5 introducing 15 bp overhangs to pBluescript SK+ and the *six*-site of $ptrA^{RM}$. Both plasmids were generated in seamless cloning reactions. The overexpressed cassettes were excised with *Mss*I. The integration of pME4916 into AfGB128 results in AfGB418 and the integration of pME4917 into AfGB128 results into AfGB419. On-locus integrations were confirmed by Southern hybridisation before and after marker recycling.

Construction of plasmids and strains for *fbx15* nuclear localisation signal deficiencies

Deletions of the *fbx15* NLS sequences were generated from gDNA of D141 with the T4 DNA ligase (Thermo Fisher Scientific). The NLS1 of *fbx15* was deleted by amplification of the *fbx15* gene in two parts without NLS1. The first part consists of the N-terminal fraction of *fbx15* till NLS1 and was amplified with the primer pair AA7/BJ63 with a length of 1.3 kb. AA7 was designed with a 15 bp overhang to the second part of *fbx15* eliminating NLS1. The second part consists of the C-terminal fraction amplified with AA6/AA75 with a length of 700 bp. Both fractions were ligated by fusion-PCR (Szewczyk *et al.*, 2006) with the primer pair AA75/BJ63 and cloned into the *Swa*I restriction site of pME4538 in a seamless cloning reaction, resulting in pME4918.

The NLS2 of *fbx15* was deleted in the same way by ligating two parts of amplified *fbx15* fractions without the NLS2. The first part, a 1.5 kb fragment, consists of the N-terminal fraction of *fbx15* till NLS2 that was amplified with the primer pair AA10/BJ63. AA10 has a 15 bp overhang to the second part of *fbx15* elimination NLS2. The second part, the 500 bp long C-terminal fraction, was amplified with AA9/AA75. Both fractions were ligated by fusion-PCR (Szewczyk *et al.*, 2006) with the primer pair AA75/BJ63 and cloned into the *Swa*I restriction site in a seamless cloning reaction, resulting in pME4919.

The double deletion *fbx15*$^{\Delta|\Delta}$ was constructed using pME4919 as template. Here, the NLS1 was deleted in addition by amplifying the first part, the N-terminal fraction of *fbx15*, with primer pair AA7/BJ63 and the second part, the C-terminal fraction of *fbx15*, with primer pair AA6/AA75 without NLS1. The fractions were ligated by fusion-PCR (Szewczyk *et al.*, 2006) with primer pair BJ63/AA75 and cloned into the *Swa*I restriction site of pME4538 in a seamless cloning reaction, resulting in pME4920.

All *fbx15* NLS-deficient gene cassettes were excised with *Mss*I before fungal integration into AfGB128. AfAA420 was constructed by integrating pME4918, AfGB421 by integrating pME4919 and AfGB422 by integrating pME4920. Validation of correct integration was verified by southern hybridisation before and after marker recycling and sequencing with the primer BJ43.

Construction of plasmids and strains for C-terminal RFP-tagged overexpressed Fbx15 nuclear localisation signal deficiencies

Overexpression versions of the *fbx15*-NLS deficiencies tagged C-terminal with *rfp* were constructed with the templates pME4044 and pME4342. For overexpression of

RFP-tagged *fbx15*$^{\Delta|NLS2}$ the same method as described for overexpressed fbx15 tagged with GFP was used to eliminate NLS1 by amplifying *fbx15* in two parts leaving out NLS1. ^{P}*gpdA* together with the first part of *fbx15* (1.7 kb), the N-terminal fraction of *fbx15* till NLS1, was amplified from pME4044 with primer pair AA5/AA7 introducing 15 bp overhangs to *fbx15* 5' flanking region and the second part of *fbx15* without NLS1. The second part, the C-terminal fraction of *fbx15* (1.6 kb) with *rfp*, was amplified with AA6/AA8 without stop codon introducing a 15 bp overhang to the *six*-site of ptrA^{RM}. Both obtained fragments were cloned into the *Swa*I restriction site of pME4538 with a seamless cloning reaction, resulting in pME4921.

For overexpression of RFP-tagged *fbx15*$^{NLS1|\Delta}$ ^{P}*gpdA* together with the first part of *fbx15* (1.9 kb), the N-terminal fraction of *fbx15* till NLS2, was amplified with primer pair AA5/AA10 introducing 15 bp overhangs to *fbx15* 5' flanking region and the second part of *fbx15* without NLS2 from pME4044. The second part, the C-terminal fraction of *fbx15* (500 bp), was amplified with AA8/AA9 from pME4342 introducing a 15 bp overhang to the *six*-site of ptrA^{RM}. The two fragments were cloned into the *Swa*I restriction site of pME4538 with a seamless cloning reaction, resulting in pME4922.

Overexpressed, C-terminal RFP-tagged *fbx15*$^{\Delta|\Delta}$ was amplified using pME4921 as template. The first part, ^{P}*gpdA* and N-terminal *fbx15* till NLS2 with a size of 1.9 kb, was amplified using primer pair AA5/AA10, where AA10 has a 15bp overhang to the second part of *fbx15* elimination NLS2 and ^{P}*gpdA* a 15 bp overhang to *fbx15* 5' flanking region. With the primer pair AA9/AA8 the C-terminal part together with *rfp* with a size of 1.4 kb was amplified. Both fragments were cloned in the *Swa*I restriction site of pME4538 to generate pME4923 with a seamless cloning reaction. The overexpression constructs of the *fbx15*-NLS deficiencies tagged with *rfp* were integrated on-locus into AfGB128 after excising the gene cassettes with *Mss*I, resulting in AfGB423 (^{P}*gpdA*:*fbx15*$^{\Delta|NLS2}$:*rfp*), AfGB424 (^{P}*gpdA*:*fbx15*$^{NLS1|\Delta}$:*rfp*) and AfGB425 (^{P}*gpdA*:*fbx15*$^{\Delta|\Delta}$:*rfp*). Correct integration was verified by Southern hybridisation before and after marker recycling and sequencing with the primer BJ43.

Construction of C-terminal GFP-tagged SsnF in the RFP-tagged overexpressed Fbx15 nuclear localisation signal deficiencies with hph marker cassette

The GFP-tagged SsnF was excised from the plasmid pME4286 (Jöhnk *et al.*, 2016) and integrated in AfGB423, in AfGB424 and in AfGB425, resulting in AfGB464, AfGB465 and AfGB466. Southern hybridisation was used for verification of correct integration by southern hybridisation.

Construction of plasmids and strains for RFP-tagged overexpressed *fbx15* phospho-site manipulations

The *rfp*-tagged overexpressed *fbx15* phospho-site manipulations were generated using the T4 DNA ligase (Thermo Fisher Scientific). Mimicking constantly dephosphorylation at Ser residues S468 and S469 was obtained by the exchange of Ser to Ala and mimicking constantly phosphorylated S468 and S469 was obtained by the exchange of Ser to arginine. ^{P}*gpdA* was amplified from pME4917 with the primer pair BJ3/BJ4. Primer pair AA76/BJ320 was used to amplify constantly mimicking dephosphorylated *fbx15*$^{S468|9A}$*:rfp* from pME4345 and for the amplification of constantly mimicking phosphorylated *fbx15*$^{S468|9D}$*:rfp* from pME4350, where AA76 has a 20 bp overhang to ^{P}*gpdA.* ^{P}*gpdA* and *fbx15*$^{S468/469A}$*:rfp* or *fbx15*$^{S468|9D}$*:rfp* were ligated by fusion-PCR (Szewczyk *et al.*, 2006) with primer pair BJ3/BJ320. The ligated fragments were integrated into the *Swa*I restriction site of pME4538 to generate pME4924 for overexpressed dephosphorylated *fbx15:rfp* or pME4925 for overexpressed phosphorylated *fbx15:rfp* in a T4 DNA ligase reaction. Gene cassettes were excised with *Mss*I and integrated into AfGB128, resulting in AfGB426 for overexpressed, dephosphorylated *fbx15*$^{S468/469A}$*:rfp* and in AfGB427 for overexpressed, phosphorylated *fbx15*$^{S468/469D}$*:rfp*. Southern hybridisation was utilised to control correct integration before and after marker recycling.

Construction of plasmids and strains for Δ*gliP*, Δ*gliZ* strains in wild type- and Δ*fbx15* background

For the plasmid construction gDNA of D141 was used as template. The 750 bp long *gliP* 5' flanking region was amplified with primer pair AA200/AA201 introducing 15 bp overhangs to pBluescript SK+ and the *six*-site of ptrA^{RM}. *gliP* 3' flanking region with a length of 800 bp was amplified with primer pair AA198/AA199 introducing 15 bp overhangs to the *six*-site of ptrA^{RM} and pBluescript SK+ and including a *Swa*I restriction site for further applications. Cloning was performed in two steps into pChS314 (C. Sasse, prs. com.). The *gliP* 5' flanking region was cloned into the *Swa*I restriction site and the *gliP* 3' flanking region was cloned into the *Pml*I restriction site in seamless cloning reactions, resulting in pME4926. The gene cassette was excised with *Mss*I and integrated on-locus into AfS35 and AfGB128, resulting in AfGB428 and AfGB430.

For pME4927 850 bp long *gliZ* 5' flanking region was amplified with primer pair AA204/AA205 introducing 15 bp overhangs to pBluescript SK^{+} and the *six*-site of ptrA^{RM}. 900 bp long *gliZ* 3' flanking region was amplified with primer pair AA202/AA203 introducing 15 bp overhangs to the *six*-site of ptrA^{RM} and pBluescript

SK+. pChS314 (C. Sasse, prs. com.) was used as backbone plasmid and cloning was performed in two steps. The *gliZ* 5' flanking region was cloned into the *Swa*I restriction site and the *gliZ* 3' flanking region was cloned into the *Pml*I restriction site in seamless cloning reactions. Excising of the gene cassette was performed with *Mss*I and integrated on-locus into AfS35 and AfGB128, resulting in AfGB429 and AfGB431. Correct integration was verified by Southern hybridisation after marker recycling.

Construction of BiFC plasmids and strains for localisation determining interactions of Fbx15 with FiAt, FidA, OefC and SrbB

BiFC studies were utilised using the bidirectional nitrate-inducible ^{P}*niiA*/^{P}*niaD* promoter and terminators (*niiA*^{T}/*niaD*^{T}) with ectopic integration in respective strains. For constructs gDNA of *fiAt*, *fidA*, *oefC* and *srbB* were used. For *fbx15* gDNA and cDNA of D141 were utilised for the experiments. Constructed plasmids were sequenced with the primers AA27, AAA28, OZG78, OZG79.

pME4301 (*cyfp*:*fbx15* (cDNA) in *Pme*I restriction site of pME3160) was used as backbone for cloning *srbB* or *oefC* gDNA fused to *nyfp*. *srbB* gDNA was amplified without stop codon with primer pair AA33/AA34 with 15 bp overhangs homologous to *nyfp* and ^{T}*niaD*. *nyfp* was amplified with the primer pair AA25/OZG387 from pME4302, where AA25 has a 15bp overhang to ^{P}*niaD*. Both fragments were cloned into the *Swa*I restriction site of pME4301 in a seamless cloning reaction, resulting in pME4929. AfGB432 was generated by ectopic integration of pME4928 into Af293.1. *oefC* gDNA was amplified without stop codon with primer pair AA29/AA30 with 15 bp overhangs homologous to *nyfp* and ^{T}*niaD*. The *nyfp* fragment used for pME4929 was also used for a seamless cloning reaction of *oefC* and *nYFP*, which were cloned into the *Swa*I restriction site of pME4301, resulting in pME4928. AfGB467 was generated by ectopic integration of pME4928 into Af293.1.

BiFC experiments for *fbx15* with *fiAt* and *fidA* were obtained using gDNA as templates. As backbone plasmid pBJ97 (*cyfp*:*fbx15* (gDNA) in *Pme*I restriction site of pME3160) was utilised. gDNA of *fiAt* without stop codon was amplified with primer pair AA83/AA84, including a 20 bp overhang to *nyfp* with AA84. *nyfp* was amplified with primer pair OZG73/OZG387 from pME4302 and ligated with *fiAt* by fusion-PCR (Szewczyk *et al.*, 2006) using primer pair AA83/OZG73. The *nyfp:fiAt* fusion fragment was cloned into the *Swa*I restriction site of pBJ97 in a T4 DNA ligase reaction, resulting in pME4930. As control the obtained fusion fragment *nyfp-fiAt* and *cyfp*, amplified with primer pair OZG75/OZG388 from pME4302, were cloned in two steps into pME3160. The *cyfp* fragment was cloned into the *Pme*I restriction site and *nyfp:fiAt* in the *Swa*I restriction site of pME3160 in a T4 DNA ligase reaction, resulting

in pME4934. AfGB433 was constructed by ectopic integration of pME4930 into Af293.1 and AfGB436 by ectopic integration of pME4934 into Af293.1.

For BiFC constructs with *fidA*, gDNA *fidA* without stop codon was amplified with primer pair AA324/AA325. *nyfp* was amplified with AA25/OZG387 and ligated with *fidA* in a fusion-PCR reaction (Szewczyk *et al.*, 2006) with primer pair AA25/AA325 including 15 bp overhangs to *nyfp* and ^{T}*niaD*. The *nyfp:fidA* fusion fragment was cloned into the *Swa*I restriction site of pBJ97 in a seamless cloning reaction, resulting in pME4931. As control *cyfp*, amplified with primer pair OZG75/OZG388, and *nyfp:fidA* fusion fragment were cloned into pME3160 in two steps. *cyfp* was cloned into the *Pme*I restriction site of pME3160 in a T4 DNA ligase reaction and the *nyfp:fidA* fusion fragment into the *Swa*I restriction site of pME3160 in a seamless cloning reaction, resulting in pME4935. Ectopic integration of pME4931 into Af293.1 result into AfGB434 and pME4935 into AfGB437.

fbx15 control for BiFC experiments was constructed by cloning of *nyfp,* amplified with primer pair AA25/AA44, into the *Swa*I restriction site of pME4301 in a seamless cloning reaction, resulting in pME4932 and ectopic integrated into Af293.1 leading to AfGB435. Correct ectopic integration of all BiFC strains was verified by PCR of gDNA.

Construction of plasmids and strains for Δ*oefC,* C-terminal GFP-tagged complementation and overexpression

For the construction of the Δ*oefC* strain 1.3 kb of *oefC* 5’ flanking region was amplified from D141 gDNA with the primer pair AA288/AA289 including 15 bp overhang to introduce overhangs to pBluescript SK+ and the *six*-site of ptrA^{RM}. 1.8 kb of *oefC* 3’ flanking region was amplified with the primer pair AA286/AA287 from D141 gDNA, which introduce 15 bp overhang homologous to pBluescript SK+ and the *six*-site of ptrA^{RM} including a *Pme*I restriction site for further integrations. pChS314 (C. Sasse) was used for stepwise cloning of *oefC* 5’- and 3’ flanking regions. *oefC* 5’ flanking region was cloned into the *Swa*I restriction site and 3’ flanking regions was cloned into the *Pmi*I restriction site, resulting in pME4936. On-locus integration into AfS35 of the excised gene cassette with *Swa*I resulted in AfGB438.

The GFP-tagged complementation plasmid pME4937 was constructed by amplifying *sgfp* with primer pair AA328/AA329 from pME4292, introducing 15 bp overhangs to pBluescript SK+ and the *six*-site of ptrA^{RM}. *oefC* was amplified with primer pair AA327/AA330 from D141 gDNA introducing 15 bp overhangs to *sgfp* and the *six*-site of ptrA^{RM}. Both fragments were integrated into the *Swa*I restriction site of pME4936, resulting in pME4937. Excised gene cassette with *Swa*I was transformed into AfGB438, resulting in AfGB439.

Overexpressed *oefC* tagged with *sgfp* was obtained with the ^{P}*gpdA*, amplified with AA351/BJ4 from pME4917 introducing a 15 bp overhang to *oefC* 5' flanking region. *sgfp-oefC* was amplified from pME4937 with primer pairs AA327/AA350 with 20 bp overhang to ^{P}*gpdA* and 15 bp overhang to ptrA^{RM}. Through fusion-PCR (Szewczyk *et al.*, 2006) ^{P}*gpdA* and *sgfp-oefC* were ligated and cloned into the *Swa*I restriction site of pME4936 in a seamless cloning reaction, leading to pME4938. The gene cassette was excised with *Swa*I and integrated into AfGB438 to generate AfGB440. All constructed strains were confirmed by Southern hybridisation after marker recycling.

Construction of Δ*oefC*/Δ*fbx15* strain and GFP-tagged *oefC* complementation and - overexpression in Δ*fbx15* background

For double deletion of Δ*oefC*/Δ*fbx15* the excided gene cassette of pME4538 was integrated into AfGB438 background strain, resulting in AfGB441. Excised gene cassette of pME4937 (GFP-tagged *oefC*) and pME4938 (overexpressed GFP-tagged *oefC*) with *Swa*I were transformed into AfGB128, resulting in AfGB442 and AfGB443. Correct integration was verified by Southern hybridisation after marker recycling.

Construction of strains for Δ*fbx15*/Δ*srbB* and Δ*srbB* complementation tagged with RFP

For double deletion of Δ*fbx15*/Δ*srbB* excised gene cassette of pChS291 (C. Sasse, prs. com.) with *Mss*I was integrated on-locus into AfGB128, resulting in AfGB446. The Δ*srbB* complementation plasmid pChS301, including the *srbB*:*rfp*:ptrA^{RM} cassette with 5'- and 3' flanking region (C. Sasse, prs. com.) was excised with *Pme*I and integrated on-locus into AfGB444, resulting in Δ*srbB* complementation strain AfGB445. Correct integration was verified by Southern hybridisation after marker recycling.

Construction of plasmids and strains for overexpressed *srbB* in wild type- and Δ*fbx15* strain background

Overexpression was induced with ^{P}*gpdA* amplified with AA63/BJ4 from pME4917, where AA63 has a 15 bp overhang to the *six*-site of ptrA^{RM}. pME4940 was constructed with D141 gDNA by amplification of the 1 kb large *srbB* 5' flanking region with primer pair AA64/srbB-1, where AA64 has a 15 bp overhang to the *six*-site of ptrA^{RM}. srbB-1 introduces a complete *Pme*I restriction site and a 15 bp overhang to pBluescript SK+. The *srbB* gene with 3' flanking region was amplified with primer pair AA65/AA66. AA65 has a 20 bp overhang to ^{P}*gpdA* and AA66 a 15 bp overhang to pBluescript SK+. ^{P}*gpdA* and *srbB-srbB* 3' flanking region were ligated by fusion-PCR

(Szewczyk *et al.*, 2006) with primer pair AA63/AA66. The *srbB* 5' flanking region, the fusion fragment ^{P}*gpdA-srbB-srbB* 3' flanking region and the ptrA^{RM} into the *EcoR*V restriction site of pBlueScript SK+. The gene cassette was excised with *Mss*I and transformed on-locus into AfGB444, resulting in AfGB447 and in AfGB128, resulting in AfGB448. Correct integration after marker recycling was verified by Southern hybridisation.

Construction of plasmids and strains for Δ*fiAt* and Δ*fbx15*/Δ*fiAt*

gDNA of D141 was used as template for the plasmid construction of Δ*fiAt*, *fiAt* 5' flanking region was amplified with primer pair AA78/AA79 and *fiAt* 3' flanking region with primer pair AA80/AA81. pME4941 was cloned in two steps were *fiAt* 5' flanking region was cloned into the *Swa*I restriction site and 3' flanking region was cloned into the *Pml*I restriction site of pChS314 harboring the ptrA^{RM} in T4 DNA ligase reactions. The gene cassette was excised with *Mss*I and integrated into AfS35, resulting in AfGB449 and AfGB128, resulting in AfGB453. Southern hybridisation was utilised for verifying correct integration on-locus after marker recycling.

Construction of plasmid and strain for overexpression for *fiAt* without and with GFP-tag by the TetOn-System

pChS3 was provided by C. Sasse as backbone plasmid containing the 5'- (1.1 kb) and 3' (1.2 kb) flanking regions of *pyroA* and the TetOn (Meyer *et al.*, 2011). *fiAt* was amplified from D141 gDNA with primer pair AA208/209 having 15 bp overhangs to tetO7-Pmin and *pyroA* 3' flanking region. *fiAt* was integrated into the *Mss*I restriction site of pChS3 in a seamless cloning reaction, resulting in pME4942. GFP-tagged overexpression of *fiAt* was constructed by amplifying *fiAt* without stop codon with primer pair AA179/AA209 introducing 20 bp overhangs to tetO7-Pmin and *sgfp* with primer pair AA285/OZG207. AA285 introduced a 15 bp overhang to *pyroA* 3' flanking region. *fiAt* and *sgfp* were ligated by fusion-PCR (Szewczyk *et al.*, 2006) with primer pair AA209/AA285 and cloned into the *MssI* restriction site of pChS3 in a seamless cloning reaction, resulting in pME4943.

Excised gene cassettes were integrated into AfGB189, resulting in AfGB450 by pME4942 and AfGB451 by pME4943. Correct integration was confirmed by Southern hybridisation.

Construction of Δ*fbx15* in overexpressed *fiAt* background strain with GFP-tag by the TetOn-System

Constructed AfGB451 was used as background strain to integrate excised gene cassette of Δ*fbx15* from pME4538 with *Mss*I, resulting in AfGB452. Southern hybridisation was used to verify on-locus integration after marker recycling.

Construction of plasmids and strains for Δ*fidA* and C-terminal GFP-tagged complementation

The Δ*fidA* strain was constructed from D141 gDNA by amplifying *fidA* 5' flanking region (1.2 kb) with primer pair AA267/AA268 introducing 15 bp overhangs to pBluescript SK+ and the *six*-site of ptrA^{RM} with a *Swa*I restriction site between *fidA* 5' flanking region and ptrA^{RM} for further cloning. *fidA* 3' flanking region (1 kb) was amplified with primer pair AA265/AA266 introducing 15 bp overhangs to the *six*-site of ptrA^{RM} and pBluescript SK+. For cloning the pChS314 (C. Sasse, prs. com.) was utilised in two step cloning. *fidA* 5' flanking region was cloned into the *Swa*I restriction site and *fidA* 3' flanking region was cloned into the *Pml*I restriction site in seamless cloning reactions, resulting in pME4944. The excised gene cassette of pME4944 was transformed into AfS35 to generate AfGB454.

The complementation plasmid pME4945 was constructed by amplification of *fidA* 5' flanking region and *fidA* without stop codon (5.5 kb) from D141 gDNA with primer pair AA267/AA269 introducing 15 bp overhangs to pBluescript SK+ and C-terminal located *sgfp*. C-terminal located *sgfp* was amplified from pME4917 with primer pair AA186/OZG207 with 15 bp overhang to the *six*-site of ptrA^{RM}. *fidA* 5' flanking region-*fidA* and *sgfp* were ligated by fusion-PCR (Szewczyk *et al.*, 2006) with primer pair AA186/AA267. Fused *fidA* 5' flanking region-*fidA*-*sgfp* and *fidA* 3' flanking region (1 kb), amplified with primer pair AA265/266 introducing 15 bp overhangs to the *six*-site of ptrA^{RM} and pBluescript SK+, were cloned in two steps into pChS314 (C. Sasse, prs. com.). *fidA* 5'-flanking region-*fidA*-*sgfp* was cloned into *Swa*I restriction site and *fidA* 3' flanking region into *Pml*I restriction site with seamless cloning reactions. The excised gene cassette was integrated into AfGB454, resulting in AfGB455. Correct integration was confirmed by Southern hybridisation after marker recycling.

Construction of plasmid and strain for overexpressed N- and C-terminal GFP-tagged FidA

^{P}*gpdA* was used for overexpression of *fidA*. ^{P}*gpdA* was amplified from pME4917 with primer pair AA359/BJ4 introducing a 15 bp overhang to *fidA* 5' flanking region. *fidA*-*sgfp* was amplified from pME4945 with primer pair AA186/AA360 introducing 15

bp overhangs to the *six*-site of ptrA^{RM} and ^{P}*gpdA*. ^{P}*gpdA* and *fidA-sgfp* were ligated by fusion-PCR (Szewczyk *et al.*, 2006) with primer pair AA186/AA359 and integrated into the *Swa*I restriction site of pME4944 in a seamless cloning reaction, resulting in pME4946. N-terminal GFP-tagged overexpressed *fidA* was obtained by amplifying ^{P}*gpdA-sgfp* with primer pair AA329/AA359 from pME4938 introducing a 15 bp overhang to *fidA* 5' flanking region. Through fusion-PCR (Szewczyk *et al.*, 2006) ^{P}*gpdA-sgfp* and *fidA* were ligated with primer pair AA359/AA361 and cloned into the *Swa*I restriction site of pME4944 in a seamless cloning reaction, resulting in pME4948.

AfGB456 was generated by integration of the excised gene cassette with *Mss*I of pME4946 into AfS35. Integration of excised gene cassette with *Mss*I of pME4948 into AfS35 resulted in AfGB458. Southern hybridisation after marker recycling was utilised to verify correct integration.

Construction of plasmids and strains for N-terminal HA- and GFP-tagged FidA

Construction of N-terminal HA-tagged *fidA* was obtained by amplification of *fidA* from D141 gDNA with AA361/AA364 introducing HA (5'- TAC CCC TAC GAC GTC CCC GAC TAC GCC – 3') with start codon by primer AA364 and 15 bp overhangs to *fidA* 5' flanking region. AA361 introduces a 15 bp overhang to the *six*-site of ptrA^{RM}. The fragment HA-*fidA* was cloned with a seamless cloning reaction into the *Swa*I restriction site of pME4944, resulting in pME4949. *ha:fidA* gene marker cassette was excised with *Mss*I and transformed into AfS35, resulting in AfGB459.

N-terminal GFP-tagged *fidA* was obtained by amplifying *sgfp* from pME4292 with primer pair AA329/AA383 introducing a 15 bp overhang to *fidA* 5' flanking region. *fidA* was amplified from D141 gDNA with primer pair AA361/AA362 introducing a 15 bp overhang to the *six*-site of ptrA^{RM} and a 20 bp overhang to *sgfp*. Through fusion-PCR (Szewczyk *et al.*, 2006) *sgfp* and *fidA* were ligated and cloned into the *Swa*I restriction site of pME4944 in a seamless cloning reaction, resulting in pME4947. The gene cassette was excised with *Mss*I and integrated into AfS35, resulting in AfGB457. Correct integration was confirmed by Southern hybridisation before and after marker recycling and PCR.

8.6 *A. nidulans* plasmid and strain construction

Construction of plasmids and strains for Δ*fbx15* and C-terminal STREP-tagged complementation with recyclable resistance marker

The Δ*fbx15* strain was constructed from ANCS07 gDNA by amplification of *fbx15* 5' flanking region (1.2 kb) with primer pair AA310/AA319 introducing 15 bp overhangs to pBluescript SK+ and the *six*-site of phleo^{RM} with a *Swa*I restriction site between *fbx15* 5' flanking region and phleo^{RM} for further applications. *fbx15* 3' flanking region (1.4 kb) was amplified with primer pair AA312/AA313 introducing 15 bp overhangs to the *six*-site of phleo^{RM} and pBluescript SK+. For cloning the pChS315 (C. Sasse, prs. com.) was utilised, harbouring the phleo^{RM} cassette, in two step cloning. *fbx15* 5' flanking region was cloned into the *Swa*I restriction site and *fbx15* 3' flanking region was cloned into the *Pme*I restriction site in seamless cloning reactions, resulting in pME4951. The excised gene cassette of pME4951 with *Mss*I was transformed into ANCS07 to generate AGB1265.

The complementation construct was generated by amplifying *fbx15* 5' flanking region and *fbx15* gene without stop codon (3.3 kb) with primer pair AA310/AA336 introducing 15 bp overhang to pBluescript SK+ and the *six*-site of phleo^{RM}. AA336 also introduce a C-terminal STREP-tag (5'- AGC GCT TGG AGC CAC CCC CAG TTC GAG AAG -3') with a stop codon. *fbx15* 3' flanking region was amplified with AA312/313 introducing 15 bp overhangs to the *six*-site of phleo^{RM} and pBluescript SK+. Both fragments were cloned into pChS315 (C. Sasse, prs. com.). *fbx15* 5' flanking region-*fbx15-strep* was cloned into *Swa*I restriction site and *fbx15* 3' flanking region was cloned into *Pme*I restriction site in seamless cloning reactions, resulting in pME4952. Gene cassette was excised with *Mss*I and transformed into AGB1265 to generate AGB1266. Correct integration on-locus was verified for AGB1265 and AGB1266 with Southern hybridisation and PCR after marker recycling.

Construction of plasmid and strain for overexpressed Fbx15 tagged with RFP

Overexpression of *fbx15* with C-terminal RFP-tag was obtained by ^{P}*gpdA* amplified from pME4917 with primer pair AA386/AA387 introducing a 15 bp overhang to *fbx15* 5' flanking region. *fbx15* was amplified from ANCS07 gDNA with primer pair AA388/AA389 without stop codon introducing 15 bp overhang to *rfp* and 20 bp overhang to ^{P}*gpdA.* The primer pair AA390/BJ319 was used to amplify *rfp* from pME4921. ^{P}*gpdA* and *fbx15* were ligated by fusion-PCR (Szewczyk *et al.*, 2006). Fused ^{P}*gpdA*- *fbx15* together with *rfp* were cloned into *Swa*I restriction site of

pME4951 in a seamless cloning reaction, resulting in pME4953. Gene cassette excised with *Mss*I was integrated into AGB1265 to generate AGB1267. Southern hybridisation was utilised to confirm correct on-locus integration.

Construction of BiFC plasmids and strains for localisation determining interactions of Fbx15 with FidA and OefC

BiFC experiments were utilised using the bidirectional nitrate-inducible ^{P}*niiA*/^{P}*niaD* promoter and terminators with ectopic integration in respective strains. gDNA of ANCS07 was used as template for *fbx15*, *fidA* and *oefC* amplification. Constructed plasmids were sequenced with the primers AA27, AAA28, OZG78, OZG79. pChS379 (C. Sasse, prs. com.) including a phleo resistance non-recyclable marker cassette (phleo^{NRM}) used as backbone plasmid. All constructed plasmids were ectopic integrated into ANCS07.

For the *fbx15-oefC* BiFC construct *cyfp* was amplified with primer pair AA24/OZG388 from pME4302 introducing 15 bp overhangs to ^{P}*niaD* and *fbx15*. *fbx15* was amplified with primer pair AA372/AA373 introducing 15 bp overhangs to *cyfp* and ^{T}*niaD* and was ligated with *cyfp* by fusion-PCR (Szewczyk *et al.*, 2006) with primer pair AA24/AA372. *nyfp* was amplified with primer pair AA25/OZG387 introducing a 15 bp overhang to ^{P}*niiA*. *oefC* was amplified with AA370/371 introducing 15 bp overhangs to *nyfp* and ^{T}*niiA*. Both fragments were ligated with primer pair AA25/AA371 by fusion-PCR (Szewczyk *et al.*, 2006). Cloning was performed in two steps cloning *cyfp-fbx15* into the *Pme*I restriction site of pChS379 and *nyfp:oefc* into the *Swa*I restriction site in seamless cloning reactions, resulting in pME4955. pME4955 was integrated into ANCS07 to generate AGB1268.

As control *cyfp*, amplified with primer pair AA24/AA44 introducing 15 bp overhangs to ^{P}*niaD* and ^{T}*niaD*, was cloned into the *Pme*I restriction site of pChS379 in a seamless cloning reaction. The previously obtained *nyfp:oefC* fusion fragment was cloned into the *Swa*I restriction site of pChS379, generating pME4958. pME4958 was integrated into ANCS07, resulting in AGB1271.

The BiFC construct for the interaction of *fbx15* and *fidA* was obtained by amplifying *fidA* with primer pair AA374/AA375 introducing 15 bp overhangs to *nyfp* and ^{T}*niiA*. *nyfp* was amplified with primer pair AA25/OZG387 introducing a 15 bp overhang to ^{P}*niiA. nyfp* and *fidA* were ligated through fusion-PCR (Szewczyk *et al.*, 2006) with primer pair AA25/AA375. Previously obtained *cyfp-fbx15* and *nyfp:fidA* were cloned into pChS379 in two steps. *cyfp-fbx15* was cloned into the *Pme*I restriction site of pChS379 and *nyfp:fidA* into the *Swa*I restriction site in seamless cloning reactions,

resulting in pME4956. AGB1269 was generated by integrating pME4956 into ANCS07.

As control *cyfp*, amplified with primer pair AA24/AA44 introducing 15 bp overhangs to ^{P}*niaD* and ^{T}*niaD*, was cloned in a seamless cloning reaction into the *Pme*I restriction site of pChS379. *nyfp-oefC,* previously obtained by fusion-PCR (Szewczyk *et al.*, 2006), was cloned into the *Swa*I restriction site of pChS379 in seamless cloning reactions, generating pME4959. To generate AGB1272, pME4959 was integrated into ANCS07.

For all BiFC experiments an *fbx15* control was generated. *nyfp*, amplified with primer pair AA25/AA44 introducing 15 bp overhangs to ^{P}*niiA* and ^{T}*niiA*. *nyfp* was cloned into the *Swa*I restriction site of pChS379 and *cyfp-fbx15* fusion fragment, previously obtained by fusion-PCR (Szewczyk *et al.*, 2006), was cloned into the *Pme*I restriction site of pChS379 in seamless cloning reactions, generating pME4957. pME4957 was integrated into ANCS07, resulting in AGB1270. All BiFC strains were verified by PCR of gDNA.

Construction of plasmids and strains for Δ*oefC* and complementation

ANCS07 gDNA was used as template to construct the Δ*oefC* strain. *oefC* 5' flanking region (1.3 kb) with primer pair AA337/AA338 introducing 15 bp overhangs to pBluescript SK+ and the *six*-site of phleo^{RM} with a *Pme*I restriction site between *oefC* 5' flanking region and phleo^{RM} for further cloning. *oefC* 3' flanking region (1.8 kb) was amplified with primer pair AA339/AA340 introducing 15 bp overhangs to the *six*-site of phleo^{RM} and pBluescript SK+. pChS315 (C. Sasse, prs. com.) was utilised for cloning in two steps. *oefC* 5' flanking region was cloned into the *Swa*I restriction site and *oefC* 3' flanking region was cloned into the *Pml*I restriction site in seamless cloning reactions, resulting in pME4960. The gene cassette was excised with *Swa*I and transformed into ANCS07 to generate AGB1273.

Construction of the complementation plasmid was generated by amplifying *oefC* 5' flanking region and *oefC* gene (3.3 kb) with primer pair AA337/AA346 introducing 15 bp overhang to pBluescript SK+ and the *six*-site of phleo^{RM}. The previously obtained *oefC* 3' flanking region and the *oefC* 5' flanking region with *oefC* were cloned into pChS315 (C. Sasse, prs. com.) in two steps. *oefC* 5' flanking region-*oefC* was cloned into *Swa*I restriction site and *oefC* 3' flanking region was cloned into *Pml*I restriction site in seamless cloning reactions, resulting in pME4961. Gene cassette was excised with *Swa*I and transformed into AGB1273 to generate AGB1274. Correct on-locus integration for AGB1273 and AGB1274 was verified with Southern hybridisation after marker recycling.

Construction of plasmids and strains for N-terminal GFP-tagged OefC in wild type- and Δ*fbx15* background strains

oefC was tagged on its N-terminus with *sgfp*. *sgfp* was amplified from pME4292 with primer pair AA328/AA342 with start codon and without stop codon introducing 15 bp overhangs to *oefC* 5' flanking region and *oefC*. *oefC* was amplified with primer pair AA343/AA344 introducing 15 bp overhang to *sgfp* and the *six*-site of phleo^{RM}. *sgfp* and *oefC* were cloned together into the *Pme*I restriction site of pME4960, resulting in pME4962. The gene cassette of pME4962 was excised with *Swa*I and transformed into AGB1273 to generate AGB1275 and into AGB1265 to generate AGB1277. Correct integration was confirmed by Southern hybridisation after marker recycling.

Construction of plasmid and strain for overexpressed N-terminal GFP-tagged OefC

^{P}*gpdA* was used to generate an overexpression of *oefC*. ^{P}*gpdA* was amplified from pME4917 with primer pair AA347/BJ4 introducing a 15 bp overhang to *oefC* 5' flanking region. *sgfp:oefC* was amplified with primer pair AA344/AA350 introducing a 15 bp overhang to the *six*-site of phleo^{RM} and a 20 bp overhang to ^{P}*gpdA* using pME4962 as template. ^{P}*gpdA* and *sgfp:oefC* were ligated with primer pair AA344/AA347 by fusion-PCR (Szewczyk *et al.*, 2006) and cloned into the *Pme*I restriction site of pME4960, resulting in pME4963. The gene cassette of pME4963 was excised with *Swa*I and integrated into AGB1273 to generate AGB1276. Southern hybridisation was utilised to verify correct on-locus integration.

Construction of plasmids and strains for Δ*fidA* and C-terminal GFP-tagged complementation strain

The Δ*fidA* strain was constructed with ANCS07 gDNA used as template by amplifying *fidA* 5' flanking region (1.2 kb) with primer pair AA272/AA273 introducing 15 bp overhangs to pBluescript SK+ and the *six*-site of phleo^{RM} with a *Swa*I restriction site between *fidA* 5' flanking region and phleo^{RM} for further integrations. With primer pair AA270/AA271 *fidA* 3' flanking region (1.2 kb) was amplified, introducing 15 bp overhangs to the *six*-site of phleo^{RM} and pBluescript SK+. The pChS315 (C. Sasse, prs. com.) was utilised for cloning in two steps. *fidA* 5' flanking region was cloned into the *Swa*I restriction site and *fidA* 3' flanking region was cloned into the *Pml*I restriction site in seamless cloning reactions, resulting in pME4965. The excised gene cassette of pME4965 with *Mss*I was transformed into AfS35 to generate AGB1278. Correct integration of AGB1278 was confirmed by Southern hybridisation before and after marker recycling.

To construct the complementation plasmid pME4966 *fidA* 5' flanking region and *fidA* without stop codon (5.3 kb) from ANCS07 gDNA with primer pair AA272/AA274 introducing 15 bp overhangs to pBluescript SK+ and C-terminal located *sgfp*. *sgfp* was amplified from pME4917 with primer pair AA186/OZG207 with 15 bp overhang to the *six*-site of phleo^{RM}. *fidA* 5' flanking region-*fidA* and *sgfp* were ligated by fusion-PCR (Szewczyk *et al.*, 2006) with primer pair AA186/AA272. The fused fragment *fidA* 5' flanking region-*fidA*:*sgfp* and *fidA* 3' flanking region (1.2 kb), amplified with primer pair AA270/AA271 introducing 15 bp overhangs to the *six*-site of phleo^{RM} and pBluescript SK+, were cloned in two steps into pChS315 (C. Sasse, prs. com.). *fidA* 5' flanking region-*fidA*:*sgfp* was cloned into *Swa*I restriction site and *fidA* 3' flanking region into *Pme*I restriction site with seamless cloning reactions. The excised gene cassette with *Mss*I was integrated into AGB1278, resulting in AGB1279. Correct integration of AGB1279 was confirmed by Southern hybridisation after marker recycling.

Construction of plasmid and strain for overexpressed N- and C-terminal GFP-tagged FidA

Overexpression of *fidA* was obtained using ^{P}*gpdA* for induction of multiple copies of the *fidA* gene transcript. Construction of overexpressed C-terminal GFP-tagged *fidA* was performed by amplifying ^{P}*gpdA* from pME4917 with primer pair AA332/BJ4 introducing a 15 bp overhang to *fidA* 5' flanking region. *fidA:sgfp* was amplified with primer pair AA186/AA333 introducing a 15 bp overhang to the *six*-site of phleo^{RM} and a 20 bp overhang to ^{P}*gpdA*. Through fusion-PCR (Szewczyk *et al.*, 2006) ^{P}*gpdA* and *fidA:sgfp* were ligated with primer pair AA186/ AA332 and cloned in a seamless cloning reaction into the *Swa*I restriction site of pME4965, resulting in pME4967.

Overexpressed, N-terminal GFP-tagged *fidA* was obtained by amplifying ^{P}*gpdA:sgfp* with primer pair AA329/AA332 from pME4963 introducing a 15 bp overhang to *fidA* 5' flanking region. *fidA* was amplified with primer pair AA354/AA366 introducing a 15 bp overhang to the *six*-site of phleo^{RM} and a 20 bp overhang to *sgfp*. Through fusion-PCR (Szewczyk *et al.*, 2006) ^{P}*gpdA:sgfp* and *fidA* were ligated with primer pair AA332/AA354 and cloned into the *Swa*I restriction site of pME4965 in a seamless cloning reaction, resulting in pME4969.

AGB1280 was generated by integration of the excised gene cassette with *Mss*I of pME4967 into AGB1278. Integration of excised gene cassette with *Mss*I of pME4969 results in AGB1282. Southern hybridisation after marker recycling was utilised to verify correct integration.

Construction of plasmid and strain for N-terminal GFP- and HA-tagged FidA

N-terminal GFP-tagged *fidA* was obtained by amplifying *sgfp* from pME4963 with primer pair AA329/AA367 introducing a 15 bp overhang to *fida* 5' flanking region. *fidA* was amplified without start codon with primer pair AA366/AA354 introducing a 15 bp overhang to the *six*-site of phleo^{RM} and a 20 bp overhang to *sgfp*. *sgfp* and *fidA* were ligated by fusion-PCR (Szewczyk *et al.*, 2006) with primer pair AA354/AA367 and cloned into the *Swa*I restriction site of pME4965 in a seamless cloning reaction, generating pME4968.

HA-tagged *fidA* was constructed by amplifying *fidA* from ANCS07 gDNA with primer pair AA354/AA368 introducing 15 bp overhangs to *fidA* 5' flanking region and the *six*-site of phleo^{RM}. AA368 also introduce the N-terminal HA-tag (5'-TAC CCC TAC GAC GTC CCC GAC TAC GCC-3') with a start codon. *ha:fidA* was cloned into the *Swa*I restriction site of pME4965 in a seamless cloning reaction, resulting in pME4970.

AGB1281 was obtained by integration of the excised gene cassette of pME4968 with *Mss*I into AGB1278. AGB1283 was obtained by integration of the excised gene cassette of pME4970 with *Mss*I into AGB1278. Correct integration was verified by Southern hybridisation after marker recycling.

Construction of plasmids and strains for cross complementations of *fbx15*^{AN}, *oefC*^{AN} into *A. fumigatus* and *fbx15*^{AF}, *oefC*^{AF} into *A. nidulans*

The *fbx15*^{AN} gene was transformed into *A. fumigatus* by amplifying *fbx15*^{AN} with primer pair AA384/AA385 introducing 15 bp overhangs to *fbx15*^{AF} 5'- flanking region and the *six*-site of ptrA^{RM}. *fbx15*^{AN} was cloned in a seamless cloning reaction into the *Swa*I restriction site of pME4538, generating pME4950. *Mss*I excised gene cassette was transformed into AfGB128, resulting in AfGB460.

fbx15^{AF} was transformed into *A. nidulans* by amplifying *fbx15*^{AF} with primer pair AA382/AA383 introducing 15 bp overhangs to *fbx15*^{AN} 5'- flanking region and the *six*-site of phleo^{RM}. *fbx15*^{AF} was cloned in a seamless cloning reaction into the *Swa*I restriction site of pME4538, generating pME4954. *Mss*I excised gene cassette was transformed into AFGB128, resulting in AGB1284.

The *oefC*^{AN} gene was integrated into *A. fumigatus* by amplifying *oefC*^{AN} with primer pair AA344/AA357 introducing 15 bp overhangs to *oefC*^{AF} 5'- flanking region and the *six*-site of ptrA^{RM}. The fragment *oefC*^{AN} was cloned into the *Pme*I restriction site of pME4936 in a seamless cloning reaction, resulting in pME4939. *Swa*I excised gene cassette was transformed into AfGB438, resulting in AfGB461.

oefC^{AF} was transformed into *A. nidulans* by amplifying *oefC*^{AF} with primer pair AA327/AA358 introducing 15 bp overhangs to *oefC*^{AN} 5'- flanking region and the *six*-

site of phleo^{RM}. *oefC*^{AF} was cloned in a seamless cloning reaction into the *Pme*I restriction site of pME4960, generating pME4964. *Swa*I excised gene cassette was transformed into AGB1273, resulting in AGB1285.

9 Genetical manipulation techniques of microorganisms

9.1 Transformation in bacteria

Transformation into *E. coli* was performed as described (Douglas Hanahan, Jessee and Bloom, 1991; Inoue, Nojima and Okayama, 1990). *E. coli* chemical competent cells were added to plasmid DNA and incubated for 30 min on ice and subsequently heat shocked at 42°C for approx. 30 to 45 s for plasmid uptake. 800 µl LB medium were added to the cells on ice. The mixture of competent cells and plasmid DNA was shaken for 30 min at 37°C on a rotary shaker and collected by centrifugation for two min at 13000 rpm. Transformants were plated on LB plates supplemented with 100 µg/ml ampicillin as selective agent. Plates were incubated o/n at 37°C upside down to obtain suitable clone shapes for further application. The successful uptake of plasmids was verified by screening *E. coli* transformants through amplification of fragments specific for respective plasmids with PCR (colony-PCR).

9.2 Transformation in *Aspergillus*

Polyethylene glycol-mediated protoplast fusion of *A. fumigatus* and *A. nidulans* was described before in Punt and van den Hondel, 1992. For *A. fumigatus* strains constructed in this study AfS35 (Krappmann, Sasse, *et al.*, 2006) and AfS35 derived strains were used as host strains. AfS35 was used as wild type (WT). Af293.1 (McCluskey *et al.*, 2010), containing a *pyrG1* mutation, was utilised for BiFC experiments as host strain. For *A. nidulans* strains generated in this study ANCS07 (C. Sasse, prs. com.) and its derivations were used as host strains. ANCS07 was used as WT. AfS35 and ANCS07 harbour the Δ*nkuA* and Δ*nkuA* mutation leading to increased homologous recombination during transformation leading to on-locus integration of linearized genetic constructs (Krappmann, Sasse and Braus, 2006; Nayak *et al.*, 2006).

A. nidulans and *A. fumigatus* host strains were cultivated vegetatively for 16 to 24 h on a rotary shaker at 37°C. Grown mycelium was harvested by filtering the medium through a Miracloth filter (Merck KGaA) and washed with sterile citrate buffer (150 mM KCl, 50 mM Na-citrate, 580 mM NaCl, pH 5.5). Protoplasts were received by transferring the washed mycellium to protoplastation solution, which was obtained by

dissolving 30mg/ml Vinoflow® Max or Vinotaste® Pro from NOVOZYMES (Bagsvaerd, Denmark) in sterile citrate buffer and sterile filtration through 0.5 µm filters (Sarstedt). For receiving *A. nidulans* transformations 15 mg/ml lysozyme (Serva Electrophoresis GmbH) was additionally supplemented to the protoplastation solution. The mixture of mycelium and protoplastation solution was incubated for 90 to 115 min at 30°C under constant agitation at 80 rpm. Received protoplasts were monitored by microscopy and sterile filtered through a sterile Miracloth filter (Merck KGaA) into a precooled sterile 50 ml centrifuge tube (Sarstedt) on ice. The protoblast-containing solution was filled up to 50 ml with 4°C cold sterile STC 1700 buffer (50 mM $CaCl_2$, 35 mM NaCl, 1.2 M sorbitol, 10 mM Tris pH 5.5) and left for 10 min on ice. Protoplasts were subsequently centrifuged at 2500 rpm at 4°C for 12 min, washed with 30 ml 4°C cold sterile STC1700. Centrifugation was repeated at 2500 rpm at 4°C for 12 min. Approx. 10 µg linearized DNA was added to the protoplasts for the integration on locus or 10 µg of circular DNA was added for ectopic integration of BiFC constructs and incubated for 30 min on ice. 1.25 ml of sterile PEG solution (50 mM $CaCl_2$, 60% (v/v) PEG4000, 10 mM Tris pH 7.5) was added gradually (250 µl, 250 µl, 850 µl) and mixed briefly by careful inverting to increase the DNA uptake of the protoplasts and immediately afterwards incubated for 40 min over ice. The DNA-protoplast mixture was washed with sterile 4°C cold STC1700, centrifuged at 2600 rpm at 4°C for 15 min and distributed on solid AMM plates, supplemented with 1.2 M sorbitol and respective selecting agents. Pyrithiamine (125 ng/ml), hygromycin G (200 µg/ml) and phleomycin (20 µg/ml) were used in this study as selective agents. After three to seven days transformants were picked and individualized on selective AMM or LM plates. In order to eliminate the marker cassettes the genome of the respective strains, individualization of transformants was performed on xylose-containing AMM plates 0.5% (w/v) glucose, 7 mM KCl, 11.2 mM KH_2PO_4, 2 mM MgSO4, 70 mM NaNO3, 0.1% (v/v) trace element solution, 0.5% (w/v) xylose, pH 5.5) (Hartmann *et al.*, 2010). Southern hybridisation was used to verify the correct integration of transformed constructs in *A. fumigatus* and *A. nidulans*.

9.3 Southern hybridisation

A. fumigatus and *A. nidulans* transformants generated in this study were confirmed by Southern hybridisation analysis (Southern, 1975). Certain restriction enzymes (Thermo Fisher Scientific) were chosen to detect a span of DNA fragments, which were cut inside the respective gene locus and outside of the integrated construct to verify on-locus integration. Digested DNA was separated by agarose gel

electrophoresis. The gel was washed in three steps under constant agitation at RT: 10 minutes in Wash buffer 1 (0.25 M HCl) for depurination, 25 min in Wash buffer 2 (1.5 M NaCl, 0.5 M NaOH) for denaturation, and 30 min in Wash buffer 3 (1.5 M NaCl, 0.5 M Tris pH 7.4) for neutralisation. An Amersham™ Hybond™-Nylon membrane from GE Healthcare (Munich, Germany) was used to transfer the gDNA fragments by dry blotting for 2h or o/n. The membrane was dried at 70°C for ten minutes and fragmented DNA was cross-linked by exposure to UV-light for three minutes per side of the membrane. DNA fragments were labelled with the probe to detect specific regions and were detected with Amersham™ Gene Images AlkPhos Direct Labelling and Detection System (GE Healthcare) according to the manufacturer's instructions. Membrane-bound DNA fragments were labelled with the probe by hybridisation at 60°C rotating o/n. The probe-labelled membrane was washed with post-hybridisation buffer 1 (2% blocking reagent, 1 mM $MgCl_2$, 2 M urea, 150 mM NaCl, 50 mM Na_3PO_4, 50 mM SDS) for ten minutes at 60°C rotating and with the pre-hybridisation buffer 2 (1 M NaCl, 1 M Tris base, pH 10) twice for five minutes under constant agitation at RT. Labelled DNA bands were detected by utilising the CDP-Star Detection Reagent (GE Healthcare), incubation for two min and exposure on an Amersham™ Hyperfilm™ ECL (GE Healthcare). An Optimax (Protec GmbH&Co.KG) film processor was used to develop the film.

10 Protein methods

10.1 Extraction of proteins

Proteins were extracted from vegetatively grown strains in liquid AMM. Mycelium was harvested through sterile Miracloth (Merck KGaA), washed with 0.96% NaCl containing 1% dimethyl sulfoxide (DMSO) and 10mM phenylmethylsulfonyl fluorid (PMSF), dried, frozen in liquid nitrogen and pulverized with a table mill (Retsch Technology GmbH). 300 µl B* buffer (1 mM EDTA, 10% (v/v) glycerol, 0.1% (v/v) NP-40, 300 mM NaCl, 100 mM Tris pH 7.5) supplemented with 1.5 mM DTT, 1 tablet/50 ml complete EDTA-free protease inhibitor cocktail (Roche Diagnostics GmbH), 1 mM PMSF, phosphatase inhibitor mix (1 mM NaF, 0.5 mM sodium-orthovanadate, 8 mM ß-glycerolphosphate disodium pentahydrate and 1.5 mM benzamidine) was added to the grounded pulverized mycelium and homogenized. After a centrifugation step for ten min at 13000 rpm at 4°C, the supernatant was transferred into a new reaction tube, stored at -20°C or used for further analysis.

10.2 GFP-/RFP-trap

Proteins tagged with GFP or RFP were pulled with GFP-trap_A and RFP-trap_A agarose beads (Chromotek). An amount of 5 ml of extracted proteins (Chapter 9.1) were incubated with 20 µl GFP-Trap_A or RFP-Trap_A beads, which were equilibrated to B* buffer used for protein extraction. Protein extracts were incubated with beads for two hours at 4°C on a rotator. Beads bound to tagged proteins were washed twice for two minutes and were transferred to a new reaction tube. Elution of the pulled proteins was performed by boiling the beads in 80 µl SDS-sample buffer for ten minutes at 95°C and used directly for SDS-PAGE followed by western hybridisation or stored at -80°C.

10.3 SDS-PAGE and western hybridisation

Protein extracts were separated according to the molecular mass by sodium dodecyl sulphate polyacrylamide gel electrophoresis (SDS-PAGE; Smith, 1984). A mixed solution of protein extract (Chapter 9.1) and sample buffer (0.3% (w/v) bromophenol blue, 30% (v/v) glycerol, 7% (w/v) SDS, 250 mM Tris-HCl pH 6.8, 15% (v/v) β-mercaptoethanol), was boiled for five min at 95°C and loaded on 10% acrylamide gels [Running gel: 2.8 ml H_2O, 3.8 ml Tris buffer pH 8.8 (stock: 1 M), 100 µl SDS (stock: 10%), 3.3 ml polyacrylamide (stock: 30%), 100 µl ammonium persulfate (APS; stock: 10%), 10 µl *N,N,N′,N′*-tetramethylethane-1,2-diamine (TEMED); stacking gel: 50 µl APS (stock: 10%), 3 ml H_2O, 650 µl polyacrylamide (stock: 30%), 50 µl SDS (stock: 10%), 5 µl TEMED; 625 µl Tris buffer pH 6.8 , for two gels], rinsed in running buffer (250 mM glycerol, 0.1% SDS, 25 mM Tris-base) with a voltage of 120-200 V in Mini-PROTEAN Tetra Cell (Bio-Rad Laboratories GmbH) at RT. As size standard the Prestained Protein Ladder (Thermo Fisher Scientific) was used.

Separated proteins from SDS gels were blotted semi wet using a Mini Trans-Blot Cell (Bio-Rad) on an Amersham™ Protran™ 0.45 µm NC nitrocellulose membranes (GE Healthcare) in transfer buffer (192 mM glycine, 0.02% (w/v) SDS, 25 mM Tris) on ice for 1h at 100 V or o/n at 35 V. PonceauS (0.2% PonceauS, 3% TCA) staining was used to control protein transfer efficiency and quantification analysis. The membrane was blocked in 1x TBST [150 mM NaCl, Tris buffered Saline and Tween-20: 50 mM Tris, 0.05% (v/v) Tween-20] with 5% (w/v) skim milk powder from Sucofin TSI GmbH&Co.KG (Zeven, Germany) or 3% (w/v) BSA (Carl Roth GmbH&Co.KG) depending on antibody requirement for 1h at RT or o/n at 4°C under constant agitation to prevent unspecific antibody-binding. The primary antibodies α-GFP mouse from Santa Cruz Biotechnology (Dallas, Texas, USA) diluted 1:1000, α-RFP

mouse (Chromotek) diluted 1:1000 and α-HA mouse (Sigma-Aldrich Chemie GmbH) diluted 1:2000 were mixed in TBST and 5% skim milk powder. The anti-phospho Ser/Thr ab17464 rabbit antibody (Abcam) diluted 1:1000 and the α-Ubiquitin clone P4D1-A11 mouse (Merck KGaA) diluted 1:5000 were mixed in TBS or TBST (0.05% Tween-20) containing 3% BSA. Membranes were incubated with primary antibodies three hours at RT or o/n at 4°C under constant agitation. Membranes were washed in TBST or TBS three times for five min at RT under constant agitation. The secondary antibodies peroxidase coupled rabbit anti-mouse (Jackson ImmunoResearch) diluted 1:2000 in TBST and 5% skim milk powder or TBST with 3% BSA or goat anti-rabbit (Invitrogen) diluted 1:2500 in TBS with 3% BSA were incubated on membranes for 1h at RT under constant agitation. Membranes were washed in TBST or TBS three times for five min at RT under constant agitation. Proteins were detected through horseradish peroxidase substrate luminol based chemiluminescence by preparing two solutions (solution 1: 2.5 mM luminol, 400 µM paracoumarat, 100 mM Tris-HCl pH 8.5; solution 2: 5.4 mM H_2O_2, 100 mM Tris-HCl pH 8.5). Both solutions were applied contemporaneous to the membrane and incubate in darkness for two min under constant agitation. Detection of signals was performed with the Fusion SL chemiluminescence detector (Peqlab Biotechnology GmbH), operated with the Fusion 15.18 software (Vilber Lourmat) or using an Amersham Hyperfilm ECL film (GE Healtcare Life Sciences) developed with the Optimax (Protec GmbH&Co.KG) film processor.

11 Secondary metabolite extraction

11.1 Extraction of vegetatively induced secondary metabolites in *A. fumigatus*

Extraction of secondary metabolites of vegetative grown cultures was performed followed by the description from Gerke and collaborators (Gerke *et al.*, 2012). $1*10^8$ of *A. fumigatus* spores were grown vegetative in AMM at 37°C on a rotary shaker for 48h. Mycelia was separated from media by filtration through Miracloth. The media were adjusted to pH 5 with HCl and mixed with equal amounts of ethyl acetate in a shaking flask to separate secondary metabolites from the forming water phase. The secondary metabolite-ethyl acetate mix was evaporated in a round bottom flask after the obtained water phase was discarded. Evaporation was performed at 37°C under constant gyration in a Hei-VAP-Advantage rotary evaporator from Heidolph Instruments GmbH&Co.KG (Schwabach, Germany) with a MWG Lauda RM6 from

Lauda-Brinkmann LP (Delran, NJ, USA) and a Laboxact KNF vacuum system (Sigma-Aldrich Chemie GmbH). Obtained secondary metabolites were resolved in 3 ml ethyl acetate, transferred into small glass tubes and evaporated at 37°C under constant gyration in an evaporator. Glass tubes were stored at - 20°C. For measurement with high-performance liquid chromatography (HPLC) secondary metabolites were resolved in 500 µl half acetonitrile, half LCMS grade water, centrifuged at 8°C at 13000rpm for ten min and transferred to a LCMS vial.

11.2 Analysis of secondary metabolites by high performance liquid chromatography (HPLC) coupled with a UV diode array detector (UV-DAD) and an evaporative light scattering detector (ELSD)

HPLC measurements were performed as described (Thieme, 2017). Dr. Jennifer Gerke executed the HPLC measurements (Department of Molecular Microbiology and Genetics, Georg-August University Göttingen, Germany).

20 µl of secondary metabolite extracts dissolved in 500 µl acetonitrile/ LCMS grade water [1:1] were analysed under gradient conditions (20% B to 100% B in 20 min) with a flow rate of 0.5 ml/min. The Geminyx III software from Goebel Instrumentelle Analytik GmbH (Au/Hallertau, Germany) was employed to analyse obtained HPLC data.

12 Microscopy

12.1 Photometric imaging

Conidiophore and cleistothecia development of *A. nidulans* strains was monitored on solid AMM media. $2*10^3$ spores were point inoculated and incubated for seven days at 37°C in light or dark with limited oxygen supply. The binocular microscope ZX12-ILLB2-200 (Olympus) equipped with a SC30 digital camera (Olympus) was used for quantification. Pictures were processed with the cellSens Dimension 1.4 software (Olympus).

12.2 Fluorescence microscopy

$2*10^3$ spores were grown vegetative in 500 µl AMM on sterile cover slips at 37°C in darkness for 18h. Media were removed carefully with paper tissue without destroying the mycelium. For stress induction 500 µl fresh AMM containing 3 mM H_2O_2 or 300 µM $CdSO_4$ was added to the samples and incubated for 1h at 37°C in dark. Media were again carefully removed, and the cover slip was put upside down on a sterile

glass slide prepared with 20 µl AMM. Cover slips were fixated with nail polish at the corners. 0.1% 4',6'-diamidino-2-phenylindole, DAPI (Carl Roth GmbH&Co.KG) or 0.1% Hoechst 33258 pentahydrate (Invitrogen) in AMM were used to stain nuclei immediately before microscopy. While monitoring stress conditions, AMM for microscopy was additionally supplemented with stress inducers, 3 mM H_2O_2 or 300 µM $CdSO_4$ and incubated for 1h. Fluorescence images were monitored with an Axiovert Observer Z1 (Carl Zeiss Microscopy GmbH) microscope equipped with a CoolSNAP ES2 (Photometrics) digital camera. Pictures were processed with the SlideBook 6.0 software package (Intelligent Imaging Innovations). Samples for microscopy were prepared on microscopic slides and cover slides from Chem-Solution GmbH (Neustadt, Germany).

13 *Galleria mellonella* larvae infection assay with *A. fumigatus* strains

The *Galleria mellonella* larvae infection assay with *A. fumigatus* strains was carried out as described in Renwick *et al.*, 2006 and Thieme, 2017 (Renwick *et al.*, 2006; Thieme, 2017). *Galleria mellonella* larvae were purchased from Fauna Topics GmbH (Marbach am Neckar, Germany). A group of 15 individual *Galleria mellonella* larvae per strain were infected with $8*10^6$ spores in 20 µl sterile 0.96% (w/v) NaCl, supplemented with 0.002% (v/v) Tween-80. In order to prevent contaminations with other microorganisms 10 µg/ml rifampicin was supplemented to each suspension. Mock infections with NaCl-Tween with rifampicin were performed for 15 larvae as control for each experimental repetition to ensure that the infection procedure itself is not responsible for observed mortality.

For the infection procedure Micro-Fine™+ 0.3 ml insulin syringes (BD Bioscience) were used, sterilized before and after each treatment with Melisepthol from Hajovital KG (Bendorf, Germany) and discarded after infection of three individuals to decrease contamination risk. Infected *Galleria mellonella* larvae and controls were kept at 30°C in darkness with litter the larvae arrived, each infection group separated from each other according to the used *A. fumigatus* strains. Survival was monitored daily. Dead larvae showing no movement upon contact and dark coloration were sorted out and stored at -20°C o/n prior to sterilization by autoclaving. Significances were determined with one-way Anova and Student's t-test by SISA (Uitenbroek, 1997).

III Results

1 Functions of Fbx15 protein encoding genes of *A. fumigatus* and *A. nidulans* partially overlap

1.1 Fbx15 is required for development in *A. nidulans* and secondary metabolism in *A. fumigatus* and *A. nidulans*

A. fumigatus Fbx15 mediates secondary metabolite homeostasis, stress tolerance as well as virulence (Jöhnk *et al.*, 2016). *A. nidulans* Fbx15 is involved in secondary metabolism indicated by the control of colony pigmentation and has a role in asexual and sexual development as the absence of *fbx15* results in decreased conidiation and block in cleistothecia formation (von Zeska Kress *et al.*, 2012).

A. fumigatus Fbx15 has a 59.8% identity to *A. nidulans* Fbx15 (Jöhnk *et al.*, 2016). *A. nidulans* Fbx15 is 653 aa long, whereas its counterpart in *A. fumigatus* consist of 655 aa. The aa sequence alignments have shown that *A. nidulans* Fbx15 contains one interaction motif. The motif shows 90% identity to motif 2 of *A. fumigatus* Fbx15 and is positioned at the same aa from 313 to 362 (Figure 12) (Jöhnk *et al.*, 2016). Fbx15 encompasses two mp NLS sequences close to the C-terminus in both fungi, named NLS1 and NLS2. The NLS1 (YEPPRKRLRRHY) of *A. nidulans* Fbx15 is positioned at aa 403 to 414. The NLS2 (VSRKRKCPID) of Fbx15 *A. nidulans* is positioned at aa 475 to 484. Two adjacent Ser residues were identified to be phosphorylated via LCMS-analysis, S468 (2%) and S469 (98%), in the human pathogen *A. fumigatus* (Jöhnk *et al.*, 2016). In *in silico* analysis via NetPhos 3.1, two adjacent Ser residues were found in *A. nidulans* Fbx15 that are phosphorylated with a probability of 52% for S445 and 99% for S446 (Figure 12).

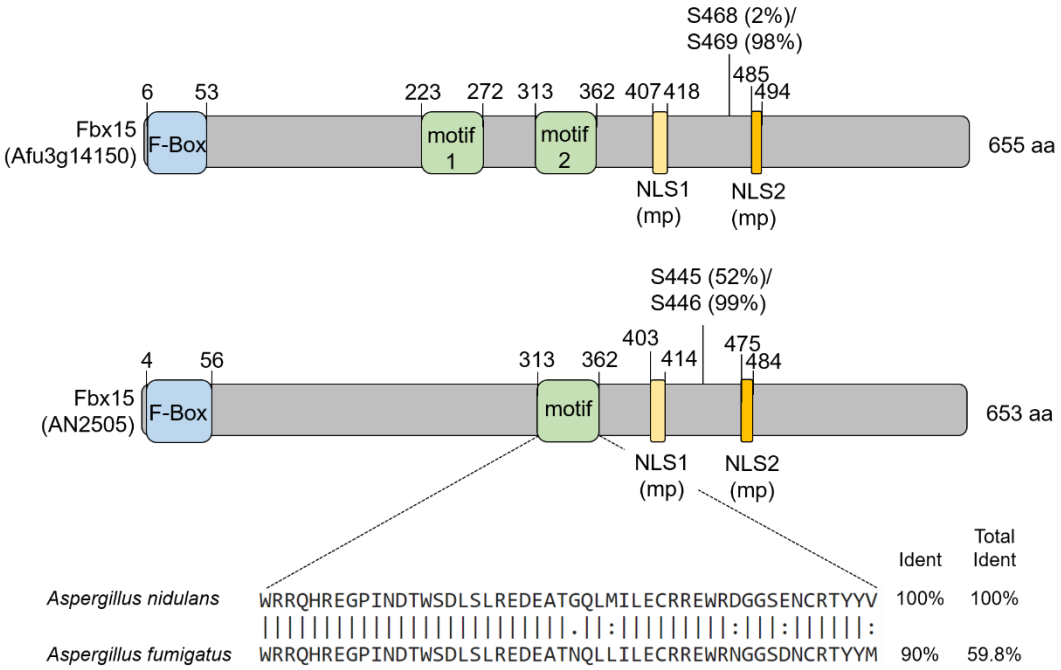

Figure 12: Comparison between the Fbx15 domain architectures of the deduced corresponding *A. fumigatus* and *A. nidulans* proteins. Deduced amino acid (aa) sequence alignments of Fbx15 shows that both F-box domains are located at the N-terminus in *A. fumigatus* Af293 at aa position 6 to 53 and *A. nidulans* FGSC A4 at aa position 4 to 56, respectively, and are followed by two motifs in *A. fumigatus* Fbx15 at aa position 223 to 272 for motif 1 (genus-specific) and at aa position 313 to 362 for motif 2. *A. nidulans* Fbx15 contains one motif with 90% identity to motif 2 of *A. fumigatus* Fbx15 at aa position 313 to 362. Two monopartite (mp) nuclear localisation signals (NLS) are identified at the C-terminal region at aa positions 407 to 418 (mp NLS1) and 485 to 494 (mp NLS2) in *A. fumigatus* Fbx15. *A. nidulans* Fbx15 contains two mp NLS sequences at aa positions 403 to 414 (mp NLS1) and 475 to 484 (mp NLS2) (http://nls-mapper.iab.keio.ac.jp/cgi-bin/NLS_Mapper_form.cgi). In *A. fumigatus* Fbx15 two adjacent serine (Ser) residues were identified to be phosphorylated, S468 with a probability of 2% and S469 with a probability of 98%. Putative adjacent phosphorylation sites at Ser residues between NLS1 and NLS2 in *A. nidulans* Fbx15 were determined with NetPhos 3.1 at S445 with a probability of 52% and S446 with a probability of 99% (http://www.cbs.dtu.dk/services/NetPhos/).

It was analysed which functions of *A. fumigatus* Fbx15 are able to be complemented by *A. nidulans* Fbx15 and *vice versa*. *A. fumigatus fbx15* gDNA was integrated in the locus of *A. nidulans fbx15* and *vice versa*. The resulting strains were compared to the corresponding Δ*fbx15* and their complementation strains. Growth assays on plates were performed in darkness with (only for *A. fumigatus*) and without limited oxygen supply enhancing cleistothecia formation in *A. nidulans* (Park *et al.*, 2019).

A. fumigatus Δ*fbx15* is known to show an orange pigmentation at the bottom of the colony compared to a pale yellowish pigmentation of WT, as well as greenish pigmented conidia like WT (Jöhnk *et al.*, 2016). *A. nidulans fbx15* gDNA introduced on-locus of *A. fumigatus* Δ*fbx15* (*fbx15*^{ANcomp}) showed a WT-like pale pigmented colony (Figure 13A, bottom).

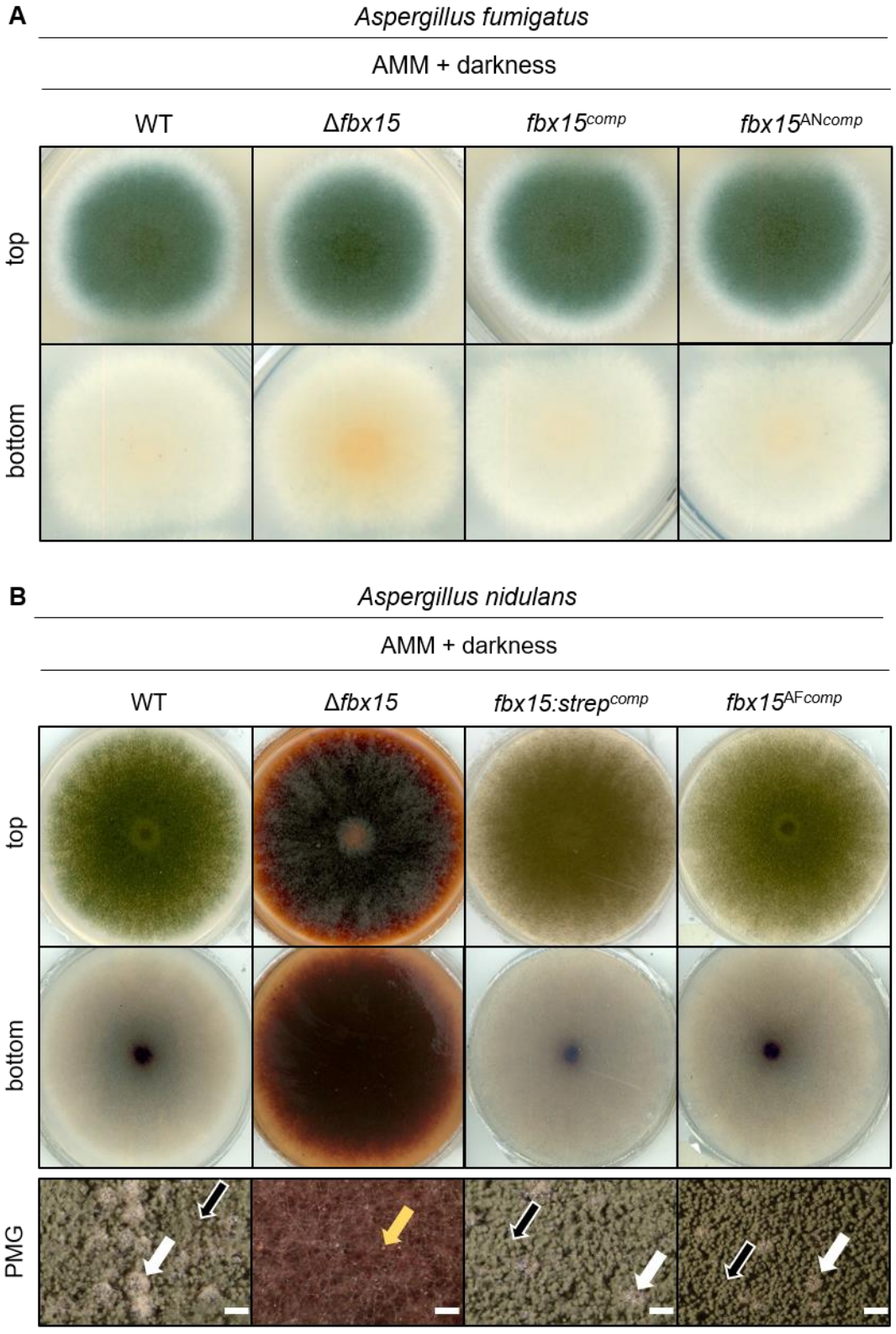
A
Aspergillus fumigatus
AMM + darkness
WT
Δfbx15
fbx15comp
fbx15ANcomp
top
bottom
B
Aspergillus nidulans
AMM + darkness
WT
Δfbx15
fbx15:strepcomp
fbx15AFcomp
top
bottom
PMG

Figure 13: The *A. fumigatus* and *A. nidulans fbx15* genes mutually complement colony pigmentation phenotypes of the corresponding deletion strains as well as developmental phenotypes of the *A. nidulans* Δ*fbx15* mutant strain. (**A**) The *A. fumigatus fbx15* gene (*fbx15*^{comp}) and the *A. nidulans fbx15* gene (*fbx15*^{ANcomp}) were integrated on-locus of the *A. fumigatus fbx15* deletion strain (Δ*fbx15*). 2*10^3 spores of *A. fumigatus* strains were point inoculated and incubated for three days on *Aspergillus* minimal medium (AMM) at 37°C in darkness. The *fbx15*^{comp} and *fbx15*^{ANcomp} strains complement the pale yellowish pigmentation of WT in Δ*fbx15* (bottom). (**B**) The *A. nidulans fbx15* gene fused to strep (*fbx15:strep*^{comp}) and the *A. fumigatus fbx15* gene (*fbx15*^{AFcomp}) were integrated on-locus of the *A. nidulans fbx15* deletion strain (Δ*fbx15*). 2*10^3 spores of *A. nidulans* strains were point inoculated on AMM and incubated at 37°C for seven days in darkness with limited oxygen supply. *A. nidulans* Δ*fbx15* shows a dark reddish pigmented colony with less and red pigmented conidia (yellow arrow) compared to a yellowish pigmented colony (bottom) with abundant green pigmented conidia (top) of wild type (WT), *fbx15:strep*^{comp} and the *fbx15*^{AFcomp} (black-white arrows). Cleistothecia formation is complemented by *fbx15:strep*^{comp} and the *fbx15*^{AFcomp} in *A. nidulans* Δ*fbx15* (white arrows). Experiments were performed with two independent transformants and two biological replicates. PMG: photomicrograph, scale bars: 200 µm.

The *A. nidulans* Δ*fbx15* colony shows a dark reddish pigmentation with a thinned layer of reddish pigmented conidiospores (yellow arrow) and a blocked cleistothecia formation (von Zeska Kress *et al.*, 2012). On-locus of *A. nidulans* Δ*fbx15* integrated gDNA of *A. nidulans fbx15* fused to *strep* (*fbx15:strep*^{comp}) and *A. fumigatus fbx15* (*fbx15*^{AFcomp}) restored the brown yellowish pigmented colony with a dense greenish pigmented conidiospore layer like WT (Figure 13B, top and bottom, black-white arrows). Cleistothecia formation was restored in *fbx15:strep*^{comp} and *fbx15*^{AFcomp}, showing cleistothecia at the top of the colonies like WT (Figure 13B, white arrows).
The data show that *A. nidulans* Fbx15 recovers the *A. fumigatus* WT-like colony pale pigmentation presumably indicating its functionality in *A. fumigatus* secondary metabolite homeostasis and *vice versa*. Moreover, *A. fumigatus* Fbx15 is functional during asexual and sexual development in *A. nidulans* as conidiation and cleistothecia formation is recovered when *A. fumigatus fbx15* gDNA is introduced on-locus of *A. nidulans* Δ*fbx15*.

1.2 *A. nidulans* Fbx15 plays only a minor role in stress response contrary to *A. fumigatus* Fbx15

A. fumigatus fbx15 can complement colony and developmental phenotypes of *A. nidulans* Δ*fbx15* and *vice versa* during non-stress conditions. An *A. nidulans* Fbx15 function in stress response like for *A. fumigatus* Fbx15 has not yet been described (von Zeska Kress *et al.*, 2012). It was examined whether there is an *A. nidulans* mediated Fbx15 controlled stress response and whether heterologous *A. nidulans* Fbx15 is capable to perform the Fbx15-mediated stress response of

A. fumigatus. Corresponding phenotypical tests of the corresponding constructed fungal strains on different stress media were performed. The following stress detergents were used to introduce different stress environments: NaCl introduce osmotic stress; cadmium sulphate ($CdSO_4$) introduce heavy metal stress; H_2O_2 introduce oxidative stress; 3-amino-1,2,4-triazole (3-AT) introduce histidine starvation as it represents a histidine analogue triggering the inhibition of histidine biosynthesis by a feedback inhibition mechanism (Hilton *et al.*, 1965; Schürch *et al.*, 1974); exchange of glucose to lactose introducing carbon source alterations.

On minimal growth conditions *A. nidulans* Δ*fbx15* did not grow on media containing introducing heavy metal stress (300 µM $CdSO_4$). Colony sizes of *A. nidulans* Δ*fbx15* were comparable to WT and *fbx15:strep*^{comp} on media containing lactose as carbon source, histidine starvation (1 mM 3-AT), osmotic stress (1 M NaCl) or oxidative stress (2 mM H_2O_2). In locus of *A. nidulans* Δ*fbx15* integrated overexpressed *A. nidulans fbx15* fused to *rfp* (oe*fbx15:rfp*) resulted in a smaller colony size during histidine starvation and cadmium ion stress conditions compared to WT and *fbx15:strep*^{comp} whereas during carbon source exchange, osmotic stress and oxidative stress conditions oe*fbx15:rfp* showed WT-like colonies. The *A. fumigatus fbx15* gene integrated in the locus of *A. nidulans* Δ*fbx15* (*fbx15*^{AFcomp}) resulted in WT-like colony growth during all tested media containing carbon source exchange and included stress inducing detergents (Figure 14A).

A. fumigatus Δ*fbx15* was sensitive against all tested stressors resulting in a decreased colony size or no growth ability as previously described in Jöhnk *et al.* (Jöhnk *et al.*, 2016) (Figure 14B). The strain containing the overexpressed *A. fumigatus fbx15* (oe*fbx15*) gene integrated in the locus of *A. fumigatus* Δ*fbx15* had no effect on growth in comparison to WT and *fbx15*^{comp} during carbon source exchange, osmotic stress, cadmium ion stress and oxidative stress conditions. Media including histidine starvation resulted in an increased colony size for oe*fbx15* compared to colony sizes of WT and *A. fumigatus* Δ*fbx15* complementation (*fbx15*^{comp}). The strain containing the *A. nidulans fbx15* gene integrated in *A. fumigatus* Δ*fbx15* (*fbx15*^{ANcomp}) restored *A. fumigatus* WT-colony sizes for carbon source exchange, osmotic stress and cadmium ion stress conditions (Figure14B, black frames). During histidine starvation and oxidative stress conditions *fbx15*^{ANcomp} showed increased colony sizes compared to *A. fumigatus* Δ*fbx15* colonies but decreased colony sizes than colonies of WT and *fbx15*^{comp} (Figure 14B).

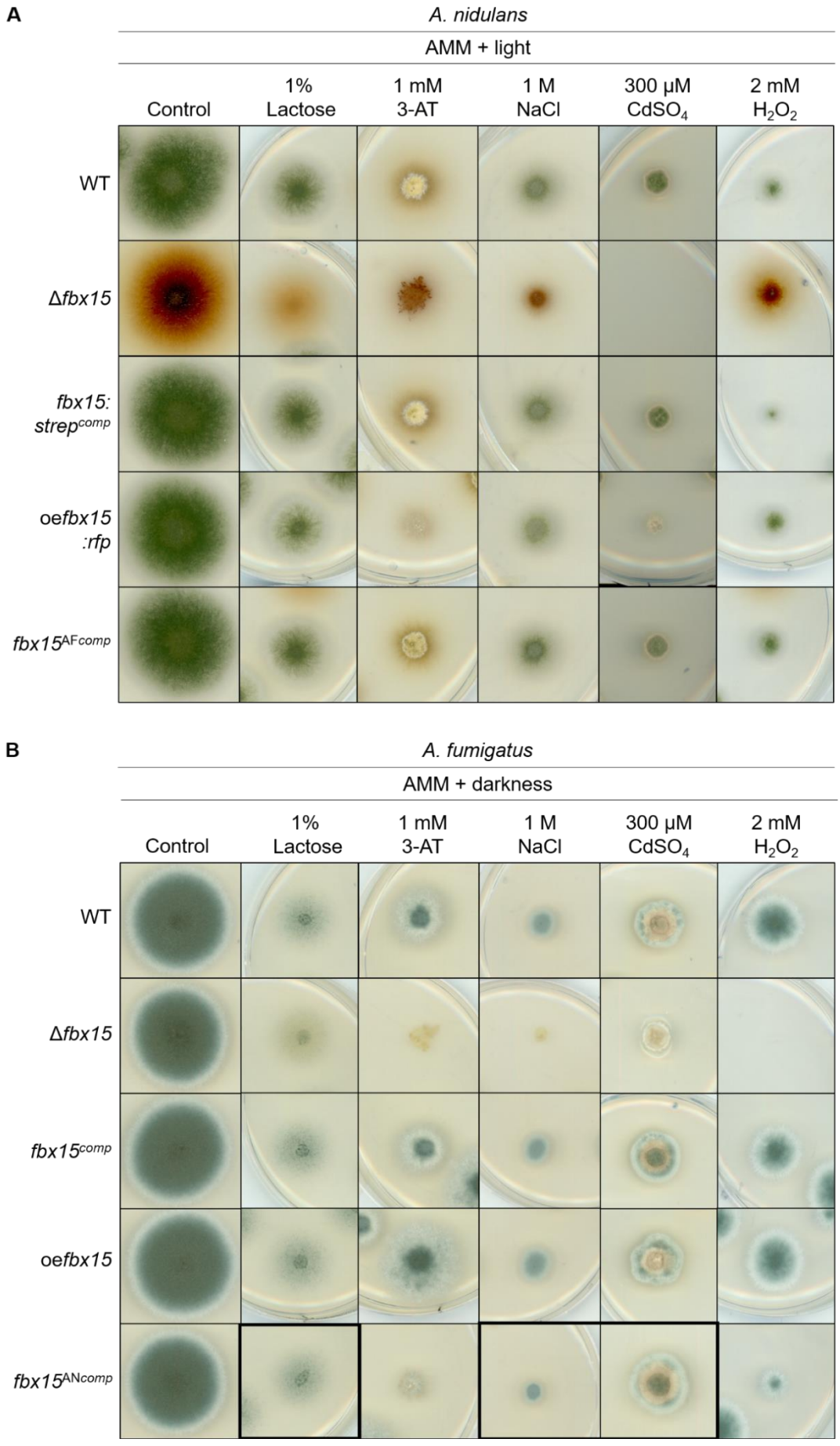
A
A. nidulans
AMM + light
Control
1% Lactose
1 mM 3-AT
1 M NaCl
300 µM CdSO4
2 mM H2O2
WT
Δfbx15
fbx15: strepcomp
oefbx15 :rfp
fbx15AFcomp
B
A. fumigatus
AMM + darkness
Control
1% Lactose
1 mM 3-AT
1 M NaCl
300 µM CdSO4
2 mM H2O2
WT
Δfbx15
fbx15comp
oefbx15
fbx15ANcomp

Figure 14: *A. nidulans fbx15* partially complements stress responses in *A. fumigatus* Δ*fbx15*. (**A**) The *A. nidulans fbx15* gene fused to strep (*fbx15:strep*^{comp}), an overexpressed *A. nidulans fbx15* gene using the constitutively active *gpdA* promoter and fused to *rfp* (oe*fbx15:rfp*) and the *A. fumigatus fbx15* gene (*fbx15*^{AFcomp}) were integrated on-locus of the *A. nidulans fbx15* deletion strain (Δ*fbx15*). 2*10^3 spores of *A. nidulans* strains were point inoculated on *A*spergillus minimal medium (AMM) and incubated at 37°C for three to five days in light without (control) and with different stressors. Δ*fbx15* does not grow on media containing cadmium sulphate (300 µM $CdSO_4$) compared to wild type (WT) and *fbx15:strep*^{comp}. On media containing lactose as sole carbon source, during histidine starvation induced by 3-amino-1,2,4-triazol (1 mM 3-AT), osmotic stress induced by natrium chloride (1 M NaCl) and oxidative stress induced by hydrogen peroxide (2 mM H_2O_2) Δ*fbx15* colonies have a comparable colony size as WT and *fbx15:strep*^{comp}. The oe*fbx15:rfp* strain shows a diminished colony growth during aa starvation and cadmium ion stress conditions compared to WT. During carbon exchange (glucose to lactose), osmotic stress and oxidative stress conditions oe*fbx15:rfp* phenocopies WT and *fbx15:strep*^{comp}. The *fbx15*^{AFcomp} strain phenocopies WT and *fbx15:strep*^{comp} on all tested media. Experiments were performed with at three biological replicates. (**B**) The *A. fumigatus fbx15* gene (*fbx15*^{comp}), an overexpressed *A. fumigatus fbx15* gene using the constitutively active *gpdA* promoter (oe*fbx15*) and the *A. nidulans fbx15* gene (*fbx15*^{ANcomp}) were integrated in the locus of *A. fumigatus* Δ*fbx15* strain. 2*10^3 spores of *A. fumigatus* strains were point inoculated on AMM and incubated at 37°C for three to five days in darkness without (-) and with different stressors. Growth on all tested stressor for Δ*fbx15* are diminished (glucose to lactose, 1 mM 3-AT, 1 M NaCl, 300 µM $CdSO_4$) or blocked (2 mM H_2O_2) compared to WT or *fbx15*^{comp} as described (Jöhnk *et al.,* 2016). Colony sizes of oe*fbx15* are in the same sizes than for WT and *fbx15*^{comp} on all tested media except 1 mM 3-AT, where the oe*fbx15* colony size is increased compared to WT and *fbx15*^{comp} colony sizes. The *fbx15*^{ANcomp} restores WT-phenotypes during osmotic stress, cadmium ion stress and exchanged carbon source (black frames). The *fbx15*^{ANcomp} colonies are decreased compared to WT- or *fbx15*^{comp} colonies but increased compared to Δ*fbx15* colonies on stress media including oxidative stress and aa starvation. Experiments were performed with at least three biological replicates.

These results show that Fbx15-mediated stress responses between *A. fumigatus*, which was earlier described (Jöhnk *et al.*, 2016), and *A. nidulans* are similar for cadmium ion heavy metal tolerance, osmotic stress and the versatility of lactose as sole carbon source. However, there is only a partial overlap in stress response because oxidative stress tolerance induced by H_2O_2 depends on *A. fumigatus* Fbx15, whereas *A. nidulans* Fbx15 is dispensable for oxidative stress tolerance but supports growth during histidine starvation induced by the analogue 3-AT. Due to these data it is indicated that the importance of Fbx15 regarding its role in stress tolerance could be due to interactions with different proteins.

1.3 Fbx15 interacting proteins

The interaction of Fbx15 with the co-repressor subunit SsnF had been analysed in more detail (Jöhnk *et al.*, 2016). Several candidate proteins were identified as possible *A. fumigatus* Fbx15 interaction partners by TAP analysis (37 candidates: Jöhnk *et al.*, 2016) or RFP-traps (66 candidates: Table S1) F-box proteins are exchangeable substrate receptors, which usually recognise proteins to be labelled with ubiquitin for 26S proteasome mediated degradation (Cardozo and Pagano, 2004). In contrast, Fbx15 is required for the nuclear location of SsnF in the nucleus, whereas SsnF stability seems to be unaffected (Jöhnk *et al.*, 2016). Among the putative Fbx15-interacting proteins are several additional control proteins for gene expression as the transcriptional regulators OefC, SrbB or FiAt (Jöhnk *et al.*, 2016). BiFC analysis were performed as additional evidence to verify a direct physical contact with Fbx15 within the cell. Direct interactions could be supported by monitoring signals for Fbx15 with the SREBP transcription factor SrbB involved in hypoxia adaptation in *A. fumigatus* (Chung *et al.*, 2014) as well as the uncharacterised putative *A. fumigatus* APSES transcription factor FiAt (Figure S1, S2, S5). BiFC analysis of *A. nidulans* Fbx15 with the in *A. nidulans* developmental relevant zinc cluster transcription factor OefC (Lee *et al.*, 2005) did not support a direct interaction in *A. fumigatus* during standard growth conditions. In contrast, *A. nidulans* Fbx15 interacts during asexual growth or heavy metal stress induced by cadmium sulphate with OefC of *A. fumigatus* or *A. nidulans* (Figure S 7 – S10, S12). However, additional experiments did not support a molecular link between Fbx15 and OefC during stress response, pathogenicity, ubiquitination or cellular localisation (Figure S 1, S3 – S7, S10 – S15).

1.3.1 *fidA* supports vegetative growth, conidiation in *A. fumigatus* and *A. nidulans* as well as cleistothecia formation in *A. nidulans*

The putative C-terminal part of a F-type ATPase F-subunit, FidA, was pulled by RFP-trap as uncharacterised, putative interaction partner of Fbx15 in *A. fumigatus* (Table S1). The annotation of *A. fumigatus* FidA as stand-alone gene is different to the one of *P. expansum* where FidA is a sequential part of a putative F-subunit (Figure 10). This fact was an impetus for launching further analysis with FidA in context to Fbx15 even if FidA was first solely pulled with the phospho-mimicking mutant Fbx15$^{S468|9D}$ (Table S1). BiFC analysis was used to verify the interaction between Fbx15 and FidA in *A. fumigatus*. Therefore, native Fbx15 was used to check, whether an interaction can be obtained under its native protein conditions. The

construct *fbx15:cYFP* with *nYFP:fidA* showed YFP signals in the cytoplasm during vegetative growth conditions in *A. fumigatus* (Figure 15A, see Figure S2 for controls). In the following, the role of FidA in *A. fumigatus* was examined. The *A. fumigatus* strain lacking the *fidA* gene (Δ*fidA*) as well as its corresponding complementation integrated on-locus of *A. fumigatus* Δ*fidA* (*fidA*^{comp}) were analysed on minimal growth conditions. Phenotypical comparisons revealed that Δ*fidA* showed a slow growing colony with a reduced conidia production resulting in a whitish colony colour compared to green conidia-rich colonies grown for WT, Δ*fbx15* and *fidA*^{comp} (Figure 15B, PMG, black arrow).

This data show that *A. fumigatus* FidA directly interacts with Fbx15 during non-stress conditions and is required for conidiations and vegetative growth contrary to Fbx15, which is dispensable for vegetative growth and conidiation in *A. fumigatus.*

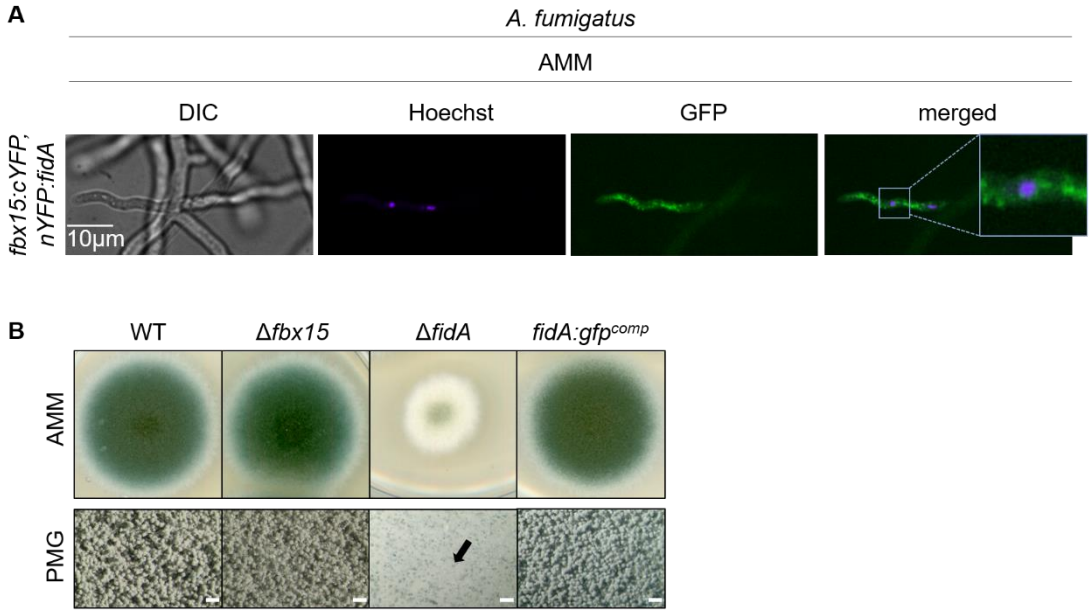

Figure 15: FidA physically interacts with Fbx15 at non-stress conditions and is needed for vegetative growth and conidiation in *A. fumigatus*. (**A**) 2*10^3 spores of *A. fumigatus* were grown vegetatively in Aspergillus minimal medium (AMM) for 18h at 37°C in darkness. The interaction was analysed via Bimolecular Fluorescence Complementation (BiFC). Fbx15 was fused to cYFP (*fbx15:cYFP*). Expressing the Fbx15 interacting developmental protein A (FidA) fused to nYFP (*nYFP:fidA*) and Fbx15 fused to cYFP (*fbx15:cYFP*) show YFP signals in the cytoplasm of *A. fumigatus* hyphae at vegetative growth. Nuclei were stained with Hoechst. Experiments were performed with two independent transformants. (**B**) 2*10^3 spores of *A. fumigatus* strains were point inoculated on *Aspergillus* minimal medium (AMM) and incubated for three days at 37°C. The *fidA* gene was integrated in the locus of Δ*fidA* resulting in *fidA:gfp*^{comp}. The Δ*fidA* strain is diminished in vegetative growth and sporulation (black arrow) contrary to Δ*fbx15, fidA:gfp*^{comp} and wild type (WT). Experiments were performed with three biological replicates. PMG: photomicrograph, scale bars: 200 µm.

BLAST analysis was performed to check whether the *A. fumigatus* Fbx15-interacting developmental relevant protein FidA also exists in the *A. nidulans* genome in the same structural composition. *In-silico* analysis revealed that FidA is also present in *A. nidulans.* FidA in *A. nidulans* is separated from the putative F-domain (F-domain: AN11565, FidA: AN7496) similar to *A. fumigatus* FidA (F-domain: Afu2g05510, FidA: Afu2g05520) in comparison to the F-type ATPase gene in *Penicillium expansum*, which harbours the corresponding FidA in the C-terminal part of the gene XP_016595530.1 (Figure 16A) (Ballester *et al.*, 2015). *A. nidulans* FidA is to 59.6% identical to *A. fumigatus* FidA with a query cover of 98% and the corresponding whole F-type ATPase the *P. expansum* gene is to 49.0% identical to *A. fumigatus* FidA with a query cover of 99% (Figure 16B).

A

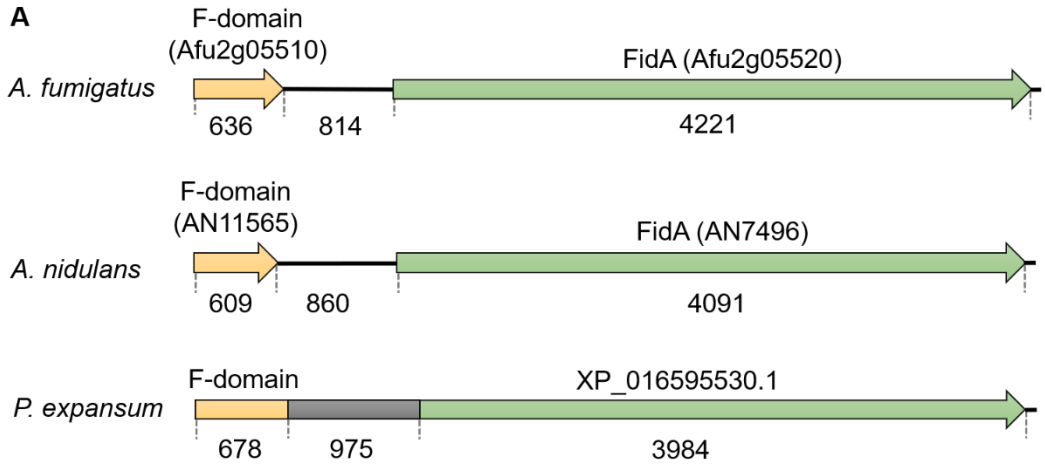

B

FidA NCBI Accession number	Organism	Query coverage	Identity
XP_749681.1	*Aspergillus fumigatus* Af293	100%	100%
XP_680765.1	*Aspergillus nidulans* FGSC A4	98%	59.6%
XP_016595530.1	*Penicillium expansum*	99%	49.0%

Figure 16: FidA is a putative C-terminal part of a F-type ATPase F-subunit in *A. fumigatus* and *A. nidulans*. Alignments were performed with NCBI-BLAST (https://blast.ncbi.nlm.nih.gov/Blast.cgi?PAGE=Proteins). (**A**) Analysis of sequential composition of the Fbx15-interacting developmental protein A (FidA). The F-domain (yellow) is separated from FidA (green) in *A. nidulans* (AN7496) and *A. fumigatus* (Afu2g05520). In *Penicillium expansum* the orthologue XP_01659553 is composite of FidA together with the corresponding F-domain. (**B**) Multiple alignment of *A. fumigatus* FidA with its counterparts in *A. nidulans and P. expansum.* 'Query coverage' describes the alignment cover of the primary amino acid sequence of *A. fumigatus* FidA in percentage. Similarities between the identified FidA homologs of other species in comparison to FidA of *A. fumigatus* are described in 'Identity' in percentage.

BiFC analysis were performed as first line of evidence to examine if Fbx15 is interacting with FidA in *A. nidulans*. The construct *fbx15:cYFP* with *nYFP:fidA* show YFP signals in the cytoplasm during vegetative growth conditions in *A. fumigatus* and asexual growth in *A. nidulans* (Figure 17A).

The role of FidA in asexual or sexual reproduction in *A. nidulans* was investigated by growth assays on plates during minimal growth conditions. *A. nidulans fidA* fused to *gfp* (*fidA:gfp*^{comp}) or overexpressed *fidA* fused to *gfp* (oe*fidA:gfp*) were integrated in the locus of *A. nidulans* Δ*fidA.* The Δ*fidA* strain was compared to WT, *fidA:gfp*^{comp} and oe*fidA:gfp*, as well as compared to Δ*fbx15* and *fbx15* complementation (*fbx15:strep*^{comp}). The Δ*fidA* colony size was reduced contrary to Δ*fbx15*, which showed a WT-like colony size like oe*fidA:gfp* during light conditions with sufficient oxygen supply enhancing asexual growth (Figure 17B, top) (Park *et al.*, 2019). The Δ*fidA* colony was dark reddish pigmented comparable to the pigmentation of the Δ*fbx15* colony and contrary to the greenish pigmented colonies of WT. The oe*fidA:gfp* colony showed a slight reddish pigmentation compared to a greenish pigmentation for WT (Figure 17B, bottom). The Δ*fbx15* and Δ*fidA* strains displayed a reduced conidia production with approx. 0.1% for Δ*fbx15* and around 1% for Δ*fidA* relative to WT or corresponding complementations *fbx15:strep*^{comp} (76%) and *fidA:gfp*^{comp} (74%). No significant differences in conidia production were observed for oe*fidA:gfp* (61%) compared to *fidA:gfp*^{comp} (74%) relative to WT. Observation of cleistothecia production in light showed that in contrast to produced cleistothecia in WT, *fidA:gfp*^{comp} and *fbx15:strep*^{comp} (black-white arrows), Δ*fidA* produced no cleistothecia like Δ*fbx15* (Figure 13, Figure 17C). The cleistothecia production of *fidA:gfp*^{comp} was approx. two-fold increased (186%) relative to WT. For oe*fidA:gfp* significantly less cleistothecia were produced with around 2% relative to WT (Figure 17C).

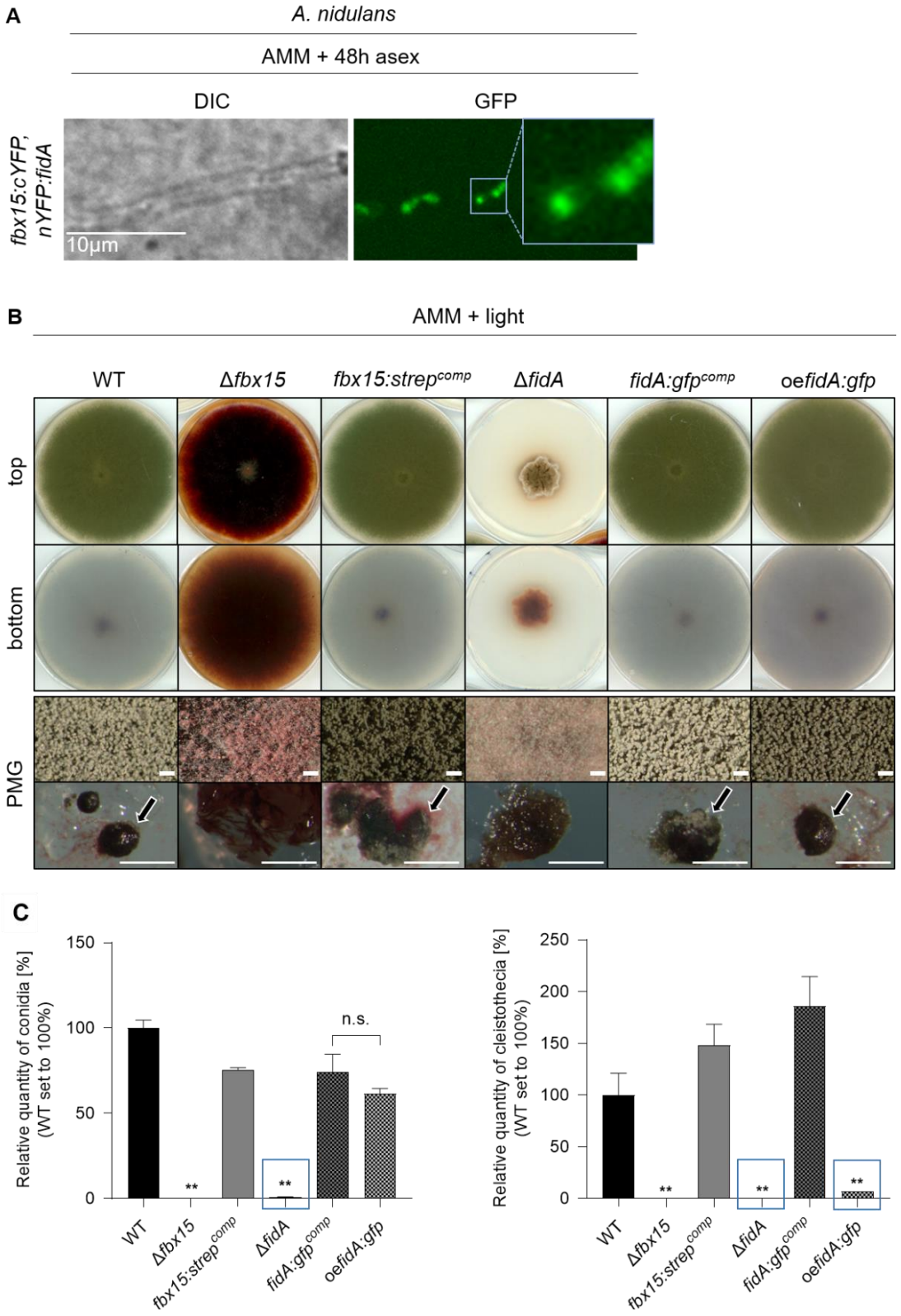
A
A. nidulans
AMM + 48h asex
DIC
GFP
fbx15:cYFP, nYFP:fidA
10µm
B
AMM + light
WT
Δfbx15
fbx15:strepcomp
ΔfidA
fidA:gfpcomp
oefidA:gfp
top
bottom
PMG
C
Relative quantity of conidia [%] (WT set to 100%)
150
100
50
0
n.s.
**
WT
Δfbx15
fbx15:strepcomp
ΔfidA
fidA:gfpcomp
oefidA:gfp
Relative quantity of cleistothecia [%] (WT set to 100%)
250
200
150
100
50
0

Figure 17*:* FidA is directly interacting with Fbx15 at asexual growth and is required for asexual and sexual development during light conditions in *A. nidulans.* (**A**) $2*10^3$ spores of *A. nidulans* were grown on solid *Aspergillus* minimal medium (AMM) and incubated for two days (2d) to induce asexual growth. The interaction was analysed through Bimolecular Fluorescence Complementation (BiFC). Expressing the Fbx15 interacting developmental protein A (FidA) fused to nYFP (*nYFP:fidA*) and Fbx15 fused to cYFP (*fbx15:cYFP*) show YFP signals at induced asexual growth. Experiments were performed with three biological replicates. (**B**) $2*10^3$ spores of *A. nidulans* strains were point inoculated on solid AMM and were incubated for seven days (7d) at 37°C in light with oxygen supply. Δ*fidA* shows a reddish pigmented colony, as well as reduced conidiation like Δ*fbx15* compared to wild type (WT) and the corresponding complementations: *fbx15* fused to *strep* on-locus integrated in Δ*fbx15* (*fbx15:strep*^{comp}) and *fidA* fused to gfp (*fidA:gfp*^{comp}) on-locus integrated into Δ*fidA* (bottom, PMG). The Δ*fidA* strain also reduced in vegetative growth. Overexpression of *fidA* by the constitutively active *gpdA* promoter (*oefidA:gfp*) results in a slight reddish pigmentated colony compared to WT or *fidA:gfp*^{comp}. For Δ*fbx15* and Δ*fidA* no cleistothecia could be identified. The *fbx15:strep*^{comp}, *fidA:gfp*^{comp} and *oefidA:gfp* strains produce cleistothecia after seven days incubation like WT (black-white arrows). (**C**) Error bars represent the SEM and were calculated from two independent transformants and three biological replicates. Significances were determined with one-way Anova and Student's t-test in comparison to WT if not indicated otherwise (P-value: *P<0.01, **P<0.001, n.s.: not significant). Quantification analysis of the asexual spores show that conidiation is strongly inhibited in Δ*fidA* (blue frame) like in Δ*fbx15* compared to WT or *fbx15:strep*^{comp} and *fidA:gfp*^{comp}. The *oefidA:gfp* strain shows no altered conidia production compared to *fidA:gfp*^{comp}. Quantification of cleistothecia shows an inhibited cleistothecia production in *oefidA:gfp* (blue frame) whereas cleistothecia production is blocked in Δ*fbx15* and Δ*fidA* (blue frame). PMG: photomicrograph, scale bars: 200 µm.

When enhancing sexual development during dark conditions with reduced oxygen supply the Δ*fidA* colony size was similar small as during light conditions contrary to Δ*fbx15*, which showed a WT-like colony size like oe*fidA:gfp* (Figure 17A, Figure 18A, top) (Park *et al.*, 2019).

Dark reddish pigmented colonies were displayed for Δ*fbx15* and Δ*fidA.* A slightly darker colony pigmentation compared to WT was observed for oe*fidA:gfp* (Figure 18A, bottom). Δ*fidA* produced primordia (yellow arrow), unlike an observed blocked fruiting body formation in Δ*fbx15* (Figure 18A, PMG) (von Zeska Kress *et al.*, 2012). Matured cleistothecia formation was observed for WT, oe*fidA:gfp* and the corresponding complementations (black-white arrow) (Figure 18A, PMG). Δ*fbx15* was strongly reduced in conidia production with around 0.1% relative to WT or *fbx15:strep*^{comp} (90%). Δ*fidA* showed similar to Δ*fbx15* a strong reduced conidia production with around 1.7% relative to WT and *fidA:gfp*^{comp} (71%). The oe*fidA:gfp* showed a reduced but no significant change in conidia production in darkness with 59% compared *fidA:gfp*^{comp} (71%). Cleistothecia were produced in oe*fidA:gfp* (107%) like WT and in *fidA:gfp*^{comp} (137%) with a significant increased amount relative to WT (Figure 18B). The ability of ascospores produced in Δ*fidA* was examined. After 21 days Δ*fidA* ascospores of mature cleistothecia were isolated and re-plated on AMM plates resulting in reproduction of Δ*fidA* (Figure 18C).

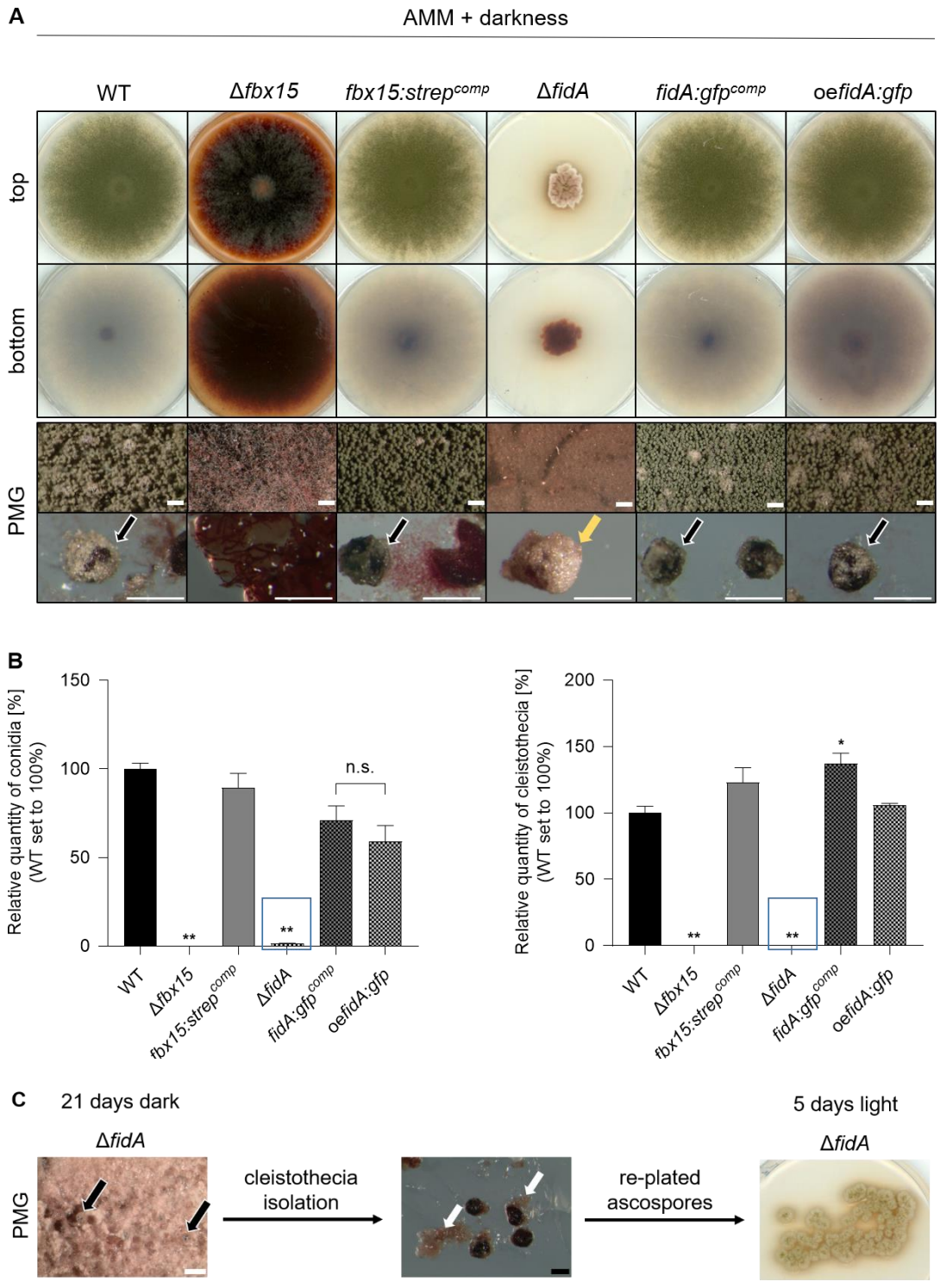
A
AMM + darkness
WT
Δfbx15
fbx15:strepcomp
ΔfidA
fidA:gfpcomp
oefidA:gfp
top
bottom
PMG
B
Relative quantity of conidia [%] (WT set to 100%)
150
100
50
0
n.s.
**
**
WT
Δfbx15
fbx15:strepcomp
ΔfidA
fidA:gfpcomp
oefidA:gfp
Relative quantity of cleistothecia [%] (WT set to 100%)
200
150
100
50
0
*
**
**
C
21 days dark
5 days light
ΔfidA
ΔfidA
PMG
cleistothecia isolation
re-plated ascospores

Figure 18: *fidA* is critical for vegetative growth, conidiation and in-time cleistothecia formation in *A. nidulans* under sexual development favouring conditions. $2*10^3$ spores of *A. nidulans* strains were point inoculated on *A*spergillus minimal medium (AMM) and incubated for seven days at 37°C in darkness with limited oxygen supply. (**A**) Δ*fidA* shows a reddish pigmentated small colony, reduced conidiation and delayed cleistothecia maturation compared to wild type (WT) and complemented *fidA* fused to *gfp* on-locus integrated into Δ*fidA* (*fidA:gfp*^{comp}) (bottom). Overexpression of *fidA* by the constitutively active *gpdA* promoter (oe*fidA:gfp*) results in a dark reddish pigmentation at the bottom of the colony. Primoridia surrounded by Hülle cells were identified for Δ*fidA* (yellow arrow), whereas no cleistothecia formation is observed for Δ*fbx15* compared to mature cleistothecia formation in WT and the corresponding complementations (*fbx15:strep*^{comp}, *fidA:gfp*^{comp}) and overexpression strain (oe*fidA:gfp*) (black-white arrows). (**B**) Error bars represent the SEM and were calculated from two independent transformants and three biological replicates. Significances were determined with one-way Anova and Student's t-test in comparison to WT if not indicated otherwise (*P*-value: ***P*<0.001, n.s.: not significant). Quantifications of conidia show a significantly reduced production for Δ*fidA* (blue frame) like Δ*fbx15* compared to WT. Conidia production in oe*fidA:gfp* is not significantly altered to *fidA:gfp*^{comp}. No matured cleistothecia are produced in Δ*fidA* (blue frame) and Δ*fbx15* compared to WT, *fbx15:strep*^{comp} and *fidA:gfp*^{comp}. The *fidA:gfp*^{comp} strain produces significantly more cleistothecia than WT. (**C**) The Δ*fidA* strain was incubated for 21 days at 37°C in darkness with limited oxygen supply on AMM. Viability of 21-days-old isolated ascospores (white arrows) from mature cleistothecia (black-white arrows) was proven by re-plating on AMM for 5 days at 37°C in light. PMG: photomicrograph, white scale bars: 200 µm, black scale bars: 500 µm.

The data of Figure 17 and Figure 18 show that the Fbx15-interacting protein *A. nidulans* FidA supports developmental processes. These data are consistent with the once obtained for *A. fumigatus* FidA indicating similar functions of FidA in *A. fumigatus* and *A. nidulans* (Figure 16). Fbx15-comparable impacts on development of *A. nidulans* in secondary metabolite homeostasis and conidiation could be due to the observed interaction verified through BiFC analysis (Figure 15 - 18) (von Zeska Kress *et al.*, 2012). However, Fbx15 is not required for development in *A. fumigatus* contrary to its interacting partner FidA indicating that the role of FidA in development is independent of Fbx15 in *A. fumigatus* (Figure 13, Figure 16) (Jöhnk *et al.*, 2016). Further interaction analysis such as stability test examining whether FidA is a candidate of the SCF^{Fbx15} complex or Fbx15-dependent localisation test as previously performed with SsnF (Jöhnk *et al.*, 2016) could not be achieved as tagged versions of FidA were either not detectable or showing multiple bands by immunoprecipitation indicating an unstable fusion protein (Figure S17).

In summary, these data further support Fbx15 interactions of *A. fumigatus* and/or *A. nidulans* to the zinc cluster transcription factor OefC, the SREBP transcription factor SrbB, the putative APSES transcription factor FiAt and to the F-type ATPase FidA. Fbx15-FidA was predominantly found in the cytoplasm (Figure 15, Figure S1, S5, S7). Fbx15 is capable to assemble to an active SCF^{Fbx15} complex at non-stress conditions predominantly in the nucleus (Jöhnk *et al.*, 2016). The analyses of the

exact molecular functions of the cytoplasmic or nuclear interactions of Fbx15 and their interplay with SCF ubiquitin ligases will be interesting topics of future research.

2 Mycotoxin production depends on *A. fumigatus* Fbx15

2.1 Gliotoxin biosynthesis-dependent GliP and GliZ are dispensable for stress adaptation in *A. fumigatus* at minimal growth

A. fumigatus Fbx15 is essential for virulence in the mouse infection model (Jöhnk *et al.*, 2016). The pathogenic potential of *A. fumigatus* is associated with its ability to produce mycotoxins such as the *A. fumigatus*-specific gliotoxin (König *et al.*, 2019; Sugui *et al.*, 2007). Fbx15 is involved in the inhibition of gliotoxin biosynthesis by the transcriptional repression of the NRPS encoding gene *gliP* and the zinc cluster transcription factor encoding gene *gliZ* next to other *gli*-cluster genes that are essential for the biosynthesis of gliotoxin (Bok *et al.*, 2006; Jöhnk *et al.*, 2016; Scharf *et al.*, 2012).

It was investigated if the obtained increased gliotoxin formation in absence of *fbx15* contributes to the observed sensitivity against stress inducers. Therefore, the single deletion strains (Δ*fbx15*, Δ*gliP*, Δ*gliZ*) and double deletion strains in Δ*fbx15* background (Δ*fbx15*/Δ*gliP*, Δ*fbx15*/Δ*gliZ*) were constructed and phenotypical analysed on media with different carbon sources and stress detergents in the background of minimal growth conditions. The Δ*gliP* - and Δ*gliZ* strains showed WT-like colonies on all tested media including lactose as sole carbon source, aa starvation (1 mM 3-AT), osmotic stress (1 M NaCl), heavy metal stress induced by cadmium (300 µM $CdSO_4$) and oxidative stress (2 mM H_2O_2) (Figure 19). The double deletions Δ*fbx15*/Δ*gliP* and Δ*fbx15*/Δ*gliZ* resulted in the same phenotypes as Δ*fbx15* with small colony sizes or blocked growth on tested stress media (Figure 19, black frames).

These results shows that during minimal growth conditions Fbx15-dependent *A. fumigatus* is independent of GliP and GliZ, which are required for gliotoxin production (Bok *et al.*, 2006; Cramer *et al.*, 2006). Moreover, GliP and GliZ are in general dispensable for stress response during minimal growth conditions in *A. fumigatus.*

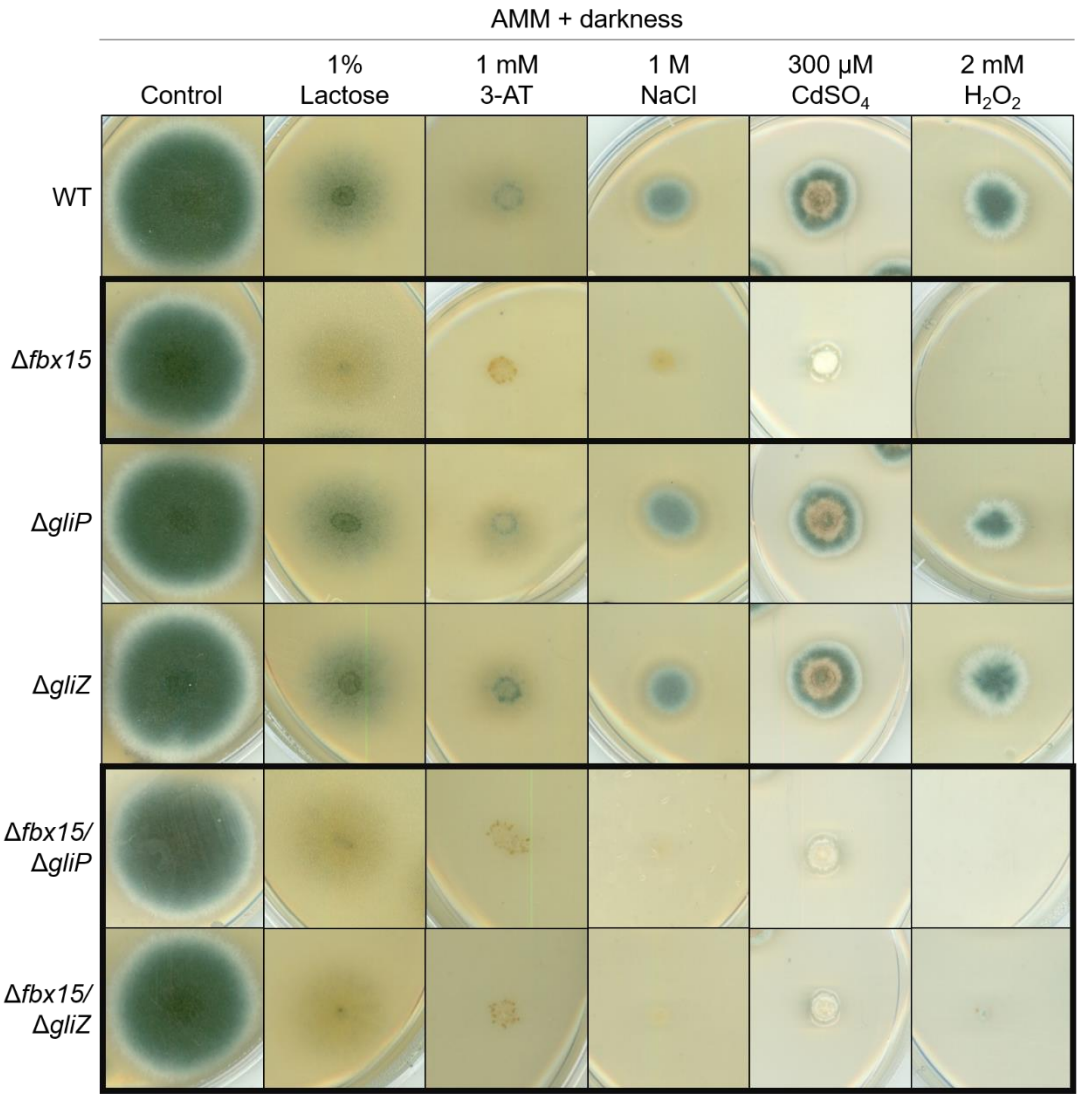

Figure 19: *A. fumigatus fbx15*-mediated stress adaptation is independent of *gliP* and *gliZ* during minimal growth conditions. Single deletions of the multimodular nonribosomal peptide synthetase (NRPS) encoding gene *gliP* (Δ*gliP*) and the Zn_2Cys_6 finger binuclear transcription factor encoding gene *gliZ* (Δ*gliZ*) and double deletions of *fbx15* with *gliP* (Δ*fbx15*/Δ*gliP*) or with *gliZ* (Δ*fbx15*/Δ*gliZ*) were compared to each other in *A. fumigatus*. $2*10^3$ spores were point inoculated on *Aspergillus* minimal medium (AMM) and incubated for three to five days in darkness at 37°C without (control) and with different stress detergents or carbon sources. Phenotypical tests were performed by using following stress inducers: lactose instead of glucose as carbon source, histidine starvation induced by 3-amino-1,2,4-triazol (1 mM 3-AT), osmotic stress induced by natrium chloride (1 M NaCl), heavy metal stress induced by cadmium sulphate (300 µM $CdSO_4$) and oxidative stress induced by hydrogen peroxide (2 mM H_2O_2). The Δ*fbx15* colonies grow slower than wild type (WT)-colonies at all tested stress conditions, whereas Δ*gliP* and Δ*gliZ* phenocopy WT. The Δ*fbx15*/Δ*gliP* and Δ*fbx15*/Δ*gliZ* strains are phenocopy Δ*fbx15* colonies on all tested stress media (black frames). Experiments were performed with two independent transformants and three biological replicates.

2.2 Gliotoxin biosynthesis-dependent GliP and GliZ are dispensable for Fbx15-mediated pathogenicity in *A. fumigatus* in the *Galleria mellonella* infection model

It is known that Δ*fbx15* results in a complete clearance of conidia in the alveoli in the CD-1 mouse model immunosuppressed with cortisone acetate as well as Δ*gliP* impairs *A. fumigatus* virulence in BALB/c and 129/Sv mouse models immunosuppressed with hydrocortisone acetate (Jöhnk *et al.*, 2016; Sugui *et al.*, 2007). It is suggested that the observed derepression of gliotoxin biosynthesis in the Δ*fbx15* strain leads to a self-intoxication of *A. fumigatus* resulting in the disability to infect host organisms and consequently lead to a loss of pathogenicity.

In vivo-infection assays were performed with the single deletion strains Δ*fbx15*, Δ*gliP,* Δ*gliP,* Δ*gliZ*, as well as the double deletion strains Δ*fbx15*/Δ*gliP* and Δ*fbx15*/Δ*gliZ* and compared to WT in the *Galleria mellonella* moth larvae infection model (Slater *et al.*, 2011). All infections were performed with the supplementation of the antibiotic rifampicin to prevent contaminations as well as injections with NaCl-Tween were performed as negative control. The survival rate of Δ*fbx15*-infected *Galleria mellonella* larvae was significantly higher with 70% after nine days post infection compared to WT-infected larvae of which 7% survived. No significant changes were observed for the survival rate of Δ*gliZ*-infected larvae with 10% survival to WT-infected larvae (7%). A significant higher survival rate than for WT-infected larvae (7%) was observed for Δ*gliP*-infected larvae with 26% nine days post infection (Figure 20A). *Galleria mellonella* larvae infected with Δ*fbx15*/Δ*gliP* and Δ*fbx15*/Δ*gliZ* resulted in no significant changes to Δ*fbx15*-infected larvae with survival rates of 60% for Δ*fbx15*/Δ*gliP* and 70% Δ*fbx15*/Δ*gliZ* compared to Δ*fbx15* with 70% survival nine days post infection (Figure 20B).

These data show that infections with *A. fumigatus* lacking *fbx15* with and without increased gliotoxin formation are comparable with each other in the *Galleria mellonella* larvae model. This indicates that the observed inhibition in pathogenicity of *A. fumigatus* when lacking *fbx15* is not caused by an increased gliotoxin production. So far it is unknown if other mycotoxins are regulated in dependency of Fbx15, which might influence the capability of *A. fumigatus* to adapt to various environmental stressors present during stress response or invasion in a putative host organism.

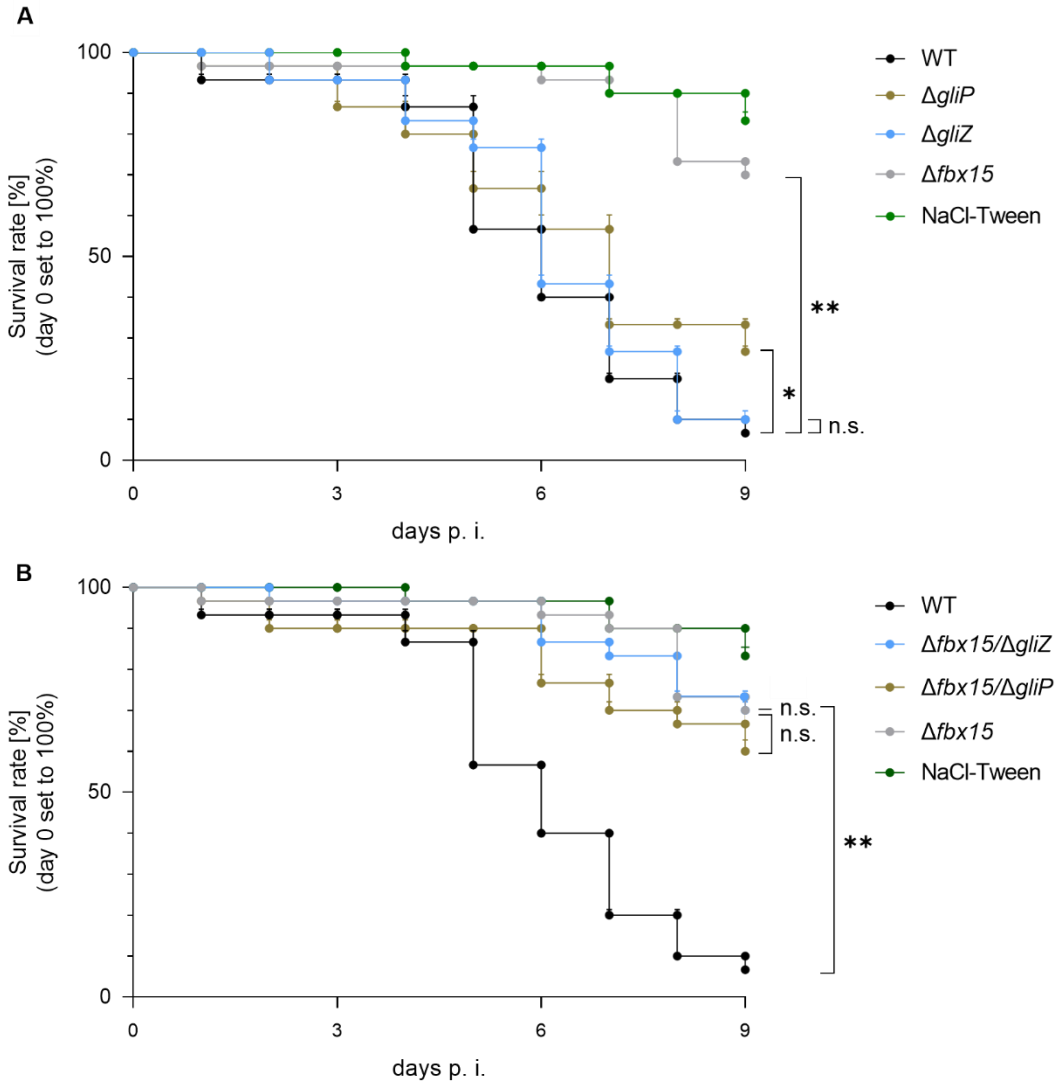

Figure 20: *A. fumigatus* Fbx15-mediated pathogenicity is independent of GliP and GliZ in the *Galleria mellonella* larvae infection model. *Galleria mellonella* larvae were infected with 5*10^{6} spores of *A. fumigatus* strains and incubated in darkness at 30°C for nine days. Larvae were treated with 10 µg/ml rifampicin to prevent death by contamination. NaCl-Tween (green) was used as negative control. (**A**) Error bars represent the standard deviation and were calculated from two biological replicates. Experiments were performed with two independent transformants for each infection series. Significances were determined with one-way Anova and Student's t-test (*P*-value: **P*<0.01, ***P*<0.001, n.s.: not significant). Single deletion strain of the Zn_2Cys_6 finger binuclear transcription factor encoding gene *gliZ* (Δ*gliZ*, blue) causes the same survival rate as wild type (WT, black) infected larvae. Infection with the single deletion strain of the multimodular nonribosomal peptide synthetase (NRPS) encoding gene *gliP* (Δ*gliP*, brown) results in a significantly higher survival rate of larvae than for WT-infected larvae. The increased survival rate of larvae-infected with the single deletion of *fbx15* (Δ*fbx15*, grey) shows the highest significant difference to WT-infected larvae (black). (**B**) Error bars represent the standard deviation and were calculated from two biological replicates. Experiments were performed with two independent transformants for each infection series. Significances were determined with one-way Anova and Student's t-test (*P*-value: ***P*<0.001, n.s.: not significant). Infections with the double deletion strains of *fbx15* with *gliZ* (Δ*fbx15*/Δ*gliZ*, blue) and with *gliP* (Δ*fbx15*/Δ*gliP*, brown) show no significant differences for the survival rate of larvae compared to Δ*fbx15*-infected larvae (grey), which is significantly higher than for WT-infected larvae (black).

2.3 *A. fumigatus* Fbx15 is required for the repression of fumagillin biosynthesis

It was investigated whether Fbx15 is involved in the regulation of other mycotoxins than gliotoxin produced in *A. fumigatus* (Jöhnk *et al.*, 2016). In order to address this question, the secondary metabolite pattern of Δ*fbx15* was compared to WT and *fbx15* complementation (*fbx15*^{comp}). HPLC-MS analysis was performed from vegetatively grown *A. fumigatus* samples. In Δ*fbx15* the production of several putative secondary metabolites was increased compared to WT and *fbx15*^{comp} (Figure 21A, arrows). Literature-based comparisons with the curves obtained by the ultraviolet/visual light (UV/Vis) spectra at retention time 16.14/16.16 min identified the antimicrobial agent fumagillin with a wavelength of a maximum absorption at 335 nm and 358 nm with a shoulder at 320 nm (Figure 21 A black arrow, Figure 21B blue frame, Figure 21C) (Chu *et al*., 2012; Hanson and Eble, 1949; McCowen *et al*., 1951). Fumagillin has a meroterpenoid chemical structure with the sum formula $C_{26}H_{34}O_7$ (Figure 21D) (McCowen *et al*., 1951). The measured exact mass of fumagillin was 459.238 in the positive ionization mode $[M+H]^+$ and 457.222 in the negative ionization mode $[M-H]^-$, which were similar to the calculated exact masses 459.2237 in $[M+H]^+$ and 457.223 $[M-H]^-$ (Figure 21E) (McCowen, Callender, and Lawlis 1951).

These data show that Fbx15 is not only required for the regulation of the biosynthesis of the mycotoxin gliotoxin at gliotoxin-inducible conditions (Jöhnk *et al.*, 2016) but also regulates the biosynthesis of the antimicrobial agent fumagillin at vegetative growth in *A. fumigatus*. The Fbx15-dependent regulation in gliotoxin biosynthesis matches with the Fbx15-dependent regulation of the cellular localisation of the co-repressor subunit SsnF. Precisely, the absence of Fbx15 leads to a derepression in gliotoxin biosynthesis and in a nuclear clearance of SsnF (Jöhnk *et al.*, 2016). The previously obtained data from Jöhnk, *et al.* and the data achieved in this study indicate that the cellular localisation of Fbx15 is essential for the regulation of the biosynthesis of certain products such as the mycotoxins gliotoxin and fumagillin.

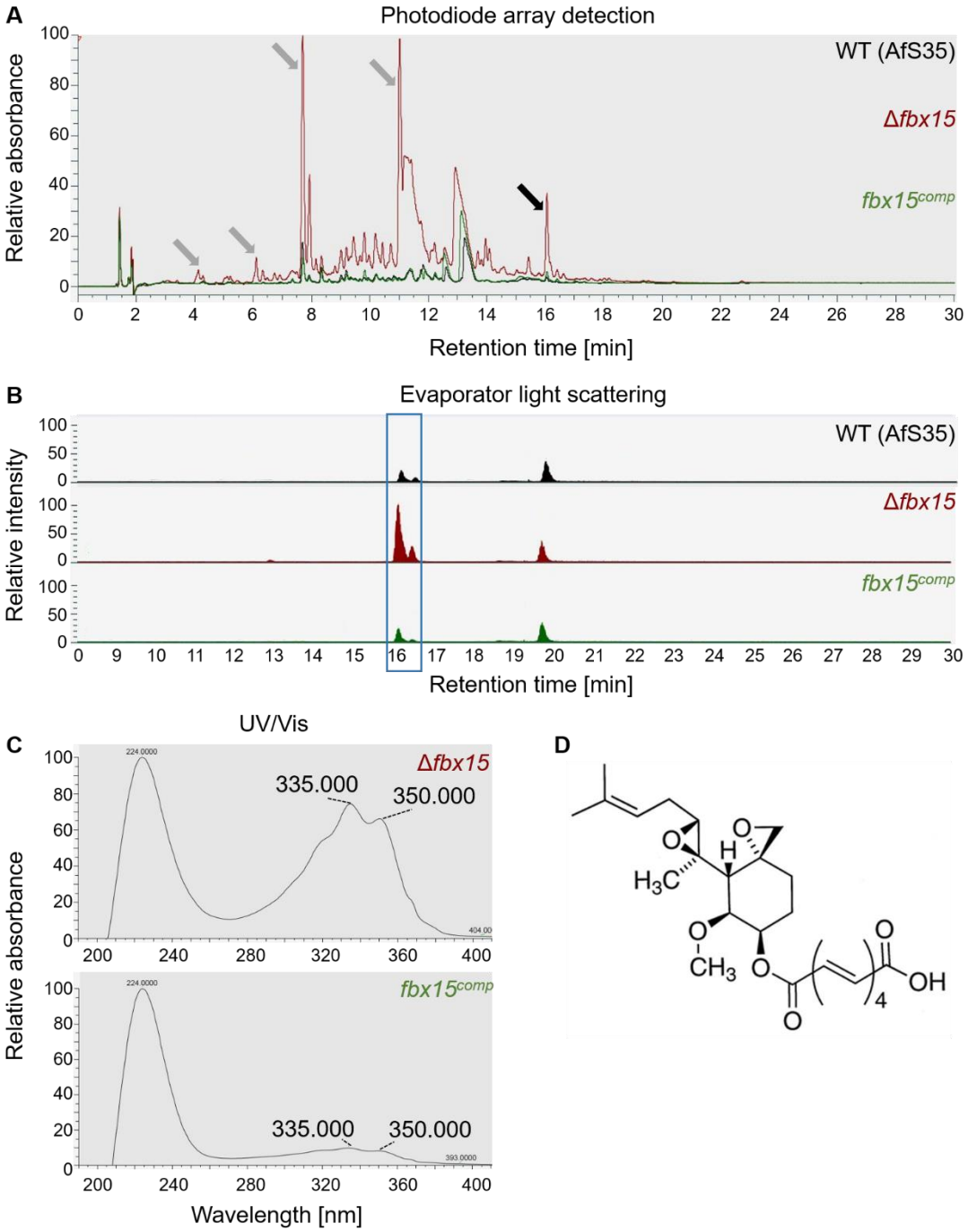

E

Metabolite	Detected as	Retention time (min)	Sum formula	Measured exact mass	Calculated exact mass	Confirmed by
Fumagillin	$[M+H]^+$, $[M-H]^-$	16.14 – 16.16	$C_{26}H_{34}O_7$	459.238^+, 457.222^-	459.2237^+, 457.223^-	A, B

Figure 21: Fbx15 negatively regulates fumagillin biosynthesis during vegetative growth conditions in *A. fumigatus*. $2*10^8$ spores of *A. fumigatus* wild type (WT), Δ*fbx15* and *fbx15* on-locus integration in Δ*fbx15* (*fbx15*^{comp}) were inoculated in *Aspergillus* minimal medium (AMM) and incubated vegetatively for 48h at 37°C. HPLC-MS analysis was performed from extracted secondary metabolites with ethyl acetate. (**A**) Overlap of the relative absorbance by photodiode array detection of secondary metabolite extracts of WT (black) and Δ*fbx15* (red), *fbx15*^{comp} (green) show that Δ*fbx15* produces more of different putative secondary metabolites compared to *fbx15*^{comp} and WT (arrows). (**B**) Evaporator light scattering data of WT and Δ*fbx15*, *fbx15*^{comp} at retention time 16 (blue box). The relative intensity of the peak at retention time 16.16 min is increased in Δ*fbx15* compared to WT (16.14 min) and *fbx15*^{comp} (16.16 min). (McCowen *et al.*, 1951). (**C**) Ultraviolet/visual light (UV/Vis) spectra of the increased peak at retention time 16.16 min in Δ*fbx15* compared to *fbx15*^{comp} identified fumagillin (Chu *et al*., 2012; Hanson and Eble, 1949; McCowen *et al.*, 1951). Relevant peaks at 335 and 350 nm were highlighted in big numbers. (**D**) Structural formula of the meroterpenoid fumagillin consisting of a partial terpenoid structure (McCowen *et al.*, 1951). (**E**) Data of fumagillin identified by HPLC-MS. Fumagillin was identified at retention time 16.14 to 16.16 and has the chemical formula $C_{26}H_{34}O_7$. The measured exact mass of fumagillin is 459.238 in the positive ionization mode $[M+H]^+$ and 457.222 in the negative ionization mode $[M-H]^-$. The calculated exact mass of fumagillin is 459.2237 in $[M+H]^+$ and 457.223 $[M-H]^-$. The identification of fumagillin was performed by the exact mass measurement [A] and the UV/Vis spectra [B] (McCowen, Callender, and Lawlis 1951).

3 *A. fumigatus* Fbx15 NLS1 or NLS2 provide nuclear location during non-stress conditions, whereas only NLS2 locates Fbx15 in the nuclear periphery during stress

3.1 Either of the two nuclear localisation signals, NLS1 and NLS2, is sufficient to facilitate the nuclear import of *A. fumigatus* Fbx15 during vegetative growth without stress

Fbx15 comprises two predicted NLS sequences NLS1: ^{407}YERPRKRLRRYY^{418} and NLS2: ^{485}VSRKRKSPID^{494} (Jöhnk *et al.*, 2016), which indicates its ability to interact with importins for a nuclear transport (Lange *et al.*, 2007). It is indicated that the cellular localisation of Fbx15 influences the localisation of the co-repressor subunit SsnF as well as the regulation of mycotoxin biosynthesis (Jöhnk *et al.*, 2016) (Figure 21).

The functions of NLS1 and NLS2 in combination or separately at non-stress conditions was analysed and monitored using the expression of Fbx15 NLS-deficient variants and comparing the cellular location to wild type. The single deletions of the DNA for either the codons for NLS1 or NLS2 of the *fbx15* gene were constructed and integrated on-locus in Δ*fbx15*. Fbx15 (Fbx15$^{NLS1|NLS2}$) with a protein length of 655 aa in the absence of NLS1 was named Fbx15$^{Δ|NLS2}$. The resulting shortened protein sequence includes 644 aa, whereas Fbx15 without NLS2 (Fbx15$^{NLS1|Δ}$) resulted in a deduced shortened protein of 646 aa. The combined deletion of NLS1 and NLS2 in

the Fbx15 sequence was named Fbx15$^{\Delta|\Delta}$ and shows a deduced shortened protein of 635 aa.

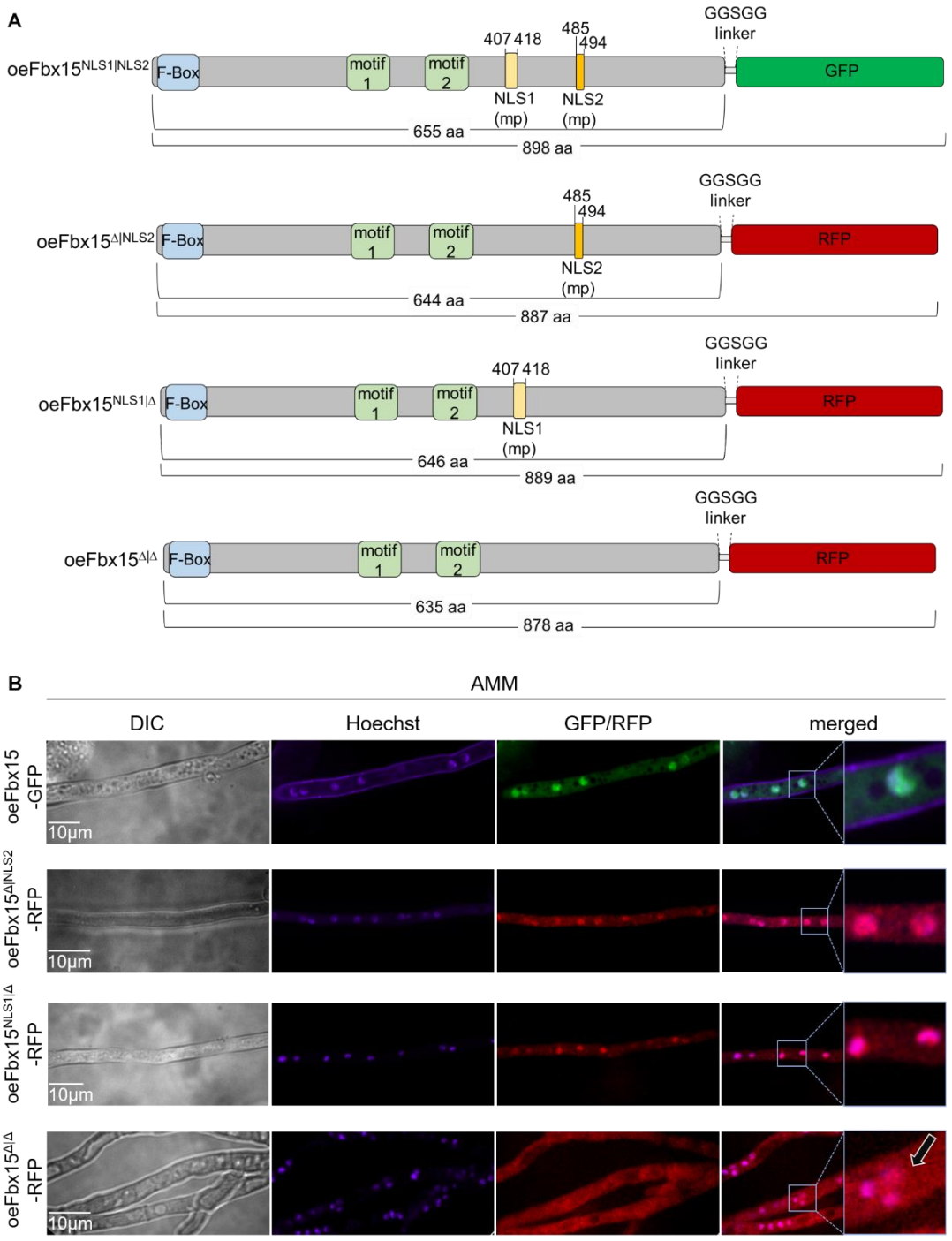

Fbx15-variant	Non-stress
oeFbx15-GFP	N + C
oeFbx15$^{\Delta|NLS2}$-RFP	N + C
oeFbx15$^{NLS1|\Delta}$-RFP	N + C
oeFbx15$^{\Delta|\Delta}$-RFP	P + C (diffuse)

Figure 22: Either NLS1 or NLS2 are sufficient to provide nuclear localisation of Fbx15 during vegetative growth in *A. fumigatus*. (**A**) Fbx15 and its NLS-variants were fused to GFP or RFP through a GGSGG-linker and were overexpressed with the constitutively active *gpdA*-promoter for visualisation in fluorescence microscopy. Overexpressed Fbx15 with an amino acid (aa) length of 655 encompasses the F-box domain, two motifs and two monopartite (mp) nuclear localisation signals (NLS), NLS1 (yellow) and NLS2 (orange). OeFbx15 was fused to GFP resulting in a total protein length of 898 aa (oeFbx15$^{NLS1|NLS2}$-GFP). OeFbx15 in absence of NLS1 has an aa length of 644 and was fused to RFP resulting in a total protein length of 887 aa (oeFbx15$^{\Delta|NLS2}$-RFP). OeFbx15 in absence of NLS2 has an aa length of 646 and was fused to RFP, resulting in a total protein length of 889 aa (oeFbx15$^{NLS1|\Delta}$-RFP). OeFbx15 in absence of NLS1 and NLS2 has an aa length of 635 and was fused to RFP, resulting in a total protein length of 878 aa (oeFbx15$^{\Delta|\Delta}$-RFP). All constructs were integrated on-locus of *A. fumigatus* Δ*fbx15*. (**B**) 2*10^3 spores of *A. fumigatus* strains were grown vegetatively in *Aspergillus* minimal medium (AMM) for 18h at 37°C in darkness. Hoechst staining was performed to visualise nuclei. OeFbx15-GFP, oeFbx15$^{\Delta|NLS2}$-RFP and oeFbx15$^{NLS1|\Delta}$-RFP are located predominantly the nucleus (N) rather then in the cytoplasm (C). OeFbx15$^{\Delta|\Delta}$-RFP fusion protein is solely diffused located in nuclear periphery (P) and cytoplasm (C) (black-white arrow). The prevalent localisations are highlighted with underscores in the tabular scheme. Experiments were performed with at least six biological replicates.

Resulting constructs were overexpressed utilising the active *gpdA*-promoter and integrated on-locus of *A. fumigatus* Δ*fbx15.* For microscopical analysis of the cellular location, WT Fbx15 (655 aa) was fused to GFP through a glycine-glycine-serine-glycine-glycine (GGSGG)-linker, resulting in a total protein length of 898 aa. The Fbx15 NLS-deficient strains were fused to RFP through a GGSGG-linker, resulting in oeFbx15$^{\Delta|NLS2}$-RFP with in total 887 aa, oeFbx15$^{NLS1|\Delta}$-RFP with in total 889 aa and oeFbx15$^{\Delta|\Delta}$-RFP with in total 878 aa (Figure 22A). Fluorescence imaging revealed that oeFbx15$^{\Delta|NLS2}$-RFP and oeFbx15$^{NLS1|\Delta}$-RFP are located in the nucleus at vegetative growth like oeFbx15-GFP. The oeFbx15$^{\Delta|\Delta}$-RFP was solely diffused located in the cytoplasm and nuclear periphery (Figure 22B, black-white arrow).

These data show that the simultaneous loss of both NLS sequences leads to a diffused localisation of Fbx15 in the cytoplasm as well as at the nuclear periphery. The most important finding is that either one of the two NLS sequences is sufficient to transfer significant amounts of Fbx15 during vegetative growth into the nucleus similar to wild type.

3.2 *A. fumigatus* Fbx15 requires NLS2 during stress response

The function of NLS1 and NLS2 during Fbx15-mediated stress response was analysed. Natively expressed Fbx15 NLS variants were constructed and compared to the overexpressed Fbx15 NLS variants previously described in Chapter 3.1. Accordingly, the *fbx15* gene lacking the codons of NLS1 (*fbx15*$^{\Delta|NLS2}$) resulting in a protein with a total length of 644aa or NLS2 (*fbx15*$^{NLS1|\Delta}$) resulting in a total protein length of 646 aa or the *fbx15* gene lacking the codons of NLS1 and NLS2 (*fbx15*$^{\Delta|\Delta}$) resulting in a deduced protein with a length of 635 aa were constructed and integrated on-locus of Δ*fbx15* (Figure 23). The resulting proteins are similar to the RFP fusion proteins (last line of Figure 22A) but lacks the C-terminal red fluorescent protein fusion (Figure 23). Phenotypes during stress conditions of the strains with the expressed NLS-deficient variants *fbx15*$^{\Delta|NLS2}$, *fbx15*$^{NLS1|\Delta}$ and *fbx15*$^{\Delta|\Delta}$ were compared to oe*fbx15*$^{\Delta|NLS2}$*:rfp*, oe*fbx15*$^{NLS1|\Delta}$*:rfp* and oe*fbx15*$^{\Delta|\Delta}$*:rfp* and WT, Δ*fbx15* and oe*fbx15*. Alterations in the ability to adapt to different stresses between normally expressed and overexpressed *fbx15*-NLS variants were elucidated.

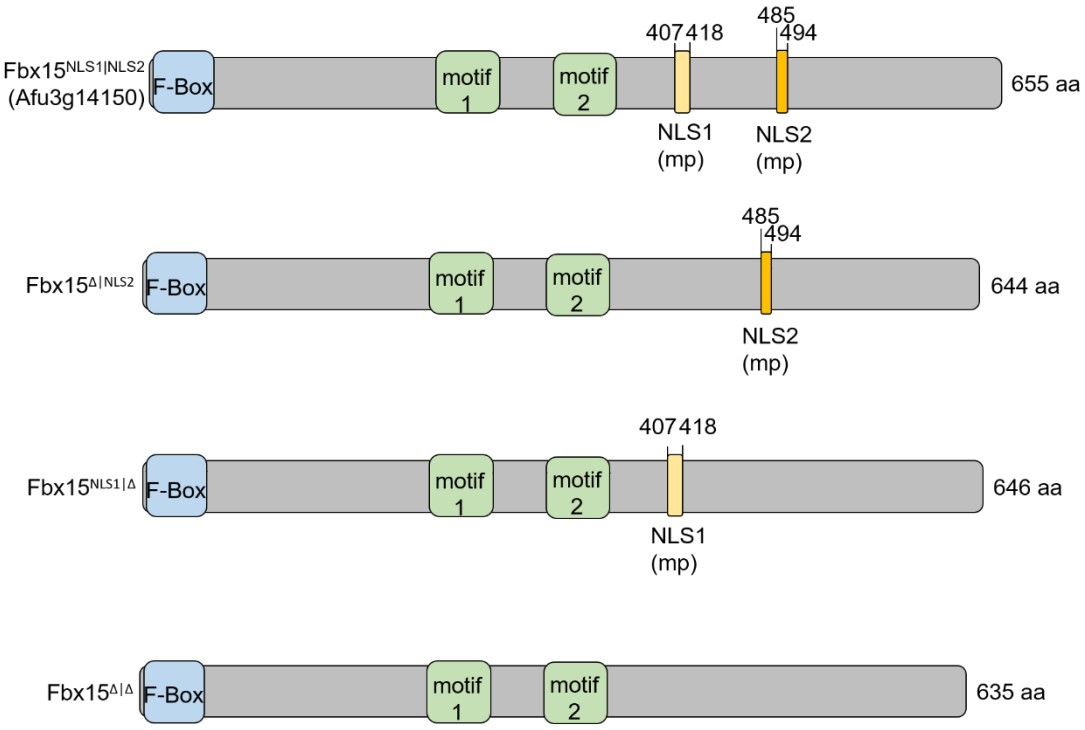

Figure 23: Scheme of natively expressed *A. fumigatus* Fbx15 NLS-deficient variants. Wild type (WT) Fbx15$^{NLS1|NLS2}$ (Afu3g14150) has a protein length of 655 amino acids (aa) and contains a F-box domain, two interaction motifs and two monopartite (mp) NLS sequences at aa 407 to 418 (NLS1) and 485 to 494 (NLS2). The single NLS-deficient strains lack either NLS1 (yellow) or NLS2 (orange) resulting in a total protein length of 644 aa for Fbx15$^{\Delta|NLS2}$ or 646 aa for Fbx15$^{NLS1|\Delta}$. In absence of NLS1 and NLS2 Fbx15 has an aa length of 635 (Fbx15$^{\Delta|\Delta}$). The constructs were integrated in the locus of *A. fumigatus* Δ*fbx15* under its native promoter.

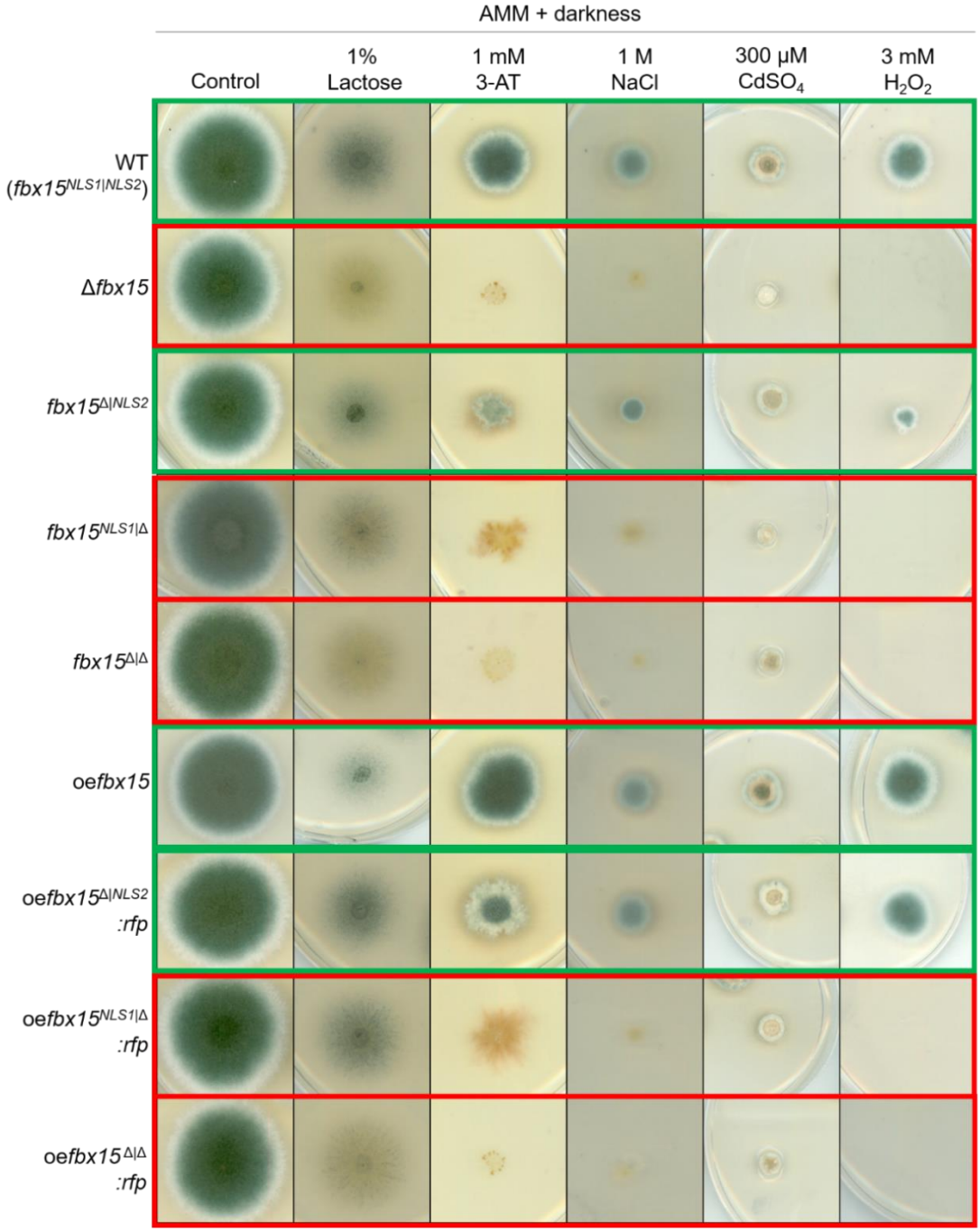

Figure 24: NLS2 is required for the stress response of *A. fumigatus*. Overexpressed *fbx15* (oe*fbx15*) and *fbx15* complementation (*fbx15*^{comp}) were integrated in the locus of Δ*fbx15.* The natively expressed NLS-deficient variants, *fbx15*$^{Δ|NLS2}$, *fbx15*$^{NLS1|Δ}$ and *fbx15*$^{Δ|Δ}$, as well as their oe variants (oe*fbx15*$^{Δ|NLS2}$*:rfp*, oe*fbx15*$^{NLS1|Δ}$*:rfp* and oe*fbx15*$^{Δ|Δ}$*:rfp*) using the constitutively active *gpdA*-promoter were fused to *rfp* and were on-locus integrated in Δ*fbx15*. $2*10^3$ spores of *A. fumigatus* strains were point inoculated on *Aspergillus* minimal medium (AMM) without (control) and with different stress detergents or carbon sources and incubated for three to five days at 37°C in darkness. Phenotypical tests were performed by using following stress inducers: lactose instead of glucose as carbon source, histidine starvation induced by 3-amino-1,2,4-triazol (1 mM 3-AT), osmotic stress induced by natrium chloride (1 M NaCl), heavy metal stress induced by cadmium sulphate (300 µM $CdSO_4$) and oxidative stress induced by hydrogen peroxide (2 mM H_2O_2). WT (*fbx15*$^{NLS1|NLS2}$) and strains containing oe*fbx15* or the *fbx15* variants lacking NLS1 (*fbx15*$^{Δ|NLS2}$*:rfp*, oe*fbx15*$^{Δ|NLS2}$*:rfp*) grow on all media (green frames). Strains lacking NLS2 (*fbx15*$^{NLS1|Δ}$, oe*fbx15*$^{NLS1|Δ}$*:rfp*) or both NLSs (*fbx15*$^{Δ|Δ}$, oe*fbx15*$^{Δ|Δ}$*:rfp*) are sensitive against all tested media containing stress inducers like Δ*fbx15* (red frames). Experiments were performed with at least three biological replicates.

All tested strains, the natively expressed and overexpressed Fbx15 NLS-deficient variants show a similar growth capability on minimal growth conditions like WT, Δ*fbx15* and the overexpression of *fbx15* (oe*fbx15*) (Figure 24, control). Phenotypic analysis on stress media also used in the Chapters 1.2 and 2.1 depicted that the deletion of the amino acid sequence harbouring the second NLS, NLS2, in *fbx15*$^{NLS1|\Delta}$ -, oe*fbx15*$^{NLS1|\Delta}$*:rfp* -, *fbx15*$^{\Delta|\Delta}$ - and oe*fbx15*$^{\Delta|\Delta}$*:rfp* strain, are sensitive as Δ*fbx15* during all tested stress conditions (Figure 24, red frames). In contrast, strains containing the deletion of the amino acid sequence harbouring only the first NLS, NLS1, in *fbx15*$^{\Delta|NLS2}$ and oe*fbx15*$^{\Delta|NLS2}$*:rfp*, are comparable tolerant to the tested stress conditions as WT and oe*fbx15* (Figure 24, green frames).

These results show that NLS2 is the stress-responsive nuclear localisation site of Fbx15, whereas NLS1 on its own is a stress-insensitive nuclear localisation site.

3.3 NLS2 is required to exclude Fbx15 from the nuclear matrix to the nuclear periphery during oxidative stress

The phenotypic analysis revealed that the presence of NLS2 within Fbx15 is a prerequisite for the appropriate fungal stress response in various conditions (Figure 24). The location of the different NLS-variants of Fbx15 were compared in the microscope. Wild type Fbx15, which is located in the nuclear matrix under non-stress conditions (Figure 23), is now excluded from the nuclear matrix and is located in the nuclear periphery during oxidative stress induced by 3 mM H_2O_2 (Jöhnk *et al.*, 2016). The lack of both NLS (oeFbx15$^{\Delta|\Delta}$-RFP) impairs any nuclear location without or with stress (Figure 25). The comparison of the Fbx15 versions carrying only a single NLS revealed a remarkable difference. The presence of only NLS1 (Fbx15$^{NLS1|\Delta}$-RFP) resulted in a Fbx15 distribution, which is different from wild type, because Fbx15 was located within the nucleus without or with stress and the fungus was unable to cope with stress. In contrast, the presence of only NLS2 (Fbx15$^{\Delta|NLS2}$-RFP) resulted in a similar location as wild type, i.e in the absence of stress nuclear location of Fbx15 and in the presence of H_2O_2 mediated stress location in the nuclear periphery (Figure 25). This is consistent with the observed stress phenotypes (Figure 25).

These data corroborate that NLS2 is the stress-responsive nuclear localisation site of Fbx15, which repress NLS1 under stress conditions in a yet unknown molecular mechanism. NLS1 on its own is a stress-insensitive nuclear localisation site.

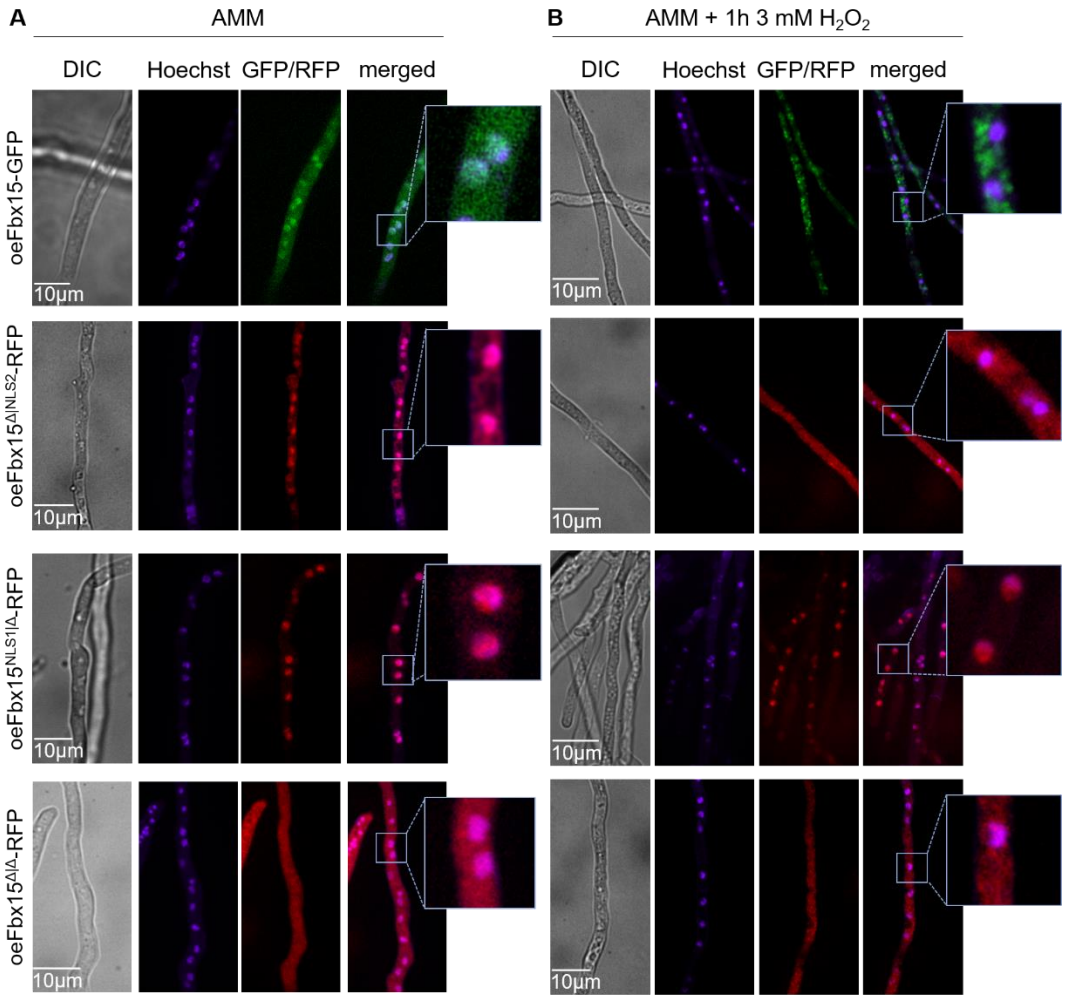

C

Fbx15-variant	Non-stress	H_2O_2-stress
oeFbx15-GFP	N + C	P + C (accumulated)
oeFbx15$^{\Delta\|NLS2}$-RFP	N + C	P + C (diffuse)
oeFbx15$^{NLS1\|\Delta}$-RFP	N + C	N + C
oeFbx15$^{\Delta\|\Delta}$-RFP	P + C (diffuse)	P + C (diffuse)

Figure 25: *A. fumigatus* Fbx15 requires NLS2 to exclude Fbx15 from the nuclear matrix to the nuclear periphery during oxidative stress conditions. Fbx15 fused to GFP, Fbx15$^{\Delta|NLS2}$ fused to RFP, Fbx15$^{NLS1|\Delta}$ fused to RFP and Fbx15$^{\Delta|\Delta}$ fused to RFP were overexpressed by using the constitutively active *gpdA*-promoter and integrated on-locus of Δ*fbx15* for visualisation in fluorescence microscopy. 2*10^3 spores of *A. fumigatus* strains were grown vegetativly in *Aspergillus* minimal medium (AMM) for 18h at 37°C and 18h-old mycelia were incubated for 1h in 3 mM H_2O_2-containing AMM at 37°C in darkness. Hoechst staining was performed to visualise nuclei. Overexpressed Fbx15$^{NLS1|\Delta}$-RFP (oeFbx15$^{NLS1|\Delta}$-RFP) is located in the nucleus (N) rather than in the cytoplasm (C) whereas GFP-/RFP signals of oeFbx15-GFP (accumulated, white arrow), oeFbx15$^{\Delta|NLS2}$-RFP and oeFbx15$^{\Delta|\Delta}$-RFP (diffused, black-white arrows) are observed solely in the nuclear periphery (P) and cytoplasm (C) at oxidative stress. In contrast Fbx15 single NLS-mutant variants (oeFbx15$^{\Delta|NLS2}$-RFP, oeFbx15$^{NLS1|\Delta}$-RFP) are located predominantly in the nucleus (N) whereas the Fbx15 double NLS-mutant variant (oeFbx15$^{\Delta|\Delta}$-RFP) is located in the nuclear periphery (P) and cytoplasm (C) (also see Figure 23). The prevalent localisations are highlighted with underscores in the tabular scheme. Experiments were performed with at least seven biological replicates.

3.4 *A. fumigatus* SsnF localisation in the nucleus during non-stress conditions and at the periphery of the nucleus during oxidative stress conditions requires NLS2, whereas NLS1 results in constitutive nuclear Fbx15 location

Nuclear localisation of the co-repressor subunit SsnF is dependent on Fbx15 in *A. fumigatus* during vegetative growth -and oxidative stress conditions (Jöhnk *et al.*, 2016). The impact of the two NLS sequences of *A. fumigatus* Fbx15 on cellular localisation of SsnF with or without stress was analysed. SsnF contains a predicted bipartite (bip) NLS at aa 679 to 703 on its own, indicating a putative Fbx15-independent ability to enter the nucleus under yet unidentified conditions (Figure 26A). The *ssnF:gfp* construct was integrated ectopically in strains expressing Fbx15 with only NLS2 (Fbx15$^{\Delta|NLS2}$-RFP), with only NLS1 (Fbx15$^{NLS1|\Delta}$-RFP) or without any NLS (Fbx15$^{\Delta|\Delta}$-RFP).

SsnF-GFP in wild type background (in nucleus without stress and in the periphery in the presence of stress), and SsnF-GFP in Δ*fbx15* background (never in the nuclear matrix) were used as control for monitoring cellular localisation of SsnF-GFP (Jöhnk *et al.*, 2016). Under normal non-stress growth conditions, a single NLS with either Fbx15 with NLS1 (Fbx15$^{\Delta|NLS2}$-RFP) or Fbx15 with NLS2 (Fbx15$^{NLS1|\Delta}$-RFP) is sufficient for nuclear localisation of SsnF-GFP like in wild type (Figure 26B, yellow arrows). The absence of both NLS1 and NLS2 in Fbx15 (Fbx15$^{\Delta|\Delta}$-RFP) never results in a location of SsnF-GFP in the nuclear matrix, but only in the nuclear envelop like a strain without Fbx15 (Δ*fbx15*; Figure 26B, orange arrows).

Oxidative stress induced by H_2O_2 results in a SsnF-GFP location which correlates to the location of the different NLS-variants analysed for Fbx15. Fbx15 lacking both NLS sequences (Fbx15$^{\Delta|\Delta}$-RFP) is never in the nuclear matrix and as well SsnF-GFP is only found in the nuclear periphery similar to the Δ*fbx15* strain lacking Fbx15. The presence of only NLS1 (Fbx15$^{NLS1|\Delta}$-RFP) without NLS2 results in a constitutive nuclear localisation of SsnF-GFP during stress in contrast to wild type (Figure 26C, yellow arrow). NLS2 alone without NLS1 (Fbx15$^{\Delta|NLS2}$-RFP) results in nuclear location of SsnF-GFP without stress and location in the nuclear periphery with stress – like it was shown for Fbx15$^{\Delta|NLS2}$ itself (Fig. 23, Fig. 26).

This correlation between the nuclear location without stress and the location in the nuclear periphery with stress for SsnF and for Fbx15 with NLS2 further supports that NLS2 is the stress-responsive element, which guides Fbx15 as well as SsnF to the correct cellular location with and without stress.

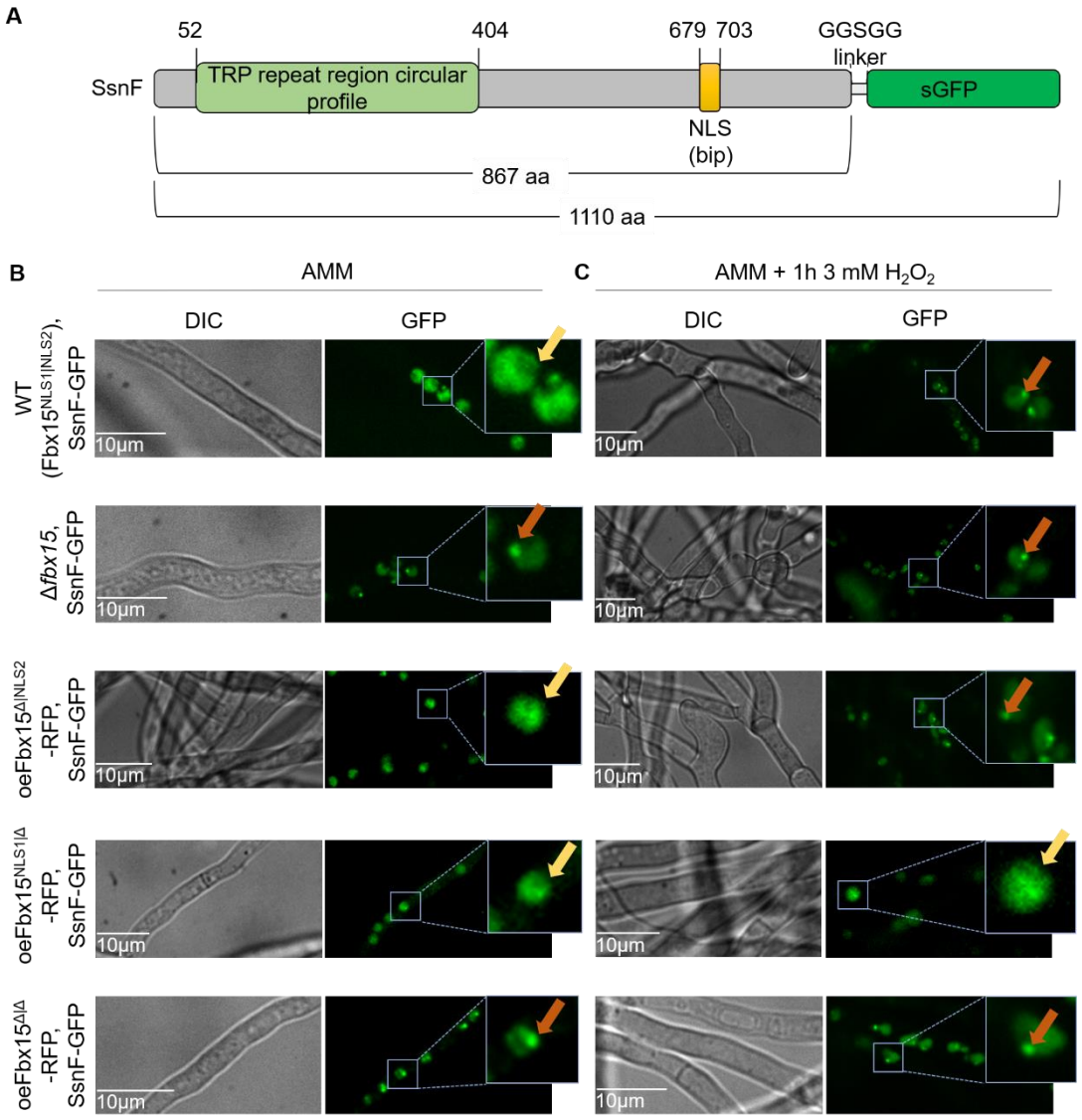

D

SsnF-GFP in Fbx15-variant	Non-stress	H_2O_2-stress
$Fbx15^{NLS1\|NLS2}$, SsnF-GFP	N	P
Δ*fbx15*, SsnF-GFP	P	P
$oeFbx15^{\Delta\|NLS2}$-RFP, SsnF-GFP	N	P
$oeFbx15^{NLS1\|\Delta}$-RFP, SsnF-GFP	N	N
$oeFbx15^{\Delta\|\Delta}$-RFP, SsnF-GFP	P	P

Figure 26: *A. fumigatus* Fbx15-NLS1 alone supports constitutive nuclear location of SsnF, whereas NLS2 distributes SsnF (with or without NLS1) during non-stress conditions to the nucleus and during stress to the periphery. (**A**) The 867 amino acids (aa) long SsnF consists of a tetratricopeptide (TRP) repeat at aa position 52 to 404 and a putative bipartite (bip) NLS at aa position 679 and 703. The 1110 aa long SsnF-GFP fusion construct was integrated ectopically in the strains expressing overexpressed Fbx15 NLS-deficiencies (oeFbx15$^{NLS1|\Delta}$-RFP, oeFbx15$^{\Delta|NLS}$-RFP and oeFbx15$^{\Delta|\Delta}$-RFP). (**B**) 2*10^3 spores of *A. fumigatus* strains were grown vegetatively in *Aspergillus* minimal medium (AMM) for 18h at 37°C in darkness. Fluorescence microscopic imaging revealed that SsnF-GFP is in the nucleus (N) during non-stress conditions in wild type (WT) expressing Fbx15$^{NLS1|NLS2}$, strains expressing oeFbx15$^{\Delta|NLS2}$-RFP or oeFbx15$^{NLS1|\Delta}$-RFP (yellow arrows), whereas SsnF-GFP accumulated in the nuclear periphery (P) in Δ*fbx15* and the strain expressing oeFbx15$^{\Delta|\Delta}$-RFP (orange arrows). (**C**) 18h-old hyphae were incubated in hydrogen peroxide (3 mM H_2O_2)-containing AMM for 1h in darkness. SsnF-GFP accumulates at the nuclear periphery (P) in WT, in the strains expressing oeFbx15$^{\Delta|NLS2}$-RFP or oeFbx15$^{\Delta|\Delta}$-RFP (orange arrows). In the strain expressing oeFbx15$^{NLS1|\Delta}$-RFP SsnF-GFP is in the nucleus (N) at oxidative stress (yellow arrows). Experiments were performed with three biological replicates.

3.5 Fbx15 cellular location during oxidative stress depends on the phosphorylation status at residues S468|9 but is not relevant during non-stress conditions

A. fumigatus NLS2 is the stress-responsive Fbx15 nuclear location site, which is as well required for the cellular distribution of Fbx15 as for the co-repressor subunit for SsnF to the nuclear matrix (without stress) or the nuclear periphery (with stress) (Figure 23, 25, 26). The phosphorylation status at S469 (98% probability to be phosphorylated) and maybe also to a minor extent of S468 (2% probability to be phosphorylated) represents an additional layer of cellular localisation control of the co-repressor subunit SsnF. It was shown that SsnF can enter the nucleus when constant phosphorylation of Fbx15 S469 is mimicked by genetically introducing a negative charge, whereas constant dephosphorylation mimicking of Fbx15 at S468 and S469 results in a cytoplasmic accumulation of SsnF at the nuclear envelope (Jöhnk *et al.*, 2016). These previous studies where completed. Both Ser residues were together replaced and substitutions mimicked phosphorylation or dephosphorylation. In this way any putative uncontrolled changes in the phosphorylation status on these Ser residues should be prevented. The localisation of Fbx15-phosphorylation variants were compared to wild type Fbx15 fused to GFP. Mimicking dephosphorylation of the S468 and S469 was achieved by exchanging the codons for Ser to Ala (Fbx15$^{S468|9A}$). Mimicking phosphorylation of the S468 and S469 was achieved by exchanging Ser to aspartate (Fbx15$^{S468|9D}$). The constructs *fbx15*$^{S468|9A}$ and *fbx15*$^{S468|9D}$ were C-terminally fused to RFP and overexpressed by utilising the *gpdA* promoter resulting in Fbx15$^{S468|9A}$- and Fbx15$^{S468|9D}$-RFP (both 916 aa long) (Figure 27A). OeFbx15$^{S468|9A}$-RFP and oeFbx15$^{S468|9D}$-RFP were

predominantly located in the nucleus like oeFbx15-GFP at vegetative growth (Figure 27B, D). OeFbx15$^{S468|9D}$-RFP is impaired in nuclear localisation resulting in a diffused localisation in the complete hyphae (Figure 27C, D, black-white arrow). In contrast, oeFbx15-GFP is located outside the nucleus in accumulated structures (Figure 27C, D, white arrow). OeFbx15$^{S468|9A}$-RFP was primarily located in the nucleus (Figure 27C, D).

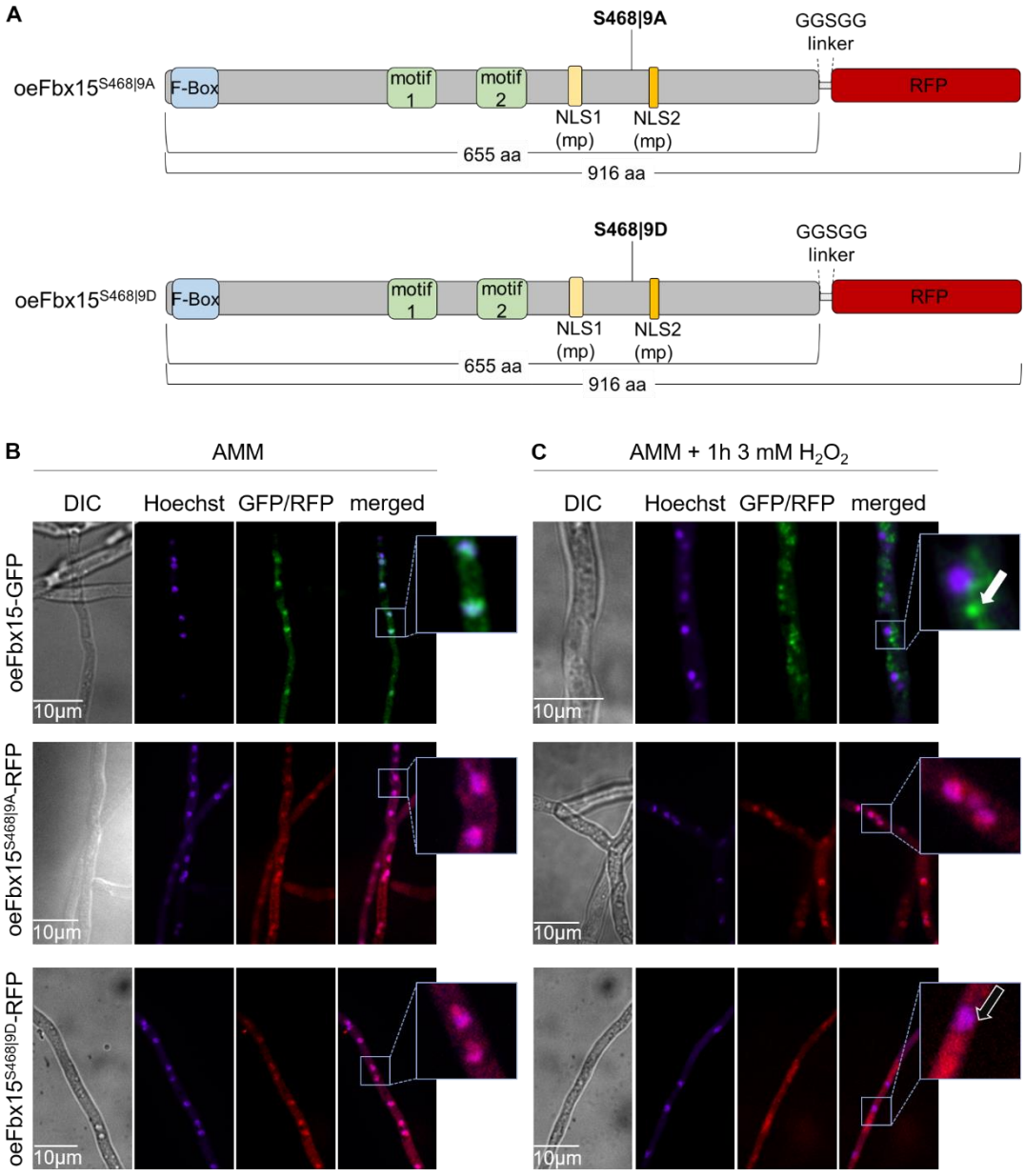

D

Fbx15-variant	Non-stress	H_2O_2-stress
oeFbx15-GFP	N + C	P + C (accumulated)
oeFbx15$^{S468|9A}$-RFP	N + C	N + C
oeFbx15$^{S468|9D}$-RFP	N + C	P + C (diffuse)

Figure 27: Phosphorylation at S468|9 is required for the cytoplasmic localisation of Fbx15 at oxidative stress in *A. fumigatus*. (**A**) The Fbx15 phospho-mimicking variants were fused to RFP through a glycine-glycine-serine-glycine-glycine (GGSGG)-linker and were overexpressed by using the constitutively active *gpdA*-promoter for microscopic visualisation. Fbx15 mimicking dephosphorylated serine (Ser) residues S468 and S469 fused to RFP was obtained by the exchange of Ser to alanine (Ala), resulting in oeFbx15$^{S468|9A}$-RFP. Fbx15 mimicking phosphorylated S468 and S469 fused to RFP was obtained by the exchange of serine to aspartate resulting in Fbx15$^{S468|9D}$-RFP. The overexpressed constructs of *fbx15*$^{S468|9A}$*:rfp* and *fbx15*$^{S468|9A}$*:rfp* were integrated in the locus of Δ*fbx15*. Hoechst staining was performed to visualise nuclei. (**B**) 2*10^3 spores of *A. fumigatus* strains were grown vegetatively in Aspergillus minimal medium (AMM) for 18h at 37°C in darkness. Overexpressed Fbx15 fused to GFP integrated in the locus of Δ*fbx15* (oeFbx15-GFP), oeFbx15$^{S468|9A}$-RFP and oeFbx15$^{S468|9D}$-RFP are predominantly in the nucleus at vegetative growth. Experiments were performed with at least eight biological replicates. (**C**) 18h-old hyphae were incubated in 3 mM H_2O_2-containing AMM for 1h at 37°C in darkness inducing oxidative stress conditions. OeFbx15$^{S468|9A}$-RFP is predominantly located in the nucleus whereas oeFbx15-GFP (accumulated, white arrow) and oeFbx15$^{S468|9D}$-RFP (diffused, black-white arrow) are solely at the nuclear periphery and in the cytoplasm. Experiments were performed with at least eight biological replicates. (**D**) Tabular scheme of the cellular localisation of oeFbx15-GFP, oeFbx15$^{S468|9A}$-RFP and oeFbx15$^{S468|9D}$-RFP at vegetative growth and oxidative stress induced by H_2O_2. N: Nucleus, C: Cytoplasm, P: Nuclear periphery. The prevalent localisations are highlighted with underscores.

These data suggest that vegetative growth conditions without stress allow the nuclear localisation of Fbx15 with a charged as well as an uncharged amino acid at S468|9 and therefore independently of the phosphorylation status. During oxidative stress a negative charge and therefore the phosphorylation status at S468|9 (Fbx15$^{S468|9D}$) is essential for excluding Fbx15 from the nuclear matrix to the cytoplasm or the nuclear periphery. Without a negative charge mimicking dephosphorylation at S468|9 (Fbx15$^{S468|9A}$) resulted in nuclear accumulation. In comparison to the obtained data described in Chapter 3.1 and 3.3 dephosphorylation at S468|9 corresponds to the localisation of Fbx15 with exclusively NLS1, whereas phosphorylation at S468|9 leads to the same cellular localisation as of Fbx15 with only NLS2.

3.6 Phosphorylation during *A. fumigatus* vegetative growth and dephosphorylation during oxidative stress is independent of the presence or absence of an intact NLS1 or NLS2 within Fbx15

A. fumigatus Fbx15 cytoplasmic localisation during oxidative stress conditions is linked to Fbx15 NLS2 and the phosphorylation status at S468|9 (Figure 25, 27). Therefore, it was examined if the NLS sequences are required for the phosphorylation status of *A. fumigatus* Fbx15 during oxidative stress conditions induced by H_2O_2. In order to address this question, the phosphorylation status of the overexpressed versions of Fbx15-GFP (oeFbx15-GFP) and its single deletion constructs of NLS1

and NLS2 fused to RFP (oeFbx15$^{\Delta|NLS2}$-RFP, Fbx15$^{NLS1|\Delta}$-RFP) were analysed during oxidative stress conditions through immunoprecipitation. The overexpressed Fbx15-variant mimicking dephosphorylation at Ser residues 468 and 469 fused to RFP (oeFbx15$^{S468|9A}$-RFP) was used as control.

OeFbx15$^{\Delta|NLS2}$-RFP, oeFbx15$^{NLS1|\Delta}$-RFP and oeFbx15$^{S468|9A}$-RFP were detected in western hybridisation with the Ser/Thr phospho antibody like oeFbx15-GFP during vegetative growth conditions. Oxidative stress conditions resulted in a significant decreased abundance of oeFbx15-GFP, oeFbx15$^{\Delta|NLS2}$-RFP and oeFbx15$^{NLS1|\Delta}$-RFP detected with the Ser/Thr phospho antibody comparable to non-stress conditions. Ser/Thr signals of oeFbx15$^{S468|9A}$-RFP were not significantly changed under oxidative stress conditions (Figure 28).

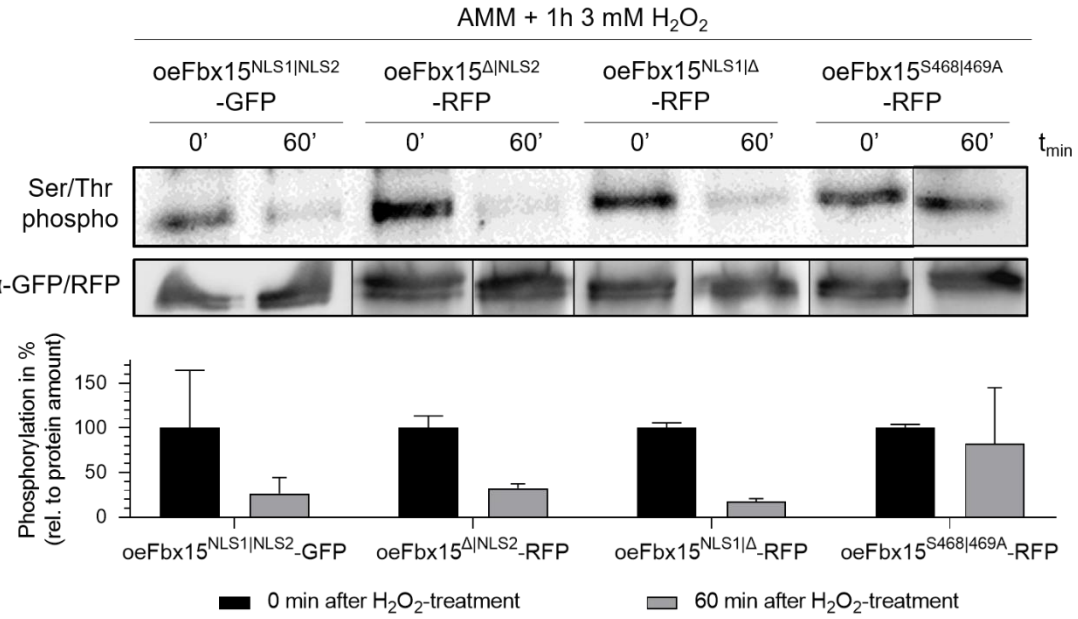

Figure 28: The phosphorylation status of *A. fumigatus* Fbx15 is independent of its NLSs during vegetative growth and oxidative stress conditions. Overexpressed Fbx15 fused to GFP (oeFbx15-GFP) was integrated on-locus of Δ*fbx15.* Overexpressed Fbx15 fused to RFP mimicking dephosphorylated serine (Ser) residues S468 and S469 by the exchange of Ser to alanine (Ala) (oeFbx15$^{S468|9A}$-RFP) and NLS1 deletion (oeFbx15$^{\Delta|NLS2}$-RFP) and NLS2 (oeFbx15$^{NLS1|\Delta}$-RFP) deletion variants were integrated in the locus of Δ*fbx15*. 2*10^8 spores of *A. fumigatus* strains were grown vegetatively in *Aspergillus* minimal medium (AMM) for 18h at 37°C. For the induction of oxidative stress 18h-old hyphae were incubated in hydrogen peroxide (3 mM H_2O_2-treatment)-containing AMM for 60 min. Immunoblotting with an antibody against phosphorylated Ser- and threonine (Thr)-residues was done with GFP-/RFP pulldown purified overexpressed GFP-/RFP-tagged Fbx15 variants before and after 1h incubation in H_2O_2-containing AMM. Dephosphorylation under oxidative stress conditions was quantified against the overall amount of GFP-/RFP-tagged Fbx15 variants. Error bars represent the SEM and were calculated from two biological replicates. Significances were determined with one-way Anova and Student’s t-test (*P*-value: **P*<0.01, n.s.: not significant). A decreased phosphorylation of oeFbx15$^{\Delta|NLS2}$-RFP and Fbx15$^{NLS1|\Delta}$-RFP upon H_2O_2-stress is shown in the same stage as for oeFbx15-GFP. For oeFbx15$^{S468|9A}$-RFP phosphorylated Ser- and Thr-residues are detected, which are not significantly different during oxidative stress conditions. Experiments were performed with two biological replicates.

These data show that NLS1 or NLS2 are dispensable for *A. fumigatus* Fbx15 overall phosphorylation status at non-stress or oxidative stress. This indicates that their impact on the proteins' cellular localisation is independently of the overall phosphorylation status of *A. fumigatus* Fbx15 at vegetative growth or oxidative stress. Moreover, S468 and S469 are not the only residues critical control the phosphorylation status of the whole *A. fumigatus* Fbx15 protein, however, they are required for the cellular localisation of Fbx15 during oxidative stress response.

This study revealed more detailed insights into the interplay between *A. fumigatus* Fbx15 and SsnF during growth without or with oxidative stress. SsnF is localised inside the nuclear matrix either with Fbx15 harbouring NLS1 or NLS2 under non-stress conditions. During oxidative stress Fbx15 NLS-deletion variants and SsnF are simultaneously located outside the nuclear matrix like the nonmutated Fbx15 protein (Table 6).

Dephosphorylation at Fbx15 S468|9 leads to an accumulation of SsnF outside the nuclear matrix (Jöhnk *et al.*, 2016), whereas, in contrast, Fbx15 itself is presumably primarily located inside the nuclear matrix at both conditions (Figure 27) (Table 6). The phosphorylation at Fbx15 S469 leads to an accumulation of SsnF in the nuclear matrix at non-stress as well as oxidative stress (Jöhnk *et al.*, 2016), whereas Fbx15 is located in the nuclear matrix at vegetative growth and outside the nuclear matrix at oxidative stress (Figure 27) (Table 6).

In summary, the two NLS sequences of Fbx15 represent a sophisticated control system for simultaneous localisation of Fbx15 and SsnF in the nuclear matrix at non-stress conditions. Fbx15 NLS2 serves as regulatory element during stress response by inhibiting the nuclear import function of NLS1 in a yet unknown mechanism. Thereby, NLS2 triggers the location of both proteins outside the nuclear matrix at oxidative stress. The phosphorylation/dephosporylation at S468|469 of Fbx15 represents an additional level of control for the location of Fbx15 and SsnF within the cell, which is primarily relevant during growth in the presence of stress.

Table 6: Summary of the cellular localisation of the *A. fumigatus* Fbx15 variants and SsnF in dependency of Fbx15 variants during non-stress - and oxidative stress conditions. + = in the nuclear matrix, - = outside the nuclear matrix (in nuclear periphery and/or cytoplasm). *Published data from Jöhnk *et al.*, 2016.

	Non-stress	**H_2O_2-stress**
$Fbx15^{NLS1\|NLS2}$	+*	-
SsnF*	+	-
$Fbx15^{\Delta\|NLS2}$	+	-
SsnF	+	-
$Fbx15^{NLS1\|\Delta}$	+	+
SsnF	+	+
oe$Fbx15^{\Delta\|\Delta}$-RFP	-	-
SsnF	-	-
$Fbx15^{S468\|9A}$ (not phos.)	+	+
SsnF*	-	-
$Fbx15^{S468\|9D}$ (similar to phos.)	+	-
SsnF*	+	+

IV Discussion

1 NLS2 takes Fbx15 and SsnF to the nuclear periphery during stress, whereas without stress NLS1 or NLS2 take both proteins into the nucleus in *A. fumigatus*

This study has revealed that the *A. fumigatus* Fbx15 second nuclear localisation signal, NLS2, is a stress-response element needed for the adaptation of *A. fumigatus* to various environmental stresses, whereas the first nuclear localisation signal, NLS1, is stress-insensitive. Precisely, both NLS sequences of Fbx15 are capable for the transport of Fbx15 in a significantly phosphorylated state together with SsnF in the nuclear matrix at vegetative growth, whereas NLS2 is besides required for the localisation of Fbx15 in a significantly dephosphorylated state and the co-repressor subunit SsnF outside the nuclear matrix at oxidative stress. Thereby, NLS2 has a putative inhibitory function regarding the activity of NLS1 (Figure 29).

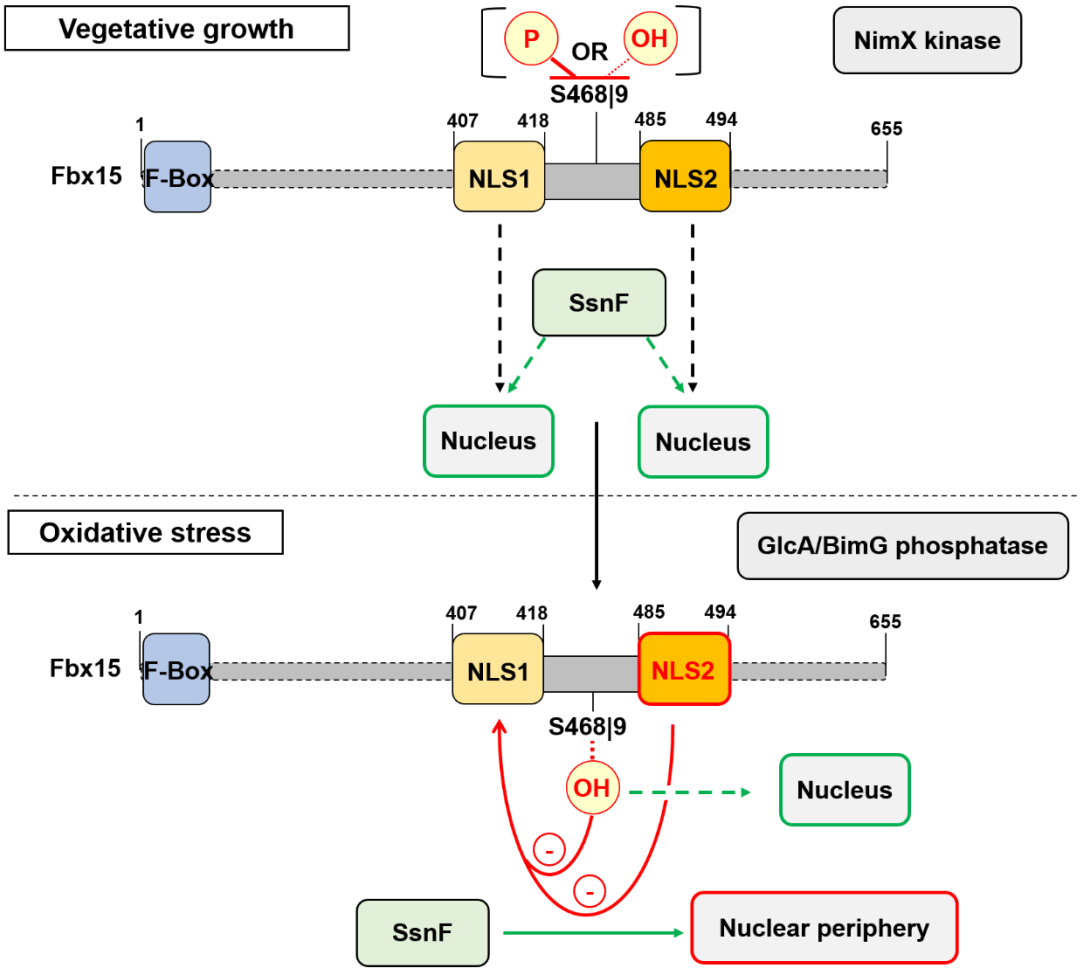

Figure 29: Model of Fbx15 NLSs functions during vegetative growth and oxidative stress conditions in *A. fumigatus*. At vegetative growth the Fbx15 nuclear localisation signals (NLS) 1 and 2 mediate independent of each other the localisation of a significant portion of Fbx15 within the nucleus (black dashed lines) together with the co-repressor subunit SsnF (green dashed lines). Unphosphorylated Fbx15 (OH, thin red dashed line) as well as presumably NimX kinase mediated phosphorylation at S468|9 (P, bold red line) provides nuclear localization of Fbx15 during growth without stress. Oxidative stress results in reduced Fbx15 phosphorylation presumably through the GlcA/BimG phosphatase and results in localisation of SsnF at the nuclear periphery (green line). The molecular mechanism of the inhibitory function of NLS2 on the nuclear import activity of NLS1 is yet unknown. The unphosporylated form of S468|9 during oxidative stress (red lines) provides an additional control level for inhibiting the nuclear localisation of Fbx15 at oxidative stress.

In general, Fbx15 phosphorylation might be favoured by the NimX kinase during non-stress vegetative growth, whereas the GlcA/BimG phosphatase acts during oxidative stress (Jöhnk *et al.*, 2016) (Figure 29). Phosphorylation of Fbx15 residues S468|9 is presumably predominant at vegetative growth but does not seem to be required for the nuclear localisation of Fbx15. During vegetative growth there is a co-localisation of Fbx15 and SsnF in the nucleus. Oxidative stress dephosphorylates S468|9 and results in nuclear localization of Fbx15, but no more co-localisation with SsnF, which is primarily found in the periphery of the nucleus or even in the cytoplasm. The displayed molecular mechanism is discussed in detail in this chapter.

1.1 NLS2 is a stress-response element, whereas NLS1 is mainly functional in mediating Fbx15 nuclear localisation

In this study it has been investigated that both NLS sequences of *A. fumigatus* Fbx15, NLS1 and NLS2, are independent of each other sufficient for the import of Fbx15 into the nucleus during non-stress conditions. However, NLS1 alone without NLS2 is not able to take Fbx15 to the nuclear periphery in accumulated structures at oxidative stress. Instead the presence of NLS1 alone leads to a nuclear accumulation of Fbx15 (Figure 25). This indicates that NLS1 is capable to interact with nuclear import relevant proteins such as importins at vegetative growth and oxidative stress. A constantly intact nuclear transport driven by a putative high affinity of NLS1 to importins results in a disturbance of required interactions with other proteins during stress response as the sole presence of NLS1 leads to similar phenotypes like the loss of the *fbx15* gene (Figure 24).

For the localisation of Fbx15 outside the nucleus at stress the presence of NLS2 is required, here tested with oxidative stress (Figure 25). Importantly, the presence of NLS2 alone leads not an accumulation of Fbx15 near the nucleus as shown for the wild type-like Fbx15 at oxidative stress (Figure 25). Putatively, NLS2 is required to inhibit the nuclear import during oxidative stress in an unknown mechanism resulting in an accumulation of Fbx15 at the nuclear periphery as *A. fumigatus* Fbx15 does not contain any NES

sequences signalising its capability for nuclear export (Jöhnk *et al.*, 2016; Wen *et al.*, 1995). The activity of NLS1 in, for instance, its interaction with importins might be inhibited in this context. This would explain why the sole presence of NLS1 leads to a clear accumulation of Fbx15 in the nucleus at oxidative stress.

These putative additional functions of NLS2 are rather untypical as NLS sequences are characterised as binding elements for importins. NLS sequences with other functions besides to the nuclear localisation of the adjacent proteins were already described. The NLS of the ubiquitin-specific protease 7 (USP7)–ring finger protein 169 (RNF169) has, besides to its function in nuclear localisation, a role in driving DNA repair and poly (ADP-ribose) polymerase inhibition resistance by mediating a direct interaction with a deubiquitylase for enhanced stability (An *et al.*, 2017). Furthermore, the NLS of the interferon cytokine IFNγ is required for the full expression of the biological activity of IFNγ independently of its cellular localisation (Subramaniam *et al.*, 2000). In consequence, NLS2 of Fbx15 could have additional functions besides a nuclear transport of Fbx15.

In case of an inhibitory function of NLS2 regarding NLS1 activity an example for a direct regulation of domains by other domains within the same protein sequence is described in Yokogawa *et al.* 2016. The described RNase Regnase-1 contains four domains: N-terminal domain (NTD), PilT N-terminus like (PIN) domain, zinc finger (ZF) domain and C-terminal domain (CTD). The RNase catalytic centre of Regnase-1 is sitting within the PIN domain which gets enhanced in its activity when the NTD interacts with the PIN domain. Thereby, the PIN domain forms a dimer interface which overlaps with the NTD binding site. Additionally, the ability to form head-to-tail oligomers of the PIN domain is essential for the proteins' RNase activity which indicates that, besides the PIN-NTD interaction, a PIN-PIN interaction is required to for the function of Regnase-1 RNase activity (Yokogawa *et al.*, 2016). Probably, NLS2 of Fbx15 may regulate NLS1 in an opposite mechanism compared to NTD-PIN interaction during oxidative stress conditions. In this process the direct or indirect interaction through other proteins of NLS2 with NLS1 leads to the inactivation of NLS1 or inhibition of its activity. How the interaction of NLS1 and NLS2 is performed is unknown.

Besides of a putative regulatory function of NLS2 regarding the NLS1 activity, NLS2 could act as a potential binding site for other proteins triggering Fbx15 nuclear export or its degradation in the nucleus. From previous studies it is known that Fbx15 is a stable protein compared to another conserved *A. fumigatus* F-box protein, SconB (Jöhnk *et al.*, 2016). On the first glance, a degradation of Fbx15 in the nucleus is therefore rather unlikely, however, a degradation of Fbx15 in the nucleus in combination with an enriched Fbx15 amount outside the nucleus resulting from an inhibited nuclear import cannot be excluded. On the other point of view, an export of Fbx15 triggered by the binding to other proteins

through NLS2 might be possible. These proteins could mediate the nuclear export of Fbx15 via a shuttle mechanism, consequently Fbx15 does not need a NES signal to get outside the nuclear matrix. Moreover, a putative function of NLS2 in the interaction of Fbx15 with other proteins is probably given in the cytoplasm at oxidative stress. This suggestion is underpinned by the fact that NLS1 alone as well as the a loss of both NLS sequences lead to the same sensitivity against oxidative stress and other stressors as observed for the *fbx15* deletion strain but these Fbx15 NLS-mutants are located differently in the cell: $Fbx15^{NLS1|\Delta}$ in the nucleus, $Fbx15^{\Delta|\Delta}$ outside the nucleus similar to WT Fbx15 or $Fbx15^{\Delta|NLS2}$ (Figure 24, Figure 25). A loss of NLS2 results therefore in a sensitivity against stressors indicating that NLS2 is a stress-response element in contrast to NLS1, whose loss and sole presence of NLS2 results in WT-like stress tolerance (Figure 24).

Taken together, NLS2 is a stress response-relevant element of Fbx15 which is required for the inhibition of NLS1 activity regarding nuclear import at oxidative stress in a so far unknown mechanism. Instead, NLS1 itself is insensitive against stress. During stress conditions NLS2 is maybe required for the interaction with other proteins relevant for the Fbx15-dependent stress response but this remains to be elucidated.

1.2 Correct localisation of SsnF requires NLS1 or NLS2 of Fbx15 at vegetative growth and a repressed NLS1 of Fbx15 at oxidative stress

This study shows that the NLS sequences of Fbx15 are involved in the cellular localisation of SsnF at vegetative growth and oxidative stress. Thereby, SsnF is located inside the nuclear matrix in presence of Fbx15 NLS1 or - NLS2 without stress as the corresponding Fbx15 NLS variants but outside the nuclear matrix in absence of both NLS sequences, NLS1 and NLS2 (Figure 22, 26). SsnF composites a bipartite NLS (Figure 26). Nonetheless, SsnF nuclear transfer is regulated by the presence of Fbx15 at vegetative growth (Jöhnk *et al.*, 2016) (Figure 26). Therefore, it is conceivable that the NLS of SsnF is either not active or gets activated by dependent on Fbx15 during vegetative growth.

NLS sequences can be intermolecular masked and unmasked through interaction partners that finally controls the nuclear import of the corresponding protein as previously described for the inhibitor of κB, which masks the NLS of the transcriptional regulator NF-κB from nuclear import (Beg *et al.*, 1992; Ganchi *et al.*, 1992; McLane and Corbett, 2009; Zabel *et al.*, 1993). In chapter 1.1 was described that NLS sequences can function in a nuclear import-independent manner. The observed binding of Fbx15 and SsnF in the cytoplasm and the final co-localisation in the nucleus (Jöhnk *et al.*, 2016) might serve as a regulatory process, in which SsnF gets intermolecular modified leading to an unmasking of its bipartite NLS and this through Fbx15, in particular its NLS2 (Figure 26). Nonetheless, the

exact mechanism how SsnF gets into the nuclear matrix – via unmasking of its NLS sequence or via a direct shuttle with Fbx15 – is yet elusive.

Moreover, the localisation of SsnF outside the nuclear matrix during oxidative stress conditions is blocked when NLS1 is solely present similar to the localisation of the corresponding Fbx15 variant. Additionally, SsnF is located outside the nuclear matrix at oxidative stress when NLS1 and NLS2 of Fbx15 are absent comparable to the cellular localisation of this particular Fbx15 variant (Figure 22, Figure 25, Figure 26). *A. fumigatus* Fbx15 NLS2 is suggested to inhibit the function or block the activity of NLS1 regarding nuclear import or promoting Fbx15 degradation in the nuclear matrix or promoting the interaction with other proteins relevant for a putative Fbx15-nuclear export at oxidative stress (chapter 1.1). Therefore, it is conceivable that this inhibitory function of *A. fumigatus* Fbx15 NLS2 on NLS1 activity or a putative NLS2-promoted degradation or interaction with other proteins affects the final co-localisation of SsnF and Fbx15 outside the nuclear matrix in a so far an unknown mechanism.

Taken together, the cellular localisation of SsnF is dependent on Fbx15 during vegetative growth conditions in *A. fumigatus.* Thereby, the bipartite NLS of SsnF gets putatively unmasked by Fbx15 though its NLS sequences, NLS1 or NLS2, or is inactivated at vegetative growth leading to a Fbx15-dependent nuclear shuttle mechanism independently on the presence of the SsnF NLS. How this shuttle mechanism is performed or if the co-localisation of SsnF and Fbx15 results from a Fbx15 NLS-dependent unmasking of the SsnF NLS sequence remains to elucidated.

1.3 NLS1 and NLS2 do not influence the phosphorylation status of Fbx15 at vegetative growth or at oxidative stress

A significant part of Fbx15 gets dephosphorylated during oxidative stress in *A. fumigatus* (Jöhnk *et al.*, 2016) (Figure 28). In this study was elucidated that the NLS sequences of *A. fumigatus* Fbx15 regulate the cellular localisation of Fbx15 independent on its overall phosphorylation status and, moreover, the overall phosphorylation of Fbx15 at vegetative growth is independent on S468|9 (Figure 28).

In general, proteins get phosphorylated through protein kinases and dephosphorylated through phosphatases (Ardito *et al.*, 2017; Barford, 1996; Slack, 2014; Zhang, 2002). *A. fumigatus* NimX is the homolog of the cyclin-dependent kinase1 NimX of *A. nidulans* (Ye *et al.*, 1999). The Ser/Thr kinase is essential in *A. fumigatus* and is the only kinase, which was identified to interact with Fbx15 in the cytoplasm (Jöhnk *et al.*, 2016). Ser - or Thr residues get phosphorylated at their alcohol groups (OH) using phosphate esters generated with gamma phosphate of ATP or GTP (Dickman and Yarden, 1999). In the

amino acid sequence of Fbx15 several Ser - and Thr residues were found next to S468 and S469 (Jöhnk *et al.*, 2016). Therefore, it is most likely the case that other Ser - and/or Thr residues of *A. fumigatus* Fbx15 are responsible for its phosphorylation status during non-stress conditions, which is presumably driven by the Ser/Thr kinase NimX but not dependent on the NLS sequences of Fbx15. Same situation could be present for the interaction of Fbx15 with the essential phosphatase GlcA, which occurs primarily during H_2O_2-stress in the cytoplasm (Jöhnk *et al.*, 2016).

In general it is unknown if *A. fumigatus* Fbx15 is able get completely dephosphorylated but this study has clarified that the overall phosphorylation status of Fbx15 is not depending on NLS1 or NLS2. The protein kinase NimX and the phosphatase GlcA/BimG might phosphorylate or dephosphorylate Fbx15, which probably take place on Ser-/ Thr residues additional to or independent of S468 and S469 but this remains to be elucidated.

1.4 The phosphorylation status at S468|9 determines Fbx15 and SsnF cellular localisation during stress

A. fumigatus Fbx15 is primarily in the nucleus during vegetative growth conditions (Jöhnk *et al.*, 2016) (Figure 22) and primarily outside the nuclear matrix upon oxidative stress (Figure 25). Thereby, Fbx15 is phosphorylated during non-stress conditions and becomes significantly dephosphorylated upon oxidative stress (Jöhnk *et al.*, 2016) (Figure 28). Mimicking dephosphorylation of Fbx15 at its most probable phosphorylation sites S469 (98%) and S468 (2%) leads to a nuclear localisation of Fbx15 as well as at non-stress - and at oxidative stress conditions (Figure 27). Mimicking dephosphorylation at S468|9 does not affect Fbx15 overall phosphorylation at vegetative growth, which suggests that additional Ser- and/or Thr residues of *A. fumigatus* Fbx15 are targets for phosphorylation at non-stress conditions. (Figure 28).

This study did not elucidate if both Ser residues are simultaneously phosphorylated in the cell. Phosphorylation at S468|9 leads to a similar Fbx15 localisation in the nuclear matrix at vegetative growth like the dephosphorylation variant at S468|9. Fbx15 is significantly dephosphorylated during oxidative stress conditions, which results in nuclear location Fbx15 (Figure 27) but without SsnF, which is located in the nuclear periphery (Jöhnk *et al.*, 2016). The small amount of S468|9 phosphorylated Fbx15 might be even localized outside of the nuclear matrix at oxidative stress (Figure 27). This suggests that the phosphorylation status at S468 and S469 for the cellular localisation of Fbx15 is only relevant during oxidative stress.

Recent studies have shown that the phosphorylation of the NLS in the mammalian GM130 reduce its binding to p115, but enhance its affinity to importin α and *vice versa* (Chang *et*

al., 2019). Mammalian GM130 is required for targeting transport vesicles to the Golgi together with the vesicle tethering factor p115 (Sönnichsen *et al.*, 1998; Waters *et al.*, 1992). Replacing the required phosphorylation site S385 of GM130 with aspartic acid mimicking constant phosphorylation results in an increased binding affinity for importin α5, which demonstrates that the specificity of the response is driven by the phosphate moiety (Chang *et al.*, 2019). It will be interesting to examine the similarities and differences to the S468 and S469 phosphorylation/dephosphorylation of Fbx15.

In summary, this study shows that Fbx15 is predominantly present in a dephosphorylated population at oxidative stress. A redundant phosphorylated population cannot be excluded, especially but not only at S468|9, as the artificial phosphorylation at S468|9 indicates Fbx15s' ability to traffic as wild type-like Fbx15 through the nuclear membrane at non-stress and stress-conditions, however, this case could not be verified in this study.

2 Fbx15-mediated secondary metabolism in *A. fumigatus* and *A. nidulans*

2.1 Fbx15 of *A. fumigatus* and *A. nidulans* are involved in secondary metabolite regulation

This study shows that both Fbx15 proteins, *A. fumigatus* - and *A. nidulans* Fbx15, complement each other's functions in the corresponding *fbx15* deletion strain regarding the regulation of secondary metabolism as *A. nidulans* Fbx15 recovers the pale pigmentation of grown colonies in *A. fumigatus* and *vice versa* (Figure 13). Differences in colour pigmentation were associated with an altered secondary metabolite regulation such as for the sterigmatocystin production in *A. nidulans*. Sterigmatocystin is a precursor of a carcinogenic aflatoxin and the enrichment of one of its precursors, norsolorinic acid, results in an orange coloured pigmentation similar to colonies in absence of *A. nidulans fbx15* (Butchko *et al.*, 1999; Hajjar *et al.*, 1989; Hsieh *et al.*, 1976; von Zeska Kress *et al.*, 2012). The global regulator LaeA is involved in the mycelial pigmentation in *A. nidulans* and *A. fumigatus* (Bok and Keller, 2004). In case of Fbx15 a similar regulation of secondary metabolites could be true in *A. fumigatus* and *A. nidulans* as the absence of both F-box proteins results in a dark red or orange pigmentation of hyphae (Jöhnk *et al.*, 2016; von Zeska Kress *et al.*, 2012) (Figure 13). LaeA coordinates the production of developmental and vegetative secondary metabolites in a BrlA-dependent manner in *A. fumigatus*. The zinc cluster transcription factor BrlA represents an activator of conidiation in *Aspergillus* (Adams *et al.*, 1988; Yu *et al.*, 2010). Interestingly, BrlA is required for the SrbA-regulated hypoxia stress response compatible to LaeA (Lind *et al.*, 2018).

A putative similar regulation could be present for the identified direct interaction of *A. fumigatus* Fbx15 and the Fbx15-interacting transcriptional regulator SrbB as both are required for the regulation of four putative identical secondary metabolite (Figure S6). So far 43 secondary metabolites were identified for *A. fumigatus* and 19 out of 44 identified genes are directly linked to secondary metabolite production (Romsdahl and Wang, 2019; Vadlapudi *et al.*, 2017). Many of the found secondary metabolite gene clusters identified in *A. fumigatus* are conserved in other pathogenic fungi such as the neosartoricin gene cluster, whose encoding gene product has a T-cell antiproliferative activity and is therefore suggested to have an immunosuppressive function (Bignell *et al.*, 2016; Raffa and Keller, 2019; Yin *et al.*, 2013). Nonetheless, the identical putative secondary metabolites regulated by *A. fumigatus* Fbx15 and SrbB could not be assign to so far identified secondary metabolites. However, the observed comparable regulation on secondary metabolite levels by *A. fumigatus* Fbx15 and SrbB at vegetative growth could indicate a putative interplay between the two proteins as they are physically interacting with each other at this circumstance.

Taken together, the Fbx15 counterparts of *A. fumigatus* and *A. nidulans* fulfil distinct as well as overlapping functions, which includes that they both are involved in the control of genes for enzymes of their respective secondary metabolism. In this context, a putative interplay between *A. fumigatus* Fbx15 and SrbB regarding the regulation of the biosynthesis of so far unidentified secondary metabolites at vegetative growth is conceivable.

2.2 *A. fumigatus* Fbx15 regulates the production of the mycotoxin fumagillin presumably indirectly through biosynthetic enzymes

Aspergillus spp. produce a wide range of secondary metabolites and are of high interest for research, medicine and biotechnology (Singh *et al.*, 2016; Yoon *et al.*, 2013). In this study the antimicrobial agent fumagillin was identified as secondary metabolite whose production is regulated by Fbx15 next to several other potential, so far unidentified secondary metabolites during non-stress minimal growth conditions in *A. fumigatus* (Figure 21). Fumagillin is a metabolite with antibiotic properties and exclusively synthesized in *A. fumigatus* (Hanson and Eble, 1949; McCowen *et al.*, 1951). First applications of fumagillin were proceed in apiculture against the microsporidian fungal disease caused by *Nosema apis* (Bailey, 1953; Katznelson and Jamieson, 1952). Fumagillin is currently the only effective drug against the *Nosema apis* related *Nosema ceranae* (Higes *et al.*, 2011; Williams *et al.*, 2011, 2008). In human medicine fumagillin is used in immunocompromised patients as prophylaxis against microsporidian

infections or to relieve symptoms after an infection with intestinal microsporidiosis (Lanternier *et al.*, 2009; Molina *et al.*, 2002, 2000).

Fumagillin is synthesized by a cluster of 21 genes (Wiemann *et al.*, 2013). The production of secondary metabolites and pathogenicity are often closely related to each as an adaptive secondary metabolite production controlled by cluster-specific transcription factors guarantees a sufficient growth depending on the present environment such as soil or in a putative host organism (Calvo *et al.*, 2002; Lind *et al.*, 2018). Fumagillin suppresses the immune response of *Galleria mellonella* larvae by inhibiting the activity of phagocytes (Fallon *et al.*, 2011). Despite of this, recent studies have investigated that fumagillin is produced in an *in vitro* pneumocyte cell line infection model and contribute to epithelial cell damage during invasive aspergillosis (Guruceaga *et al.*, 2018). In absence of *A. fumigatus fbx15* is not able to invade in the alveoli in mice at early stage of infection (Jöhnk *et al.*, 2016). As the increased fumagillin biosynthesis in absence of *fbx15* does not result in a WT-like or increased pathogenicity of *A. fumigatus* in the *Galleria mellonella* larvae infection model, it is suggested that Fbx15 is involved in earlier stages during infection than fumagillin. This assumption is supported by an observed loss of virulence when *fbx15* is absent even if fumagillin biosynthesis is de-repressed but known to promote pathogenicity. Also, a direct regulation by the control on localisation level or stability of essential proteins for fumagillin biosynthesis can be excluded because none of the biosynthetic proteins were identified as putative interaction partners of Fbx15 in previous analysis, similarly to gliotoxin biosynthesis-associated proteins (Jöhnk *et al.*, 2016; Wiemann *et al.*, 2013). Therefore, a Fbx15-dependent regulation of fumagillin indirectly through biosynthetic enzymes, that are involved in the fumagillin production in a direct - or more direct manner than Fbx15 is conceivable.

Noteworthy, a derepressive function of fumagillin biosynthesis in dependency of *fbx15* is observed during vegetative growth conditions and not during infection. Protein activities can differ upon environmental circumstances as previously described for VeA (Mooney and Yager, 1990; Stinnett *et al.*, 2007). This would support a putative environmental specificity of Fbx15 regarding fumagillin biosynthesis. In consequence the observed derepressive function of Fbx15 on fumagillin biosynthesis at vegetative growth must not occur during infection.

Taken together, fumagillin biosynthesis is Fbx15-dependent regulated at vegetative growth. This effect might be dispensable for *A. fumigatus* pathogenicity when lacking *fbx15*.

2.3 Fbx15-dependent inhibition of gliotoxin production is independent for Fbx15-dependent *A. fumigatus* virulence in the *Galleria mellonella* infection model and stress response during minimal growth conditions

This study has shown that the deficiency in gliotoxin biosynthesis by deletion of *gliZ* or *gliP* did not result in any altered stress adaptation on AMM compared to *A. fumigatus* AfS35 WT indicating a specialised role of gliotoxin under certain milieus as found in potential host organism. Moreover, the disruption in gliotoxin biosynthesis in absence of *fbx15* did not lead to differences in the sensitivity against tested stressors when compared to the sole deletion of the *fbx15* gene (Figure 19). This shows that the reported Fbx15-dependent regulation in gliotoxin production (Jöhnk *et al.*, 2016) is dispensable for the Fbx15-dependent role in stress adaptation. This indicates either that the repressive function of Fbx15 on gliotoxin production is only present during gliotoxin-inducible conditions or that an overproduction of gliotoxin is dispensable for the adaptation to stress.

Gliotoxin biosynthesis is blocked when the gene *gliP* is deleted and results in an attenuated pathogenicity of *A. fumigatus* in non-neutropenic mice immunosuppressed with hydrocortisone (Sugui *et al.*, 2007). Previous studies have shown that gliotoxin biosynthesis is promoted in the *Galleria mellonella* model but is dispensable for *A. fumigatus* vegetative growth (Reeves *et al.*, 2004). However, in other studies deletion of *gliP* and incorporated block in gliotoxin biosynthesis does not alter virulence in *A. fumigatus* using neutropenic BALC/c mice immunosuppressed with a combination of cyclophosphamide and cortisone acetate suggesting virulence in dependency of gliotoxin formation is host-specific (Kupfahl *et al.*, 2006). This suggestions were supported by the *gliZ* deficient strain, which shows no alterations in pathogenicity compared to WT in mice immunocompromised by intraperitoneal injection of cyclophosphamide (Bok *et al.*, 2006). Larvae of the greater wax moth *Galleria mellonella* share similar innate immune responses with mammals as shown for insects hemocytes, such as phagocytosis or superoxide production, and mammalian phagocytes (Browne *et al.*, 2013; Kavanagh and Reeves, 2004). In this study was demonstrated that a *gliP* deficiency results in an impaired virulence in the *Galleria mellonella* infection model. Nonetheless, suggestions that Fbx15-dependent regulation of gliotoxin biosynthesis is connected to Fbx15-mediated virulence in *A. fumigatus* is presumably not true as no significant changes in the survival rates of Δ*fbx15*/Δ*gliP* and Δ*fbx15*/Δ*gliZ* compared to Δ*fbx15* were observed (Figure 20).

This study has shown that the loss in pathogenicity of *A. fumigatus* when lacking *fbx15* is not reasoned by the Fbx15-dependent regulation of gliotoxin biosynthesis in the *Galleria mellonella* infection model. However, it is not clear if this repressive function of Fbx15 has in impact on infection in other host organisms such as mice or humans.

3 Contribution of asexual and sexual development and stress response by *A. fumigatus* - and *A. nidulans* Fbx15

3.1 Fbx15 functions are different during asexual and sexual development in *A. fumigatus* and *A. nidulans*

A. fumigatus Fbx15 was already described to be crucial for stress adaptation as well as required for developmental processes such as asexual and sexual development in *A. nidulans* (Jöhnk *et al.*, 2016; von Zeska Kress *et al.*, 2012). *A. fumigatus* Fbx15 rescues the Δ*fbx15* phenotype in *A. nidulans* regarding sexual and asexual development (Figure 12). Instead Δ*fbx15* phenotype during stress response in *A. fumigatus* is partially complemented by the introduction of *A. nidulans* Fbx15 suggesting a heterologous conserved molecular function of *fbx15* as Fbx15 is dispensable for asexual development in *A. fumigatus* (Figure 13) (Jöhnk *et al.*, 2016). In fact, *A. fumigatus* and *A. nidulans* are already different during development. Sexual development only occurs under harsh conditions in *A. fumigatus* whereas the formation of cleistothecia is enhanced in darkness with moderate temperatures in *A. nidulans* (Bayram *et al.*, 2010a; Ruger-Herreros *et al.*, 2011; O'Gorman *et al.*, 2009). Contradictious functions for one protein and its homolog in *A. fumigatus* and *A. nidulans* was already described for the transcriptional regulator SclB. SclB is repressed by the velvet domain VosA in *A. nidulans* and required its conidiation. Nonetheless, in *A. fumigatus* SclB is dispensable for conidiation but can take over the function in conidiation of SclB in *A. nidulans* (Thieme *et al.*, 2018). It was suggested that *A. nidulans* and *A. fumigatus* conidiation cascades significant differ between each other. This suggestions are underpinned by the fact that crucial counterparts required for conidiation in *A. nidulans* have other functions in *A. fumigatus* like the velvet proteins (Mah and Yu, 2006; Park *et al.*, 2012; Thieme *et al.*, 2018; Yu, 2010; Yu *et al.*, 2006). An assumed putative different functionality of Fbx15 between *A. fumigatus* and *A. nidulans* is supported by the fact that stress response in *A. nidulans* is only partially mediated by Fbx15 (Figure 14). This could contribute to identified differences in the domain architecture and therefore different involvement in molecular pathways in comparison to *A. fumigatus* Fbx15 (Figure 12) (Jöhnk *et al.*, 2016). During stress response different cascades get activated or inhibited to ensure a successful adaptation to environmental changes (Chen and Thorner, 2007). The genomes of *A. nidulans* and *A. fumigatus* are to 66% identical, suggesting putative molecular differences according to responses to environmental changes, which were elucidated in this study in focus of Fbx15 (Figure 14) (Galagan *et al.*, 2005).

A. fumigatus Fbx15 complements WT-like conidiation and cleistothecia formation in the deletion of *fbx15* in *A. nidulans*, which might indicate a putative unknown function of

A. fumigatus Fbx15 concerning asexual and sexual development (Figure 13). Nonetheless, in *A. fumigatus* no macroscopic differences in conidiation were observed in a loss of *fbx15*, which indicates rather a dispensable function of *fbx15* in developmental relevant processes such as asexual development (Jöhnk *et al.*, 2016). Noteworthy, the absence of the key regulator in secondary metabolism LaeA shows similar negligible effects on the asexual development in *A. fumigatus* on macroscopic levels like Fbx15 (Bok and Keller, 2004; Jöhnk *et al.*, 2016). Instead, microscopic analysis on the conidiospore composition in dependency LaeA revealed its influence on the structural composition in the hydrophobin layer resulting in an increased phagocytosis in absence of *laeA*, consequently a decreased pathogenicity (Bok and Keller, 2004; Dagenais *et al.*, 2010; Girardin *et al.*, 1999). The hydrophin layer of *A. fumigatus* spores contains the rodlet protein/hydrophobin (RodAp) which amount is significantly decreased in spores lacking *laeA* (Dagenais *et al.*, 2010). As the impact on the loss of *fbx15* is similar to the loss of *laeA* regarding the pathogenic potential and secondary metabolism homeostasis in combination with a non-macroscopic difference in asexual development in *A. fumigatus*, a similar influence on the conidiospore composition identified in the dependency on *laeA* could be conceivable for *fbx15* (Bok and Keller, 2004; Dagenais *et al.*, 2010; Girardin *et al.*, 1999; Jöhnk *et al.*, 2016).

In case of sexual reproduction *A. fumigatus* compromised all essential genes, which get activated during harsh conditions in a long term process (Galagan *et al.*, 2005; O'Gorman *et al.*, 2009). *A. fumigatus* Fbx15 interacts physically with the putative APSES transcription factor FiAt as shown in this study. APSES transcription factors are solely present in filamentous fungi and associated with the regulation of cellular processes and pathogenicity (Aramayo *et al.*, 1996; Dutton *et al.*, 1997; LeeJ. Y. *et al.*, 2013; Yao *et al.*, 2017; Zhao *et al.*, 2014). In this study the role of FiAt in stress response or pathogenicity using the *Galleria mellonella* infection model could not be identified (Figure S1, S4). The protein sequence of FiAt shows 'best hits' to the non-*Aspergillus* spp. organisms NCU06560 in *Neurospora crassa* and to Bqt4 in the fission yeast *S. pombe* (Cerqueira *et al.*, 2014; Hu *et al.*, 2019). The inner nuclear membrane protein Bqt4 is essential for the association of chromosomes to the nuclear envelop by interacting with different protein partners such as the telomere protein Rap1. A loss of Bqt4 results in a partial deficit in meiotic telomere clustering with decreased frequency in meiotic recombination which leads to a defective spore formation (Chikashige *et al.*, 2009). The N-terminal domain of Bqt4 is a protein-interaction module required to recognize a consensus motif whereby the interaction to other proteins (Hu *et al.*, 2019). FiAt in *A. fumigatus* was analysed under vegetative conditions and asexual growth. Sexual recombination by meiotic division needs two mating types, MAT1-1 and MAT1-2, and certain media, temperature as well as a long

period of over six month in *A. fumigatus* (O'Gorman *et al.*, 2009). However, an interaction of Fbx15 and the APSES transcription factor FiAt was examined under vegetative growth conditions and not during sexual reproduction indicating an independent relationship of FiAt and Fbx15 in *A. fumigatus* to sexual development (Figure S1) (Jöhnk *et al.*, 2016). Nonetheless, a Fbx15-mediated sexual reproduction in *A. fumigatus* cannot be excluded as sexual development was not analysed in dependency of *fbx15*.

Taken together, Fbx15 of *A. fumigatus* and *A. nidulans* share structural and functional similarities in a conserved manner. However, *A. fumigatus* and *A. nidulans* differ in developmental processes and stress response regarding molecular pathways, which is supported by the main function of *A. nidulans* Fbx15 in development whereas *A. fumigatus* Fbx15 is essential in stress response and virulence. Nonetheless, an impact on asexual and sexual development by *A. fumigatus* Fbx15 could not be excluded and remains to be elucidated.

3.2 Fbx15 interacts with its interaction partners predominantly in the cytoplasm

Proteins must be localised in certain compartments depending on their region of action such as transcriptional regulators in the nucleus (Whiteside and Goodbourn, 1993; Xu and Massagué, 2004). In this study it was identified that *A. fumigatus* Fbx15 interacts physically with the transcriptional regulators SrbB and OefC, as well as the putative APSES transcriptional regulator FiAt and the putative F-type ATPase relative protein FidA in the cytoplasm in *A. fumigatus* and/or *A. nidulans* during different non--stress and/or stress conditions similar located as the interaction of Fbx15 with SsnF (Figure 15, Figure S1, S5, S7, S12) (Jöhnk *et al.*, 2016). It is known that a cytoplasmic localisation of transcription factors can be coupled with their inactivated form as shown for NF-κB (Beg *et al.*, 1992). Fbx15 with SsnF co-localise in the nucleus, whereas their physical interaction occurs in the cytoplasm during vegetative growth indicating a positive effect of Fbx15 on SsnF activity in the nucleus in an SCF^{Fbx15} indirect manner as previously proven (Jöhnk *et al.*, 2016). In this study a direct interplay of the functions of FiAt with Fbx15 in *A. fumigatus* or OefC with Fbx15 in *A. nidulans* regarding localisation and/or pathogenicity or as SCF^{Fbx15} substrate could not be elucidated (Figure S1, S3, S4, S9 – S15) whereas a nuclear transport dependent on *A. fumigatus* Fbx15 for FidA and SrbB is unknown.

F-box proteins were first described as substrate receptors in SCF E3 ubiquitin ligase complexes (Feldman *et al.*, 1997; Skowyra *et al.*, 1997). However, in humans 12% of all 69 F-box proteins were identified to have a SCF-independent role (Nelson *et al.*, 2013). The F-box protein Fbxo7 has SCF-independent functions next to the participation in the

degradation of proteins involved in hepatocellular carcinoma and NF-κB activity as part of the SCF^{Fbxo7} complex like acting as a regulator of the cell cycle by acting as a scaffold for the formation of cyclin D/Cdk6 complexes (Hsu *et al.*, 2004; Kuo *et al.*, 2012; Laman *et al.*, 2005; Nelson *et al.*, 2013). In case of FiAt, FidA and SrbB a direct interaction with *A. fumigatus* Fbx15 was observed during non-stress conditions, precisely when Fbx15 is phosphorylated and able to assemble to an active SCF^{Fbx15} complex as previously described (Jöhnk *et al.*, 2016). Consequently, this could be an indicator for a stability-dependent interaction in a SCF^{Fbx15} E3 ubiquitin ligase complex manner as Fbx15 is phosphorylated at non-stress conditions (Figure 15, Figure S1, Figure S5). However, a same local interaction of *A. fumigatus* Fbx15 was examined with SsnF, which was identified to be not a substrate of the SCF^{Fbx15} E3 ubiquitin ligase complex (Jöhnk *et al.*, 2016). Therefore, a physical interaction of *A. fumigatus* Fbx15 with interaction partners in the cytoplasm is not a clear evidence for a SCF^{Fbx15}-dependent interplay.

Taken together, the interaction of Fbx15 of *A. fumigatus* and *A. nidulans* with so far analysed interaction partners is solely localised in the cytoplasm during non-stress and/or stress conditions, where most of them are transcriptional regulators. However, the only Fbx15-dependent molecular function was identified for *A. fumigatus* Fbx15, which represents an unusual function for F-box proteins in the regulation of the cellular localisation of the co-repressor subunit SsnF.

3.3 FidA is presumably not a part of a F-type ATPase but crucial for development in a putative Fbx15-interacting manner in *A. fumigatus* and *A. nidulans*

FidA was identified as the putative C-terminal part of a F-type ATPase subunit F in the orthologous gene XP_016595530.1 in *Penicillium expansum*, which interacts with Fbx15 of *A. fumigatus* and *A. nidulans* and indicates the involvement in a conserved interplay for developmental processes (Figure 10, Figure 15– 18) (Table S1). In *A. fumigatus* and *A. nidulans* FidA is annotated separately from the F-domain (AN11565/Afu2g05510) (Figure 10, Figure S17). F-type ATPases are composite of two compartments: F_0-particel and F_1-particle, which are synthesised by the involvement of so far 25 identified genes in *S. cerevisiae*. The F_0-particle is integral in the membrane, whereas the F_1-particle is peripheral (Song *et al.*, 2018). FidA as potential part of and F-type ATPase F-subunit would be part of the membrane-bound F_0-particle (Pedersen and Amzel, 1993) (Figure 30).

FidA was initially described due to genome -, transcriptome - and functional analysis in *P. expansum* (Ballester *et al.*, 2015) (http://blast.ncbi.nlm.nih.gov/Blast.cgi). However, *A. nidulans* AN11565 is highly similar to the already identified and characterized *ATP17*

gene in *Saccharomyces cerevisiae*, which encodes the F-domain, respectively the F-subunit of the F-type ATPase (Table S2). This fact could be an evidence for an annotation mistake in the protein sequence of the F-subunit, in which FidA is presumably not a part of the F-type ATPase F-subunit in *A. nidulans* and *A. fumigatus*. However, FidA in *A. fumigatus* and *A. nidulans* plays a role in vegetative growth and developmental processes such as conidiation, in-time cleistothecia formation as well as secondary metabolite homeostasis in *A. nidulans.* These properties correlate to the observed functional impact the previous described *ATP17* in *S. cerevisiae*, whose deficiency results in diminished growth on glycerol medium (Spannagel *et al.*, 1997).

Moreover, the protein structure of FidA in *A. fumigatus* and *A. nidulans* is intrinsically disordered (Figure S16). Several orthologs of the F-domain as stand-alone gene are found in other fungi such as *Saccharomyces cerevisiae*, *Saccharomyces pombe*, *Candida albicans* and *Neurospora crassa*, named *ATP17* and is associated with the F-subunit in the F_0-particle (Figure 30, blue) (Table S2) (Song *et al.*, 2018).

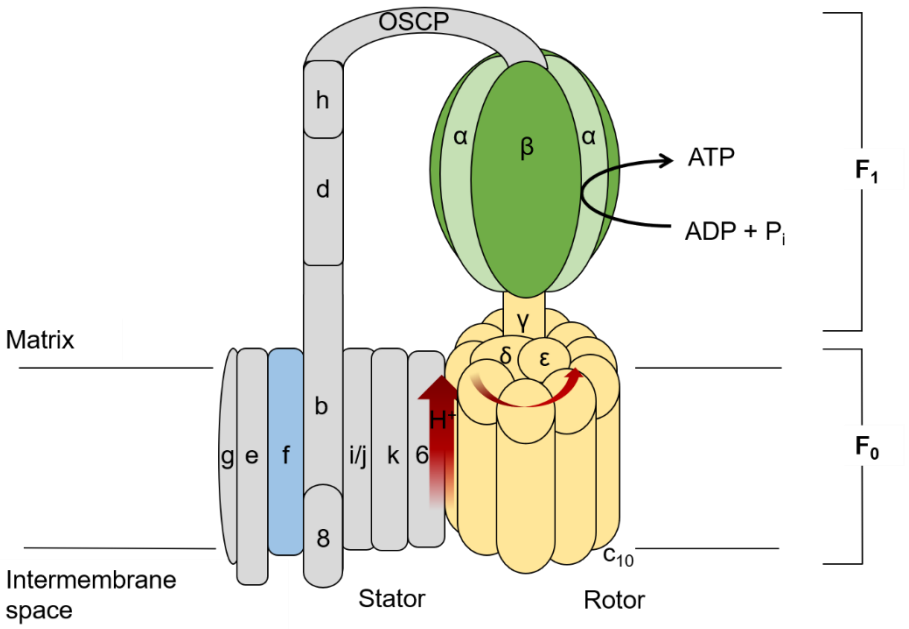

Figure 30: **Structural model of the mitochondrial F_0F_1-ATPase.** The mitochondrial F-type ATPase in eukaryotic cells comprises a stator (in grey: 6, k, i/j, 8, f, e, g, b, h, d and OSCP), a rotator (in yellow: c_{10} ring, δ, γ, ε) and the activity-bearing subunits (in green: three αβ heterodimers). The ATPase is subdivided into two major particles: The membrane-bound F_0-particle which includes the stator and the c-ring of the rotator; and the soluble F_1-particle including the αβ heterodimers and the δ, γ, ε-subunits of the rotator. The F_1-particle represents the catalytic activity and is bound to the proton channel F_0-particle by the OSCP subunit. The F-subunit is highlighted in blue. Modified from Song *et al.*, 2018.

As FidA shows similar properties to known characteristics of F-subunits or in general ATPases it could not be excluded that FidA is a putative part of a F-type ATPase. However,

FidA is presumably not a part of the F-subunit as this subunit is already annotated as AN11565/Afu2G05510 with high similarities to the already described which were already described *Saccharomyces cerevisiae* ATP17 (Table S2) (Spannagel *et al.*, 1997).

4 Conclusion and outlook

The main result of this study is that the Fbx15 NLS2 of the pathogenic fungus *A. fumigatus* is a stress response-element, whereas NLS1 is mainly required for the nuclear localisation of Fbx15. Thereby, NLS2 is required for the localisation outside the nuclear matrix of Fbx15 and its interaction partner SsnF, a conserved co-repressor subunit (Smith and Johnson, 2000).

Pathogenic fungi such as *A. fumigatus* are threatening as they are capable to adapt to various stress inducers (Debeaupuis *et al.*, 1997; Rocchi *et al.*, 2015). In this work the function of the domain architecture at the C-terminus of *A. fumigatus* Fbx15 was further analysed concerning the proteins' function during stress response, especially during H_2O_2-stress. The C-terminal part of *A. fumigatus* Fbx15, which composites of two monopartite NLS sequences and two Ser residues previously identified to be phosphorylated, is crucial for its cellular localisation and accumulation within the cell during non-stress and oxidative stress conditions. The NLS2 sequence of *A. fumigatus* Fbx15 has additional roles in stress response beyond the function in the nuclear localisation of Fbx15 as a putative binding site for interacting proteins as well as possessing a putative regulatory function regarding NLS1 activity to import factors. For future research it would be of high interest to analyse how the NLS-deficiency affects the interplay to *A. fumigatus* Fbx15 interacting partners. Especially analysis of *A. fumigatus* Fbx15 lacking NLS2 would be of interest, which has the most considerable impact on *A. fumigatus* Fbx15 functionality and the recruitment of SsnF outside the nuclear matrix upon stress response after SsnF entered the nucleus before at non-stress conditions in *A. fumigatus*. Thereby, the analysis of SsnF depending on its bipartite NLS have to be performed to clarify when this NLS is active and when Fbx15 takes into account in this process. In this context, it would be of high interest to answer the question how SsnF gets from the nuclear matrix to the nuclear periphery: Are there any contact points such as nuclear porins or ER membrane proteins? Moreover, in this work it was elucidated that S468 and S469, the two Ser residues previously identified to be phosphorylated, are dispensable for the phosphorylation of the whole *A. fumigatus* Fbx15 protein. Nonetheless, both aa must be intact to ensure the cytoplasmic localisation of *A. fumigatus* Fbx15 (this study) as well as its interaction with SsnF during these circumstances as previously described (Jöhnk *et al.*, 2016). The suggestions of a putative given specific phosphate moiety at these Ser residues needs to

be clarified. Therefore, it would be of interest to elucidate whether *A. fumigatus* Fbx15 has to be heterogenous phosphorylated at oxidative stress. Therefore, the localisation of *A. fumigatus* Fbx15 with mimicked phosphorylated S469 in combination with mimicked dephosphorylated S468 or solely phosphorylated S469 should be analysed, i.e. on protein – and localisation level.

The domain architecture of *A. nidulans* Fbx15 is to around 60% identical to *A. fumigatus* Fbx15 and compromises also two NLS sequences at its C-terminus with putative phosphorylation sites in between of them but only one motif, which is to 90% identical to motif 2 of *A. fumigatus* Fbx15 (Jöhnk *et al.*, 2016). However, despite of' structural similarities *A. nidulans* Fbx15 is primarily involved in developmental processes and not in stress response as previously described (von Zeska Kress *et al.*, 2012). Indications could be found that Fbx15 might play a role in the sexual reproduction of the pathogenic fungus *A. fumigatus*. These suggestions were supported by the interaction of *A. fumigatus* Fbx15 with interaction partners (FiAt, FidA), which are involved in sexual reproduction in *A. nidulans* (FidA) or are predicted to be involved in sexual reproduction in *A. fumigatus* (FiAt). It would be of high interest to verify this assumption by analysing the cryptic sexual reproduction of *A. fumigatus* as well as to analyse the *A. fumigatus* conidiospore composition on microscopic levels in dependency of Fbx15.

A. fumigatus Fbx15 is required for the pale pigmentation of colonies, which is also observable for *A. nidulans* Fbx15 indicating a role of *A. nidulans* Fbx15 in secondary metabolism (von Zeska Kress *et al.*, 2012). Further analysis would help to understand how *A. fumigatus* Fbx15 affects secondary metabolism and may elucidate if the regulation of secondary metabolism by Fbx15 contributes to its connection to virulence as a part of a regulatory network in *A. fumigatus*. As the involvement of Fbx15 in regulating the pigmentation of colonies in *A. fumigatus* and *A. nidulans* is conserved, it would be interesting to know whether both proteins are involved in similar pathways in secondary metabolite regulation by identifying identical metabolites, whose biosynthesis are regulated or promoted by Fbx15 in both fungi.

A. fumigatus Fbx15 regulates the gliotoxin formation required for the repression of the antimicrobial agent fumagillin biosynthesis, which contributes to the fungal pathogenicity (Fallon *et al.*, 2010; Guruceaga *et al.*, 2018). However, it was discovered that the *A. fumigatus* Fbx15-mediated regulation of mycotoxin biosynthesis, here shown for gliotoxin formation, is presumably not responsible for the pathogenicity mediated by Fbx15 in the *Galleria mellonella* larvae infection model as well as Fbx15-mediated stress response during minimal growth conditions. Nonetheless, it would be of interest to examine whether the regulation of fumagillin biosynthesis is required for the *A. fumigatus* pathogenicity dependent on Fbx15. Concerning the regulation of secondary metabolism

A. fumigatus Fbx15 might act in a network with the transcriptional regulator SrbB, a SREBP family member, in the control of a so far not identified, putative secondary metabolite during vegetative growth indicating a putative shared pathway.

In summary, this study shows that *A. fumigatus* Fbx15 location is controlled by the complex interplay between two NLS sequences and as a second layer of control by dephosphorylation during oxidative stress. Both NLS sequences can act independently like classical NLS facilitating the nuclear localisation of Fbx15. This is the situation during vegetative growth, NLS2 acts in addition as stress response-element triggering the localisation of Fbx15 outside the nucleus by inhibiting NLS1. Thereby, the cellular localisation of SsnF, which can interact with Fbx15 and can function in the nucleus as part of a transcriptional repressor complex is simultaneously controlled. The function of Fbx15 is partially conserved between *A. fumigatus* and *A. nidulans* in the regulation of secondary metabolism and has additional features in *A. fumigatus*.

Many F-box proteins are existing, and it is an exciting question how many of these proteins may be controlled in their functions by multiple containing NLS sequences and maybe controlling the localisation of other proteins concerning the nucleus, the nuclear periphery and/or cytoplasm. Moreover, it will be exciting to determine the contact points for protein delivery to the nuclear periphery are to identify other proteins, which are involved and necessary for this process.

.

References

Abdul Rehman SA, Kristariyanto YA, Choi SY, Nkosi PJ, Weidlich S, Labib K, Hofmann K, Kulathu Y (2016) MINDY-1 is a member of an evolutionarily conserved and structurally distinct new family of deubiquitinating enzymes. **Mol. Cell** 63, 146–155.

Adams TH, Boylan MT, Timberlake WE (1988) BrlA is necessary and sufficient to direct conidiophore development in *Aspergillus nidulans*. **Cell** 54, 353–362.

Adams TH, Wieser JK, Yu JH (1998) Asexual sporulation in *Aspergillus nidulans*. **Microbiol. Mol. Biol. Rev.** 62, 35–54.

Adav SS, Ravindran A, Sze SK (2015) Quantitative proteomic study of *Aspergillus fumigatus* secretome revealed deamidation of secretory enzymes. **J. Proteomics** 119, 154–168.

Alberts B, Johnson A, Lewis J, Morgan D, Raff M, Roberts K, Walter P (2014) Cell chemistry and bioenergetics - catalysis and the use of energy by cells. In: *Molecular biology of the cell (6th edition)*. pp. 51–73.

Alkhayyat F, Chang Kim S, Yu JH (2015) Genetic control of asexual development in *Aspergillus fumigatus*. **Adv. Appl. Microbiol.** 90, 93–107.

Amin AD, Vishnoi N, Prochasson P (2013) A global requirement for the HIR complex in the assembly of chromatin. **Biochim. Biophys. Acta - Gene Regul. Mech.** 1819, 264–276.

An L, Jiang Y, Ng HHW, Man EPS, Chen J, Khoo US, Gong Q, Huen MSY (2017) Dual-utility NLS drives RNF169-dependent DNA damage responses. **Proc. Natl. Acad. Sci. U. S. A.** 114, E2872-2881.

Aramayo R, Peleg Y, Addison R, Metzenberg R (1996) Asm-1+, a *Neurospora crassa* gene related to transcriptional regulators of fungal development. **Genetics** 144, 991–1003.

Ardito F, Giuliani M, Perrone D, Troiano G, Lo Muzio L (2017) The crucial role of protein phosphorylation in cell signalingand its use as targeted therapy. **Int. J. Mol. Med.** 40, 271–280.

Ariño J, Velázquez D, Casamayor A (2019) Ser/Thr protein phosphatases in fungi: Structure, regulation and function. **Microb. Cell** 6, 217–256.

Arnaud MB, Cerqueira GC, Inglis DO, Skrzypek MS, Binkley J, Chibucos MC, Crabtree J, Howarth C, Orvis J, Shah P, Wymore F, Binkley G, Miyasato SR, Simison M, Sherlock G, Wortman JR (2012) The *Aspergillus* Genome Database (AspGD): Recent developments in comprehensive multispecies curation, comparative genomics and community resources. **Nucleic Acids Res.** 40, D653-659.

Ashu EE, Hagen F, Chowdhary A, Meis JF, Xu J (2017) Global population genetic analysis of *Aspergillus fumigatus*. **mSphere** 2, e00019-17.

de Assis LJ, Ulas M, Ries LNA, El Ramli NAM, Sarikaya-Bayram O, Braus GH, Bayram O, Goldman GH (2018) Regulation of *Aspergillus nidulans* CreA-mediated catabolite repression by the F-box proteins Fbx23 and Fbx47. **MBio** 9, e00840-18.

Bahn YS (2015) Exploiting fungal virulence-regulating transcription factors as novel antifungal drug targets. **PLoS Pathog.** 11, e1004936.

Bai C, Sen P, Hofmann K, Ma L, Goebl M, Harper JW, Elledge SJ (1996) SKP1 connects cell cycle regulators to the ubiquitin proteolysis machinery through a novel motif, the F-box. **Cell** 86, 263–274.

Bailey L (1953) Effect of fumagillin upon *Nosema apis* (Zander). **Nature** 171, 212–213.

Bakti F, Király A, Orosz E, Miskei M, Emri T, Leiter É, Pocsi I (2017) Study on the glutathione metabolism of the filamentous fungus *Aspergillus nidulans*. **Acta Microbiol. Immunol. Hung.** 64, 255–272.

Balibar CJ, Walsh CT (2006) GliP, a multimodular nonribosomal peptide synthetase in *Aspergillus fumigatus*, makes the diketopiperazine scaffold of gliotoxin. **Biochemistry** 45, 15029–15038.

Ballester AR, Marcet-Houben M, Levin E, Sela N, Selma-Lázaro C, Carmona L, Wisniewski M, Droby S, González-Candelas L, Gabaldón T (2015) Genome, transcriptome, and functional analyses of *Penicillium expansum* provide new insights into secondary metabolism and pathogenicity. **Mol. Plant-Microbe Interact.** 28, 232–248.

von Ballmoos C, Wiedenmann A, Dimroth P (2009) Essentials for ATP synthesis by F_1F_0 ATP synthases. **Annu. Rev. Biochem.** 78, 649–672.

Barford D (1996) Molecular mechanisms of the protein serine/threonine phosphatases. **Trends Biochem. Sci.** 21, 407–412.

Bauer NC, Doetsch PW, Corbett AH (2015) Mechanisms regulating protein localization. **Traffic** 16, 1039–1061.

Bayram Ö, Braus GH (2012) Coordination of secondary metabolism and development in fungi: The velvet family of regulatory proteins. **FEMS Microbiol. Rev.** 36, 1–24.

Bayram Ö, Braus GH, Fischer R, Rodriguez-Romero J (2010) Spotlight on *Aspergillus nidulans* photosensory systems. **Fungal Genet. Biol.** 47, 900–908.

Bayram Ö, Krappmann S, Ni M, Jin WB, Helmstaedt K, Valerius O, Braus-Stromeyer S, Kwon NJ, Keller NP, Yu JH, Braus GH (2008) VelB/VeA/LaeA complex coordinates light signal with fungal development and secondary metabolism. **Science** 320, 1504–1506.

Beck T, Hall MN (1999) The TOR signalling pathway controls nuclear localization of nutrient-regulated transcription factors. **Nature** 402, 689–692.

Beffa T, Staib F, Lott Fischer J, Lyon PF, Gumowski P, Marfenina OE, Dunoyergeindre S, Georgen F, Roch-Susuki R, Gallaz L, Latgé JP (1998) Mycological control and surveillance of biological waste and compost. **Med. Mycol. Suppl.** 36, 137–145.

Beg AA, Ruben SM, Scheinman RI, Haskill S, Rosen CA, Baldwin AS (1992) IκB interacts with the nuclear localization sequences of the subunits of NF-κB: A mechanism for cytoplasmic retention. **Genes Dev.** 6, 1899–1913.

Berner N, Reutter K-R, Wolf DH (2018) Protein quality control of the endoplasmic reticulum and ubiquitin–proteasome-triggered degradation of aberrant proteins: Yeast pioneers the path. **Annu. Rev. Biochem.** 87, 751–782.

Bertram PG, Choi JH, Carvalho J, Ai W, Zeng C, Chan TF, Zheng XFS (2000) Tripartite regulation of Gln3p by TOR, Ure2p, and phosphatases. **J. Biol. Chem.** 275, 35727–35733.

Bhattacharyya S, Yu H, Mim C, Matouschek A (2014) Regulated protein turnover: Snapshots of the proteasome in action. **Nat. Rev. Mol. Cell Biol.** 15, 122–133.

Bhatti AA, Haq S, Bhat RA (2017) Actinomycetes benefaction role in soil and plant health. **Microb. Pathog.** 111, 458–467.

Bien CM, Espenshade PJ (2010) Sterol regulatory element binding proteins in fungi: Hypoxic transcription factors linked to pathogenesis. **Eukaryot. Cell** 9, 352–359.

Bignell E, Cairns TC, Throckmorton K, Nierman WC, Keller NP (2016) Secondary metabolite arsenal of an opportunistic pathogenic fungus. **Philos. Trans. R. Soc. B Biol. Sci.** 371, 20160023.

Bischoff FR, Görlich D (1997) RanBP1 is crucial for the release of RanGTP from importin β-related nuclear transport factors. **FEBS Lett.** 419, 249–254.

Bischoff FR, Ponstingl H (1991) Catalysis of guanine nucleotide exchange on Ran by the mitotic regulator RCC1. **Nature** 354, 80–82.

Bode HB, Bethe B, Höfs R, Zeeck A (2002) Big effects from small changes: Possible ways to explore nature's chemical diversity. **ChemBioChem** 3, 619–627.

Bok JW, Chung DW, Balajee SA, Marr KA, Andes D, Nielsen KF, Frisvad JC, Kirby KA, Keller NP (2006) GliZ, a transcriptional regulator of gliotoxin biosynthesis, contributes to *Aspergillus fumigatus* virulence. **Infect. Immun.** 74, 6761–6768.

Bok JW, Keller NP (2004) LaeA, a regulator of secondary metabolism in *Aspergillus* spp. **Eukaryot. Cell** 3, 527–535.

Bongomin F, Gago S, Oladele RO, Denning DW (2017) Global and multi-national prevalence of fungal diseases—estimate precision. **J. Fungi** 3, E57.

Bonnett CR, Cornish EJ, Harmsen AG, Burritt JB (2006) Early neutrophil recruitment and aggregation in the murine lung inhibit germination of *Aspergillus fumigatus* conidia. **Infect. Immun.** 74, 6528–6539.

Bos JL, Rehmann H, Wittinghofer A (2007) GEFs and GAPs: Critical elements in the control of small G proteins. **Cell** 129, 865–877.

Brakhage AA, Langfelder K (2002) Menacing mold: The molecular biology of *Aspergillus fumigatus*. In: *Annual Review of Microbiology*. Vol56, pp. 433–455.

Braus G, Krappmann S, Eckert S (2002) Sexual development in Ascomycetes fruit body formation of *Aspergillus nidulans*. In: *Osewacz, H.D. (Ed.). Molecular Biology of Fungal Development. CRC Press, New York,*. pp. 215–244.

Breitenbach M, Weber M, Rinnerthaler M, Karl T, Breitenbach-Koller L (2015) Oxidative stress in fungi: Its function in signal transduction, interaction with plant hosts, and lignocellulose degradation. **Biomolecules** 5, 318–342.

Browne N, Heelan M, Kavanagh K (2013) An analysis of the structural and functional similarities of insect hemocytes and mammalian phagocytes. **Virulence** 4, 597–603.

Bultman KM, Kowalski CH, Cramer RA (2017) *Aspergillus fumigatus* virulence through the lens of transcription factors. **Med. Mycol.** 55, 24–38.

Butchko R, Adams TH, Keller N (1999) A visual screen to detect *Aspergillus nidulans* mutants defective in aflR regulation. **Genetics** 153, 715–720.

Calvo AM, Wilson RA, Woo Bok J, Keller NP (2002) Relationship between secondary metabolism and fungal development. **Microbiol. Mol. Biol. Rev.** 66, 447–459.

Canosa I, Rojo F, Alonso JC (1996) Site-specific recombination by the β protein from the streptococcal plasmid pSM19035: Minimal recombination sequences and crossing over site. **Nucleic Acids Res.** 24, 2712–2717.

Cardozo T, Pagano M (2004) The SCF ubiquitin ligase: Insights into a molecular machine. **Nat. Rev. Mol. Cell Biol.** 5, 739–751.

Carvalho J, Zheng XF (2003) Domains of Gln3p interacting with karyopherins, Ure2p, and the target of rapamycin protein. **J. Biol. Chem.** 278, 16878–16886.

de Castro E, Sigrist CJA, Gattiker A, Bulliard V, Langendijk-Genevaux PS, Gasteiger E, Bairoch A, Hulo N (2006) ScanProsite: Detection of PROSITE signature matches and ProRule-associated functional and structural residues in proteins. **Nucleic Acids Res.** 34, W362-365.

Cerqueira GC, Arnaud MB, Inglis DO, Skrzypek MS, Binkley G, Simison M, Miyasato SR, Binkley J, Orvis J, Shah P, Wymore F, Sherlock G, Wortman JR (2014) The *Aspergillus* genome database: Multispecies curation and incorporation of RNA-Seq data to improve structural gene annotations. **Nucleic Acids Res.** 42, D705-710.

Chandra D, Londino J, Alexander S, Bednash JS, Zhang Y, Friedlander RM, Daskivich G, Carlisle DL, Lariviere WR, Nakassa ACI, Ross M, St. Croix C, Nyunoya T, Sciurba F, Chen B, Mallampalli RK (2019) The SCF^{FBXO3} ubiquitin E3 ligase regulates inflammation in atherosclerosis. **J. Mol. Cell. Cardiol.** 126, 50–59.

Chang C, Chen C, Grauffel C, Pien Y, Lim C, Tsai S, Hsia K (2019) Ran pathway-independent regulation of mitotic Golgi disassembly by importin- α. **Nat. Commun.** 10, 4307.

Chaudhary N, Marr KA (2011) Impact of *Aspergillus fumigatus* in allergic airway diseases. **Clin. Transl. Allergy** 1, 1–7.

Chazalet V, Debeaupuis JP, Sarfati J, Lortholary J, Ribaud P, Shah P, Cornet M, Vu Thien H, Gluckman E, Brücker G, Latgé JP (1998) Molecular typing of environmental and patient isolates of *Aspergillus fumigatus* from various hospital settings. **J. Clin. Microbiol.** 36, 1494–1500.

Chen RE, Thorner J (2007) Function and regulation in MAPK signaling pathways: Lessons learned from the yeast *Saccharomyces cerevisiae*. **Biochim. Biophys. Acta - Mol. Cell Res.** 1773, 1311–1340.

Chi NC, Adam EJH, Visser GD, Adam SA (1996) RanBP1 stabilizes the interaction of Ran with p97 in nuclear protein import. **J. Cell Biol.** 135, 559–569.

Chikashige Y, Yamane M, Okamasa K, Tsutsumi C, Kojidani T, Sato M, Haraguchi T, Hiraoka Y (2009) Membrane proteins Bqt3 and -4 anchor telomeres to the nuclear envelope to ensure chromosomal bouquet formation. **J. Cell Biol.** 187, 413–427.

Christensen M, Samson RA, van Reenen-Hoekstra ES (1989) Introduction to food-borne fungi. **Mycologia** 81, 942–943.

Christmann M, Schmaler T, Gordon C, Huang X, Bayram Ö, Schinke J, Stumpf S, Dubiel W, Braus GH (2013) Control of multicellular development by the physically interacting deneddylases DEN1/DenA and COP9 signalosome. **PLoS Genet.** 9, e1003275.

Chu M, Mierzwa R, He L, Xu L, Patel M, Patel D, Chan T-M (2012) Structure of Sch 528647: A new antitumor antibiotic related to fumagillin. **J. Antibiot. (Tokyo).** 54, 1096–1099.

Chung D, Barker BM, Carey CC, Merriman B, Werner ER, Lechner BE, Dhingra S, Cheng C, Xu W, Blosser SJ, Morohashi K, Mazurie A, Mitchell TK, Haas H, Mitchell AP, Cramer RA (2014) ChIP-seq and in vivo transcriptome analyses of the *Aspergillus fumigatus* SREBP SrbA reveals a new regulator of the fungal hypoxia response and virulence. **PLoS Pathog.** 10, e1004487.

Church M, Smith KC, Alhussain MM, Pennings S, Fleming AB (2017) Sas3 and Ada2(Gcn5)-dependent histone H3 acetylation is required for transcription elongation at the de-repressed FLO1 gene. **Nucleic Acids Res.** 45, 4413–4430.

Clague MJ, Heride C, Urbé S (2015) The demographics of the ubiquitin system. **Trends Cell Biol.** 25, 417–426.

Cooney DG, Emerson R (1965) Thermophilic fungi - an account of their biology, activities, and classification. **Q. Rev. Biol.** 40, 292.

Corrochano LM (2007) Fungal photoreceptors: Sensory molecules for fungal development and behaviour. **Photochem. Photobiol. Sci.** 6, 725–736.

La Cour T, Kiemer L, Mølgaard A, Gupta R, Skriver K, Brunak S (2004) Analysis and prediction of leucine-rich nuclear export signals. **Protein Eng. Des. Sel.** 17, 527–36.

Cramer RA, Gamcsik MP, Brooking RM, Najvar LK, Kirkpatrick WR, Patterson TF, Balibar CJ, Graybill JR, Perfect JR, Abraham SN, Steinbach WJ (2006) Disruption of a nonribosomal peptide synthetase in *Aspergillus fumigatus* eliminates gliotoxin production. **Eukaryot. Cell** 5, 972–980.

Czapek F (1902) Untersuchungen über die Stickstoffgewinnung und Eiweiß-bildung der Pflanzen. **Beitr. Chem. Physiol. u. Pahtol.** 1, 540–560.

Dagenais TRT, Giles SS, Aimanianda V, Latgé JP, Hull CM, Keller NP (2010) *Aspergillus fumigatus* LaeA-mediated phagocytosis is associated with a decreased hydrophobin layer. **Infect. Immun.** 78, 823–829.

Daly MJ (2009) A new perspective on radiation resistance based on *Deinococcus radiodurans*. **Nat. Rev. Microbiol.** 7, 237–245.

Dancis A, Yuan DS, Haile D, Askwith C, Eide D, Moehle C, Kaplan J, Klausner RD (1994) Molecular characterization of a copper transport protein in *S. cerevisiae*: An unexpected role for copper in iron transport. **Cell** 76, 393–402.

Debeaupuis JP, Sarfati J, Chazalet V, Latgé JP (1997) Genetic diversity among clinical and environmental isolates of *Aspergillus fumigatus*. **Infect. Immun.** 65, 3080–3085.

Denning DW, Cadranel J, Beigelman-Aubry C, Ader F, Chakrabarti A, Blot S, Ullmann AJ, Dimopoulos G, Lange C (2016) Chronic pulmonary aspergillosis: Rationale and clinical guidelines for diagnosis and management. **Eur. Respir. J.** 47, 45–68.

DeRisi JL, Iyer VR, Brown PO (1997) Exploring the metabolic and genetic control of gene expression on a genomic scale. **Science** 278, 680–686.

Deshaies RJ, Joazeiro CAP (2009) RING domain E3 ubiquitin ligases. **Annu. Rev. Biochem.** 78, 399–434.

Dhingra S, Andes D, Calvoa AM (2012) VeA regulates conidiation, gliotoxin production, and protease activity in the opportunistic human pathogen *Aspergillus fumigatus*. **Eukaryot. Cell** 11, 1531–1543.

Dibrova D V., Galperin MY, Mulkidjanian AY (2010) Characterization of the N-ATPase, a distinct, laterally transferred Na_+-translocating form of the bacterial F-type membrane ATPase. **Bioinformatics** 26, 1473–1476.

Dickman MB, Yarden O (1999) Serine/threonine protein kinases and phosphatases in filamentious fungi. **Fungal Genet. Biol.** 26, 99–117.

Dingwall C, Laskey RA (1991) Nuclear targeting sequences - a consensus? **Trends Biochem. Sci.** 16, 478–481.

Doedt T, Krishnamurthy S, Bockmühl DP, Tebarth B, Stempel C, Russell CL, Brown AJP, Ernst JF (2004) APSES proteins regulate morphogenesis and metabolism in *Candida albicans*. **Mol. Biol. Cell** 15, 3167–3180.

Dolan SK, O'Keeffe G, Jones GW, Doyle S (2015) Resistance is not futile: Gliotoxin biosynthesis, functionality and utility. **Trends Microbiol.** 23, 419–428.

Dox AW (1910) The intracellular enzymes of *Penicillium* and *Aspergillus* with special references to those of *Penicillium camemberti*. **U.S. Dept. Agr. Bur. Anim. Ind. Bull.,** 120

Drocourt D, Calmels T, Reynes JP, Baron M, Tiraby G (1990) Cassettes of the *Streptoalloteichus hindustanus* ble gene for transformation of lower and higher eukaryotes to phleomycin resistance. **Nucleic Acids Res.** 18, 4009.

Duda DM, Borg LA, Scott DC, Hunt HW, Hammel M, Schulman BA (2008) Structural insights into NEDD8 activation of Cullin-RING ligases: Conformational control of conjugation. **Cell** 134, 995–1006.

Dutton JR, Johns S, Miller BL (1997) StuAp is a sequence-specific transcription factor that regulates developmental complexity in *Aspergillus nidulans*. **EMBO J.** 16, 5710–5721.

Dyer PS, O'Gorman CM (2012) Sexual development and cryptic sexuality in fungi: Insights from *Aspergillus* species. **FEMS Microbiol. Rev.** 36, 165–192.

Elramli N, Karahoda B, Sarikaya-Bayram O, Frawley D, Ulas M, Oakley CE, Oakley BR, Seiler S, Bayram O (2019) Assembly of a heptameric STRIPAK complex is required for coordination of light-dependent multicellular fungal development with secondary metabolism in *Aspergillus nidulans*. **PLoS Genet.** 15, e1008053.

Ene I V., Bennett RJ (2014) The cryptic sexual strategies of human fungal pathogens. **Nat. Rev. Microbiol.** 12, 239–251.

Espinosa V, Jhingran A, Dutta O, Kasahara S, Donnelly R, Du P, Rosenfeld J, Leiner I, Chen CC, Ron Y, Hohl TM, Rivera A (2014) Inflammatory monocytes orchestrate innate antifungal immunity in the lung. **PLoS Pathog.** 10, e1003940.

Fallon JP, Reeves EP, Kavanagh K (2010) Inhibition of neutrophil function following exposure to the *Aspergillus fumigatus* toxin fumagillin. **J. Med. Microbiol.** 59, 625–633.

Fallon JP, Reeves EP, Kavanagh K (2011) The *Aspergillus fumigatus* toxin fumagillin suppresses the immune response of *Galleria mellonella* larvae by inhibiting the action of haemocytes. **Microbiology** 157, 1481–1488.

Fang W, Latgé JP (2018) Microbe profile: *Aspergillus fumigatus*: A saprotrophic and opportunistic fungal pathogen. **Microbiol. (United Kingdom)** 164, 1009–1011.

Fayed A (2018) Sudden death in middle aged woman with invasive pulmonary aspergillosis. **J. Pulm. Respir. Med.** 8, 149–155.

Feldman RMR, Correll CC, Kaplan KB, Deshaies RJ (1997) A complex of Cdc4p, Skp1p, and Cdc53p/cullin catalyzes ubiquitination of the phosphorylated CDK inhibitor Sic1p. **Cell** 91, 221–230.

Fischbach MA, Walsh CT (2006) Biochemistry: Directing biosynthesis. **Science** 314, 603–605.

Flipphi M, Sun J, Robellet X, Karaffa L, Fekete E, Zeng AP, Kubiecek CP (2009) Biodiversity and evolution of primary carbon metabolism in *Aspergillus nidulans* and other *Aspergillus* spp. **Fungal Genet. Biol.** 46, S19-44.

Fogarty WM (1994) Enzymes of the genus *Aspergillus*. In: *Aspergillus*. pp. 177–218.

Fornerod M, Ohno M, Yoshida M, Mattaj IW (1997) CRM1 is an export receptor for leucine-rich nuclear export signals. **Cell** 90, 1051–1060.

Fountain JC, Bajaj P, Nayak SN, Yang L, Pandey MK, Kumar V, Jayale AS, Chitikineni A, Lee RD, Kemerait RC, Varshney RK, Guo B (2016) Responses of *Aspergillus flavus* to oxidative stress are related to fungal development regulator, antioxidant enzyme, and secondary metabolite biosynthetic gene expression. **Front. Microbiol.** 7, 2048.

Fox H, Hickey PC, Fernández-Ábalos JM, Lunness P, Read ND, Doonan JH (2002) Dynamic distribution of BIMG(PP1) in living hyphae of *Aspergillus* indicates a novel role in septum formation. **Mol. Microbiol.** 45, 1219–1230.

Fridell RA, Fischer U, Luhrmann R, Meyer BE, Meinkoth JL, Malim MH, Cullen BR (2002) Amphibian transcription factor IIIA proteins contain a sequence element functionally equivalent to the nuclear export signal of human immunodeficiency virus type 1 Rev. **Proc. Natl. Acad. Sci.** 93, 2936–2940.

Futai M, Noumi T, Maeda M (1989) ATP synthase (H+-ATPase): Results by combined biochemical and molecular biological approaches. **Annu. Rev. Biochem.** 58, 111–136.

Futai M, Omote H, Sambongi Y, Wada Y (2000) Synthase (H+-ATPase): Coupling between catalysis, mechanical work, and proton translocation. **Biochim. Biophys. Acta - Bioenerg.** 1458, 276–288.

Futai M, Sun-Wada GH, Wada Y (2005) Proton translocating ATPases: Introducing unique enzymes coupling catalysis and proton translocation through mechanical rotation. In: *Handbook of ATPases: Biochemistry, Cell Biology, Pathophysiology*. pp. 235–260.

Galagan JE, Calvo SE, Cuomo C, Ma LJ, Wortman JR, Batzoglou S, Lee SI, Baştürkmen M, Spevak CC, Clutterbuck J, Kapitonov V, Jurka J, Scazzocchio C, Farman M, Butler J, Purcell S, Harris S, Braus GH, Draht O, *et al.* (2005) Sequencing of *Aspergillus nidulans* and comparative analysis with *A. fumigatus* and *A. oryzae*. **Nature** 438, 1105–1115.

Gallagher L, Owens RA, Dolan SK, O'Keeffe G, Schrettl M, Kavanagh K, Jones GW, Doyle S (2012) The *Aspergillus fumigatus* protein GliK protects against oxidative stress and is essential for gliotoxin biosynthesis. **Eukaryot. Cell** 11, 1226–1238.

Ganchi PA, Sun SC, Greene WC, Ballard DW (1992) IκB/MAD-3 masks the nuclear localization signal of NF-κB p65 and requires the transactivation domain to inhibit NF-κB p65 DNA binding. **Mol. Biol. Cell** 3, 1339–1352.

García-Sánchez S, Mavor AL, Russell CL, Argimon S, Dennison P, Enjalbert B, Brown AJP (2005) Global roles of Ssn6 in Tup1- and Nrg1-dependent gene regulation in the fungal pathogen, *Candida albicans*. **Mol. Biol. Cell** 16, 2913–2925.

Gardiner DM, Howlett BJ (2005) Bioinformatic and expression analysis of the putative gliotoxin biosynthetic gene cluster of *Aspergillus fumigatus*. **FEMS Microbiol. Lett.** 248, 241–248.

Gerke J, Bayram Ö, Feussner K, Landesfeind M, Shelest E, Feussner I, Braus GH (2012) Breaking the silence: Protein stabilization uncovers silenced biosynthetic gene clusters in the fungus *Aspergillus nidulans*. **Appl. Environ. Microbiol.** 78, 8234–8244.

Gerke J, Braus GH (2014) Manipulation of fungal development as source of novel secondary metabolites for biotechnology. **Appl. Microbiol. Biotechnol.** 98, 8443–8455.

Ghosh S, Hoselton SA, Schuh JM (2015) Allergic inflammation in *Aspergillus fumigatus*-induced fungal asthma. **Curr. Allergy Asthma Rep.** 15, 59.

Girardin H, Paris S, Rault J, Bellon-Fontaine MN, Latgé JP (1999) The role of the rodlet structure on the physicochemical properties of *Aspergillus* conidia. **Lett. Appl. Microbiol.** 29, 364–369.

Glickman MH, Ciechanover A (2002) The ubiquitin-proteasome proteolytic pathway: Destruction for the sake of construction. **Physiol. Rev.** 82, 373–428.

Glotzer M, Murray AW, Kirschner MW (1991) Cyclin is degraded by the ubiquitin pathway. **Nature** 349, 132–138.

Goldenberg SJ, Cascio TC, Shumway SD, Garbutt KC, Liu J, Xiong Y, Zheng N (2004) Structure of the Cand1-Cul1-Roc1 complex reveals regulatory mechanisms for the assembly of the multisubunit cullin-dependent ubiquitin ligases. **Cell** 119, 517–528.

Gong L, Yeh ETH (1999) Identification of the activating and conjugating enzymes of the NEDD8 conjugation pathway. **J. Biol. Chem.** 274, 12036–12042.

Goodbourn S, R. CA (1990) Negative regulation of transcriptional initiation in eukaryotes. **BBA - Rev. Cancer** 296, 521–541.

Goodley JM, Clayton YM, Hay RJ (1994) Environmental sampling for aspergilli during building construction on a hospital site. **J. Hosp. Infect.** 26, 27–35.

Görlich D, Dabrowski M, Bischoff FR, Kutay U, Bork P, Hartmann E, Prehn S, Izaurralde E (1997) A novel class of RanGTP binding proteins. **J. Cell Biol.** 138, 65–80.

Görlich D, Kutay U (2002) Transport between the cell nucleus and the cytoplasm. **Annu. Rev. Cell Dev. Biol.** 15, 607–660.

Görlich D, Panté N, Kutay U, Aebi U, Bischoff FR (1996) Identification of different roles for RanGDP and RanGTP in nuclear protein import. **EMBO J.** 15, 5584–5594.

Gounalaki N, Tzamarias D, Vlassi M (2000) Identification of residues in the TPR domain of Ssn6 responsible for interaction with the Tup1 protein. **FEBS Lett.** 473, 37–41.

Gravelat FN, Beauvais A, Liu H, Lee MJ, Snarr BD, Chen D, Xu W, Kravtsov I, Hoareau CMQ, Vanier G, Urb M, Campoli P, Al Abdallah Q, Lehoux M, Chabot JC, Ouimet MC, Baptista SD, Fritz JH, Nierman WC, *et al.* (2013) *Aspergillus* galactosaminogalactan mediates adherence to host constituents and conceals hyphal β-glucan from the immune system. **PLoS Pathog.** 9, e1003575.

Green SR, Johnson AD (2004) Promoter-dependent roles for the Srb10 cyclin-dependent kinase and the Hda1 deacetylase in Tup1-mediated repression in *Saccharomyces cerevisiae*. **Mol. Biol. Cell** 15, 4191–4202.

Grimm MJ, Vethanayagam RR, Almyroudis NG, Dennis CG, Khan ANH, D'Auria AC, Singel KL, Davidson BA, Knight PR, Blackwell TS, Hohl TM, Mansour MK, Vyas JM, Röhm M, Urban CF, Kelkka T, Holmdahl R, Segal BH (2013) Monocyte- and macrophage-targeted NADPH oxidase mediates antifungal host defense and regulation of acute inflammation in mice. **J. Immunol.** 190, 4175–4184.

Gu ZC, Enenkel C (2014) Proteasome assembly. **Cell. Mol. Life Sci.** 71, 4729–4745.

Guruceaga X, Ezpeleta G, Mayayo E, Sueiro-Olivares M, Abad-Diaz-De-Cerio A, Aquirre Urízar JM, Liu HG, Wiemann P, Bok JW, Filler SG, Keller NP, Hernando FL, Ramirez-Garcia A, Rementeria A (2018) A possible role for fumagillin in cellular damage during host infection by *Aspergillus fumigatus*. **Virulence** 9, 1548–1561.

Hagiwara D, Suzuki S, Kamei K, Gonoi T, Kawamoto S (2014) The role of AtfA and HOG MAPK pathway in stress tolerance in conidia of *Aspergillus fumigatus*. **Fungal Genet. Biol.** 73, 138–149.

Hajjar JD, Bennett JW, Bhatnagar D, Bahu R (1989) Sterigmatocystin production by laboratory strains of *Aspergillus nidulans*. **Mycol. Res.** 93, 548–551.

Hanahan D (1985) DNA cloning: A practical approach. In: *IRL Press*.

Hanahan D, Jessee J, Bloom FR (1991) Plasmid transformation of *Escherichia coli* and other bacteria. **Methods Enzymol.** 204, 63–113.

Hanks SK, Hunter T (1995) Protein kinases 6: The eukaryotic protein kinase superfamily : Kinase (catalytic) domam structure and classification. **FASEB J. Off. Publ. Fed. Am. Soc. Exp. Biol.** 9, 576–596.

Hanlon SE, Rizzo JM, Tatomer DC, Lieb JD, Buck MJ (2011) The stress response factors Yap6, Cin5, Phd1, and Skn7 direct targeting of the conserved co-repressor Tup1-Ssn6 in *S. cerevisiae*. **PLoS One** 6, e19060.

Hanson FR, Eble TE (1949) An antiphage agent isolated from *Aspergillus* sp. **J. Bacteriol.** 58, 527–529.

Hartmann T, Dümig M, Jaber BM, Szewczyk E, Olbermann P, Morschhäuser J, Krappmann S (2010) Validation of a self-excising marker in the human pathogen *Aspergillus fumigatus* by employing the β-rec/*six* site-specific recombination system. **Appl. Environ. Microbiol.** 76, 6313–6317.

Heinekamp T, Thywißen A, Macheleidt J, Keller S, Valiante V, Brakhage AA (2012) *Aspergillus fumigatus* melanins: Interference with the host endocytosis pathway and impact on virulence. **Front. Microbiol.** 3, 1–7.

Helmschrott C, Sasse A, Samantaray S, Krappmann S, Wagener J (2013) Upgrading fungal gene expression on demand: Improved systems for doxycycline-dependent silencing in *Aspergillus fumigatus*. **Appl. Environ. Microbiol.** 79, 1751–1754.

Henkel T, Zabel U, van Zee K, Müller JM, Fanning E, Baeuerle PA (1992) Intramolecular masking of the nuclear location signal and dimerization domain in the precursor for the p50 NF-κB subunit. **Cell** 68, 1121–1133.

Hermann TE, Kurtz MB, Champe SP (1983) Laccase localized in hulle cells and cleistothecial primordia of *Aspergillus nidulans*. **J. Bacteriol.** 154, 955–964.

Higes M, Nozal MJ, Alvaro A, Barrios L, Meana A, Martín-Hernández R, Bernal JL, Bernal JL (2011) The stability and effectiveness of fumagillin in controlling *Nosema ceranae* (Microsporidia) infection in honey bees (*Apis mellifera*) under laboratory and field conditions. **Apidologie** 42, 364–377.

Hilton JL, Kearney PC, Ames BN (1965) Mode of action of the herbicide, 3-amino-1,2,4-triazole(amitrole): Inhibition of an enzyme of histidine biosynthesis. **Arch. Biochem. Biophys.** 112, 544–547.

Hohl TM, Feldmesser M (2007) *Aspergillus fumigatus*: Principles of pathogenesis and host defense. **Eukaryot. Cell** 6, 1953–1963.

Horikoshi M, Hai T, Lin YS, Green MR, Roeder RG (1988) Transcription factor ATF interacts with the TATA factor to facilitate establishment of a preinitiation complex. **Cell** 54, 1033–1042.

Horta MAC, Thieme N, Gao Y, Burnum-Johnson KE, Nicora CD, Gritsenko MA, Lipton MS,

Mohanraj K, de Assis LJ, Lin L, Tian C, Braus GH, Borkovich KA, Schmoll M, Larrondo LF, Samal A, Goldman GH, Benz JP (2019) Broad substrate-specific phosphorylation events are associated with the initial stage of plant cell wall recognition in *Neurospora crassa*. **Front. Microbiol.** 10, 2317.

Hospenthal DR, Kwon-Chung KJ, Bennett JE (1998) Concentrations of airborne *Aspergillus* compared to the incidence of invasive aspergillosis: Lack of correlation. **Med. Mycol.** 36, 165–168.

Hsieh DPH, Lin MT, Yao RC, Singh R (1976) Biosynthesis of aflatoxin. Conversion of norsolorinic acid and other hypothetical intermediates into aflatoxin B1. **J. Agric. Food Chem.** 24, 1170–1174.

Hsu JM, Lee YCG, Yu CTM, Huang CYF (2004) Fbx7 functions in the SCF complex regulating Cdk1-cyclin B-phosphorylated hepatoma up-regulated protein (HURP) proteolysis by a proline-rich region. **J. Biol. Chem.** 279, 32592–32602.

Hu C, Inoue H, Sun W, Takeshita Y, Huang Y, Xu Y, Kanoh J, Chen Y (2019) Structural insights into chromosome attachment to the nuclear envelope by an inner nuclear membrane protein Bqt4 in fission yeast. **Nucleic Acids Res.** 47, 1573–1584.

Hua X, Yokoyama C, Wu J, Briggs MR, Brown MS, Goldstein JL, Wang X (1993) SREBP-2, a second basic-helix-loop-helix-leucine zipper protein that stimulates transcription by binding to a sterol regulatory element. **Proc. Natl. Acad. Sci.** 90, 11603–11607.

Hua Z, Vierstra RD (2011) The cullin-RING ubiquitin-protein ligases. **Annu. Rev. Plant Biol.** 62, 299–334.

Huang DT, Ayrault O, Hunt HW, Taherbhoy AM, Duda DM, Scott DC, Borg LA, Neale G, Murray PJ, Roussel MF, Schulman BA (2009) E2-RING expansion of the NEDD8 cascade confers specificity to cullin modification. **Mol. Cell** 33, 483–495.

Igamberdiev AU, Kleczkowski LA (2015) Optimization of ATP synthase function in mitochondria and chloroplasts via the adenylate kinase equilibrium. **Front. Plant Sci.** 6, 10.

Inoue H, Nojima H, Okayama H (1990) High efficiency transformation of *Escherichia coli* with plasmids. **Gene** 96, 23–28.

Issi L, Farrer RA, Pastor K, Landry B, Delorey T, Bell GW, Thompson DA, Cuomo CA, Rao RP (2017) Zinc cluster transcription factors alter virulence in *Candida albicans*. **Genetics** 205, 559–576.

Jhingran A, Mar KB, Kumasaka DK, Knoblaugh SE, Ngo LY, Segal BH, Iwakura Y, Lowell CA, Hamerman JA, Lin X, Hohl TM (2012) Tracing conidial fate and measuring host cell antifungal activity using a reporter of microbial viability in the lung. **Cell Rep.** 2, 1762–1773.

Jia X, Zhang X, Hu Y, Hu M, Tian S, Han X, Sun Y, Han L (2018) Role of actin depolymerizing factor cofilin in *Aspergillus fumigatus* oxidative stress response and pathogenesis. **Curr. Genet.** 64, 619–634.

Jöhnk B (2016) Stress response SCF Ubiquitin ligase F-box protein Fbx15 controls nuclear co-repressor localization and virulence of the opportunistic human fungal pathogen *Aspergillus fumigatus*. Dissertation. Faculty of biology and psychology. Georg-August University Goettingen.

Jöhnk B, Bayram Ö, Abelmann A, Heinekamp T, Mattern DJ, Brakhage AA, Jacobsen ID, Valerius O, Braus GH (2016) SCF Ubiquitin ligase F-box protein Fbx15 controls nuclear co-repressor localization, stress response and virulence of the human pathogen *Aspergillus fumigatus*. **PLOS Pathog.** 12, e1005899.

Junge W, Nelson N (2015) ATP synthase. **Annu. Rev. Biochem.** 84, 631–657.

Jungmann J, Reins HA, Lee J, Romeo A, Hassett R, Kosman D, Jentsch S (1993) MAC1, a nuclear regulatory protein related to Cu-dependent transcription factors is involved in Cu/Fe utilization and stress resistance in yeast. **EMBO J.** 12, 5051–5056.

Kalderon D, Roberts BL, Richardson WD, Smith AE (1984) A short amino acid sequence able to specify nuclear location. **Cell** 39, 499–509.

Kato N, Brooks W, Calvo AM (2003) The expression of sterigmatocystin and penicillin genes in *Aspergillus nidulans* is controlled by *veA*, a gene required for sexual development. **Eukaryot. Cell** 2, 1178–1186.

Katznelson H, Jamieson CA (1952) Control of *Nosema* disease of honeybees with fumagillin. **Science** 115, 70–71.

Kavanagh K, Reeves EP (2004) Exploiting the potential of insects for *in vivo* pathogenicity testing of microbial pathogens. **FEMS Microbiol. Rev.** 28, 101–112.

Keller NP, Turner G, Bennett JW (2005) Fungal secondary metabolism - from biochemistry to genomics. **Nat. Rev. Microbiol.** 3, 937–947.

Kelsall IR, Kristariyanto YA, Knebel A, Wood NT, Kulathu Y, Alpi AF (2019) Coupled monoubiquitylation of the co-E3 ligase DCNL1 by Ariadne-RBR E3 ubiquitin ligases promotes cullin-RING ligase complex remodeling. **J. Biol. Chem.** 294, 2651–2664.

Kimura N, Tsuge T (1993) Gene cluster involved in melanin biosynthesis of the filamentous fungus *Alternaria alternata*. **J. Bacteriol.** 175, 4427–4435.

Kipreos ET, Pagano M (2000) The F-box protein family. **Genome Biol.** 1, reviews3002.1–reviews3002.7.

Knowles JR (2003) Enzyme-catalyzed phosphoryl transfer reactions. **Annu. Rev. Biochem.** 49, 877–919.

Knutsen AP, Bush RK, Demain JG, Denning DW, Dixit A, Fairs A, Greenberger PA, Kariuki B, Kita H, Kurup VP, Moss RB, Niven RM, Pashley CH, Slavin RG, Vijay HM, Wardlaw AJ (2012) Fungi and allergic lower respiratory tract diseases. **J. Allergy Clin. Immunol.** 129, 280–291.

Ko GA, Cho SK (2018) Phytol suppresses melanogenesis through proteasomal degradation of MITF via the ROS-ERK signaling pathway. **Chem. Biol. Interact.** 286, 132–140.

Köhler AM, Harting R, Langeneckert AE, Valerius O, Gerke J, Meister C, Strohdiek A, Braus GH (2019) Integration of fungus-specific CandA-C1 into a trimeric CandA complex allowed splitting of the gene for the conserved receptor exchange factor of CullinA E3 ubiquitin ligases in Aspergilli. **MBio** 10, pii: e01094-19.

Komander D, Rape M (2012) The ubiquitin code. **Annu. Rev. Biochem.** 81, 203–229.

König S, Pace S, Pein H, Heinekamp T, Kramer J, Romp E, Straßburger M, Troisi F, Proschak A, Dworschak J, Scherlach K, Rossi A, Sautebin L, Haeggström JZ, Hertweck C, Brakhage AA, Gerstmeier J, Proschak E, Werz O (2019) Gliotoxin from *Aspergillus fumigatus* abrogates leukotriene B_4 formation through inhibition of leukotriene A_4 hydrolysis. **Cell Chem. Biol.** 26, 524-534.e5.

Koressaar T, Remm M (2007) Enhancements and modifications of primer design program Primer3. **Bioinformatics** 23, 1289–1291.

Kosugi S, Hasebe M, Entani T, Takayama S, Tomita M, Yanagawa H (2008) Design of peptide inhibitors for the importin α/β nuclear import pathway by activity-based profiling. **Chem. Biol.** 15, 940–949.

Kosugi Shunichi, Hasebe M, Matsumura N, Takashima H, Miyamoto-Sato E, Tomita M, Yanagawa H (2009) Six classes of nuclear localization signals specific to different binding grooves of importin α. **J. Biol. Chem.** 284, 478–485.

Kosugi S., Hasebe M, Tomita M, Yanagawa H (2009) Systematic identification of cell cycle-dependent yeast nucleocytoplasmic shuttling proteins by prediction of composite motifs. **Proc. Natl. Acad. Sci.** 106, 10171–10176.

Kozakiewicz Z, Smith D (1994) Physiology of *Aspergillus*. In: *Aspergillus*. pp. 23–40.

Krappmann S, Braus GH (2005) Nitrogen metabolism of *Aspergillus* and its role in pathogenicity. **Med. Mycol.** 43, S31-40.

Krappmann S, Jung N, Medic B, Busch S, Prade RA, Braus GH (2006) The *Aspergillus nidulans* F-box protein GrrA links SCF activity to meiosis. **Mol. Microbiol.** 61, 76–88.

Krappmann S, Sasse C, Braus GH (2006) Gene targeting in *Aspergillus fumigatus* by homologous recombination is facilitated in a nonhomologous end- joining-deficient genetic background. **Eukaryot. Cell** 5, 212–215.

Kubodera T, Yamashita N, Nishimura A (2000) Pyrithiamine resistance gene (ptra) of *Aspergillus oryzae*: Cloning, characterization and application as a dominant selectable marker for transformation. **Biosci. Biotechnol. Biochem.** 64, 1416–1421.

Kuo TC, Chang PY, Huang SF, Chou CK, Chao CCK (2012) Knockdown of HURP inhibits the proliferation of hepacellular carcinoma cells via downregulation of gankyrin and accumulation of p53. **Biochem. Pharmacol.** 83, 758–768.

Kupfahl C, Heinekamp T, Geginat G, Ruppert T, Härtl A, Hof H, Brakhage AA (2006) Deletion of the *gliP* gene of *Aspergillus fumigatus* results in loss of gliotoxin production but has no effect on virulence of the fungus in a low-dose mouse infection model. **Mol. Microbiol.** 62, 292–302.

Kutay U, Ralf Bischoff F, Kostka S, Kraft R, Görlich D (1997) Export of importin α from the nucleus is mediated by a specific nuclear transport factor. **Cell** 90, 1061–1071.

Kwon-Chung KJ, Sugui JA (2009) What do we know about the role of gliotoxin in the pathobiology of *Aspergillus fumigatus*? **Med. Mycol.** 47, S97-103.

Laity JH, Lee BM, Wright PE (2001) Zinc finger proteins: New insights into structural and functional diversity. **Curr. Opin. Struct. Biol.** 11, 39–46.

Laman H, Funes JM, Ye H, Henderson S, Galinanes-Garcia L, Hara E, Knowles P, McDonald N, Boshoff C (2005) Transforming activity of Fbxo7 is mediated specifically through regulation of cyclin D/cdk6. **EMBO J.** 24, 3104–3116.

Lange A, Mills RE, Lange CJ, Stewart M, Devine SE, Corbett AH (2007) Classical nuclear localization signals: Definition, function, and interaction with importin α. **J. Biol. Chem.** 282, 5101–5105.

Lanternier F, Boutboul D, Menotti J, Chandesris MO, Sarfati C, Mamzer-Bruneel MF, Calmus Y, Méchaï F, Viard JP, Lecuit M, Bougnoux ME, Lortholary O (2009) Microsporidiosis in solid organ transplant recipients: Two enterocytozoon bieneusi cases and review: Short communication. **Transpl. Infect. Dis.** 11, 83–88.

Latgé JP (1999) *Aspergillus fumigatus* and aspergillosis. **Clin. Microbiol. Rev.** 12, 310–350.

Lee B-Y, Han S-Y, Choi HG, Kim JH, Han K, Han D-M (2005) Screening of growth- or development-related genes by using genomic library with inducible promoter in *Aspergillus nidulans*. **J. Microbiol.** 43, 523–528.

Lee DH, Goldberg AL (1998) Proteasome inhibitors: Valuable new tools for cell biologists. **Trends Cell Biol.** 8, 397–403.

Lee IR, Morrow CA, Fraser JA (2013) Nitrogen regulation of virulence in clinically prevalent fungal pathogens. **FEMS Microbiol. Lett.** 345, 77–84.

Lee JY, Kim LH, Kim HE, Park JS, Han KH, Han DM (2013) A putative APSES transcription factor is necessary for normal growth and development of *Aspergillus nidulans*. **J. Microbiol.** 51, 800–806.

Lee PY, Costumbrado J, Hsu C-Y, Kim YH (2012) Agarose gel electrophoresis for the separation of DNA fragments. **J. Vis. Exp.**, e3923.

Lennarz W, Lane M (2013) Ubiquitin system. In: *Encyclopedia of Biological Chemistry (2nd edition)*. pp. 473–476.

Levine M, Manley JL (1989) Transcriptional repression of eukaryotic promoters. **Cell** 59, 405–408.

Li C, Wen A, Shen B, Lu J, Huang Y, Chang Y (2011) FastCloning: A highly simplified, purification-free, sequence- and ligation-independent PCR cloning method. **BMC Biotechnol.** 11, 92.

Li L, Stoeckert CJ, Roos DS (2003) OrthoMCL: Identification of ortholog groups for eukaryotic genomes. **Genome Res.** 13, 2178–2189.

Liang N, Jakobsson T, Fan R, Treuter E (2019) The nuclear receptor-co-repressor complex in control of liver metabolism and disease. **Front. Endocrinol. (Lausanne).** 10

Lind AL, Lim FY, Soukup AA, Keller NP, Rokas A (2018) An LaeA- and BrlA-dependent cellular network governs tissue-specific secondary metabolism in the human pathogen *Aspergillus fumigatus*. **mSphere** 3, e00050-18.

Liu Z, Karmarkar V (2008) Groucho/Tup1 family co-repressors in plant development. **Trends Plant Sci.** 13, 137–144.

Lo HJ, Köhler JR, Didomenico B, Loebenberg D, Cacciapuoti A, Fink GR (1997) Nonfilamentous *C. albicans* mutants are avirulent. **Cell** 90, 939–949.

Lohr D, Venkov P, Zlatanova J (1995) Transcriptional regulation in the yeast *GAL* gene family: A complex genetic network. **FASEB J.** 9, 777–787.

Lowes D, Al-Shair K, Newton PJ, Morris J, Harris C, Rautemaa-Richardson R, Denning DW (2017) Predictors of mortality in chronic pulmonary aspergillosis. **Eur. Respir. J.** 49, pii: 1601062.

MacPherson S, Larochelle M, Turcotte B (2006) A fungal family of transcriptional regulators: The zinc cluster proteins. **Microbiol. Mol. Biol. Rev.** 70, 583–604.

Mah JH, Yu JH (2006) Upstream and downstream regulation of asexual development in *Aspergillus fumigatus*. **Eukaryot. Cell** 5, 1585–1595.

Malik VS (1980) Microbial secondary metabolism. **Trends Biochem. Sci.** 5, 68–72.

Martinelli SD (1994) *Aspergillus nidulans* as an experimental organism. **Prog. Ind. Microbiol.** 29, 33–58.

Mattaj IW, Englmeier L (1998) Nucleocytoplasmic transport: The soluble phase. **Annu. Rev. Biochem.** 67, 265–306.

McCluskey K, Wiest A, Plamann M (2010) The fungal genetics stock center: A repository for 50 years of fungal genetics research. **J. Biosci.** 35, 119–126.

McCowen MC, Callender ME, Lawlis JF (1951) Fumagillin (H-3), a new antibiotic with amebicidal properties. **Science** 113, 202–203.

McLane LM, Corbett AH (2009) Nuclear localization signals and human disease. **IUBMB Life** 61, 697–706.

McNeilly D, Schofield A, Stone SL (2018) Degradation of the stress-responsive enzyme formate dehydrogenase by the RING-type E3 ligase Keep on Going and the ubiquitin 26S proteasome system. **Plant Mol. Biol.** 96, 265–278.

Meister A, Anderson ME (1983) Glutathine. **Ann. Rev. Biochem.** 52, 711–760.

Meister C, Thieme KG, Thieme S, Köhler AM, Schmitt K, Valerius O, Braus GH (2019) COP9 signalosome interaction with UspA/Usp15 deubiquitinase controls VeA-mediated fungal multicellular development. **Biomolecules** 9, E238.

Merlet J, Burger J, Gomes JE, Pintard L (2009) Regulation of cullin-RING E3 ubiquitin-ligases by neddylation and dimerization. **Cell. Mol. Life Sci.** 66, 1924–1938.

Meyer V, Wanka F, van Gent J, Arentshorst M, van den Hondel CAMJJ, Ram AFJ (2011) Fungal gene expression on demand: An inducible, tunable, and metabolism-independent expression system for *Aspergillus niger*. **Appl. Environ. Microbiol.** 77, 2975–2983.

Millet N, Moya-Nilges M, Sachse M, Krijnse Locker J, Latgé J, Mouyna I (2019) *Aspergillus fumigatus* exoβ(1-3)glucanases family GH55 are essential for conidial cell wall morphogenesis. **Cell. Microbiol.** 19, e13102.

Mims CW, Richardson EA, Timberlake WE (1988) Ultrastructural analysis of conidiophore development in the fungus *Aspergillus nidulans* using freeze-substitution. **Protoplasma** 144, 132–141.

Mircescu MM, Lipuma L, van Rooijen N, Pamer EG, Hohl TM (2009) Essential role for neutrophils but not alveolar macrophages at early time points following *Aspergillus fumigatus* infection. **J. Infect. Dis.** 200, 647–656.

Molina JM, Goguel J, Sarfati C, Michiels JF, Desportes-Livage I, Balkan S, Chastang C, Cotte L, Maslo C, Struxiano A, Derouin F, Decazes JM (2000) Trial of oral fumagillin for the treatment of intestinal microsporidiosis in patients with HIV infection. **AIDS** 14, 1341–1348.

Molina JM, Tourneur M, Sarfati C, Chevret S, de Gouvello A, Gobert JG, Balkan S, Derouin F, and Francis Derouin MD for the AN de R sur le S 090 SG (2002) Fumagillin treatment of intestinal microsporidiosis. **N. Engl. J. Med.** 346, 1963–1969.

Mooney JL, Yager LN (1990) Light is required for conidiation in *Aspergillus nidulans*. **Genes Dev.** 4, 1473–1482.

Müller V, Lemker T, Lingl A, Weidner C, Coskun Ü, Grüber G (2006) Bioenergetics of archaea: ATP synthesis under harsh environmental conditions. **J. Mol. Microbiol. Biotechnol.** 10, 167–180.

Mullins J, Harvey R, Seaton A (1976) Sources and incidence of airborne *Aspergillus fumigatus* (Fres). **Clin. Exp. Allergy** 6, 209–217.

Murphy R, Wente SR (1996) An RNA-export mediator with an essential nuclear export signal. **Nature** 383, 357–360.

Nakayama KI, Nakayama K (2006) Ubiquitin ligases: Cell-cycle control and cancer. **Nat. Rev. Cancer** 6, 369–381.

Nakielny S, Dreyfuss G (1999) Transport of proteins and RNAs in and out of the nucleus. **Cell** 99, 677–690.

Natorff R, Sieńko M, Brzywczy J, Paszewski A (2003) The *Aspergillus nidulans metR* gene encodes a bZIP protein which activates transcription of sulphur metabolism genes. **Mol. Microbiol.** 49, 1081–1094.

Nayak T, Szewczyk E, Oakley CE, Osmani A, Ukil L, Murray SL, Hynes MJ, Osmani SA, Oakley BR (2006) A versatile and efficient gene-targeting system for *Aspergillus nidulans*. **Genetics** 172, 1557–1566.

Nelson DE, Randle SJ, Laman H (2013) Beyond ubiquitination: The atypical functions of Fbxo7 and other F-box proteins. **Open Biol.** 3, 130131.

O'Gorman CM, Fuller HT, Dyer PS (2009) Discovery of a sexual cycle in the opportunistic fungal pathogen *Aspergillus fumigatus*. **Nature** 457, 471–474.

Orejas M, MacCabe AP, Pérez-González JA, Kumar S, Ramón D (2001) The wide-domain carbon catabolite repressor CreA indirectly controls expression of the *Aspergillus nidulans xlnB* gene, encoding the acidic endo-β-(1,4)-xylanase X(24). **J. Bacteriol.** 183, 1517–1523.

Osaka F, Kawasaki H, Aida N, Saeki M, Chiba T, Kawashima S, Tanaka K, Kato S (1998) A new NEDD8-ligating system for cullin-4A. **Genes Dev.** 12, 2263–2268.

Osmani SA, Mirabito PM (2004) The early impact of genetics on our understanding of cell cycle regulation in *Aspergillus nidulans*. **Fungal Genet. Biol.** 41, 401–410.

Owens RA, Hammel S, Sheridan KJ, Jones GW, Doyle S (2014) A proteomic approach to investigating gene cluster expression and secondary metabolite functionality in *Aspergillus fumigatus*. **PLoS One** 9, e106942.

Pagano M, Tam SW, Theodoras AM, Beer-Romero P, Del Sal G, Chau V, Yew PR, Draetta GF, Rolfe M (1995) Role of the ubiquitin-proteasome pathway in regulating abundance of the cyclin-dependent kinase inhibitor p27. **Science** 269, 682–685.

Palaiomylitou M, Tartas A, Vlachakis D, Tzamarias D, Vlassi M (2008) Investigating the structural stability of the Tup1-interaction domain of Ssn6: Evidence for a conformational change on the complex. **Proteins Struct. Funct. Genet.** 70, 72–82.

Pan ZQ, Kentsis A, Dias DC, Yamoah K, Wu K (2004) Nedd8 on cullin: Building an expressway to protein destruction. **Oncogene** 23, 1985–1997.

Paoletti M, Seymour FA, Alcocer MJC, Kaur N, Calvo AM, Archer DB, Dyer PS (2007) Mating type and the genetic basis of self-fertility in the model fungus *Aspergillus nidulans*. **Curr. Biol.** 17, 1384–1389.

Paris S, Debeaupuis JP, Crameri R, Carey M, Charlès F, Prévost MC, Schmitt C, Philippe B, Latgé JP (2003) Conidial hydrophobins of *Aspergillus fumigatus*. **Appl. Environ. Microbiol.** 69, 1581–1588.

Paris S, Wysong D, Debeaupuis JP, Shibuya K, Philippe B, Diamond RD, Latgé JP (2003) Catalases of *Aspergillus fumigatus*. **Infect. Immun.** 71, 3551–3562.

Park H, Myers CL, Sheppard DC, Phan QT, Sanchez AA, Edwards JE, Filler SG (2005) Role of the fungal Ras-protein kinase A pathway in governing epithelial cell interactions during oropharyngeal candidiasis. **Cell. Microbiol.** 7, 499–510.

Park HS, Bayram Ö, Braus GH, Kim SC, Yu JH (2012) Characterization of the velvet regulators in *Aspergillus fumigatus*. **Mol. Microbiol.** 84, 937–953.

Park HS, Lee MK, Han KH, Kim MJ, Yu JH (2019) Developmental decisions in *Aspergillus nidulans*. In: *Hoffmeister D, Gressler M, (eds), Biology of the fungal cell. The mycota (a comprehensive treatise on fungi as experimnetal systems for basic and applied research)*, Vol8, pp. 63–80.

Parnell EJ, Stillman DJ (2011) Shields up: The Tup1-Cyc8 repressor complex blocks coactivator recruitment. **Genes Dev.** 25, 2429–2435.

Pashkova N, Gakhar L, Winistorfer SC, Yu L, Ramaswamy S, Piper RC (2010) WD40 repeat propellers define a ubiquitin-binding domain that regulates turnover of F-box proteins. **Mol. Cell** 40, 433–443.

Pauw B de, Thomas J. Walsha, Donnellya JP, Stevens D a., Edwards JE, Calandra T, Pappas PG, Maertens J, Lortholary O, Kauffman C a., Denning DW, Patterson TF, Maschmeyer G, Bille J, Dismukes WE, Herbrecht R, Hope WW, Kibbler CC, Kullberg BJ, *et al.* (2008) Revised definitions of invasive fungal disease from the European Organization for Research and treatment of cancer/invasive. **Clin. Infect. Dis** 46, 1813–1821.

Pedersen PL, Amzel LM (1993) ATP synthases. Structure, reaction center, mechanism, and regulation of one of nature's most unique machines. **J. Biol. Chem.** 268, 9937–9940.

Pedersen PL, Carafoli E (1987) Ion motive ATPases. I. Ubiquity, properties, and significance to cell function. **Trends Biochem. Sci.** 12, 146–150.

Perfect JR, Cox GM, Lee JY, Kauffman CA, de Repentigny L, Chapman SW, Morrison VA, Pappas P, Hiemenz JW, Stevens DA, Grp MS (2001) The impact of culture isolation of *Aspergillus* species: A hospital-based survey of aspergillosis. **Clin. Infect. Dis.** 33, 1824–1833.

Perrin RM, Fedorova ND, Bok, Jin W, Cramer RA, Wortman JR, Kim HS, Nierman WC, Keller NP (2007) Transcriptional regulation of chemical diversity in *Aspergillus fumigatus* by LaeA. **PLoS Pathog.** 3, e50.

Petroski MD, Deshaies RJ (2005a) Function and regulation of cullin-RING ubiquitin ligases. **Nat. Rev. Mol. Cell Biol.** 6, 9–20.

Petroski MD, Deshaies RJ (2005b) Mechanism of lysine 48-linked ubiquitin-chain synthesis by the cullin-RING ubiquitin-ligase complex SCF-Cdc34. **Cell** 123, 1107–1120.

Pócsi I, Prade RA, Penninckx MJ (2004) Glutathione, altruistic metabolite in fungi. **Adv. Microb. Physiol.** 49, 1–76.

Pöggeler S, Nowrousian M, Teichert I, Beier A, Kück U (2018) Fruiting-body development in Ascomycetes. In: *Physiology and Genetics*. pp. 325–355.

Pollack JK, Harris SD, Marten MR (2009) Autophagy in filamentous fungi. **Fungal Genet. Biol.** 46, 1–8.

Poon IKH, Jans DA (2005) Regulation of nuclear transport: Central role in development and transformation? **Traffic** 6, 173–186.

Ptashne M (1988) How eukaryotic transcriptional activators work. **Nature** 335, 683–689.

Punt PJ, van den Hondel CAMJJ (1992) Transformation of filamentous fungi based on hygromycin b and phleomycin resistance markers. **Methods Enzymol.** 216, 447–457.

Raffa N, Keller NP (2019) A call to arms: Mustering secondary metabolites for success and survival of an opportunistic pathogen. **PLoS Pathog.** 15, e1007606.

Rambach G, Blum G, Latgé JP, Fontaine T, Heinekamp T, Hagleitner M, Jeckström H, Weigel G, Würtinger P, Pfaller K, Krappmann S, Löffler J, Lass-Flörl C, Speth C (2015) Identification of *Aspergillus fumigatus* surface components that mediate interaction of conidia and hyphae with human platelets. **J. Infect. Dis.** 212, 1140–1149.

Reeves EP, Messina CGM, Doyle S, Kavanagh K (2004) Correlation between gliotoxin production and virulence of *Aspergillus fumigatus* in *Galleria mellonella*. **Mycopathologia** 158, 73–79.

Reichard U, Buttner S, Eifert H, Staib F, Ruchel R (1990) Purification and characterisation of an extracellular serine proteinase from *Aspergillus fumigatus* and its detection in tissue. **J. Med. Microbiol.** 33, 243–251.

Ren H, Santner A, Pozo JC Del, Murray JAH, Estelle M (2008) Degradation of the cyclin-dependent kinase inhibitor KRP1 is regulated by two different ubiquitin E3 ligases. **Plant J.** 53, 705–716.

Renwick J, Daly P, Reeves EP, Kavanagh K (2006) Susceptibility of larvae of *Galleria mellonella* to infection by *Aspergillus fumigatus* is dependent upon stage of conidial germination. **Mycopathologia** 161, 377–384.

Rexach M, Blobel G (1995) Protein import into nuclei: Association and dissociation reactions involving transport substrate, transport factors, and nucleoporins. **Cell** 83, 683–692.

Ribbeck K, Lipowsky G, Kent HM, Stewart M, Görlich D (1998) NTF2 mediates nuclear import of Ran. **EMBO J.** 17, 6587–6598.

Rivière Y, Blank V, Kourilsky P, Israël A (1991) Processing of the precursor of NF-κB by the HIV-1 protease during acute infection. **Nature** 350, 625–626.

Robbins J, Dilwortht SM, Laskey RA, Dingwall C (1991) Two interdependent basic domains in nucleoplasmin nuclear targeting sequence: Identification of a class of bipartite nuclear targeting sequence. **Cell** 64, 615–623.

Rocchi S, Reboux G, Millon L (2015) Résistance aux antifongiques azolés d'origine environnementale: Quelles alternatives pour l'avenir ? **J. Mycol. Med.** 25, 249–256.

Rojo F, Alonso JC (1994) A novel site-specific recombinase encoded by the *Streptococcus pyogenes* plasmid pSM19035. **J. Mol. Biol.** 238, 159–172.

Rojo F, Weise F, Alonso JC (1993) Purification of the β product encoded by the *Streptococcus pyogenes* plasmid pSM19035. A putative DNA recombinase required to resolve plasmid oligomers. **FEBS Lett.** 328, 169–173.

Romsdahl J, Wang CCC (2019) Recent advances in the genome mining of: *Aspergillus* secondary metabolites (covering 2012-2018). **Medchemcomm** 10, 840–866.

Roy A, Shin YJ, Cho KH, Kim J-H (2013) Mth1 regulates the interaction between the Rgt1 repressor

and the Ssn6-Tup1 corepressor complex by modulating PKA-dependent phosphorylation of Rgt1. **Mol. Biol. Cell** 24, 1493–1503.

Ruger-Herreros C, Rodríguez-Romero J, Fernández-Barranco R, Olmedo M, Fischer R, Corrochano LM, Canovas D (2011) Regulation of conidiation by light in *Aspergillus nidulans*. **Genetics** 188, 809–822.

Rybak K, See PT, Phan HTT, Syme RA, Moffat CS, Oliver RP, Tan KC (2017) A functionally conserved Zn_2Cys_6 binuclear cluster transcription factor class regulates necrotrophic effector gene expression and host-specific virulence of two major pleosporales fungal pathogens of wheat. **Mol. Plant Pathol.** 18, 420–434.

Samar D, Kieler JB, Klutts JS (2015) Identification and deletion of Tft1, α predicted glycosyltransferase necessary for cell wall β-1,3;1,4-glucan synthesis in *Aspergillus fumigatus*. **PLoS One** 10, e0117336.

Sarikas A, Hartmann T, Pan ZQ (2011) The cullin protein family. **Genome Biol.** 12, 220.

Sato I, Shimizu M, Hoshino T, Takaya N (2009) The glutathione system of *Aspergillus nidulans* involves a fungus-specific glutathione S-transferase. **J. Biol. Chem.** 284, 8042–8053.

Scazzocchio C (2006) *Aspergillus* genomes: secret sex and the secrets of sex. **Trends Genet.** 22, 521–525.

Scharf DH, Heinekamp T, Remme N, Hortschansky P, Brakhage AA, Hertweck C (2012) Biosynthesis and function of gliotoxin in *Aspergillus fumigatus*. **Appl. Microbiol. Biotechnol.** 93, 467–472.

Scherer M, Fischer R (1998) Purification and characterization of laccase II of *Aspergillus nidulans*. **Arch. Microbiol.** 170, 78–84.

Schindelin J, Arganda-Carrera I, Frise E, Kayniig V, Longair M, Pietzsch T, Preibisch S, Rueden C, Saalfeld S, Schmid B, Tinevez J-Y, White DJ, Hartenstein V, Kevin E, Tomancak P, Cardona A (2009) Fiji - an open platform for biological image analysis. **Nat. Methods** 9, 676–682.

Schjerling P, Holmberg S (1996) Comparative amino acid sequence analysis of the C_6 zinc cluster family of transcriptional regulators. **Nucleic Acids Res.** 24, 4599–4607.

Schmaler-Ripcke J, Sugareva V, Gebhardt P, Winkler R, Kniemeyer O, Heinekamp T, Brakhage AA (2009) Production of pyomelanin, a second type of melanin, via the tyrosine degradation pathway in *Aspergillus fumigatus*. **Appl. Environ. Microbiol.** 75, 493–503.

Schmidt MW, McQuary PR, Wee S, Hofmann K, Wolf DA (2009) F-box-directed CRL complex assembly and regulation by the CSN and CAND1. **Mol. Cell** 35, 589–597.

Schmittgen TD, Livak KJ (2008) Analyzing real-time PCR data by the comparative C(T) method. **Nat. Protoc.** 3, 1101–1108.

Schoberle TJ, Nguyen-Coleman CK, Herold J, Yang A, Weirauch M, Hughes TR, McMurray JS, May GS (2014) A novel C_2H_2 transcription factor that regulates *gliA* expression interdependently with GliZ in *Aspergillus fumigatus*. **PLoS Genet.** 10, e1004336.

Schrettl M, Carberry S, Kavanagh K, Haas H, Jones GW, O'Brien J, Nolan A, Stephens J, Fenelon O, Doyle S (2010) Self-protection against gliotoxin-a component of the gliotoxin biosynthetic cluster, *gliT*, completely protects *Aspergillus fumigatus* against exogenous gliotoxin. **PLoS Pathog.** 6, e1000952.

Schürch A, Miozzari J, Hütter R (1974) Regulation of tryptophan biosynthesis in *Saccharomyces cerevisiae*: mode of action of 5-methyl-tryptophan and 5-methyl-tryptophan sensitive mutants. **J. Bacteriol.** 117, 1131–1140.

Schuster E, Dunn-Coleman N, Frisvad J, Van Dijck P (2002) On the safety of *Aspergillus niger* - a review. **Appl. Microbiol. Biotechnol.** 59, 426–435.

Seo JA, Han KH, Yu JH (2004) The *gprA* and *gprB* genes encode putative G protein-coupled receptors required for self-fertilization in *Aspergillus nidulans*. **Mol. Microbiol.** 53, 1611–1623.

Serrano-Bueno G, Madroñal JM, Manzano-López J, Muñiz M, Pérez-Castiñeira JR, Hernández A, Serrano A (2019) Nuclear proteasomal degradation of *Saccharomyces cerevisiae* inorganic pyrophosphatase Ipp1p, a nucleocytoplasmic protein whose stability depends on its subcellular localization. **Biochim. Biophys. Acta - Mol. Cell Res.** 1866, 1019–1033.

Shaaban M, Shaaban KA, Abdel-Aziz MS (2012) Seven naphtho-γ-pyrones from the marine-derived fungus *Alternaria alternata*: Structure elucidation and biological properties. **Org. Med. Chem. Lett.** 2, 6.

Sharma K, D'Souza RCJ, Tyanova S, Schaab C, Wiśniewski JR, Cox J, Mann M (2014) Ultradeep human phosphoproteome reveals a D distinct regulatory nature of Tyr and Ser/Thr-based signaling. **Cell Rep.** 8, 1583–1594.

Shen J, Spruck C (2017) F-box proteins in epigenetic regulation of cancer. **Oncotarget** 8, 110650–110655.

Sheppard DC, Doedt T, Chiang LY, Kim HS, Chen D, Nierman WC, Filler SG (2005) The *Aspergillus fumigatus* StuA protein governs the up-regulation of a discrete transcriptional program during the acquisition of developmental competence. **Mol. Biol. Cell** 16, 5866–5879.

Shi H Bin, Chen N, Zhu XM, Liang S, Li L, Wang JY, Lu JP, Lin FC, Liu XH (2019) F-box proteins MoFwd1, MoCdc4 and MoFbx15 regulate development and pathogenicity in the rice blast fungus *Magnaporthe oryzae*. **Environ. Microbiol.** 21, 3027–3045.

Shlezinger N, Irmer H, Dhingra S, Beattie SR, Cramer RA, Braus GH, Sharon A, Hohl TM (2017) Sterilizing immunity in the lung relies on targeting fungal apoptosis-like programmed cell death. **Science** 357, 1037–1041.

Sieńko M, Natorff R, Skoneczny M, Kruszewska J, Paszewski A, Brzywczy J (2014) Regulatory mutations affecting sulfur metabolism induce environmental stress response in *Aspergillus nidulans*. **Fungal Genet. Biol.** 65, 37–47.

Sigler PB (1988) Acid blobs and negative noodles. **Nature** 333, 210–212.

Singh B, Satyanarayana T (2019) Thermophilic molds in environmental management. In: *Fungi from different environments*. pp. 355–379.

Singh BK, Park SH, Lee HB, Goo YA, Kim HS, Cho SH, Lee JH, Ahn GW, Kim JP, Kang SM, Kim EK (2016) Kojic acid peptide: A new compound with anti-tyrosinase potential. **Ann. Dermatol.** 28, 555–561.

Skaar JR, D'Angiolella V, Pagan JK, Pagano M (2009) SnapShot: F Box proteins II. **Cell** 137, 1358.e1.

Skaar JR, Pagan JK, Pagano M (2013) Mechanisms and function of substrate recruitment by F-box proteins. **Nat. Rev. Mol. Cell Biol.** 14, 369–381.

Skowyra D, Craig KL, Tyers M, Elledge SJ, Harper JW (1997) F-box proteins are receptors that recruit phosphorylated substrates to the SCF ubiquitin-ligase complex. **Cell** 91, 209–219.

Slack JMW (2014) Molecular biology of the cell. In: *Principles of Tissue Engineering (4th edition)*. pp. 127–145.

Slater JL, Gregson L, Denning DW, Warn PA (2011) Pathogenicity of *Aspergillus fumigatus* mutants assessed in *Galleria mellonella* matches that in mice. **Med. Mycol.** 49, S107-113.

Smith A, Brownawell A, Macara IG (2004) Nuclear import of Ran is mediated by the transport factor NTF2. **Curr. Biol.** 8, 1403–1406.

Smith BJ (1984) SDS polyacrylamide gel electrophoresis of proteins. In: *Proteins*. Humana Press, New Jersey, New Jersey, Vol1, pp. 41–56.

Smith RL, Johnson AD (2000) Turning genes off by Ssn6-Tup1: A conserved system of transcriptional repression in eukaryotes. **Trends Biochem. Sci.** 25, 325–330.

Smith TD, Calvo AM (2014) The *mtfA* transcription factor gene controls morphogenesis, gliotoxin

production, and virulence in the opportunistic human pathogen *Aspergillus fumigatus*. **Eukaryot. Cell** 13, 766–775.

Sohn KT, Yoon KS (2002) Ultrastructural study on the cleistothecium development in *Aspergillus nidulans*. **Mycobiology** 30, 117–127.

Son S, Osmani SA (2009) Analysis of all protein phosphatase genes in *Aspergillus nidulans* identifies a new mitotic regulator, Fcp1. **Eukaryot. Cell** 8, 573–585.

Song J, Pfanner N, Becker T (2018) Assembling the mitochondrial ATP synthase. **Proc. Natl. Acad. Sci. U. S. A.** 115, 2850–2852.

Sonneborn A, Bockmühl DP, Ernst JF (1999) Chlamydospore formation in *Candida albicans* requires the Efg1p morphogenetic regulator. **Infect. Immun.** 67, 5514–5517.

Sonneborn A, Tebarth B, Ernst JF (1999) Control of white-opaque phenotypic switching in *Candida albicans* by the Efg1p morphogenetic regulator. **Infect. Immun.** 67, 4655–4660.

Sönnichsen B, Lowe M, Levine T, Jämsä E, Dirac-Svejstrup B, Warren G (1998) A role for giantin in docking COPI vesicles to Golgi membranes. **J. Cell Biol.** 140, 1013–1021.

Southern EM (1975) Detection of specific sequences among DNA fragments separated by gel electrophoresis. **J. Mol. Biol.** 98, 503–517.

Spannagel C, Vaillier J, Arselin G, Graves PV, Velours J (1997) The subunit f of mitochondrial yeast ATP synthase - characterization of the protein and disruption of the structural gene *ATP17*. **Eur. J. Biochem.** 247, 1111–1117.

Spikes S, Xu R, Nguyen CK, Chamilos G, Kontoyiannis DP, Jacobson RH, Ejzykowicz DE, Chiang LY, Filler SG, May GS (2008) Gliotoxin production in *Aspergillus fumigatus* contributes to host-specific differences in virulence. **J. Infect. Dis.** 197, 479–486.

St-Germain G, Summerbell R (2003) Identifying filamentous fungi: A clinical laboratory handbook. **Rev. Inst. Med. Trop. Sao Paulo** 45, 152.

Steinbach WJ (2018) 244 - *Aspergillus* species. In: *Principles and Practice of Pediatric Infectious Diseases (5th edition)*. Elsevier, pp. 1238-1244.e2.

Steinert K, Wagner V, Kroth-Pancic PG, Bickel-Sandkötter S (1997) Characterization and subunit structure of the ATP synthase of the halophilic archaeon *Haloferax volcanii* and organization of the ATP synthase genes. **J. Biol. Chem.** 272, 6261–6269.

Stinnett SM, Espeso EA, Cobeño L, Araújo-Bazán L, Calvo AM (2007) *Aspergillus nidulans* VeA subcellular localization is dependent on the importin α carrier and on light. **Mol. Microbiol.** 63, 242–255.

Stoldt VR, Sonneborn A, Leuker CE, Ernst JF (1997) Efg1p, an essential regulator of morphogenesis of the human pathogen *Candida albicans*, is a member of a conserved class of bHLH proteins regulating morphogenetic processes in fungi. **EMBO J.** 16, 1982–1991.

Subramaniam PS, Larkin J, Mujtaba MG, Walter MR, Johnson HM (2000) The COOH-terminal nuclear localization sequence of interferon γ regulates STAT1 α nuclear translocation at an intracellular site. **J. Cell Sci.** 113, 2771–2781.

Sugareva V, Härtl A, Brock M, Hübner K, Rohde M, Heinekamp T, Brakhage AA (2006) Characterisation of the laccase-encoding gene *abr2* of the dihydroxynaphthalene-like melanin gene cluster of *Aspergillus fumigatus*. **Arch. Microbiol.** 186, 345–355.

Sugui JA, Pardo J, Chang YC, Zarember KA, Nardone G, Galvez EM, Müllbacher A, Gallin JI, Simon MM, Kwon-chung KJ (2007) Gliotoxin is a virulence factor of *Aspergillus fumigatus*: *gliP* deletion attenuates virulence in mice immunosuppressed with hydrocortisone. **Eukaryot. Cell** 6, 1562–1569.

Szewczyk E, Nayak T, Oakley CE, Edgerton H, Xiong Y, Taheri-Talesh N, Osmani SA, Oakley BR (2006) Fusion PCR and gene targeting in *Aspergillus nidulans*. **Nat. Protoc.** 1, 3111–3120.

Tafforeau L, Le Blastier S, Bamps S, Dewez M, Vandenhaute J, Hermand D (2006) Repression of ergosterol level during oxidative stress by fission yeast F-box protein Pof14 independently of SCF. **EMBO J.** 25, 4547–4556.

Tao L, Yu JH (2011) AbaA and WetA govern distinct stages of *Aspergillus fumigatus* development. **Microbiology** 157, 313–326.

Tekaia F, Latgé JP (2005) *Aspergillus fumigatus*: Saprophyte or pathogen? **Curr. Opin. Microbiol.** 8, 385–392.

Teunissen AWRH, Van Den Berg JA, Yde Steensma H (1995) Transcriptional regulation of flocculation genes in *Saccharomyces cerevisiae*. **Yeast** 11, 435–446.

Thieme KG (2017) The zinc cluster transcription factor ZtfA is an activator of asexual development and secondary metabolism and regulates the oxidative stress response in the filamentous fungus *Aspergillus nidulans*. Dissertation. Faculty of biology and psychology. Georg-August University Goettingen.

Thieme KG, Gerke J, Sasse C, Valerius O, Thieme S, Karimi R, Heinrich AK, Finkernagel F, Smith K, Bode HB, Freitag M, Ram AFJJ, Braus GH (2018) Velvet domain protein VosA represses the zinc cluster transcription factor SclB regulatory network for *Aspergillus nidulans* asexual development , oxidative stress response and secondary metabolism. **PLoS Genet.** 14, e1007511.

Thön M, Al-Abdallah Q, Hortschansky P, Brakhage AA (2007) The thioredoxin system of the filamentous fungus *Aspergillus nidulans*: Impact on development and oxidative stress response. **J. Biol. Chem.** 282, 27259–27269.

Todd RB, Andrianopoulos A (1997) Evolution of a fungal regulatory gene family: The $Zn(II)_2Cys_6$ binuclear cluster DNA binding motif. **Fungal Genet. Biol.** 21, 388–405.

Tyers M, Jorgensen P (2000) Proteolysis and the cell cycle: with this RING I do thee destroy. **Curr. Opin. Genet. Dev.** 10, 54–64.

Tzamarias D, Struhl K (1994) Functional dissection of the yeast Cyc8-Tupl transcriptional co-repressor complex. **Nature** 369, 758–761.

Uitenbroek DG (1997) SISA Binomial. *Southampton: D.G. Uitenbroek. Retrieved January 01, 2017, from the World Wide Web*: https://www.quantitativeskills.com/sisa/distributions/binomial.htm.

Untergasser A, Cutcutache I, Koressaar T, Ye J, Faircloth BC, Remm M, Rozen SG (2012) Primer3-new capabilities and interfaces. **Nucleic Acids Res.** 40, e115.

Vadlapudi V, Borah N, Yellusani KR, Gade S, Reddy P, Rajamanikyam M, Vempati LNS, Gubbala SP, Chopra P, Upadhyayula SM, Amanchy R (2017) *Aspergillus* secondary metabolite database, a resource to understand the secondary metabolome of *Aspergillus* genus. **Sci. Rep.** 7, 7325.

Valiante V, Macheleidt J, Föge M, Brakhage AA (2015) The *Aspergillus fumigatus* cell wall integrity signalling pathway: Drug target, compensatory pathways and virulence. **Front. Microbiol.** 6, 325.

Valsecchi I, Dupres V, Stephen-Victor E, Guijarro JI, Gibbons J, Beau R, Bayry J, Coppee JY, Lafont F, Latgé JP, Beauvais A (2018) Role of hydrophobins in *Aspergillus fumigatus*. **J. Fungi** 4, 2.

Vandeputte P, Ischer F, Sanglard D, Coste AT (2011) *In vivo* systematic analysis of *Candida albicans* Zn_2-Cys_6 transcription factors mutants for mice organ colonization. **PLoS One** 6, e26962.

Verstrepen KJ, Fink GR (2009) Genetic and epigenetic mechanisms underlying cell-surface variability in protozoa and fungi. **Annu. Rev. Genet.** 43, 1–24.

Voutsina A, Fragiadakis GS, Gkouskou K, Alexandraki D (2019) Synergy of Hir1, Ssn6, and Snf2 global regulators is the functional determinant of a Mac1 transcriptional switch in *S. cerevisiae*

copper homeostasis. **Curr. Genet.** 65, 799–816.

Walker JE (2013) The ATP synthase: The understood, the uncertain and the unknown. **Biochem. Soc. Trans.** 41, 1–16.

Wang D, Sun J, Yu HL, Li CX, Bao J, Xu JH (2012) Maximum saccharification of cellulose complex by an enzyme cocktail supplemented with cellulase from newly isolated *Aspergillus fumigatus* ECU0811. **Appl. Biochem. Biotechnol.** 166, 176–186.

Wang R, Brattain MG (2007) The maximal size of protein to diffuse through the nuclear pore is larger than 60 kDa. **FEBS Lett.** 581, 3164–3170.

Ward JJ, McGuffin LJ, Bryson K, Buxton BF, Jones DT (2004) The DISOPRED server for the prediction of protein disorder. **Bioinformatics** 20, 2138–2139.

Waters MG, Clary DO, Rothman JE (1992) A novel 115-kD peripheral membrane protein is required for intercisternal transport in the Golgi stack. **J. Cell Biol.** 118, 1015–1026.

Wei D, Sun Y (2010) Small RING finger proteins RBX1 and RBX2 of SCF E3 ubiquitin ligases: The role in cancer and as cancer targets. **Genes and Cancer** 1, 700–707.

Wen W, Meinkotht JL, Tsien RY, Taylor SS (1995) Identification of a signal for rapid export of proteins from the nucleus. **Cell** 82, 463–473.

Whiteside ST, Goodbourn S (1993) Signal transduction and nuclear targeting: Regulation of transcription factor activity by subcellular localisation. **J. Cell Sci.** 104, 949–955.

Wiemann P, Guo C-J, Palmer JM, Sekonyela R, Wang CCC, Keller NP (2013) Prototype of an intertwined secondary-metabolite supercluster. **Proc. Natl. Acad. Sci.** 110, 17065–17070.

Willems AR, Schwab M, Tyers M (2004) A hitchhiker's guide to the cullin ubiquitin ligases: SCF and its kin. **Biochim. Biophys. Acta - Mol. Cell Res.** 1695, 133–170.

Willger SD, Puttikamonkul S, Kim KH, Burritt JB, Grahl N, Metzler LJ, Barbuch R, Bard M, Lawrence CB, Cramer RA (2008) A sterol-regulatory element binding protein is required for cell polarity, hypoxia adaptation, azole drug resistance, and virulence in *Aspergillus fumigatus*. **PLoS Pathog.** 4, e1000200.

Williams GR, Sampson MA, Shutler D, Rogers REL (2008) Does fumagillin control the recently detected invasive parasite *Nosema ceranae* in western honey bees (*Apis mellifera*)? **J. Invertebr. Pathol.** 99, 342–344.

Williams GR, Shutler D, Little CM, Burgher-Maclellan KL, Rogers RELL (2011) The microsporidian *Nosema ceranae*, the antibiotic Fumagilin-B®, and western honey bee (*Apis mellifera*) colony strength. **Apidologie** 42, 15–22.

Wu L, Osmani SA, Mirabito PM (1998) A role for NIMA in the nuclear localization of cyclin B in *Aspergillus nidulans*. **J. Cell Biol.** 141, 1575–1587.

Wyatt TT, Wösten HAB, Dijksterhuis J (2013) Fungal spores for dispersion in space and time. **Adv. Appl. Microbiol.** 85, 43–91.

Xiong X, Sun S, Li Y, Zhang X, Sun J, Xue F (2019) The cotton WRKY transcription factor *GhWRKY70* negatively regulates the defense response against *Verticillium dahliae*. **Crop J.** 7, 393–402.

Xu L, Massagué J (2004) Nucleocytoplasmic shuttling of signal transducers. **Nat. Rev. Mol. Cell Biol.** 5, 209–219.

Yaguchi T (2011) The genus *Aspergillus*. **Japanese J. Med. Mycol.** 52, 193–197.

Yang D, Hu Y, Yin Z, Gao Q, Zhang Y, Chan FY, Zeng G, Weng L, Wang L, Wang Y (2020) *Candida albicans* ubiquitin and heat shock factor-type transcriptional factors are involved in 2-dodecenoic acid-mediated inhibition of hyphal growth. **Microorganisms** 8, 75.

Yao G, Zhang F, Nie X, Wang X, Yuan J, Zhuang Z, Wang S (2017) Essential APSES transcription

factors for mycotoxin synthesis, fungal development, and pathogenicity in *Aspergillus flavus*. **Front. Microbiol.** 8, 2277.

Ye XS, Lee SL, Wolkow TD, McGuire SL, Hamer JE, Wood GC, Osmani SA (1999) Interaction between developmental and cell cycle regulators is required for morphogenesis in *Aspergillus nidulans*. **EMBO J.** 18, 6994–7001.

Yin WB, Chooi YH, Smith AR, Cacho RA, Hu Y, White TC, Tang Y (2013) Discovery of cryptic polyketide metabolites from dermatophytes using heterologous expression in *Aspergillus nidulans*. **ACS Synth. Biol.** 2, 629–634.

Yokogawa M, Tsushima T, Noda NN, Kumeta H, Enokizono Y, Yamashita K, Standley DM, Takeuchi O, Akira S, Inagaki F (2016) Structural basis for the regulation of enzymatic activity of Regnase-1 by domain-domain interactions. **Sci. Rep.** 6, 22324.

Yokoyama C, Wang X, Briggs MR, Admon A, Wu J, Hua X, Goldstein JL, Brown MS (1993) SREBP-1, a basic-helix-loop-helix-leucine zipper protein that controls transcription of the low density lipoprotein receptor gene. **Cell** 75, 187–197.

Yoon J, Kikuma T, Maruyama JI, Kitamoto K (2013) Enhanced production of bovine chymosin by autophagy deficiency in the filamentous fungus *Aspergillus oryzae*. **PLoS One** 8, e62512.

Yu J-H (2010) Regulation of development in *Aspergillus nidulans* and *Aspergillus fumigatus*. **Mycobiology** 38, 229–237.

Yu J-H, Kwon N-J, Shin K-S, Gao N, Ni M (2010) Regulation of *Aspergillus* conidiation. In: *Cellular and Molecular Biology of Filamentous Fungi (1st edition) Chapter 35*. pp. 559–576.

Yu JH, Mah JH, Seo JA (2006) Growth and developmental control in the model and pathogenic Aspergilli. **Eukaryot. Cell** 5, 1577–1584.

Zabel U, Henkel T, Silva MS, Baeuerle PA (1993) Nuclear uptake control of NF-κB by MAD-3, an IκB protein present in the nucleus. **EMBO J.** 12, 201–211.

von Zeska Kress MR, Harting R, Bayram Ö, Christmann M, Irmer H, Valerius O, Schinke J, Goldman GH, Braus GH (2012) The COP9 signalosome counteracts the accumulation of cullin SCF ubiquitin E3 RING ligases during fungal development. **Mol. Microbiol.** 83, 1162–1177.

Zhang C, Meng X, Gu H, Ma Z, Lu L (2018) Predicted glycerol 3-phosphate dehydrogenase homologs and the glycerol kinase GlcA coordinately adapt to various carbon sources and osmotic stress in *Aspergillus fumigatus*. **G3 Genes, Genomes, Genet.** 8, 2291–2299.

Zhang Z-Y (2002) Protein tyrosine phosphatases: Structure and function, substrate specificity, and inhibitor development. **Annu. Rev. Pharmacol. Toxicol.** 42, 209–234.

Zhang Z, Reese JC (2004) Ssn6-Tup1 requires the ISW2 complex to position nucleosomes in *Saccharomyces cerevisiae*. **EMBO J.** 23, 2246–2257.

Zhao Y, Su H, Zhou J, Feng H, Zhang K-QQ, Yang J (2014) The APSES family proteins in fungi: Characterization, evolution and functions. **Fungal Genet. Biol.** 81, 271–280.

Zheng J, Yang X, Harrell JM, Ryzhikov S, Shim EH, Lykke-Andersen K, Wei N, Sun H, Kobayashi R, Zhang H (2002) CAND1 binds to unneddylated CUL1 and regulates the formation of SCF ubiquitin E3 ligase complex. **Mol. Cell** 10, 1519–1526.

Zhou S, Zhang P, Zhou H, Liu X, Li SM, Guo L, Li K, Yin WB (2019) A new regulator RsdA mediating fungal secondary metabolism has a detrimental impact on asexual development in *Pestalotiopsis fici*. **Environ. Microbiol.** 21, 416–426.

Supplementary Material

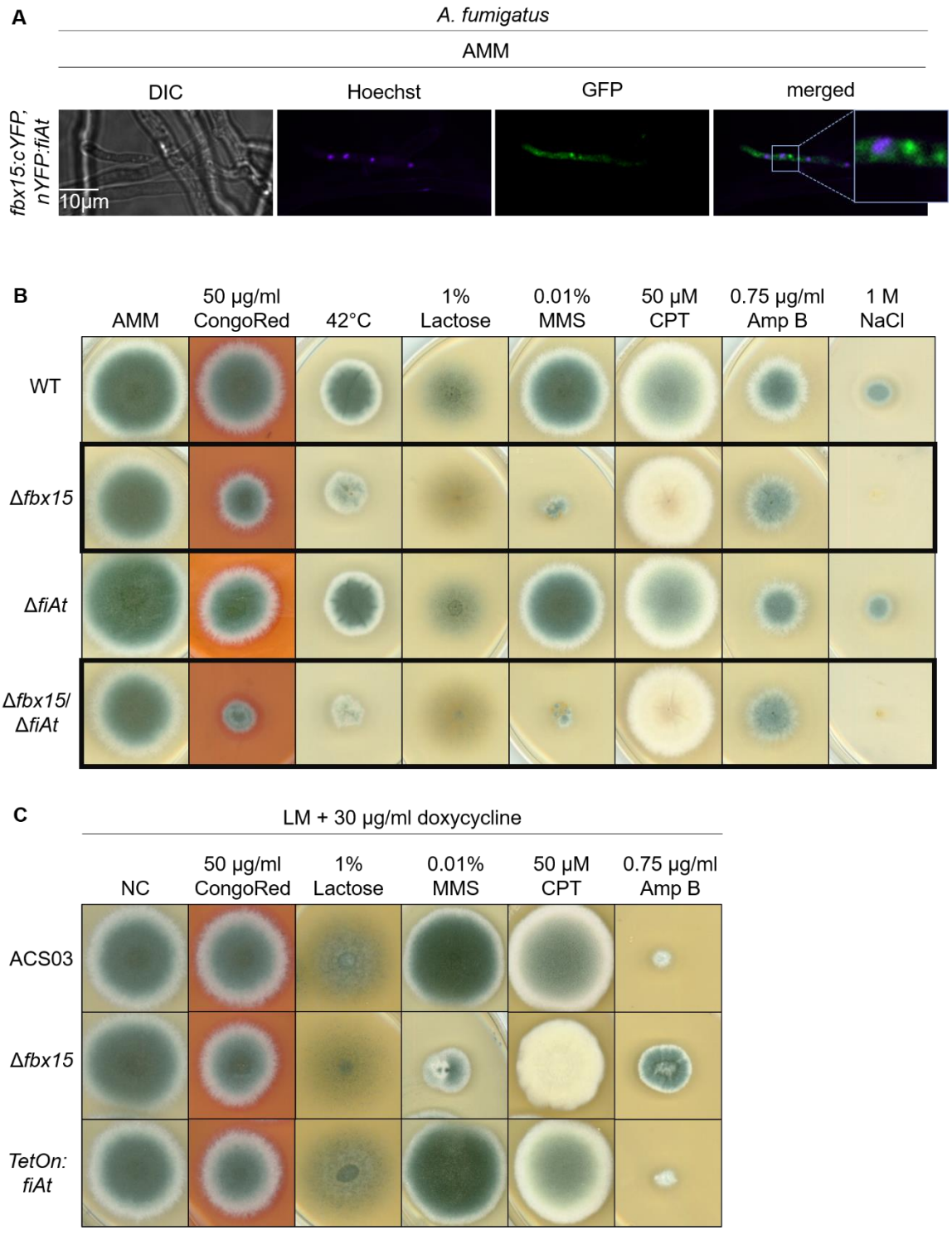

Figure S1: *fiAt* is dispensable for Fbx15-mediated stress response in *A. fumigatus*. (**A**) 2*10^3 spores of *A. fumigatus* were grown vegetatively in Aspergillus minimal medium (AMM) for 18h at 37°C in darkness: The location of the physical interaction was analysed through Bimolecular Fluorescence Complementation (BiFC). YFP signals for the putative Fbx15 interacting APSES transcription factor (FiAt) fused to nYFP (*nYFP:fiAt*) and Fbx15 fused to cYFP (*fbx15:cYFP*) are shown in the cytoplasm in hyphae during vegetative growth conditions. Nuclei were stained with Hoechst. (**B**) 2*10^3 spores of *A. fumigatus* strains were point inoculated on *Aspergillus* minimal medium (AMM) and incubated for three to five days at 37°C without (control) and with stressors in darkness. Δ*fiAt* phenocopies wild type (WT) all tested stressors including cell wall stress induced by 50 µl/ml CongoRed, heat induced by the incubation at 42°C, carbon source stress induced by exchanging glucose to lactose, DNA damage induced by methyl methanesulfonate (0.01% MMS) OR camptothecin (50 µM CPT), drug tolerance analysed with amphotericin B (0.75 µg/ml Amp B) and osmotic stress induced by natrium chloride (1 M NaCl). Δ*fbx15*-phenotypes dominate in Δ*fbx15*/Δ*fiAt* on all tested stress media (black frames). (**C**) Overexpressed *fiAt* fused to *pyroA* was integrated in the locus of *pyroA* under an doxycycline-inducible *tetOn* promoter in *A. fumigatus* resulting in ^{P}*tetOn:fiAt*. 2*10^3 spores of *A. fumigatus* strains were grown for three days at 37°C on London medium (LM) supplemented with 30 µM/ml dox without (NC) and with stressors in darkness. The ^{P}*tetOn:fiAt* strain phenocopies the reference strain ^{P}*tetOn:rfp*. In contrast to the phenotypes observed on AMM, stress sensitivity of Δ*fbx15* is reduced on LM + dox at cell wall stress and drug resistance resulting in an increased stress tolerance for Δ*fbx15*. Experiments were performed with two independent transformants and three biological replicates.

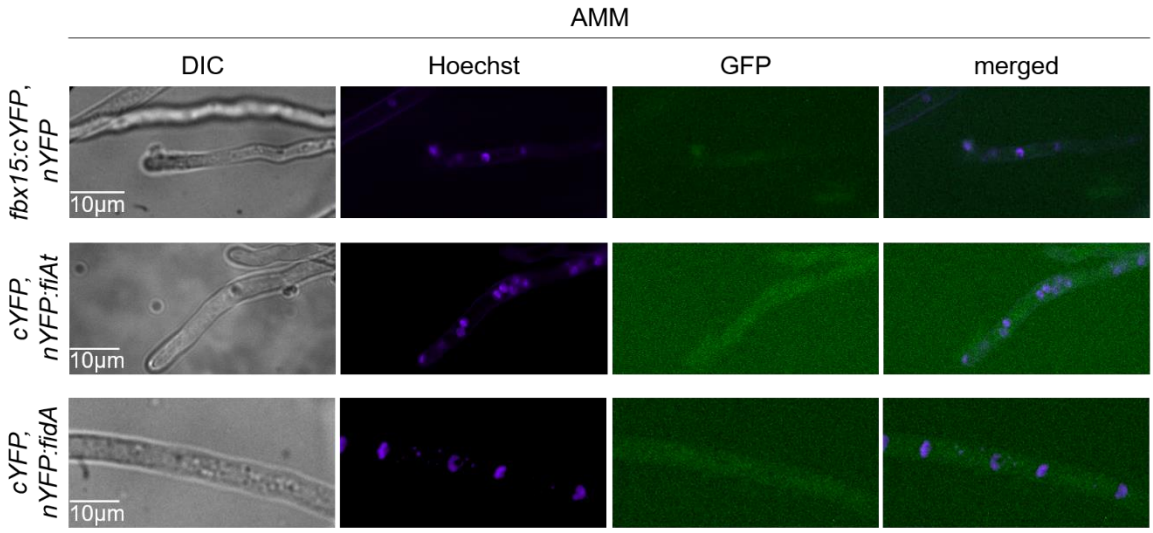

Figure S2: Controls of the interaction analysis of Fbx15 with FiAt and FidA do not produce YFP signals at vegetative growth or cadmium ion stress in *A. fumigatus*. 2*10^3 spores of *A. fumigatus* strains were grown vegetatively in *Aspergillus* minimal medium (AMM) for 18h at 37°C in darkness. The negative controls expressing *nYFP* with *fbx15:cYFP*; *cYFP* with *nYFP:fiAt* or *cYFP* with *nYFP:fidA* were ectopically integrated into *A. fumigatus* and show no YFP signals during vegetative growth. Hoechst dye was used to visualise nuclei. Experiments were performed with at least two independent transformants and three biological replicates.

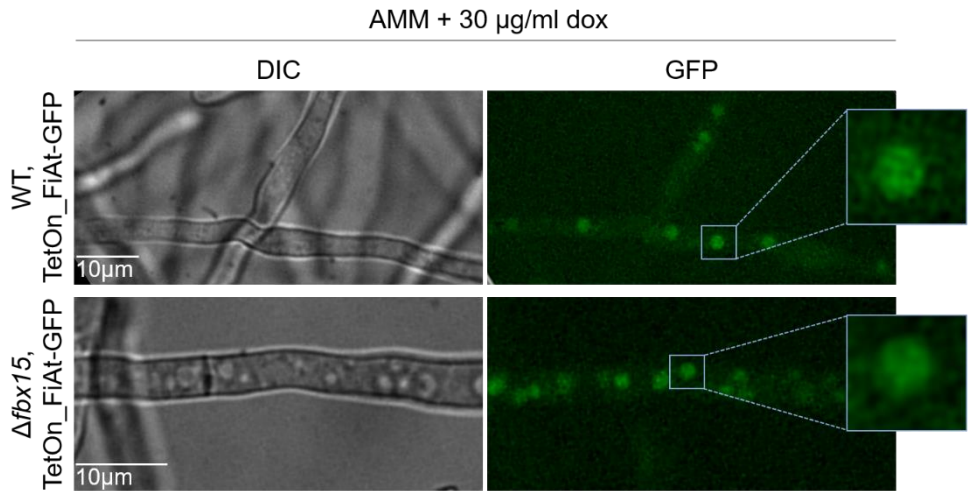

Figure S3: Nuclear localisation of FiAt is independent of Fbx15 in *A. fumigatus* at vegetative growth. 2*10^3 spores of *A. fumigatus* strains were grown vegetatively in *Aspergillus* minimal medium (AMM) for 18h at 37°C in darkness. Overexpressed *fiAt* was ectopically integrated in Fluorescence microscopic imaging reveals that overexpressed FiAt (TetOn_FiAt-GFP) is located in spots, presumably nuclei, in presence or absence of *fbx15*. Experiments were performed with two independent transformants and two biological replicates.

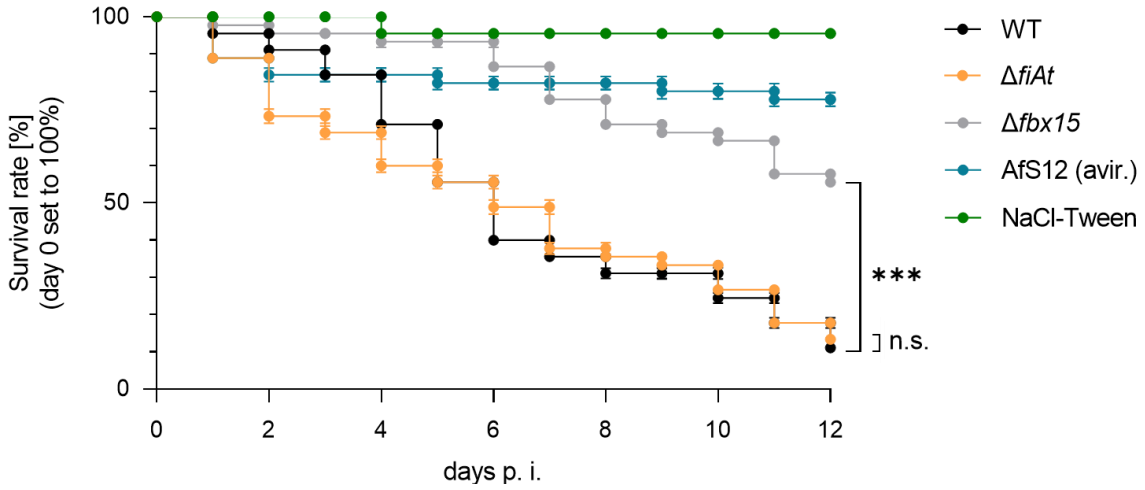

Figure S4: *fiAt* is dispensable for *A. fumigatus* virulence in the *Galleria mellonella* larvae infection model. *Galleria mellonella* larvae were injected with 5*10^6 spores of *A. fumigatus* strains and incubated in darkness at 30°C for 12 days. 10 µg/ml rifampicin were used to prevent death by contaminations. Standard deviation from three biological replicates were calculated. Significances were determined with one-way Anova and Student's t-test (*P*-value: ****P*<0.0001, n.s.: not significant). The survival rate of larvae injected with Δ*fiAt* (yellow) is not significantly altered compared to that of wild type-infected larvae (WT, black). The survival rate of Δ*fbx15*-infected larvae (grey) is significantly higher compared to larvae infected with WT (black). Larvae injected with NaCl-Tween (green) or the avirulent strain AfS12 (blue) were used as negative controls.

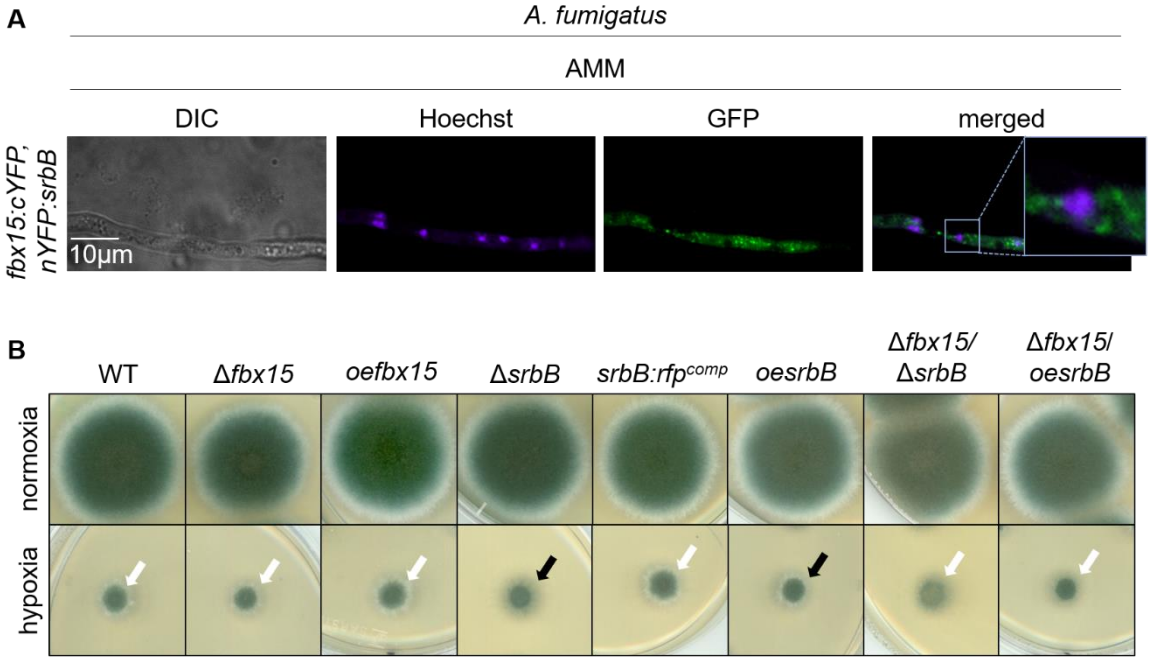

Figure S5: *fbx15* is dispensable for hypoxia adaptation unlike *srbB* in *A. fumigatus*. (**A**) 2*10^3 spores of *A. fumigatus* were grown vegetatively in Aspergillus minimal medium (AMM) for 18h at 37°C in darkness. The location of the physical interaction was analysed via Bimolecular Fluorescence Complementation (BiFC). The *A. fumigatus* strain expressing the SREBP transcription factor SrbB fused to nYFP (*nYFP:srbB*) and Fbx15 fused to cYFP (*fbx15:cYFP*) shows YFP signals in the cytoplasm at vegetative growth. Nuclei were stained with Hoechst. Experiments were performed with three biological replicates. (**B**) 2*10^3 spores of *A. fumigatus* strains were point inoculated on *Aspergillus* minimal medium (AMM) and incubated for four days at 37°C with sufficient oxygen supply (normoxia) or reduced oxygen supply (~3% O_2, hypoxia) in darkness. Overexpressed *fbx15* using the constitutively active *gpdA* promoter (oe*fbx15*) and native expressed *fbx15* (*fbx15*^{comp}) were integrated on-locus of Δ*fbx15.* The *srbB* gene fused to *rfp* (*srbB:rfp*^{comp}) and overexpressed *srbB* (oe*srbB*) using the constitutively active *gpdA* promoter were integrated on-locus of Δ*srbB*. Oe*fbx15,* oe*srbB* and Δ*fbx15* in combination with oe*srbB* (Δ*fbx15*/oe*srbB*) phenocopy wild type (WT) and *fbx15*^{comp} during hypoxia conditions resulting in colonies harbouring a white mycelia ring (white arrows). Δ*srbB* and Δ*fbx15*/Δ*srbB* show less hyphal growth compared to WT (black arrows). Experiments were performed with two independent transformants or four biological replicates.

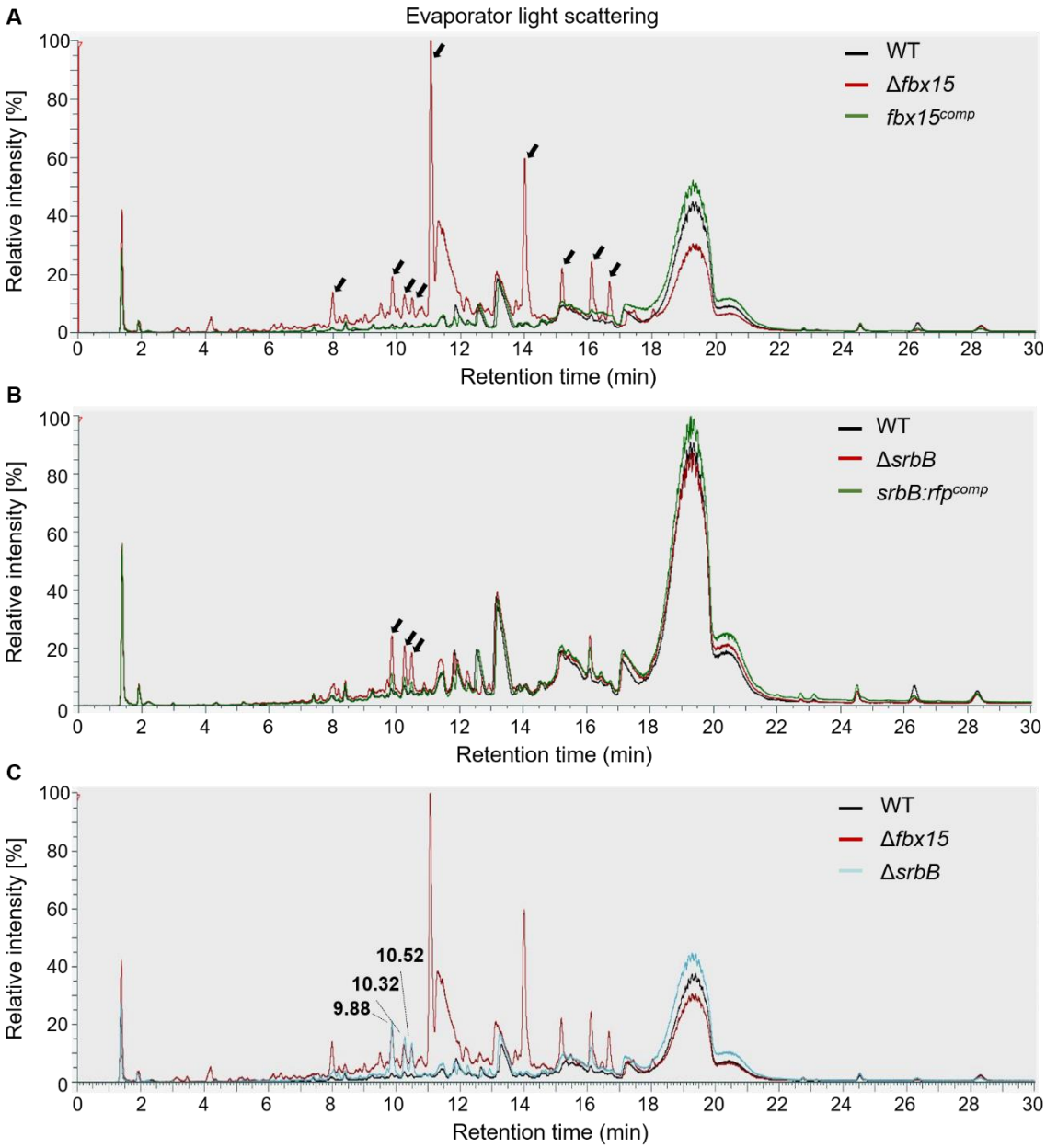

Figure S6: Fbx15 and SrbB are required for the regulation of four identical, unidentified secondary metabolites during vegetative growth conditions in *A. fumigatus*. 2*10^8 spores of *A. fumigatus* strains were grown vegetatively in *Aspergillus* minimal medium (AMM) for two days at 37°C. HPLC analysis were performed from extracted secondary metabolites with ethyl acetate. (**A**) The *fbx15* gene (*fbx15*^{comp}) was integrated on-locus of Δ*fbx15.* The Δ*fbx15* (red) produces secondary metabolites, which are less induced in WT (black) or *fbx15*^{comp} (green) (arrows). (**B**) The *srbB* gene fused to *rfp* (*srbB:rfp*^{comp}) was integrated on-locus of Δ*srbB.* Δ*srbB* (red) leads to a higher production of certain secondary metabolites compared to WT (black) and *srbB*^{comp} (green) (arrows). (**C**) Four similar increased peaks of Δ*fbx15* (red) and Δ*srbB* (blue) are identified at retention times 9.88, 10.32 and 10.52 min (bold numbers).

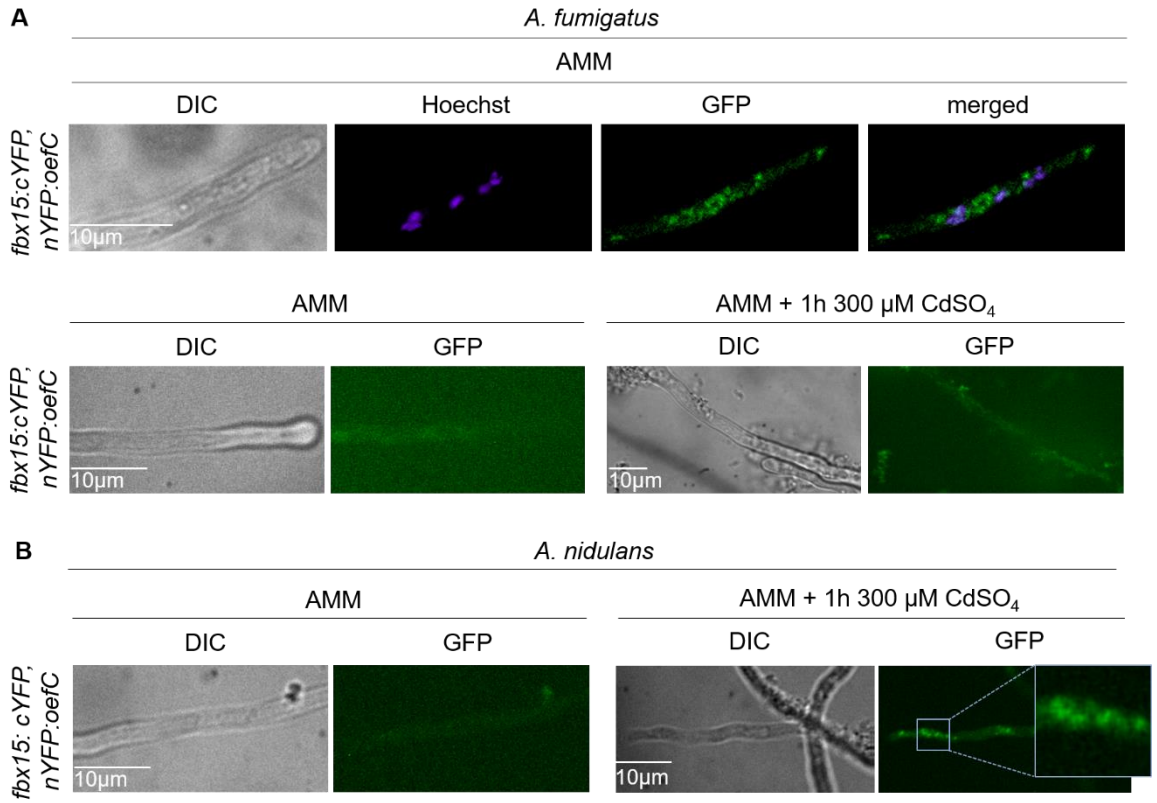

Figure S7: Fbx15 interact with the transcriptional regulator OefC at cadmium ion stress in *A. nidulans* but not significantly in *A. fumigatus*. The interaction was analysed through Bimolecular fluorescence complementation (BiFC). $2*10^3$ spores of *A. fumigatus* - or *A. nidulans* strains were grown vegetatively in *Aspergillus* minimal medium (AMM) for 18h at 37°C in darkness. For cadmium ion stress induction fresh cadmium sulphate (300 µM $CdSO_4$)-containing AMM was applied to 18h-old hyphae and incubated in darkness for 1h prior to microscopy. The location of the physical interaction was analysed through Bimolecular Fluorescence Complementation (BiFC). (**A**) *A. fumigatus* Fbx15 fused to cYFP (*fbx15:cYFP*) and the zinc cluster transcription factor OefC fused to nYFP (*nYFP:oefC*) were ectopically integrated into *A. fumigatus*. Hyphae stained with Hoechst show YFP signals in the cytoplasm at vegetative growth. Without Hoechst staining no YFP-signals are observed for the interaction of *fbx15:cYFP* with *nYFP:oefC* during vegetative growth - or heavy metal stress conditions induced by the incubation in cadmium sulphate (300 µM $CdSO_4$)-containing AMM for 1h. Experiments were performed with three biological replicates. (**B**) YFP signals for *fbx15:cYFP* with *nYFP:oefC* are observed in the cytoplasm of hyphae during cadmium ion stress. No YFP signals are observed during vegetative growth expressing *fbx15:cYFP, nYFP:oefC*. Experiments were performed with two independent transformants.

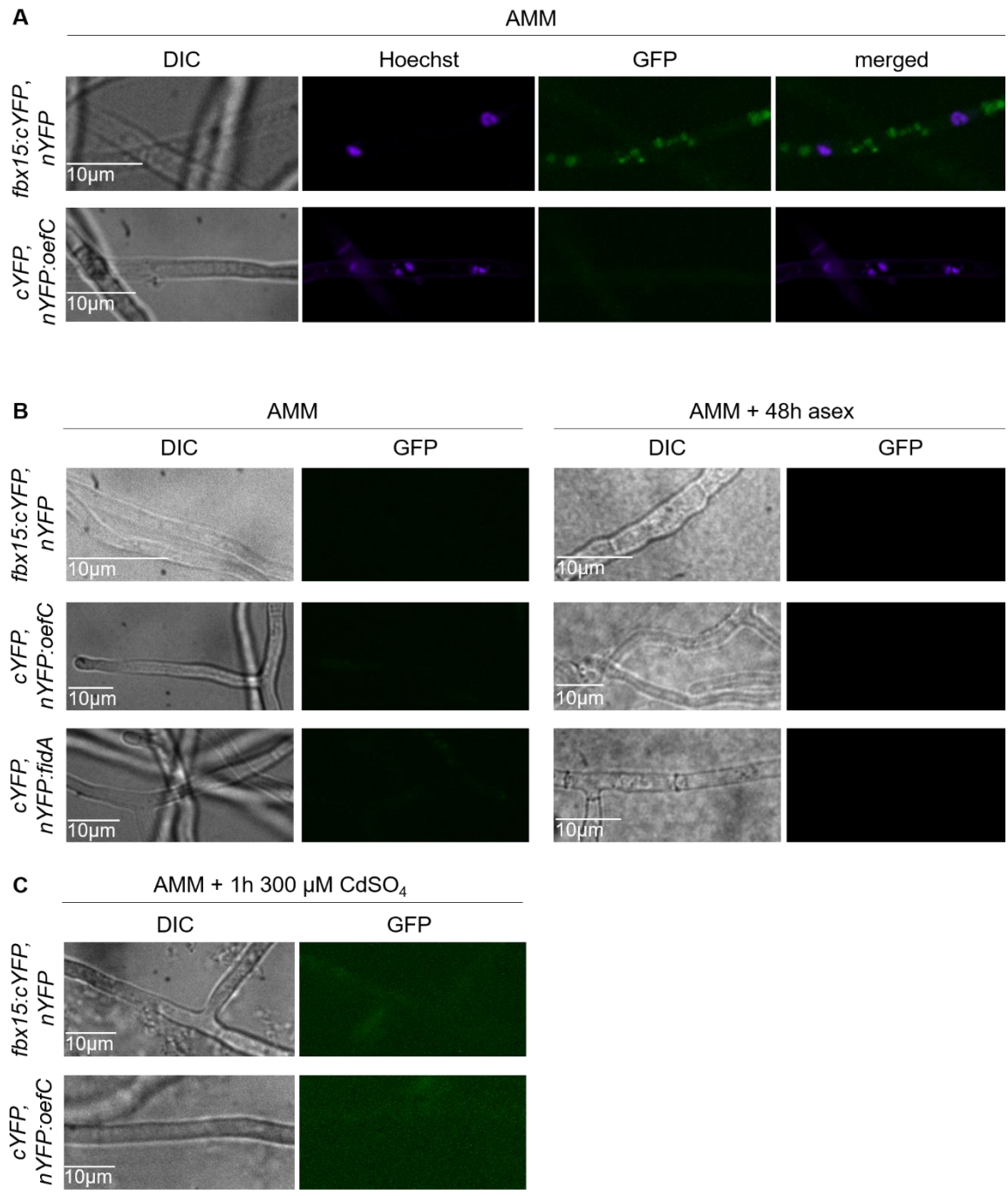

Figure S8: Controls of the interaction analysis of Fbx15 with OefC and FidA do not produce significant YFP signals at vegetative - or asexual growth and cadmium ion stress in *A. nidulans* without Hoechst staining. $2*10^3$ spores of *A. nidulans* strains were grown vegetatively in Aspergillus minimal medium (AMM) for 18h at 37°C in darkness or asexual growth induced by a 48h incubation of $2*10^3$ spores on solid AMM at 37°C in light. Heavy metal stress conditions were induces by a 1h incubation in cadmium sulphate (300 µM $CdSO_4$)-containing AMM for on 18h-old vegetatively grown hyphae. Experiments were performed with two independent transformants or three biological replicates. (**A**) The controls expressing *fbx15:cYFP* and *nYFP* (*fbx15:cYFP, nYFP*), *cYFP* and *nYFP:oefC* (*cYFP, nYFP:oefC*) were ectopically integrated into *A. nidulans*. Hoechst staining results in YFP signals for *fbx15:cYFP, nYFP*, whereas the control *cYFP, nYFP:oefC* does not show YFP signals at vegetative growth. (**B**) Without Hoechst staining the controls *fbx15:cYFP, nYFP* and *cYFP, nYFP:oefC* or *cYFP, nYFP:fidA* show not YFP signals at vegetative growth or induces asexual growth. (**C**) No YFP signals were observed in the controls *fbx15:cYFP* and *nYFP*; *cYFP* and *nYFP:oefC* during heavy metal stress conditions.

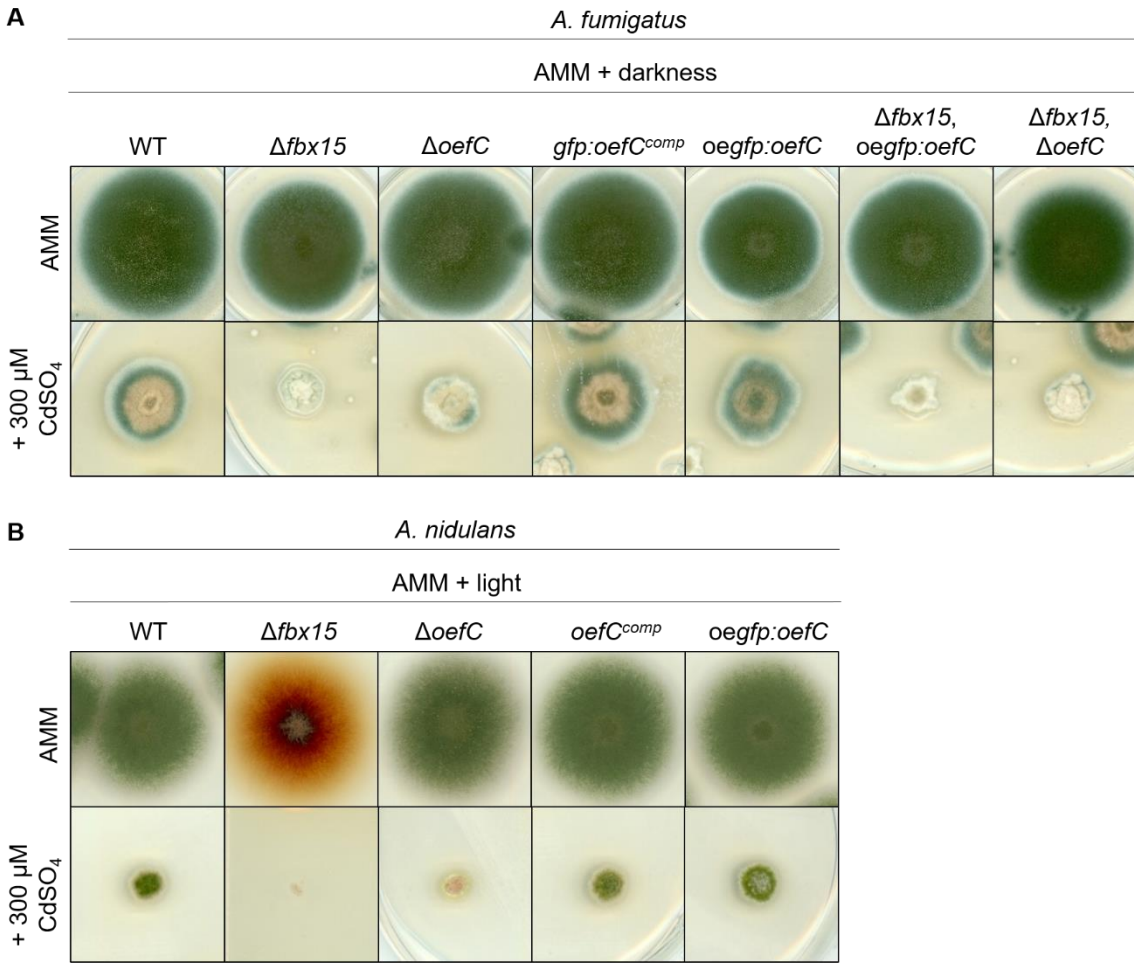

Figure S9: *oefC* is required for cadmium ion stress tolerance in *A. fumigatus* and *A. nidulans*. 2*10^3 spores of *A. fumigatus* - or *A. nidulans* strains were point inoculated on *A*spergillus minimal medium (AMM) and 300µM $CdSO_4$-containing AMM and were incubated at 37°C for five days in in darkness (*A. fumigatus*) or in light (*A. nidulans*). (**A**) *A. fumigatus oefC* fused to *gfp* (*gfp:oefC*^{comp}) and overexpressed *oefC* fused to *gfp* (oe*gfp:oefC*) were on-locus integrated in Δ*oefC*, as well as oe*oefC* fused to *gfp* (Δ*fbx15*, oe*gfp:oefC*) was on-locus integrated in Δ*fbx15*/Δ*oefC. A. fumigatus* Δ*fbx15* and Δ*oefC* are reduced in conidiation and its colony size is smaller compared to wild type (WT) at heavy metal stress induced by cadmium ions. The Δ*fbx15*/oe*gfp:oefC* and Δ*fbx15*/Δ*oefC* phenocopy Δ*fbx15* in colony size at heavy metal stress. (**B**) *A. nidulans oefC* (*oefC*^{comp}) and oe*oefC* fused to *gfp* (oe*gfp:oefC*) were on-locus integrated in Δ*oefC*. The colony size of *A. nidulans* Δ*oefC* is smaller compared to WT at heavy metal stress. The oe*gfp:oefC* strain results in an increased colony size than WT or *oefC*^{comp} at heavy metal stress. *A. nidulans* Δ*fbx15* is strongly reduced in growth compared to WT.

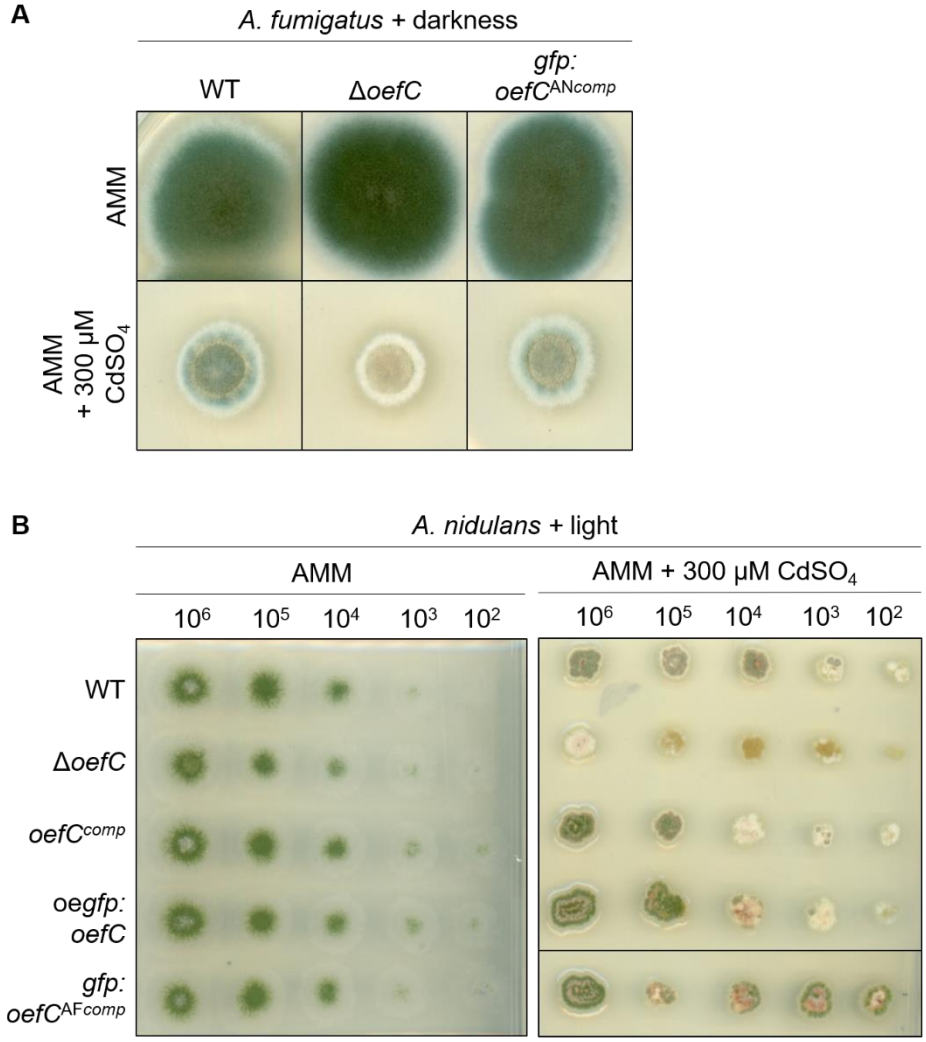

Figure S10: *oefC*-dependent cadmium ion stress tolerance is conserved among *A. fumigatus* and *A. nidulans*. (**A**) *A. nidulans oefC* fused to *gfp* (*gfp:oefC*^{ANcomp}) was integrated on-locus of *A. fumigatus* Δ*oefC*. 2*10^3 spores of *A. fumigatus* strains were incubated for five days at 37°C in darkness on *Aspergillus* minimal medium (AMM) and 300µM $CdSO_4$-containing AMM. Growth on $CdSO_4$-containing AMM results in a smaller colony size with less conidiation for Δ*oefC* compared to wild type (WT). The *gfp:oefC*^{ANcomp} strain rescues the WT-phenotype during cadmium ion stress conditions ($CdSO_4$) in *A. fumigatus*. (**B**) *A. nidulans oefC (oefC*^{comp}*),* overexpressed *oefC* fused to *gfp (*oe*gfp:oefC)* and *A. fumigatus oefC* (*oefC*^{AFcomp}) were on-locus integrated in *A. nidulans* Δ*oefC. A. nidulans* Δ*oefC*. A dilution series of 3*10^6 to 3*10^2 spores of *A. nidulans* strains were point inoculated on AMM without and with cadmium ion stress (300µM $CdSO_4$) and were incubated for five days at 37°C in light. Growth on $CdSO_4$-containing AMM results in a smaller colony sizes with less conidiation for Δ*oefC* compared to WT and *oefC*^{comp} and oe*gfp:oefC*. The *gfp:oefC*^{AFcomp} rescues the WT-colony sizes during cadmium ion stress conditions in *A. nidulans*. Experiments were performed with two biological replicates.

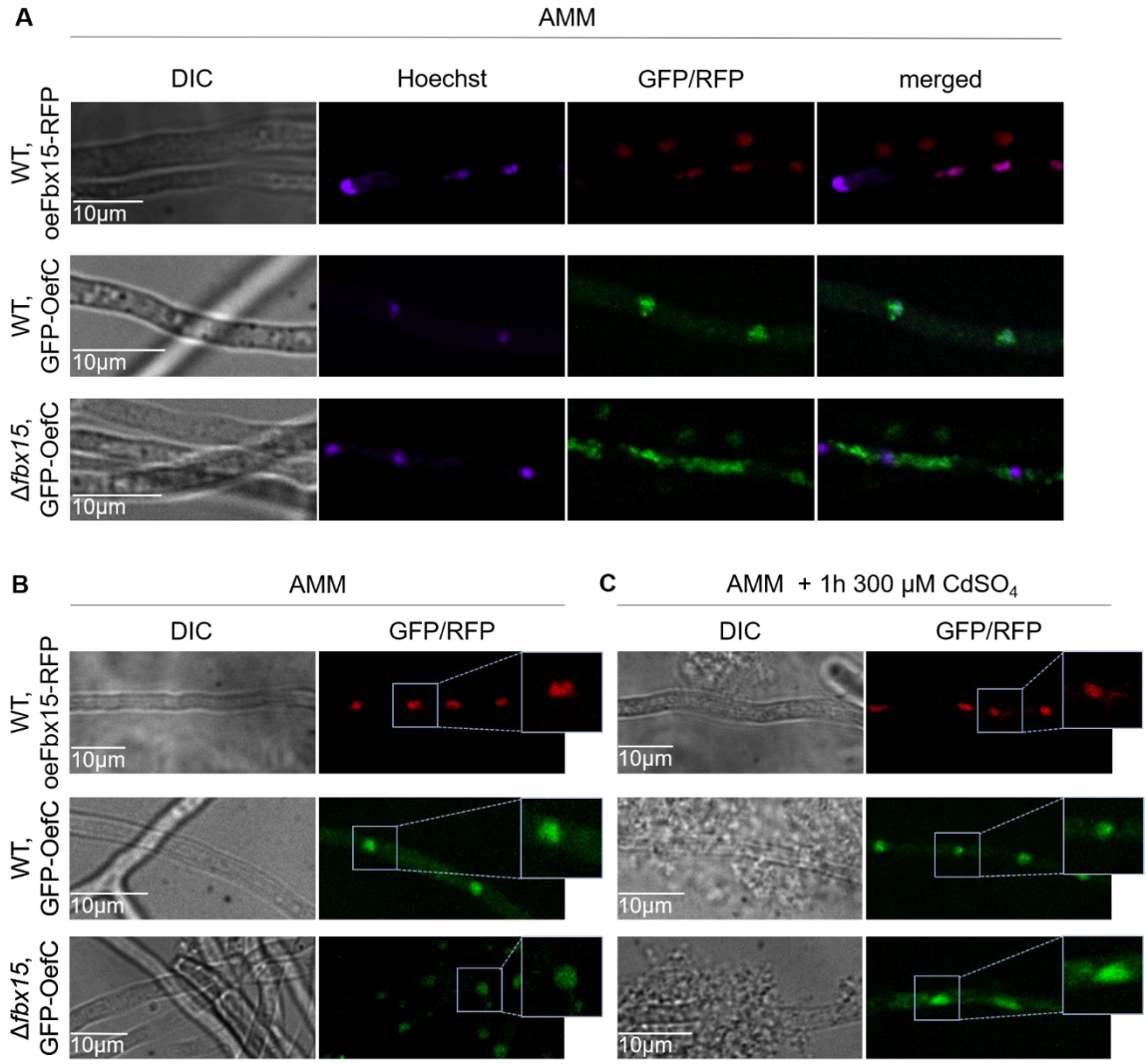

Figure S11: OefC nuclear localisation is independent of Fbx15 during non-stress or cadmium ion stress in *A. nidulans*. 2*10^3 spores of *A. nidulans* strains were grown vegetatively in *Aspergillus* minimal medium (AMM) for 18h at 37°C in darkness. (**A**) Hoechst staining results in cytoplasmic localisation of GFP-OefC in Δ*fbx15* background. (**B**) GFP-OefC is in spots presumably nuclei during vegetative growth in presence or absence of *fbx15* when nuclei are not stained with Hoechst. oeFbx15-RFP is in the nucleus at vegetative growth. (**C**) For heavy metal stress induction 300 µM $CdSO_4$-containing AMM was applied to grown hyphae and incubated in darkness for 1h. oeFbx15-RFP is primarily in the nucleus during heavy metal stress conditions. Experiments were performed with three biological replicates.

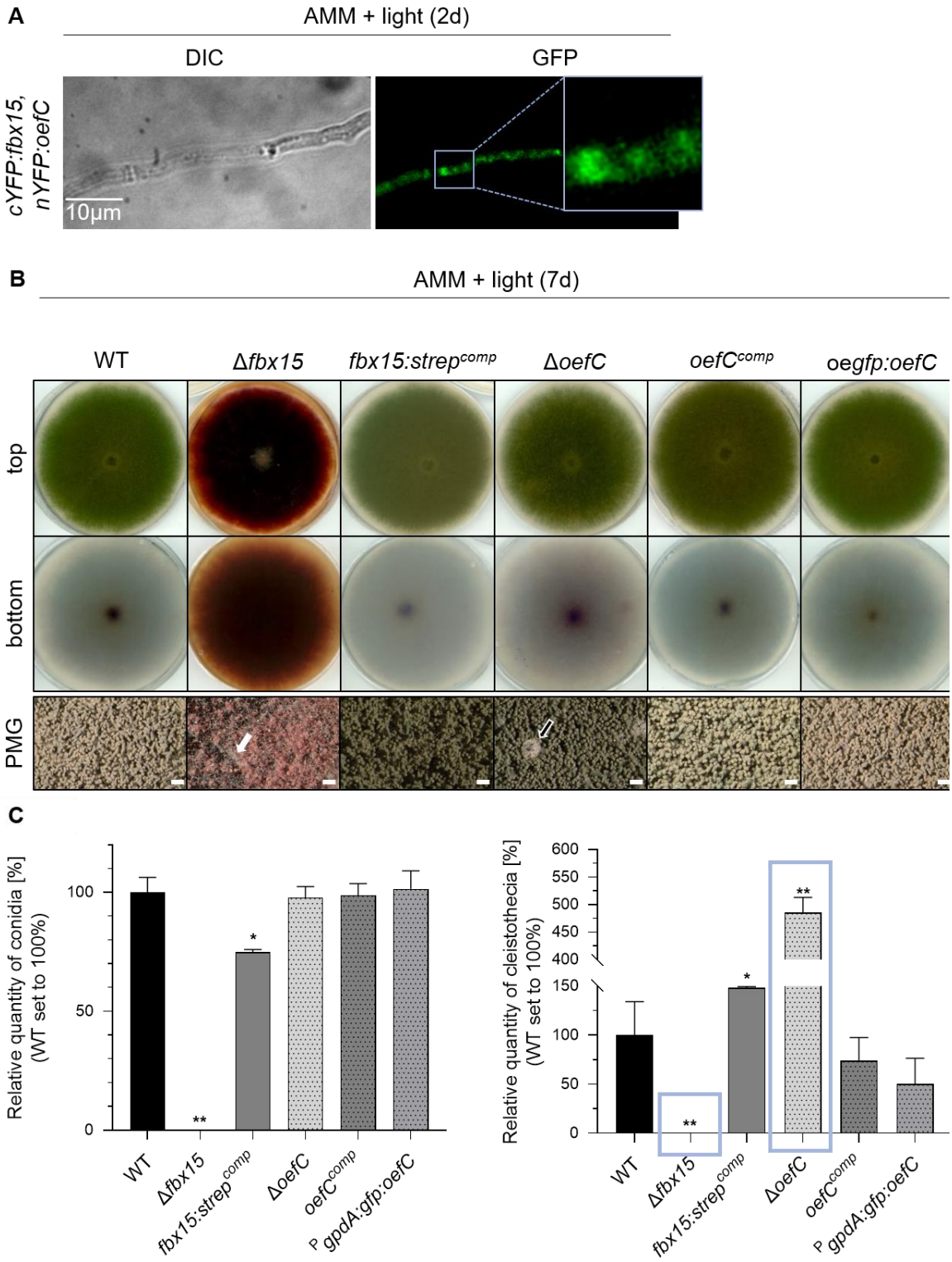
A
AMM + light (2d)
DIC
GFP
cYFP:fbx15,
nYFP:oefC
10µm
B
AMM + light (7d)
WT
Δfbx15
fbx15:strepcomp
ΔoefC
oefCcomp
oegfp:oefC
top
bottom
PMG
C
Relative quantity of conidia [%]
(WT set to 100%)
100
50
0
**
*
WT
Δfbx15
fbx15:strepcomp
ΔoefC
oefCcomp
PgpdA:gfp:oefC
Relative quantity of cleistothecia [%]
(WT set to 100%)
600
550
500
450
400
150
100
50
0
**
*
**
WT
Δfbx15
fbx15:strepcomp
ΔoefC
oefCcomp
PgpdA:gfp:oefC

Figure S12: *oefC* modulates cleistothecia formation and secondary metabolism in light in *A. nidulans*. (**A**) $2*10^3$ spores of *A. nidulans* were grown vegetatively in Aspergillus minimal medium (AMM) on solid AMM and incubated for two days (2d) to induce asexual growth. The interaction was analysed via Bimolecular Fluorescence Complementation (BiFC). YFP signals for *fbx15:cYFP* and the zinc cluster transcription factor OefC fused to nYFP (*nYFP:oefC*) are observed in the cytoplasm of hyphae during asexual growth. Experiments were performed with either two independent transformants or at least three biological replicates. (**B**) The *A. nidulans oefC* gene (*oefC*^{comp}) and the overexpressed *oefC* gene using the constitutively active *gpdA* promoter fused to *gfp* (oe*gfp:oefC*) were integrated on-locus of the *oefC* deletion strain (Δ*oefC*) and compared to wild type (WT), Δ*fbx15* and its on-locus complementation (*fbx15:strep*^{comp}). $2*10^3$ spores of *A. nidulans* strains were point inoculated on *Aspergillus* minimal medium (AMM) and incubated for seven days (7d) at 37°C in light with oxygen supply. The Δ*oefC* colony shows a reddish pigmentation compared to WT, *oefC*^{comp} and oe*gfp:oefC* (bottom) and cleistothecia are observed at the surface of the colony (black-white arrow). The Δ*fbx15* colony shows its characteristic phenotype with less conidia (white arrow) and dark red pigmentation (bottom) compared to WT and *fbx15:strep*^{comp}. (**C**) Error bars represent the SEM and were calculated from six biological replicates. Significances were determined with one-way Anova and Student's t-test (*P*-value: **P*<0.01, ***P*<0.001). Quantification of conidia in light conditions reveals no differences in Δ*oefC* compared to WT or *oefC*^{comp} and oe*gfp:oefC*, whereas significant decreased conidia are quantified for Δ*fbx15.* Cleistothecia amount is significantly increased in Δ*oefC* compared to WT, *oefC*^{comp} and oe*gfp:oefC* in light conditions. Δ*fbx15* is blocked in cleistothecia production (blue frames).

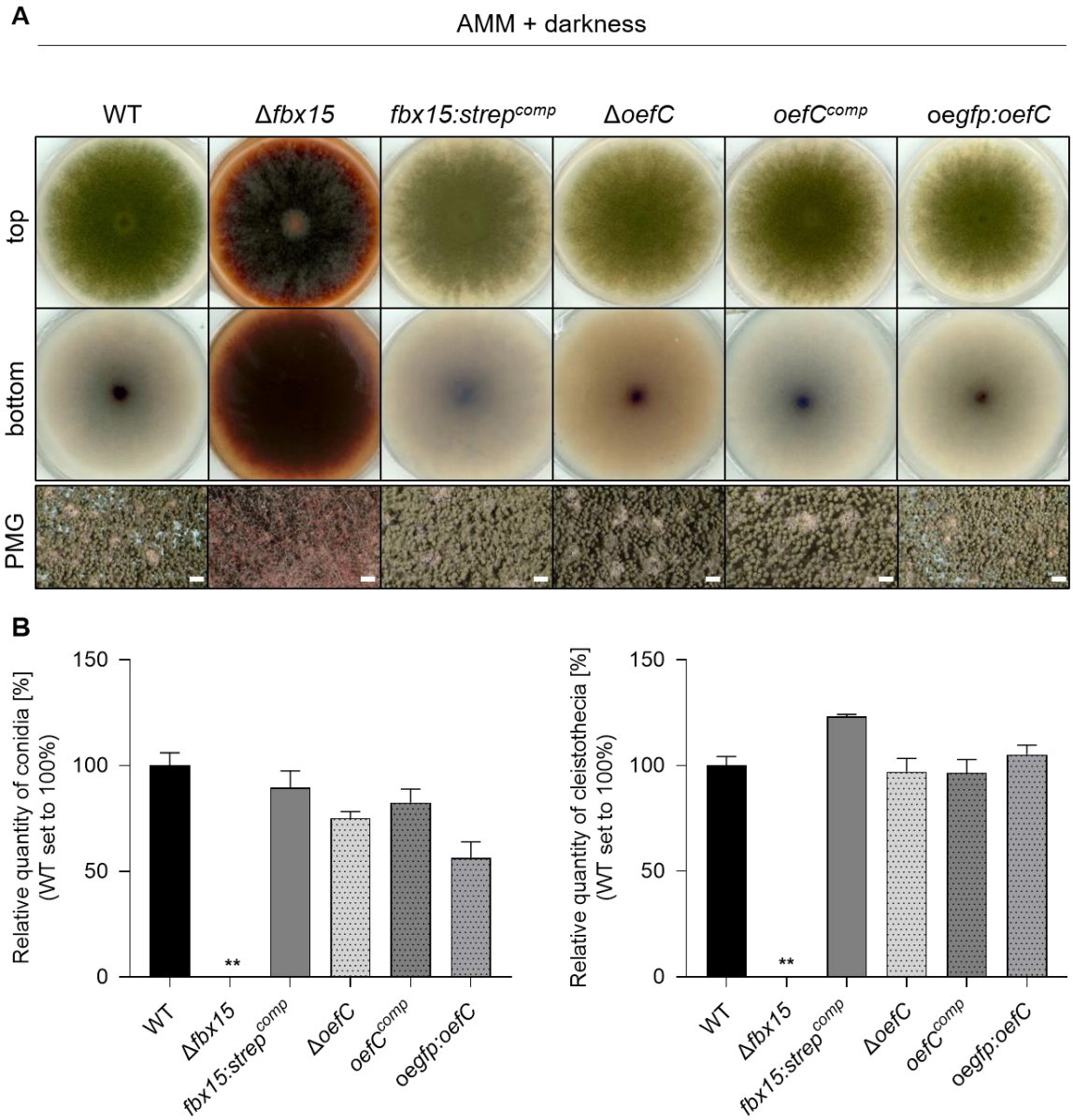

Figure S13: *oefC* is dispensable for asexual or sexual development but regulates secondary metabolism in darkness in *A. nidulans.* The *A. nidulans oefC* gene (*oefC*^{comp}) and overexpressed *oefC* gene using the constitutively active *gpdA* promoter fused to *gfp* (oe*gfp:oefC*) were integrated on-locus of the *oefC* deletion strain (Δ*oefC*) and compared to wild type (WT), Δ*fbx15* and its on-locus complementation (*fbx15:strep*^{comp}). 2*10^3 spores of *A. nidulans* strains were point inoculated on *Aspergillus* minimal medium (AMM) and incubated for seven days at 37°C in darkness with limited oxygen supply. (**A**) In darkness Δ*fbx15* shows its characteristic phenotype with extreme reduced conidiation, no cleistothecia formation and extreme reddish pigmentated colony compared to the greenish pigmentation of WT- and *fbx15:strep*^{comp} colonies. The Δ*oefC* colony shows a yellowish pigmentation (bottom) compared to the greenish pigmentation of WT-, *gfp:oefC*^{comp} or oe*gfp:oefC* colonies. (**B**) Error bars represent the SEM and were calculated from six biological replicates. Significances were determined with one-way Anova and Student's t-test (*P*-value: ***P*<0.001). Quantifications of conidia and cleistothecia in darkness revealed that the production of spores is strongly reduced and cleistothecia formation is blocked in Δ*fbx15* compared to *fbx15:strep*^{comp} and WT. No significant differences of conidia or cleistothecia formation was observed in Δ*oefC* and in oe*gfp:oefC* compared to WT and/or *gfp:oefC*^{comp}. PMG: photomicrograph, scale bars: 200 µm.

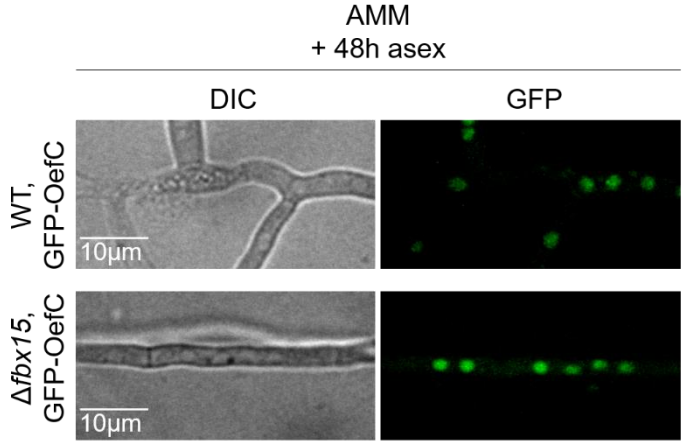

Figure S14: OefC is independent of Fbx15 localised in the nucleus during asexual growth in *A. nidulans*. The *oefC* gene fused to *gfp* was integrated on-locus of Δ*oefC* resulting in wild type (WT), GFP-OefC or integrated on-locus of Δ*fbx15* resulting in Δ*fbx15*, GFP-OefC. 2*10^3 spores of *A. nidulans* strains were grown on solid *Aspergillus* minimal medium (AMM) for 48h at 37°C in light. GFP-OefC is localised in spots, presumably nuclear, at asexual growth in presence or absence of *fbx15*. Experiments were performed with three biological replicates.

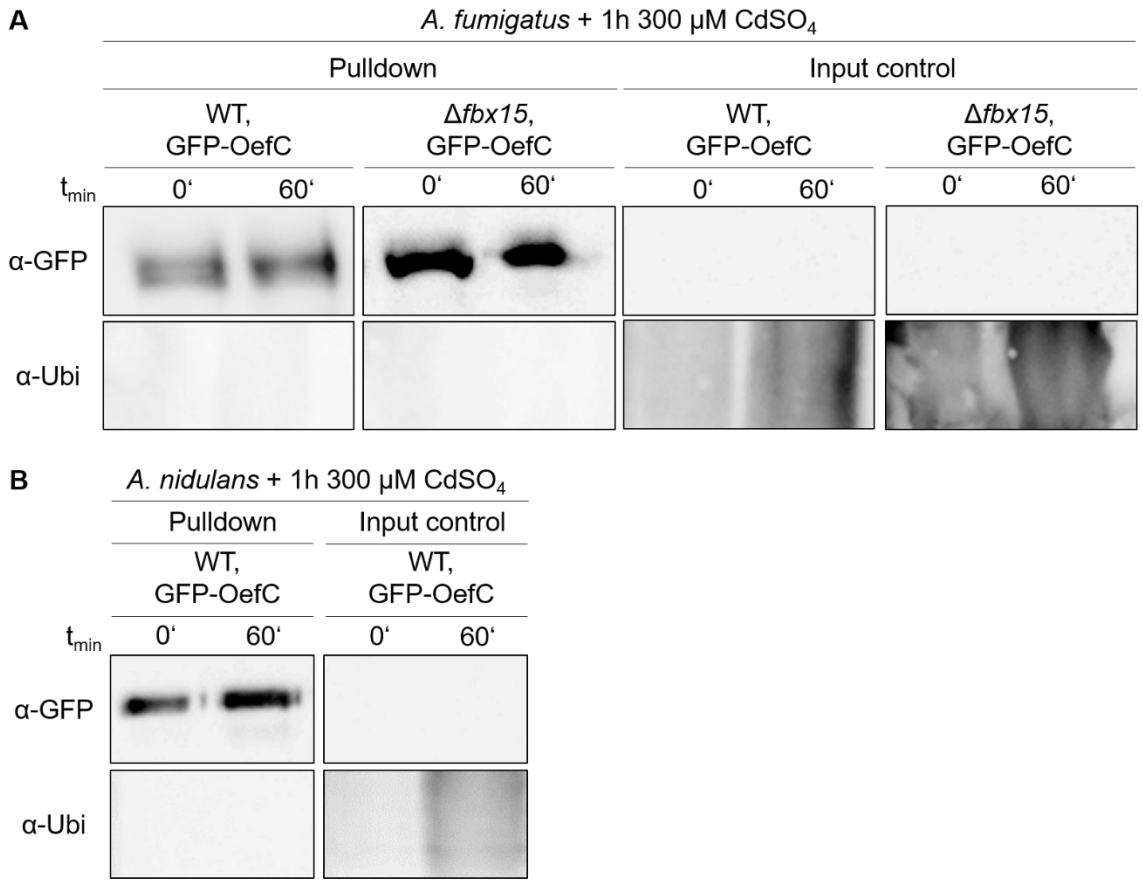

Figure S15: OefC is not ubiquitinated under non-stress or cadmium ion stress conditions in a Fbx15-dependent or -independent manner in *A. fumigatus* or *A. nidulans*. 2*10^8 spores of *A. fumigatus* or *A. nidulans* strains were grown vegetatively for 20h at 37°C in *Aspergillus* minimal medium (AMM) in light. (**A**) *A. fumigatus oefC* fused to *gfp* was on-locus integrated in *A. fumigatus* Δ*oefC* and in *A. fumigatus* Δ*fbx15*/Δ*oefC* resulting in wild type (WT), GFP-OefC and Δ*fbx15*, oeGFP-OefC. GFP-pulldown experiments reveal that GFP-OefC does not show ubiquitin signals under vegetative growth conditions and/or application of 300 µM $CdSO_4$ for 1h in context of the SCF^{Fbx15} complex in *A. fumigatus*. Crude extract used as input control shows an stronger ubiquitin band during cadmium ion stress conditions compared to vegetative growth conditions in WT, GFP-OefC and Δ*fbx15*, oeGFP-OefC. (**B**) *A. nidulans oefC* fused to *gfp* was on-locus integrated in *A. nidulans* Δ*oefC* resulting in WT, GFP-OefC. GFP-pulldown experiments show that no ubiquitin signals for the approx. 110 kDa large WT, GFP-OefC protein under vegetative growth conditions and/or application of 300 µM $CdSO_4$ for 1h in *A. nidulans*. Crude extract of WT, GFP-OefC used as input control shows an stronger ubiquitin band during cadmium ion stress conditions compared to vegetative growth conditions. Experiments were performed with two biological replicates.

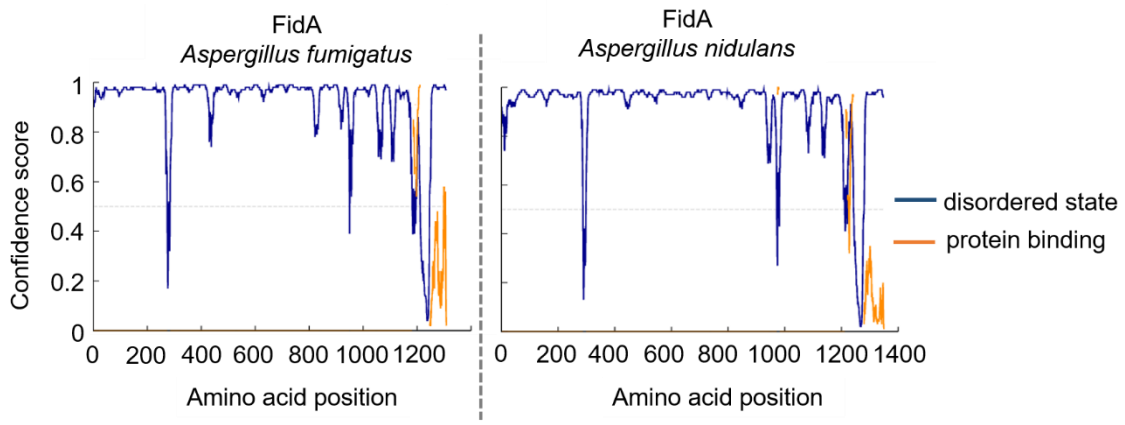

Figure S16: **FidA has an intrinsically disordered structure in *A. fumigatus* and *A. nidulans***. Computational analysis show that FidA has no known domain with a complete disordered state (blue) and a protein binding side (yellow) on its C-terminus (DISOPRED program (http://bioinf.cs.ucl.ac.uk/psipred/) (Ward *et al.*, 2004)).

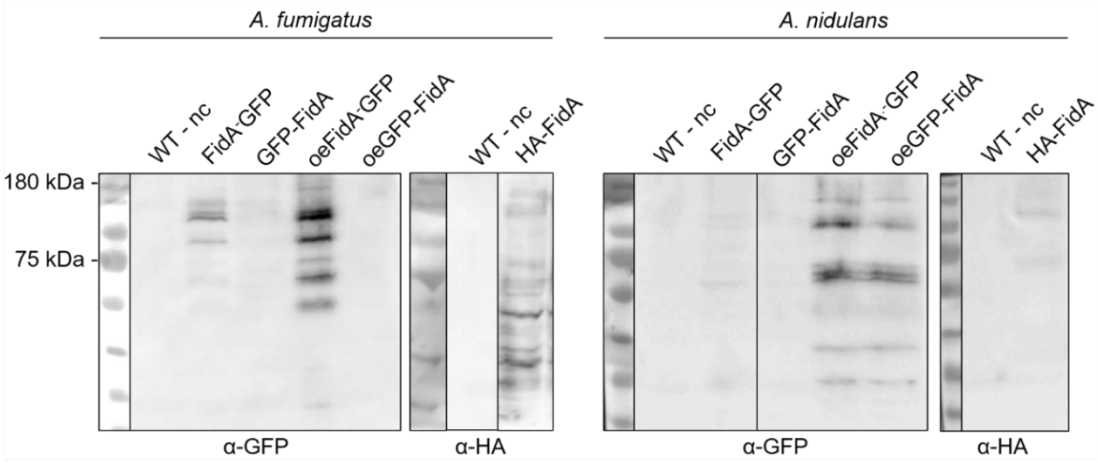

Figure S17: Tagged versions of FidA are unstable in *A. fumigatus* and *A. nidulans*. $2*10^8$ spores of *A. fumigatus* and *A. nidulans* strains were grown vegetatively in *Aspergillus* minimal medium (AMM) for 18h at 37°C. Immunoprecipitation with α-GFP and α-HA antibody reveals that FidA labelled with N-terminal HA, and GFP on C- or N-terminus is unstable in *A. fumigatus* and/or *A. nidulans* (FidA-GFP, GFP-FidA, oeFidA-GFP, oeGFP-FidA and HA-FidA). AfS35 wild type (WT, *A. fumigatus*) and Δ*nkuA* WT (*A. nidulans*) were used as negative controls (nc). Native and/or overexpressed FidA has a predicted protein size of ~ 170 kDa with GFP-tag and ~140 kDa with HA-tag.

Table S1: Putative interaction partners of *A. fumigatus* Fbx15 identified via RFP-pulldown. In total 66 proteins from vegetatively grown cultures were pulled with Fbx15 and/or Fbx15$^{S468|9D}$ tagged with RFP, which were identified in at least two out of three biological replicates with MS/MS count ≥ 5, unique peptides ≥ 3 and LFQ (label-free quantification) intensity ≥ 20. Sys. name: systematic name, Std. name: standard name, Unchar.: uncharacterised. Corresponding descriptions were obtained from AspGD (http://www.aspgd.org/). The further analysed protein Afu2g05520 is shaded in green. Data were obtained from Jöhnk (unpublished).

Sys. name	Std. name	Description	Fbx15	Fbx15 [S468|9D]
Afu3g14150	Fbx15	Bait protein	x	x
SCF subunit and related proteins				
Afu1g12960	Unchar.	Putative orthologe of *A. nidulans* CulA, predicted SCF ubiquitin ligase complex subunit CulA	x	x
Afu5g06060	SkpA	Putative sulfur metabolism regulator	x	x
Afu5g05790	Unchar.	Putative ortholog of *S. cerevisiae* HRT1, putative ubiquitin protein ligase activity		x
Afu2g08150	Unchar.	Putative ortholog of *A. nidulans* NeddH, has a putative role in protein neddylation and SCF ubiquitin ligase complex localisation		x
Transcription factors and nuclear proteins				
Afu2g11840	Cyc8/SsnF	Transcriptional co-repressor	x	x
Afu6g05150	Unchar.	Putative ortholog of *A. nidulans* RcoA/Tup1, has putative histone binding, transcription corepressor activity	x	x
Afu8g05570	Unchar.	Putative ortholog of *S. cerevisiae* SIN3, putative transcription corepressor activity		x
Afu1g10860	Unchar.	Putative ortholog of *S. pombe* Nup107, putative nuclear pore		x
Afu2g08560	Unchar.	Putative ortholog of *A. nidulans* Nup82, has putative nuclear pore localisation		x
DNA/RNA processing				
Afu4g09010	Unchar.	Putative ortholog of *S. pombe* Usp105, putative U1 snRNP localisation		x
Afu5g06040	Unchar.	Putative ortholog of *S. cerevisiae* RAD23, has putative role in cellular response to DNA damage stimulus	x	x
Afu7g01840	Unchar.	Putative ortholog of *S. pombe* Syn1, putative plasma membrane localisation	x	x
Afu6g12300	Unchar.	RNP domain protein	x	x
Afu4g04350	Unchar.	Putative ortholog of *S. pombe* CWF11, putatively has U2-type spliceosomal complex	x	x
Afu1g13060	Unchar.	Putative orthologe of *S. cerevisiae* NAM7, predicted ATP-dependent RNA helicase of the SFI superfamily		x
Afu2g02780	Unchar.	Putative ortholog of *S. pombe* Rnc1, has putative mRNA 3'-UTR AU-rich region binding	x	x
Metabolic enzymes				

Afu7g01010	ADH1	Putative ortholog of *S. pombe* ADH1, putative alcohol dehydrogenase		x
Afu5g10120	Unchar.	Putative ortholog of *S. cerevisiae* LYS1, protein similar to nonribosomal peptide synthases (NRPS-like)	x	x
Afu1G06860	PtcF	Putative ortholog of *S. cerevisiae* PTC5, putative protein serine/threonine phosphatase activity		x
Afu5g08890	Lys4	Putative ortholog of *A. nidulans* LysF, putative homoaconitase	x	x
Afu4g09140	Car2	Putative ortholog of *S. pombe* Car2, L-ornithine aminotransferase	x	x
Afu3g10300	Unchar.	Putative ortholog of *A. nidulans* GalE, putative galactokinase with a role in galactose catabolism		x
Afu6g07720	AcuF	Putative ortholog of *S. cerevisiae* PCK1, putative phosphoenolpyruvate carboxykinase		x
Afu6g08720	Unchar.	Putative ortholog of *S. cerevisiae* MEU1, putative 5'-methylthioadenosine phosphorylase	x	x
Afu1g04670	Unchar.	Putative PSP1 domain protein		x
Afu6g13450	Unchar.	Putative ortholog of *S. cerevisiae* NIT1, has domain(s) with predicted hydrolase activity		x
Afu5g09860	Unchar.	Putative ortholog of *S. cerevisiae* YYJL068C, putative esterase		x
Afu2g09130	Unchar.	Putative ortholog of *N. crassa* Nuo24, putative NADH-ubiquinone dehydrogenase	x	x
Afu5g08270	Unchar.	Putative HAD superfamily hydrolase	x	
Afu5g11290	Unchar.	Putative ortholog of *S. pombe* Dao1, has predicted D-amino-acid oxidase activity and role in D-alanine metabolic process	x	x
Afu3g02270	Cat1	Mycelial catalase	x	x
Afu2g14970	Unchar.	Putative ortholog of *S. cerevisiae* AIM17, gamma-butyrobetaine hydroxylase subfamily protein	x	x
Afu6g02260	Unchar.	putatively has glyoxysome and mitochondrial membrane localisation		x
Afu5g07210	Met2	Homoserine O-acetyltransferase	x	
Afu6g04920	AciA/Fdh	Putative ortholog of *A. nidulans aciA*, putative NAD-dependent formate dehydrogenase		x
Afu4g03900	MFP	Putative ortholog of *S. cerevisiae* FOX2, putative multifunctional beta-oxidation protein		x
Au5g02480	Unchar.	Putative ortholog of *S. cerevisiae* GSY1, putative glycogen sythase		x
Afu2g06000	Unchar.	Putative ortholog of *S. pombe* GDH2, putative NAD+ dependent glutamate dehydrogenase		x
Afu5g05820	Unchar.	Putative ortholog of *S. cerevisiae* THR1, putative homoserine kinase activity	x	x
Afu1g07200	Unchar.	Has domain(s) with predicted catalytic activity		x

Afu5g03500	Unchar.	Putative ortholog of *S. pombe* GLS2, has putative domain(s) with predicted hydrolase activity		x
Afu2g04010	TpsB	Putative trehalose-6-phosphate synthase	x	
Afu6g12950	TpsA	Trehalose-6-phosphate synthase	x	
Afu3g13970	Unchar.	Putative ortholog of *S. pombe* Psd3, has putative phosphatidylserine decarboxylase activity		x
Afu5g09910	Unchar.	Putative ortholog of *S. cerevisiae* HBN1, putative p-nitroreductase family protein	x	x
Afu5g06500	Unchar.	Putative ortholog of *N. crassa* Acd-3, acyl-CoA dehydrogenase family protein with a predicted role in fatty acid beta oxidation		x
Afu5g06710	Unchar.	Putative ortholog of *S. cerevisiae* YMR027W, has predicted phosphatase activity		x
Protein degradation				
Afu2g09030	DppV	Dipeptidyl-peptidase V, secreted dipeptidyl-peptidase	x	x
Afu8g04730	Unchar.	Putative ortholog of *S. pombe* ppp16, putative oligopeptidase family protein		x
Protein folding				
Afu4g12850	Clx4	Calnexin	x	x
Signal transduction				
Afu3g12510	Unchar.	Putative ortholog of *S. pombe* Sec18, has putative domain(s) with predicted ATP binding		x
Afu3g08620	Unchar.	Putative ortholog of *S. cerevisiae* LSB1, has putative role in negative regulation of Arp2/3 complex-mediated actin nucleation and actin cortical patch		x
Afu3g13440	Unchar.	Stomatin family protein	x	x
Afu6g02090	Unchar.	Putative ortholog of *S. cerevisiae* VMA4, putative vacuolar proton-transporting V-type ATPase	x	x
Afu7g03870	Unchar.	Putative ortholog of *S. cerevisiae* PAN1, predicted Arp2/3 complex binding activity		x
Afu6g11890	Unchar.	Putative ortholog of *S. cerevisiae* VPS1, putative dynamin GTPase	x	x
Afu4g08040	Unchar.	Putative ortholog of *S. pombe* Ypt5, has putative GTP binding activity	x	x
Afu6g14220	Unchar.	Putative ortholog of *A. nidulans* KinA, has putative ATP-dependent microtubule motor activity		x
Afu5g05550	Unchar.	Putative ortholog of *S. cerevisiae* MYO2, putative class V myosin	x	x
Other proteins				
Afu1g11120	Unchar.	Has putative domain(s) with predicted cytoplasm and nucleus localisation		x
Afu6g02870	Unchar.	Has putative domain(s) with predicted cell outer membrane	x	x
Proteins with unknown function				
Afu2g05520	Unchar.	conserved hypothetical protein		x

Afu8g03950	Unchar.	conserved hypothetical protein		x
Afu1g09770	Unchar.	conserved hypothetical protein		x
Afu1g09630	Unchar.	conserved hypothetical protein		x
Afu1g04280	Unchar.	conserved hypothetical protein		x

Table S2: **Homologs of *A. nidulans* AN11565/ATP17 identified by NCBI-BLAST.** 'Query coverage' describes the alignment cover of the primary amino acid sequence of *A. nidulans* AN11565/ATP17 in percentage. Similarities between the identified ATP17 homologs of other species in comparison to ATP17 of *A. nidulans* ATP17 are described in 'Identity' in percentage. NCBI-BLAST: https://blast.ncbi.nlm.nih.gov/Blast.cgi?PAGE=Proteins.

F-subunit ATP17	**Organism**	**Query coverage**	**Identity**
AN11565/ATP17	*Aspergillus nidulans* FGSC A4	100%	100%
ATP17	*Saccharomyces cerevisiae* S288C	88%	54.74%
atp17	*Schizosaccharomyces pombe* 972	90%	42.86%
ATP17	*Candida albicans* SC5314	100%	49.51%
NCU05220	*Neurospora crassa* OR74A	100%	68.32%

List of Figures

List of Tables

List of Supplementary Material

Abbreviations

5´	upstream flanking region
3´	downstream flanking region
3-AT	3-amino-1,2,4-triazole
°C	degree Celsius
Δ	deletion
µg	microgram
µl	microlitre
µm	micrometre
µM	micromolar
A or Ala	alanine
ADP	Adenosine diphosphate
AIDS	acquired Immune Deficiency Syndrome
AMP	Adenosine monophosphate
Amp B	Amphotericin B
AMM	*Aspergillus* minimal medium
AMP^R	ampicillin resistance marker cassette
Approx.	approximately
APS	ammonium persulfate
APSES	Asm1p, Phd1p, Sok2p, Efg1p and StuAp
ATP	Adenosine triphosphate
ATPase	Adenosine triphosphate synthase
bHLH	basic helix-loop-helix
BiFC	Bimolecular fluorescence complementation
bip	bipartite
BLAST	basic local alignment search tool
bp	base pair(s)
BSA	bovine serum albumin
CAND1	cullin-associated Nedd8-dissociated protein A
cDNA	complementary DNA
CGD	chronic granulomatous disease
COP9	constitutive photomorphogenesis 9
CP	core particle
CPT	camptothecin
CSN	COP9 signalosome
C-terminus	carboxy terminus
D	asparagine
DBD	DNA binding domain

DHN	1,8-dihydroxynaphthalene
DKP	diketopiperazine
DIC	differential interference contrast
DMATS	dimethylallyl tryptophan synthase
DNA	deoxyribonucleic acid
Dox	doxycycline
DTT	dithiothreitol
DUB	deubiquitinating enzyme
EDTA	2,2´,2´´,2´´´-(Ethane-1,2-diyldinitrilo) tetra-acetic acid
ELSD	evaporative light scattering detector
g	gram
gDNA	genomic DNA
GSH	reduced form of glutathione
Fbx	F-box
FidA	Fbx15-interacting developmental protein A
FiAt	Fbx15-interacting APSES transcription factor
GDP	guanine diphosphate
GEF	guanine exchange factor
GFP	green fluorescent protein
gpdA	*A. nidulans* glyceraldehyde-3-phosphate dehydrogenase promoter
GOI	gene of interest
GTP	guanine triphosphate
H_2O_2	hydrogen peroxide
h	hour(s)
H2A	histone
hph^{NRM}	hygromycin resistance non-recyclable marker cassette
HPLC	High performance liquid chromatography
kb	kilobase(s)
kDA	kilo Dalton
l	litre
LB	lysogeny broth
LCMS	liquid chromatography mass spectrometry
LM	London medium
LRR	leucine rich repeats
M	molar
mg	milli gram(s)
MHR	middle homologous region
min	minute(s)
ml	millilitre(s)
mM	millimolar
MMS	methyl methanesulfonate
mp	monopartite

mRNA	messenger RNA
NADP(H)	Nicotinamide adenine dinucleotide phosphate
NEDD8	neural-precursor-cell-expressed developmentally down-regulated 8
NES	nuclear export signal
NLS	nuclear localisation signal
nm	nanometre (s)
NPC	nuclear pore complex
NRPS	Non-ribosomal peptide synthetase
N-terminus	amino terminus
o/n	over night
oe	overexpression
ORF	open reading frame
PCR	polymerase chain reaction
PDA	photodiode assay detection
PKS	polyketide synthase
P-value	probability value
phleo^{NRM}	phleomycin resistance non-recyclable marker cassette
phleo^{RM}	phleomycin resistance recyclable marker cassette
ptrA^{NRM}	pyrithiamine resistance non-recyclable marker cassette
ptrA^{RM}	pyrithiamine resistance recyclable marker cassette
qRT	quantitative reverse transcriptase
Ran	RAs-related nuclear protein
RING	Really interesting new gene
ROS	reactive oxygen species
RFP	red fluorescence protein
RP	regulatory particle
rpm	revolutions per minute
RNA	ribonucleic acid
RT	room temperature
s	second(s)
S or Ser	serine
SCF	SkpA/CulA/F-box
SDS	sodium dodecyl sulphate
SEM	standard error of the mean
SISA	*Simple Interactive Statistical Analysis*
SOD	superoxide dismutase
SREBP	sterol regulatory element binding protein
SrbA	sterol regulatory element binding protein A
SrbB	sterol regulatory element binding protein B
OefC	overexpressed fluffy C
TAP	Tandem Affinity Purification
TC	terpene cyclase

TEMED	*N,N,N′,N′*-tetramethylethane-1,2-diamine
Thr	Threonine
Tris	2-Amino-2-hydroxymethyl-propane-1,3-diol
^{T}*trpC*	*A. nidulans* tryptophan biosynthesis gene terminator
Ubi	Ubiquitin
UBD	Ubiquitin binding domain
UPS	Ubiquitin proteasome system
UV	ultra-violet
UV-DAD	UV diode array detector
V	Voltage
v/v	volume per volume
WT	wild type
w/v	weight per volume
YFP	yellow fluorescence protein

Acknowledgements

I am very grateful for the people who supported me in any possible way during the last four years and thereby helped me to develop this thesis.

First Prof. Dr. Gerhard Braus, without your support I would have not been able to do my PhD in the field of filamentous fungi. Especially in the last months you provided me with valuable advices and suggestions to finalise my thesis. The experiences I made while working on my PhD had a strong impact on my personal development, thanks for that!

I thank my thesis committee members, apl. Prof. Dr Kai Heimel and Prof. Dr. Ralf Kehlenbach. I really enjoyed our meetings, which always helped me to keep the focus on the important objectives of my project.

I thank Prof. Dr. Stefanie Pöggeler, Prof. Dr. Rolf Daniels and PD Dr. Michael Hoppert for being members of my examination board.

I sincerely appreciate the support of Dr. Christoph Sasse during my PhD time. You listened to me, whenever I had questions or worries, gave me advices or another perspective. Thank you!

Dr. Jennifer Gerke is the specialist in the institute regarding secondary metabolite analysis. Without your help I would still not have been able to understand the FreeStyle Software. Thank you for your support and the measurement of my samples.

So many plasmids I constructed would not be existing without your impressive pipetting skills, thanks Dr. Rebekka Harting. Also, thank you for your proof-reading efforts, Rockbuddy!

Dear, Dr. Blaga Popova, thanks for the years of mental support and help concerning imaging. Working with you has always been a pleasure!

I am thankful for the friendships I made through the years: Cindy Meister, you are a genius for me. In my opinion you are a gifted scientist and I am glad to know you. Thanks for your input regarding my results and the humorous comments. Correcting my errors has never been so funny. Whenever I was clueless how to handle my projects or running out of time you were always there and helped me regardless what you had to do for your own PhD project. For this I want to express my gratitude, Fruzsina Bakti. You inspire me! Anna Maria Köhler, thank you for the time you spent for proof-reading, although you recently had your lovely daughter, thanks a lot! While we are at it, thank you Bine for proof-reading my discussion. As a young mother of the little Mieke you still found the time to help me. That means a lot to me, thank you! Anja Strohdiek, my namesake, always in a good mood and very good in making corrections! Thank you for your help! Liu Li, thanks for your proof-reading and thanks for the joyful time at the DGHM in February ’19 in Göttingen! And thank

you, Lara Schmitt, for proof-reading and for the valuable advices concerning writing my thesis! Annalena Höfer, I have spent the longest period of my time at the university with you. Thanks for our conversations that calmed me down when I was going crazy. Miriam Leonard and Jessica Starke, I always have you as a duo in mind. Maybe it's because both of you were registered in the Canada project and worked close together. I am thankful to know you both and I am proud to call you my friends!

Thank you, Verena Große, for your help in daily lab life over the years and also Wangping for ensuring a pleasant atmosphere in the lab!

All in all, I want to thank the whole 'Microbiology and Molecular Genetics' Department. The daily work was full of laughter and great discussions. Some persons I want to thank moved already to other places all over the world. Basti, thank you for the first year in which you introduced me to the Fbx15 project and your RFP-traps you provided for me! Karl and again Bine, I really miss the conversations with you both since you left and started a new episode in your lives in Munich together with your cute daughter Mieke.

Alena, thank you for being my best friend! I never want to miss the wine evenings or wednesdays at Thanners! We shared a very stressful period of our lives but now we can say 'We did it!'. I am looking forward to the coming years with you!

At the end I want to thank the most related persons that contributed to my today's personality, my family. Father, our family was always the first priority for you. No matter how hard work was, my brother, my sister and I could always count on you. Today, I hope I can be there for you, helping you getting healthy again.

My mother is the strongest person I have ever known. You raised three children as a blind woman, and I cannot understand even now how you handled this. I would already be unable to cope with one child. And even today you are always there for me. Whenever I called you, because things got out of control, you calmed me down. You always supported me in my decisions and raised me to a self-confident adult. Thank you for being my mom!

I thank my sister and my brother for the lucky childhood I joined with you both. Christian, as husband of my sister, you became my second brother. Thank you for being part of our family and your help when my mother, my brother, my sister and I were helpless with the illness of my father.

Finally, thank you Dominik for your strong support over the last years. You are already a part of my family and living without you would be a big loss. I cannot imagine how the last months would have been without you. The past six months contributed so far to the most stressful time in my life but with you by my side, it was bearable. I can always count on you and I am excited about the future with you!

And most importantly, I thank my tom cat Barney for being the cutest, fluffiest and most adorable animal in the world. As I always say to you: "You are my heart!"